The Function of Toll-like receptor 2 in Infection and Inflammation

Hu, W.

The Function of Toll-like receptor 2 in Infection and Inflammation

Wanbin Hu

2021, Leiden

Colophon

Title: The Function of Toll-like receptor 2 in Infection and Inflammation

Author: Wanbin Hu

Ph.D. thesis, University of Leiden, Leiden, The Netherlands

ISBN: 978-94-92597-88-5

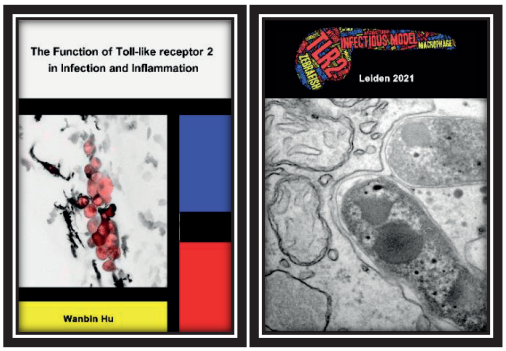

Cover design: Wanbin Hu
Cover lay out:
Cover Front: The design was inspired by the painting “Composition with red, yellow and blue” (by Piet Mondriaan). The confocal picture in the middle box shows the co-localization of macrophages (black) with clusters of *Mycobacterium avium* bacteria (red) in infected zebrafish larvae at 4 days post infection.
Cover back: Word cloud in the shape of a 1 day post fertilization zebrafish larva. The font size in the word cloud is based on its occurrence frequency in the thesis. The transmission electron microscope image shows two *Mycobacterium avium* bacteria inside a phagosome. The image was taken from zebrafish larva tail fin infected with *Mycobacterium avium* strain MAC101. The transmission electron microscope image was taken by Gerda Lamers.

Printing company: Printsupport4U

The studies described in this thesis were performed at the Institute of Biology Leiden, Leiden University.
The work was supported by a grant from the Innovative Medicines Initiative 2 Joint Undertaking (IMI2 JU) under the RespiriNTM project (Grant No. 853932) and the China Scholarship Council (CSC no. 201708210177).
The publication of this thesis was financially supported by Leiden University.

The Function of Toll-like receptor 2 in Infection and Inflammation

Proefschrift

ter verkrijging van
de graad van doctor aan de Universiteit Leiden,
op gezag van rector magnificus prof.dr.ir. H. Bijl,
volgens besluit van het college voor promoties
te verdedigen op 16 december 2021
klokke 15.00 uur

door

Wanbin Hu

geboren te Luoyang, Henan, China

op 8 mei 1991

Promotores:	Prof. Dr. H. P. Spaink
	Prof. Dr. F. J. Verbeek
Promotiecommissie:	Prof. Dr. G. P. van Wezel
	Prof. Dr. B.E. Snaar-Jagalska
	Prof. Dr. R. M. H. Merks
	Prof. Dr. T. H. M. Ottenhoff
	Prof. Dr. W. Bitter (Vrije Universiteit Amsterdam)

路漫漫其修远兮，吾将上下而求索。

The road ahead is long and has no ending; yet high and low I will search with my will unbending.

——Qu Yuan

For my family and friends

献给远方的家人和所有的朋友

Table of contents

Scope of this thesis

Innate immunity is considered as the first line in defense against microbial invasion and it is also involved in responses to tissue injury [1-3]. The innate immune system consists of physical/chemical barriers, humoral components, innate immune cells, and innate signaling molecules [1]. The host maintains its homeostasis and initiates adaptive immune responses by modulating the innate immune system [1, 2]. Innate immune disorders can increase the susceptibility of hosts to invading pathogen infections [4]. Thus, better comprehension of events involved in innate immunity is essential for understanding human pathogenesis and the subsequent discovery of new targets for therapeutic applications.

Toll-like receptor (TLR) signaling, as a crucial part of the innate immune system, has been widely investigated after its initial discovery in *Drosophila* [5, 6]. TLR2, which is conserved in most vertebrates, is one of the most crucial toll-like receptors because its function in microbial defense is the broadest, and the most promiscuous [7]. It has been reported that TLR2 is involved in the immune modulation during infectious diseases [8, 9], chronic and acute inflammatory diseases [10, 11], cancers [12], and even metabolic disorders [13]. At present, the function of TLR2 is still controversial in some studies and its role in several diseases is still inconclusive [7]. It is clear that TLR2 is a promising therapeutic target, but its dual role in both activation and suppression of innate immune responses makes further clinical research challenging [14]. Thus, further studies on the function of toll-like signaling and TLR2 in the innate immune system are necessary.

In this thesis, the functions of toll-like signaling in infection and inflammation are studied by using the zebrafish larval model. Firstly, we studied the function of Toll-like signaling in the absence and presence of pathogenic microbial infection at the transcriptome level. Then, we studied the role of Toll-like signaling on the regulation of leukocyte migration in response to tissue damage and infection, respectively. For this, sophisticated cell tracking and mathematic analyses were performed using fluorescent live imaging based on a confocal laser scanning microscopy. In the end, we set up a comparative zebrafish infection model and found specialized roles of the *tlr2* gene in defense against various mycobacterial species. This thesis provides better understanding of the functions of TLR2 in innate immune responses and provides a large amount of data for future mathematical modeling and deep learning, which makes further *in silico* biological studies possible.

In the general introduction, we address the current cell biological knowledge about the function of TLR2 that makes it a promising therapeutic target for combatting infectious and inflammatory diseases. Subsequently, we discuss the advantages of transparent zebrafish larvae for cell tracking methods to uncover new functions of TLR2.

Chapter 1

General introduction:

The role of TLR2: from cell biology to therapeutic target

1

1. Innate immunity and Toll-like receptors

1.1 Innate immunity

The host cells, rely on membrane-localized and germline-encoded pattern recognition receptors (PRRs) to initiate protective innate immune responses [2, 3]. PRRs recognize invading microbial pathogens through pathogen-associated molecular patterns (PAMPs) of the pathogens in combination with recognition of danger-associated molecular patterns (DAMPs) produced by infected or damaged tissues [2, 3, 15]. PRRs are comprised of four well-characterized groups, including Toll-like receptors (TLRs), retinoic acid-inducible gene-I (RIG)-I-like receptors (RLRs), the nucleotide-binding oligomerization domain (NOD)-like receptors (NLRs), and C-type lectin receptors (CLRs) [16]. TLRs and CLRs belong to transmembrane proteins, while RLRs and NLRs are cytoplasmic proteins [16]. TLRs are the most important and widely studied PRRs (See Fig 1).

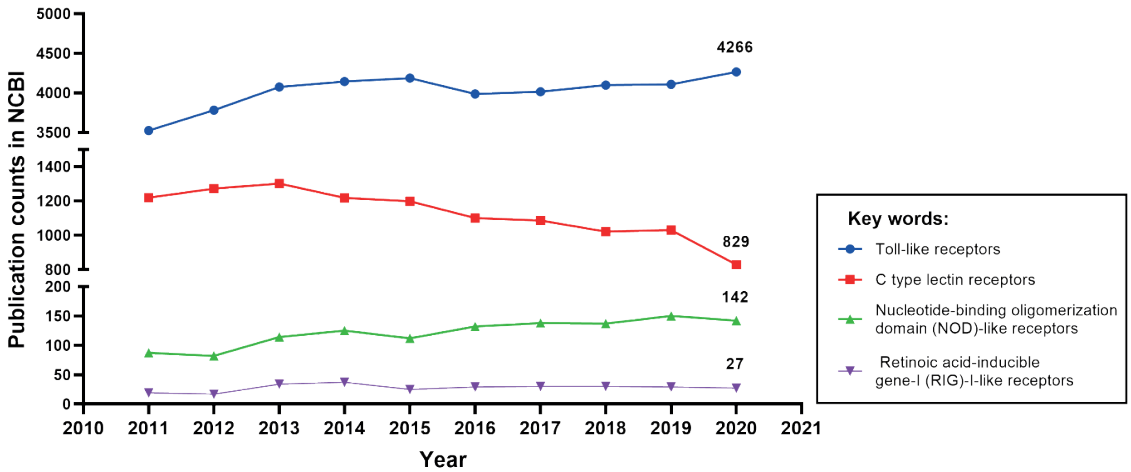

Figure 1 Publication counts for four PRRs in the NCBI data base.

1.2 The structure of TLRs

The function of TLRs has been studied extensively in the last decades (Fig 1). Their capacity as a key control factor of innate immune responses makes them attractive therapeutic targets. TLRs are homologs of the *toll* gene that was first discovered to be involved in embryonic development in *Drosophila* [5, 6]. The investigation of TLRs became very intense after their function in defense against microbial infection in *Drosophila* and vertebrates was demonstrated [17]. TLRs are made up of an ectodomain, also known as the periplasmic extracellular domain,

a cytoplasmic signaling domain, and a single transmembrane domain [3, 18]. The ectodomain of TLRs contains leucine-rich repeats (LRRs) and selectively recognizes PAMPs and DAMPs [3]. We summary the different PAMPs and DAMPs are recognized by the specific TLRs in Fig 2. The cytoplasmic signaling domain of TLRs comprises an evolutionary conserved Toll/IL-1 receptor (TIR) homology domain that is responsible for signal transduction [3]. Different species have different numbers of genes that encode TLRs. In the human genome, 10 TLRs are encoded, whereas the mouse and zebrafish genomes encode at least 12 and 17 TLRs, respectively [19-21]. TLRs can be divided into two subgroups based on their cellular location. TLRs are expressed either on the cell surface or in intracellular compartments. In humans, TLR1, 2, 4, 5, 6 and 10 are expressed on the cell surface, while TLR3, 7, 8 and 9 are localized in intracellular membranes [3, 22]. In mice, the cellular distribution of the conserved TLRs is assumed to be the same as the distribution in humans, while TLR12 is expressed on the cell surface and TLR13 is probably expressed within endosomes [22]. Interestingly, TLR11 can be expressed on both cell surface and intracellular compartments [23].

1.3 TLR2, an important member of the TLR family

After the identification of TLR2 in 1998, much progress has been made in our understanding of its function [9, 24]. Its functions, in the recognition of a large number of ligands, including PAMPs and DAMPs, are complicating the studies of the underlying recognition mechanisms (Fig 2). In addition, the ubiquitous distribution of TLR2 on various types of cells, e.g., immune, endothelial, and epithelial cells, also determines its wide range of functions [9]. Considering the broad functions of TLR2, the drive for the development of TLR2 related therapeutic targeted vaccine or treatment has accelerated in the last decades [7, 25, 26]. However, some studies on TLR2 are still controversial [7]. It is because of the complex functions of TLR2 that its role in immune regulation is not black or white [8]. For example, TLR2 plays a dual role in infection processes. TLR2 has been shown to play a protective role during infection by triggering a strong pro-inflammatory response which is considered beneficial for bacterial clearance [27, 28]. However, excessive inflammation caused by TLR2 can lead to tissue damage and even affect healing of damaged tissues [11]. The mechanisms of TLR2 signaling and its regulation are discussed in detail below.

2. Regulation of TLR2 signaling

2.1 TLR2 signaling pathway

The binding of the LRR domain in TLRs and its ligands stimulates the recruitment of adaptor proteins to interact with the intracellular TIR domain in TLRs to trigger the downstream cascades. Myeloid differentiation factor (Myd88) is a well-known adaptor protein that interacts with almost all TLRs except TLR3 [3]. TIR domain-containing adaptor protein (Tirap), which is also called Myd88 adaptor-like (Mal), is required in the TLR2/6 signaling via Myd88 while it is not necessary in the TLR2/1 signaling [29]. In addition to Myd88 and Tirap, other adaptor proteins in mammalian cells include TIR domain-containing adaptor protein inducing interferon-β (TRIF), TIR-containing adaptor molecule (TICAM), TRIF-related adaptor molecule (TRAM), and sterile α- and armadillo motif-containing protein (SARM) [30]. The recruitment of distinct adaptor proteins can trigger different downstream signaling pathways. Recent reviews have discussed in detail the known differences between downstream signaling pathways of the mammalian TLR receptors [3, 31, 32] and therefore we only briefly describe TLR2 signaling here and summarize it in Fig 3.

After the interaction of TLR2 and its associated adaptor proteins, the IRAK complex is activated to recruit TRAF6. Activated TRAF6 triggers the activity of a complex of TAK1/ TABs to stimulate both the activation of the MAPKs and the IKK complex (IKK1, 2, and IKK-γ, also named NEMO). The MAPKs family includes, but is not limited to JNKs and p38. The IKK complex promotes the nuclear translocation of NF-κB. In the end, the production of pro-inflammatory cytokines is induced by the AP-1 and NF-κB, which in turn controls inflammation and modulates cell survival and proliferation [9, 33].

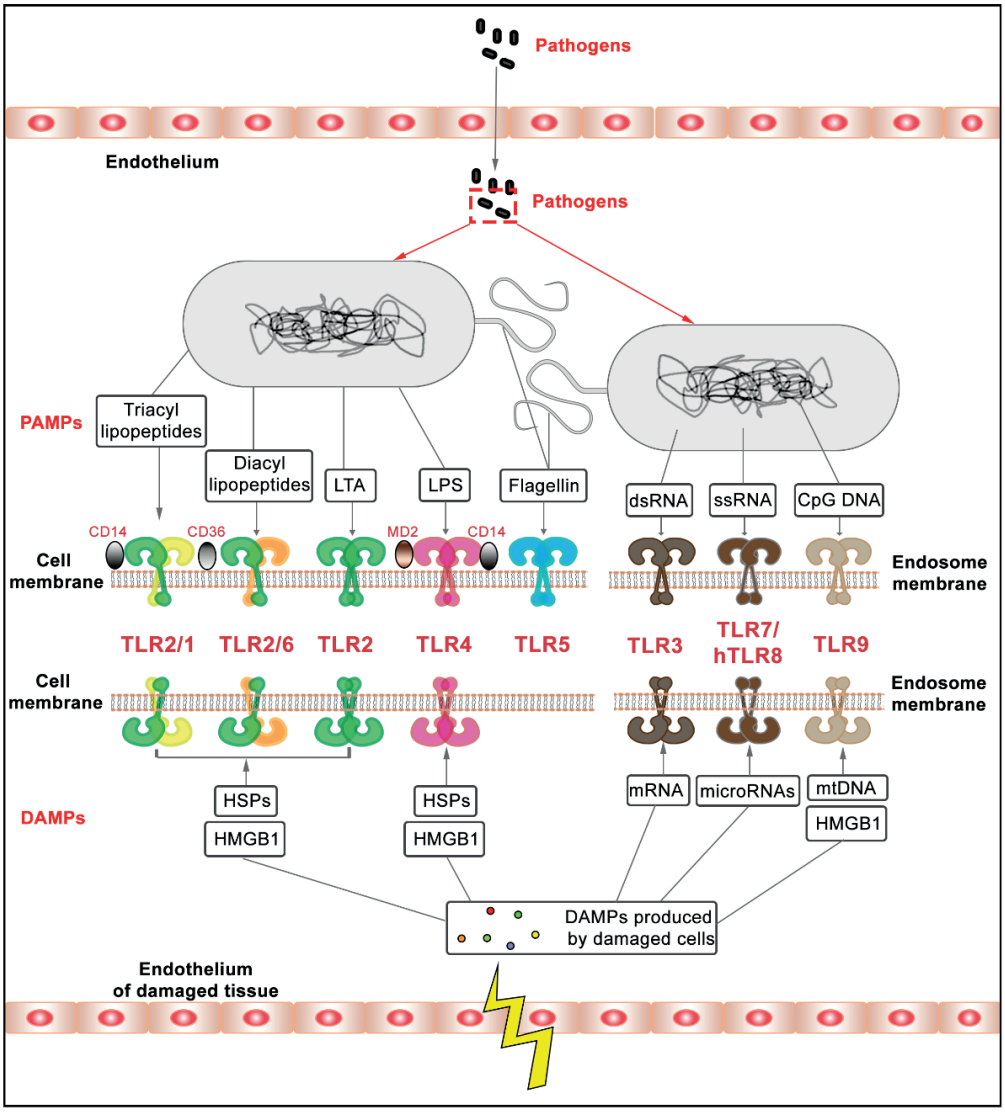

Figure 2 TLRs and its ligands. TLRs can recognize PAMPs from invading microbial pathogens and DAMPs from infected or damaged tissue. TLR2, its heterodimers and TLR4 recognize pathogens through their cell wall surface components. TLR2 conjugates with TLR1 or with TLR6 to sense triacyl or diacyl lipopeptides, and lipoteichoic acid (LTA) on the cell wall of gram-positive bacteria, and mycobacteria [9, 34-36]. The process of the recognition of triacyl or diacyl lipopeptides by heterodimers needs the participation of accessory molecules. For example, CD14 and CD36 are well characterized as ligand delivery molecules to enhance TLR2 responses to ligands especially with a lower concentration of ligands, although the participation of these molecules is not essential [9, 36]. TLR4 can sense Gram-negative bacteria through the lipopolysaccharide (LPS) located on their outer membrane [35]. During this process, the formation of a complex of TLR4 with MD2 and CD14 is essential for recognizing LPS [35, 37]. TLR5 functions in the recognition of flagellin from bacterial surfaces. There is still relatively little knowledge about the function of TLRs in the recognition of DAMPs compared with its function in there cognition of PAMPs. TLR3, 7, and 9 have been reported to play a role to sense these nucleic acids released from damaged cells [38, 39]. It has been demonstrated that TLR2 and TLR4 can be activated by the intracellular proteins or extracellular matrix components released from damaged cells [38, 39]. It is controversial that DAMPs directly interact with extracellular TLRs, during this DAMPs recognition process [38]. It has been shown that recognition can be indirect for instance by the involvement of high-mobility group box 1 protein (HMGB1), which is a widely studied endogenous danger signal that induces inflammatory response through its interaction with DAMPs recognized by TLR2, TLR4 and TLR9 [40, 41].

2.2 Negative regulation in TLR2 signaling

Accumulating evidence has been reported that the activation of TLR2 signaling is a benefit for the host defense against invading pathogens [42-44]. Excessive activation of TLR signaling, can lead to over-expression of pro-inflammatory cytokines, which have been implicated in chronic inflammatory diseases, autoimmune diseases, and even aggravation of infection diseases [45-47]. For example, a deficiency of TLR2 in diabetic mice can accelerate wound healing, which indicates that excessive activation of TLR2 signaling might be harmful for wound healing [48]. Thus, it appears that TLR2 signaling needs to be tightly regulated by negative regulation mechanisms that are still poorly understood. Recent reviews have summarized many different mechanisms of negative regulation and their molecular components [49-52]. Negative regulators are including the following categories of molecules: ubiquitin ligases, deubiquitinases, transcriptional regulators, and microRNA, which induce different negative regulations [52]. The mechanisms inhibiting TLR2 signaling are based on (1) prevention of receptor-ligand binding; (2) dissociation of adaptor complexes; (3) inhibition of TLR2 downstream kinase signaling; (4) negative transcriptional regulation by TLR2 and other factors as described below [50, 51].

Soluble TLR2, which is a smaller isoform of the TLR2 protein that has been reported to be secreted by human monocytes, has been characterized to compete with TLR2 located on cell membranes to bind with the ligands to inhibit TLR2 signaling [53, 54]. As a negative regulator that leads to dissociation of adaptor complexes it has been shown that a short form of Myd88 (sMyd88) is unable to bind with IRAK4 and thereby its expression can inhibit NF-κB activation [55]. Another described mechanism for inhibition adaptor signaling is the induction of TIRAP degradation by the suppressor of cytokine signaling 1 (SOCS1) [56]. Moreover, TRIF can be degraded by a disintegrin and metalloprotease 15 (ADAM15) in a TRIF-dependent pathway [57]. In terms of TLR2 downstream kinase signaling inhibition, Toll-interacting protein (TOLLIP) inhibits the TLR2 signaling by targeting with IRAK1 to suppress its phosphorylation or directly interacting with TLR2 [58, 59]. Thus, TOLLIP is widely utilized as an inhibitor to inhibit TLR2 signaling [59]. IRAK-M is another IRAK inhibitor, which belongs to the IRAK kinase family but cannot induce NF-κB activation [60]. In addition, tyrosine phosphatase SHP-1, CD300a, and CD300f are also reported as IRAKs inhibitors. SHP-1 inhibits IRAK1 activation by interaction with a kinase tyrosine-based inhibitory motif (KTIM) [61], and CD300a/f can associate with SHP-1 to inhibit signaling [62]. In addition to the inhibitors

targeting IRAKs, proteins bind with TRAF6 , namely A20 (also called TNF- α induced protein 3, TNFAIP3), a non-receptor tyrosine kinase Sky, NLR family member X1 (NLRX1), and the cylindromatosis protein (CYLD) have also been shown to be negative regulators of TLR2 signaling [63]. Furthermore, A20 and NLRX1 can also block the activation of the IKK complex [64]. The last category is the negative regulatory of transcription. The transcription of some pro-inflammatory genes, like IL-6, are negatively regulated by transcription factor 3 (ATF3) [65], A TLR-inducible IkB protein (IkBNS) [66], and B-cell CLL/lymphoma 3 (Bcl-3) [67]. It is not yet known how these negative regulators are controlled. It has been hypothesized that Myd88 might be involved in a feedback loop that could be under control of TLR2 or other Toll like receptors [68]. Therefore, it is very likely that TLR2 is an important control factor of negative regulation of transcription of genes involved in inflammation.

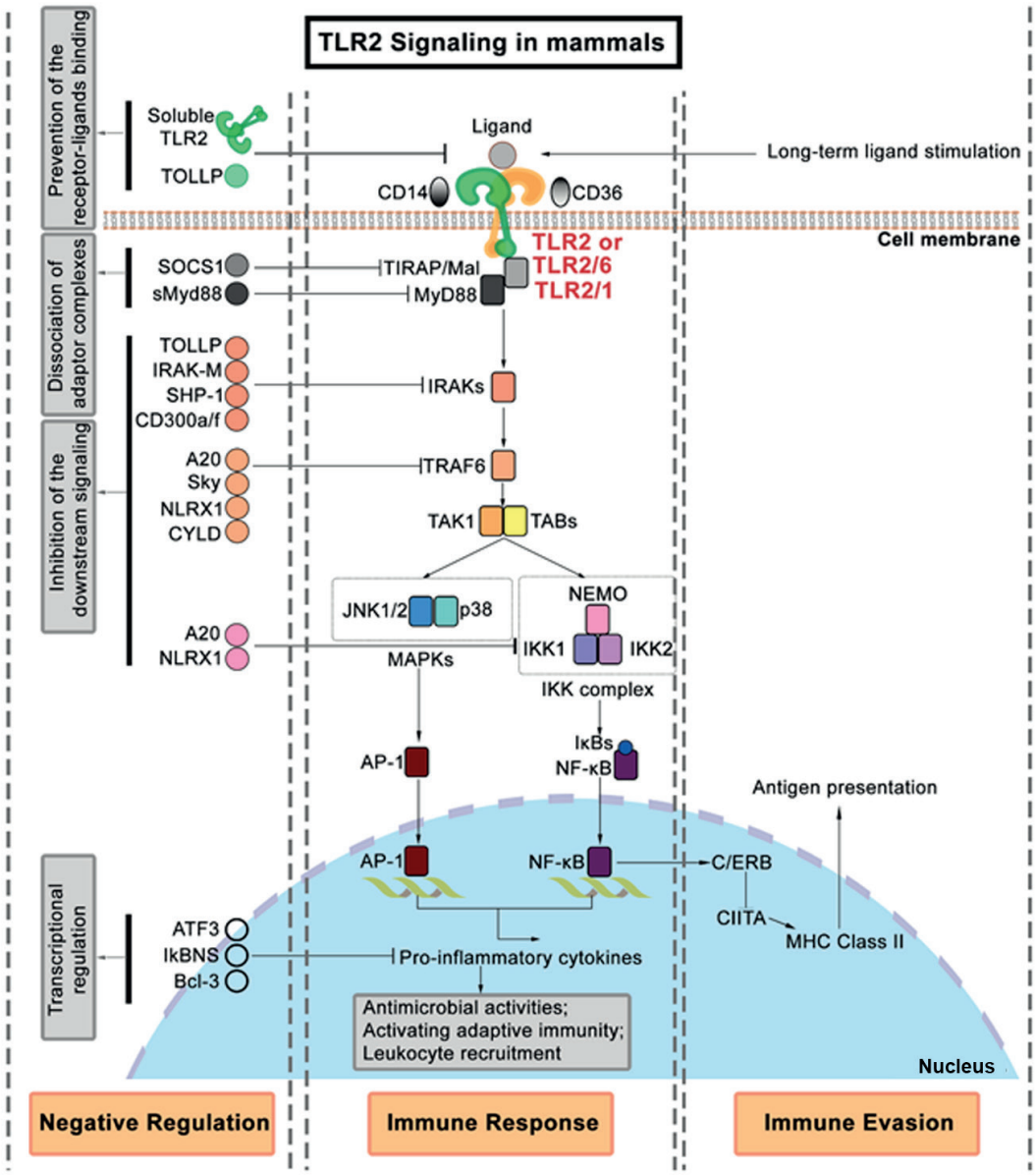

Figure 3 A brief overview of the TLR2 signaling pathway in mammals [9, 33]. To be noted, the shown TLR2 signaling components are not exclusive for this TLR receptor, and the phosphorylation and ubiquitination processes are not mentioned in this figure. TLR2 or its heterodimers are ubiquitously located on the cell membranes. The TLR2 signaling activation through TLR2/1 requires the participant of accessory molecule CD14, while TLR2/6 requires CD36. The TLR2 signaling pathway is activated after TLR2 ligand-recognition (PAMPs or DAMPs). Subsequently, the adaptor proteins, Myd88 and Tirap/Mal, are recruited. After a series of cascades involving NF-κB and MAPKs, various transcription factors are activated to induce pro-inflammatory cytokines.

3. TLR2 function in mycobacterial infection studies

3.1 Tuberculosis and non-tuberculosis disease

Tuberculosis (TB) is a communicable disease, which is caused by infection with *Mycobacterium tuberculosis* (Mtb) [69]. At present, TB remains one of the top 10 diseases which give rise to death and currently its death toll is higher than that caused by other major infectious disease such as malaria, AIDS or COVID-19 [69]. It has been reported that in recent years, incidence and death of TB are falling, but it is not reaching any of the global TB eradication goals set by the WHO [70]. Currently, in the COVID-19 pandemic situation the numbers of deaths due to tuberculosis are rapidly rising due to a lack of diagnostic and treatment capacity [69]. Nontuberculous mycobacteria (NTM) diseases are defined as caused by mycobacterial pathogens other than Mtb and *Mycobacterium leprae* [71]. Besides TB, NTM infection diseases have recently attracted wide attention because the disease prevalence of NTM infection diseases is increasing sharply since 2000 [72]. It is hard to combat TB or NTM infection incidence due to the rapid increase in multi-drug resistant mycobacterial strains [69, 73]. Therefore, there is an urgent need to discover novel preventive or therapeutic strategies for TB and NTM infection diseases. Currently, host-directed therapies (HDT) are one of the most promising strategies to combat NTM infectious diseases by making the NTM antibiotic treatment regimens more effective [73, 74]. In mycobacterial infection, TLR2 is a key receptor to recognize mycobacteria, modulate immune cells recruitment, modulate phagocytosis, and trigger pro-inflammatory responses to eliminate the invading mycobacteria [9]. Thus, it is helpful to discover new host directed therapeutic targets by better understanding the mechanism of TLR2 modulating the host-mycobacterial interactions.

3.2 TLR2 recognizes mycobacterial components

As we described in this introduction, TLR2 plays a crucial role in recognizing bacteria such as Mtb through their cell wall components [75]. TLR2 lipoprotein ligands of the cell surface of Mtb include 19-kDa lipoprotein (Rv3763, LpqH), 24-kDa lipoproteins (Rv1270c, LprA and Rv1411c, LprG), and 38-kDa glycolipoprotein (PhoS1). Other categories of TLR2 ligands include lipoarabinomannan (LAM), lipomannans (LM), phosphatidylinositol dimannoside (PIMs) and trehalose dimycolate (TDM). and mycobacterial heat shock protein 70 (HSP70). The TLR2 ligands from Mtb are briefly summarized and described in Table 1 [76]. As we described in this introduction these ligands activate macrophages by activating NF-κB through TLR2 (Fig 3). However, prolonged TLR2 signaling triggered by these ligands might help Mtb

to evade immune surveillance. For example, long-term exposure of macrophages to LpqH, LprG, LprA, PhoS1, LM, and PIM leads to IL-10, IL-4, and TGF-β expression, which in turn inhibits the activation of macrophages [76]. Furthermore, it has been demonstrated that prolonged TLR2 signaling activated by LpqH and LprG inhibits the expression of MHC class II molecules and exogenous antigen processing for presentation to $CD4^+$ T cell, which can be a basis for Mtb immune evasion (Fig 3) [77-80].

3.3 TLR2 is associated with susceptibility to various mycobacteria

The structural integrity of TLR2 is crucial for defense against invading pathogens. Single nucleotide polymorphisms (SNPs) in human TLR2 have been reported to associate with increased susceptibility to infectious diseases [81]. For example, one of the TLR2 polymorphisms, Arg753Gln has been demonstrated to lead to higher susceptibility to TB [82]. Moreover, the TLR2 polymorphism R753Q impairs the activation of TLR2 signaling upon *M. smegmatis* infection [83]. These studies indicate that TLR2 plays a protective role in mycobacterial infection diseases, although a small number of studies found no effect of TLR2 polymorphism [8, 84, 85]. Thus, an animal model for TLR2 polymorphisms is needed to investigate the functions of the polymorphisms in tuberculosis.

Mice is a widely used animal model to study the function of TLR2 in resistance to mycobacterial infection. The evidence for the role of TLR2 in defense against NTM infection is still limited, and no correlation has been found between TLR2 polymorphism and human susceptibility to NTM infection until now [86]. Interestingly, $TLR2^{-/-}$ mutant mice were more susceptible to *M. avium* infection [87]. It has been demonstrated that TLR2 deficient mice, but not TLR4 deficient mice, were more susceptible to a high dose Mtb infection than wild type mice [88-90]. However, the results of the studies of the role of TLR2 in low-dose Mtb infection are controversial. As a result, it is not clear at which infectious stages TLR2 functions in defense against Mtb infection: it is undecided whether it functions at an acute infectious stage or chronic infectious stage. Some researchers hypothesize that TLR2 plays a protective role during Mtb chronic infection while it does not affect Mtb acute infection [89, 91, 92]. In contrast, Tjärnlund et al. demonstrated that TLR2 has a function in Mtb acute infection (at 3 weeks post infection, wpi) but not in Mtb chronic infection (at 8 wpi) [27]. Interestingly, other studies found no significant differences between TLR2 defective mice or wild type mice upon low-dose Mtb infection, in both acute or chronic infection [88, 93, 94]. The reasons for these different results may be because (1) different Mtb strains were used. Most researchers used the Mtb H37Rv

strain, while some studies utilized the Mtb Kurono strain or the Mtb Erdman strain. (2) They application of different infection methods. Aerosol challenging is the most extensively used method, but some studies also use intranasal (i.n.), intravenous (i.v.), or intratracheal infection methods (i.t.). (3) Differences in the definition of acute or chronic infection. For example, how long is an infection considered a chronic infection? In some studies, 8 weeks are considered as a chronic infection, while other studies 21 weeks is taken as a threshold. In summary the lack of standardization in mice studies has given rise to many uncertainties as to the function of TLR2 in defense against tuberculosis.

3.4 Macrophage-mycobacterium interactions mediated by TLR2

Macrophages are not only the primer cells to recognize the invasion of mycobacteria, but are also the main cellular components of granulomas [95]. TLR2 plays an essential role in mediating the interaction of macrophages and mycobacteria. At the early infection stage, TLR2 enhances the entrance of Mtb bacteria into macrophages by binding PE_PGR33, a mycobacterial protein from the Mtb [96]. The binding of TLR2 and PE_PGR33 can activate macrophages by inducing the expression of TNF-α and some other pro-inflammatory cytokines (Table 1), while it can also trigger the PI3K pathway that can impair the macrophage antimicrobial responses [96]. In addition to promoting inflammatory responses, TLR2 also plays a role in promoting apoptosis of macrophages [97], which is an important defense mechanism of the host against intracellular pathogens. For example, Sánchez et al. has reported that the apoptosis triggered by Mtb infection is depending on the TLR2 signaling pathway [98]. In addition, it has been demonstrated that the apoptosis induced by ESAT-6 is a TLR2-depentent event [99]. ESAT-6, an abundantly secreted protein of Mtb is an important virulence factor. Furthermore, TLR2-dependent microRNA-155 (miR-155) expression is required to elicit macrophage apoptosis by *Mycobacterium bovis BCG* [100]. The antimicrobial activity of macrophages is an essential function of the host to combat invading mycobacteria and is mediated by TLR2 [101]. In human macrophages, the stimulation of TLR2 by mycobacteria results in the upregulation of Cyp27B1 and VDR, which have a function in the induction of transcription of antimicrobial factors, like the antimicrobial peptide cathelicidin [102, 103]. To be noted, mouse macrophages and human macrophages utilize different mechanisms to kill intracellular Mtb through TLR2 activation [28]. TLR2 activation leading to killing of intracellular bacilli is an iNOS-dependent process in mouse macrophages, whereas human macrophages do not depend on it [27]. Thus, other animal models are needed to confirm the

TLR2-mediated mechanisms of triggering macrophage antimicrobial activity. There is only one *in vitro* study describing how mycobacteria can directly control macrophage migration by rearranging the cytoskeleton via activation of TLR2 [104]. Konowich et al. have demonstrated by using various chimeric mice that TLR2 signaling in hematopoietic cells plays a role in controlling bacterial burden and granuloma integrity, while TLR2 signaling in non-hematopoietic cells may play a role in promoting granulomatous inflammation and bacterial dissemination [92]. Furthermore, Carlos et al. found that $TLR2^{-/-}$ mice displayed increased bacterial burden, diminished myeloid cell recruitment, and defective granuloma formation [90]. Interestingly, the adoptive transfer of TLR2 positive mast cells into these $TLR2^{-/-}$ mice reversed the phenotype [90]. In conclusion, TLR2 participates in mediating macrophage-mycobacteria interactions in many ways during phagocytosis, apoptosis, antimicrobial activity, cell recruitment, and granuloma formation. But, the mechanisms underlying these function of TLR2 are still not clear and need to be further studied.

3.5 Neutrophil-mycobacterium interactions mediated by TLR2

In addition to macrophages, neutrophils are innate immune cells that have an important function in defense against mycobacterial infection. A large number of neutrophils can be detected in TB lesions and in the sputum of TB patients, which indicates that neutrophils play a crucial role during Mtb infection [105, 106]. There is consensus that neutrophils are activated upon mycobacterial infection via TLR2-mediated recognition of LAM on the surface of bacteria (Table 1) [107]. However, the reports on the function of TLR2 in regulation of the recruitment of neutrophils during mycobacterial infection are contradictory. In $TLR2^{-/-}$ mutant mice, the bacterial burden after Mtb infection was increased compared to the wild type, and this was accompanied by increased neutrophil influx in the lungs and tissue damage [108]. Conversely, after alveolar epithelial cells were infected by *Mycobacterium bovis BCG in vitro*, the recruitment of neutrophils was significantly reduced by blocking TLR2 [109]. Moreover, injection of non-mannose-capped lipoarabinomannan (AraLAM), which is a TLR-ligand from *Mycobacterium smegmatis*, led to a stronger reduction of neutrophils influx in the pulmonary compartment in $TLR2^{-/-}$ mice than compared to WT mice [110]. These results demonstrate that it is important to study, the function of TLR2 in neutrophils migration in further detail.

3.6 Therapeutic targeting of TLR2 signaling in mycobacterial infection disease

TLR2, as one of the most important representatives of PRRs, can recognize many mycobacterial components which are known as PAMPs. Some of these TLR2 ligands constitute the main

protein component of TB vaccines or adjuvants [96]. For example, the ESAT-6 and PPE18 proteins (Rv1196) are important components of the M72/AS01 and H56/IC31 vaccine candidates [96]. In addition, the mycobacterial MPT38 and PE_PGRS33 proteins have been reported to be TLR2-targeted secreted proteins that are promising pulmonary TB vaccines [96, 111]. At present, *Mycobacterium bovis Bacille Calmette and Guérin* (BCG) remains the only available vaccine for TB, but it is only validated for prevention of TB in children [112, 113]. Furthermore, there is no effective vaccine for infection disease caused by NTM strains.

TLR2 plays a dual role to trigger both pro-inflammatory and anti-inflammatory responses after infection. Thus, modulation of TLR2 signaling has become a popular approach for the design of host-directed therapeutics against infectious diseases. A recent review has described in detail how TLR2 could be used as a therapeutic target to cure bacterial infections [114]. TLR2 ligands from mycobacteria constitute a large group of natural TLR2- agonists and TLR2- antagonists which we summarize in Table 1. These TLR2 agonists or antagonists not only can be used to study the function of TLR2 in infectious diseases, but also provide new possibilities as therapeutic that target TLR2 signaling to treat hyper-inflammation and auto-inflammatory diseases. For example, recombinant PPE18 protein (rPPE18), which is a TLR2 ligand derived from Mtb, has been demonstrated to be a promising novel therapeutic to control sepsis [115]. Because rPPE18 significantly decreases the secretion of serum pro-inflammatory cytokines and reduces organ damage in mice infected with high doses of *E. coli* bacteria [115].

4. Zebrafish as a model to study the innate immune system

4.1 General advantages of the zebrafish larval model

In the last decades, extensive disease models have been established for using zebrafish larvae to study hematology [116, 117], oncology [118] and other pathogenic processes [119]. Zebrafish models contributed to uncovering pathogenic mechanisms and to the discovery and efficacy screening of innovative drugs [120, 121]. As an animal model, zebrafish possesses various advantages. The zebrafish larvae already have a functional innate immune system within 5 days post-fertilization, when the adaptive immune system is still not functional, providing a great advantage for studying the mechanisms of acute inflammation[122]. Moreover, its optical transparency and small size are the most significant advantages of the zebrafish embryos and larvae, because it provides an ideal *in vivo* system to directly observe cell- cell or cell- microbe interactions [122]. This is very difficult to achieve in other vertebrate

models. In addition, the large number of zebrafish offspring makes it possible for omics studies of large groups of larvae. In this thesis, we make use of these advantages of zebrafish larvae to investigate the role of the innate immune system in inflammation and defense against mycobacteria.

4.2 Confocal real-time imaging as a tool for investigating cell function in zebrafish larvae

Cell migration is an important physiological parameter for many pathological processes, including inflammatory responses, immune defense and metastasis of malignant tumor cells. Single-cell tracking using confocal real-time imaging is one of the most popular methods to analyze cell migration. Transgenic zebrafish larvae with fluorescently labeled cells are highly suited for non-invasive real-time imaging because of their transparency at early developmental stages. To visualize and quantify the trajectories of cell migration, a large number of algorithms and software programs have been developed in the last decades. In this thesis we also have developed new automated methods for cell tracking (chapter 3). Notwithstanding these efforts, for much biological research it is needed to track the cell movements manually. In the discussion chapter of this thesis, we will discuss future research directions that could make such time-consuming steps of cell migration research less of a bottleneck.

Overview of this thesis

TLR2 plays a pivotal role in triggering the innate immune responses in inflammation and infection. This makes TLR2 an attractive therapeutic target for developing cures to many diseases. However, its dual role in inflammation and infection makes it very difficult to use the available results from basic research for the development of clinical trials. In addition, it is still not clear and controversial what is the function of TLR2 in regulating phagocytic cell migration. In this thesis, we used the advantage of the transparent zebrafish larval model to observe the dynamics of cell migration *in vivo* under various conditions. We not only aimed to acquire new insights into the function of Tlr2 in regulating cell migration in inflammation and infection, but also aimed to extend our understanding of the role it thereby plays in host defense against pathogens.

The role of TLR2 in host defense against Mtb is still controversial in reports based on rodent *in vivo* studies. In addition, its function in host innate immunity during infection is still not clear.

Moreover, there is still a lack of research of the systemic transcriptome regulation of TLR downstream signaling in a whole animal model after infection. Therefore, **in Chapter 2**, we study the function of *tlr2* in defense against *Mycobacterium marinum* (Mm) infection in zebrafish by measuring infection phenotypes and corresponding transcriptome responses. We show that infection of a *tlr2* mutant in zebrafish larvae leads to a higher Mm bacterial burden, accompanied with a lower number of granulomas and increased extracellular bacterial growth, compared to wild type siblings. These results suggest that Tlr2 plays a protective role in defense against mycobacteria at early infection stages. To obtain explanations and genetic markers for further studies of the effect of the *tlr2* mutation on infection we performed deep RNA sequencing to study the whole transcriptome profile in our mycobacterial infection model at the systems level. From this RNAseq analysis, we found that the role of Tlr2 in controlling mycobacterial infection can be explained by several mechanisms, like reduction of mycobacterial dissemination by dampening of CXCR3-CXCL11 signaling, and modulation of anti-mycobacterial activity by regulating vitamin D signaling.

In a previous study, Torraca et al. found the CXCR3-CXCL11 axis signaling executes an important function in regulating macrophage recruitment in zebrafish larvae [123]. In chapter 2, we found that the expression of *cxcl11aa* and *cxcl11ac* is significantly decreased in the *tlr2* mutant infected with *M. marinum*. Considering that the expression of many chemokines is controlled by Tlr2, we hypothesized that Tlr2 is a key factor in the control of chemokine expression in order to regulate cell recruitment in innate immunity. To test this hypothesis, **in Chapter 3**, we first investigated the function of Tlr2 and Myd88 in leukocytes migration behavior upon tissue damage by using a zebrafish tail wounding model. In this chapter, live fluorescent imaging was performed to study the effect of the *tlr2* mutation and *myd88* mutation on leukocyte migration upon tail wounding. We observed reduced numbers of recruited neutrophils and macrophages at the wounding area in both *tlr2* mutants and *myd88* mutants, compared to their wild type sibling controls. Extensive mathematical analyses have been performed of the cell migration trajectories in the zebrafish larvae upon wounding. Through these analyses, we demonstrated that both *tlr2* and *myd88* control the migration direction of neutrophils upon wounding. Furthermore, in both the *tlr2* and the *myd88* mutants, macrophages migrated more slowly toward the wound edge.

The migration of leukocytes is important during the infection process for bacterial clearance, containment, dissemination, and granuloma formation at the early mycobacterial infectious

stage [124-127]. However, the role of Tlr2 in modulating leukocyte migration in infection is still not clear. In chapter 3, we show that *tlr2* is involved in regulating leukocyte migration in response to inflammatory signaling. Thus, we hypothesize that *tlr2* could also be involved in the regulation of migratory behavior of macrophages and neutrophils to the sites of mycobacterial infection. To test this hypothesis, in **Chapter 4,** we studied the function of *tlr2* during the infection with two different NTM mycobacterial species with special attention to the responsive cell migration behavior. In this chapter, *M. marinum* Mma20 strain and *M. avium* MAC 101 strain were used to study the function of *tlr2* in infection. *M. marinum* infected zebrafish larvae is a recognized model for tuberculosis infection, whereas *M. avium* was never studied in zebrafish before. Thus, we first developed a zebrafish larval infection model for studying *M. avium* infection. The results show that *M. avium* bacteria can infect zebrafish larvae effectively leading to the formation of granulomas. Moreover, we compared the innate immune response of zebrafish larvae to infection with these two different species of NTM, specifically with regard to the bacterial burden, granuloma-like cluster formation, and transcriptomic gene expression profiles. Subsequently, we utilized this model to study the function of *tlr2* in regulating leukocyte migration using a tail fin infection method.

In the last **Chapter 5,** we summarize the findings from the thesis and discuss the challenges and perspective for further research of TLR signaling by using the zebrafish larval model. In addition, we briefly discuss some unpublished results from ongoing studies into the function of TLR2 in system metabolism.

Table 1 Mycobacterial ligands of TLR2

Species	Ligand (s)	Ligand (s) abbreviation	PRRs	Accessory molecules	Observations	References
M. tuberculosis	***Lipoproteins***					
	19-kDa lipoprotein (Rv3763)	**LpqH**	TLR2/1	CD14	Inhibits MHC- expression and antigen processing; IFN-γ-induced genes is inhibited by prolonged LpqH stimulation	[77-79]
	24-kDa lipoprotein (Rv1270c)	**LprA**	TLR2/1	CD14/CD36	Induces cytokine response and regulate APC function	[79, 128]
	24-kDa lipoprotein (Rv1411c)	**LprG**	TLR2/1; TLR2	CD14	Long-term exposure of LprG inhibits the processing of MHC-II antigen; Short-term exposure of LprG induces the production of TNF-α	[79, 80]
	24-kDa lipoprotein (Rv1016c)	**LpqT**	TLR2	Unknown	Induces TLR2 dependent apoptosis in macrophage and inhibits MHC- expression and antigen processing	[129]
	38-kDa glycolipoprotein	**PhoS1**	TLR2/1, TLR4	Unknown	Activates the ERK1/2 and p38 MAPK signaling, which in turn induce TNF-α and IL-6 expression	[79, 130]
	Lipoylated and glycosylated Mtb lipoprotein (Rv2873)	**MPT83**	TLR2	unknown	MPT83 induced cytokine production was decreased in the TLR2 defective mice	[131]
	Lipoglycans/Glycolipids					
	Lipoarabinomannan	**LAM**	TLR2/1; TLR2	CD14	Mtb LAM induces the production of pro- and anti-inflammatory cytokine to activate neutrophils	[75, 107]
	Arabinosylated lipoarabinomannan	**AraLAM**	TLR2	Unknown	Induces the pro-inflammatory responses	[132]
	Lipomannans	**LM**	TLR2/1; TLR2;	CD40/CD86	Induces TNF-α and NO secretion to activate macrophages	[133, 134]
	phosphatidylinositol dimannoside	**PIM2/6**	TLR2	Unknown	Induces the expression of TNF-α to activate macrophages	[75, 135]
	Trehalose dimycolate	**TDM**	TLR2	CD14/MARCO	Induces NF-κB signaling	[136]

Table 1 Continued. Mycobacterial ligands of TLR2

Species	Ligand (s)	Ligand (s) abbreviation	PRRs	Accessory molecules	Observations	References
M. tuberculosis	***Others***					
	Heat shock protein 70	**HSP70**	TLR2	Unknown	Inhibits the secretion of IL-6 in TLR2-deficient macrophages	[137]
	55-kDa flavin containing monooxygenase (Rv3083)	**MymA**	TLR2	CD40/CD80/ CD86/HLA-DR	Upregulates the expression of TLR2 and its co-simulatory molecules. Activates macrophage by inducing TNF- α and IL-12.	[138]
	PE_PGRS proteins (Rv1818c)	**PE_PGRS33**	TLR2	CD14	Contributes to Mtb enter macrophage by interacting with TLR2	[139, 140]
	Secreted antigenic targets of 6-kDa (ESAT-6) family proteins (Rv1198)	**EsxL**	TLR2	Unknown	Induces TNF-α and IL-6 through TLR2 dependent NF-κB and MAPK signaling	[141]
	PE/PPE protein (Rv1196)	**PPE18**	TLR2	Unknown	Interacts with TLR2 to produce IL-10 and SOCS3 to in turn inhibit TLR2 signaling	[142, 143]
	PE/PPE protein (Rv1789)	**PPE26**	TLR2	CD80/CD86	Activates macrophage by inducing pro-inflammatory cytokine TNF-α, IL-6 and IL-12	[144]
	PE/PPE protein (Rv1808)	**PPE32**	TLR2	Unknown	Induces both anti-inflammatory cytokine IL-10 and pro-inflammatory cytokines TNF-α and IL-6	[145]
	PE/PPE protein (Rv3425)	**PPE57**	TLR2	CD40/CD80/ CD86	Activates macrophage by inducing pro-inflammatory cytokine TNF-α, IL-6 and IL-12	[146]
	Leucine-responsive regulatory protein	**Lrp**	TLR2	Unknown	Inhibit LPS-induced pro-inflammatory cytokine production IL-12 and TNF-α	[147]
M. avium	Glycopeptidolipids	**GPLs**	TLR2, TLR4	Unknown	Promotes the activation of macrophages depended on a TLR2 and MyD88 manner. TLR2 senses GPLs needs its specific acetylation and methylation;	[148-150]
M. abscessus	TLR2-enriched fraction	**TLR2eF**	TLR2	Unknown	TLR2eF mildly protects Mab infected ΔF508 mice and its littermates	[151]
	Glycopeptidolipids	**GPLs**	TLR2	Unknown	The switch of Mab from the smooth to the rough morphotype depends on the present of bacterial surface GLPs.	[152]
M. smegmatis	Phosphoinositol-capped LAM	**PILAM**	TLR2/ TLR1	Unknown	High affinity binding to TLR2 and strong pro-inflammatory response	[133, 153]
	Arabinosylated lipoarabinomannan	**AraLAM**	TLR2	CD14?	The lung inflammation induced by AraLAM is diminished in TLR2 deficiency mice	[110]
	Dimannoside hosphatidyl-myo-inositol mannosides	**PIM2/6**	TLR2	Unknown	Induces the expression of TNF to activate primary macrophages	[135]

Reference

1. Riera Romo M, Perez-Martinez D, Castillo Ferrer C. Innate immunity in vertebrates: an overview. Immunology. 2016;148(2):125-39. Epub 2016/02/16. doi: 10.1111/imm.12597. PubMed PMID: 26878338; PubMed Central PMCID: PMCPMC4863567.

2. Hato T, Dagher PC. How the Innate Immune System Senses Trouble and Causes Trouble. Clin J Am Soc Nephrol. 2015;10(8):1459-69. Epub 2014/11/22. doi: 10.2215/CJN.04680514. PubMed PMID: 25414319; PubMed Central PMCID: PMCPMC4527020.

3. Kumar H, Kawai T, Akira S. Pathogen recognition by the innate immune system. Int Rev Immunol. 2011;30(1):16-34. Epub 2011/01/18. doi: 10.3109/08830185.2010.529976. PubMed PMID: 21235323.

4. Hara T, Nakashima Y, Sakai Y, Nishio H, Motomura Y, Yamasaki S. Kawasaki disease: a matter of innate immunity. Clin Exp Immunol. 2016;186(2):134-43. Epub 2016/06/28. doi: 10.1111/cei.12832. PubMed PMID: 27342882; PubMed Central PMCID: PMCPMC5054572.

5. Hashimoto C, Hudson KL, Anderson KV. The Toll gene of Drosophila, required for dorsal-ventral embryonic polarity, appears to encode a transmembrane protein. Cell. 1988;52(2):269-79. Epub 1988/01/29. doi: 10.1016/0092-8674(88)90516-8. PubMed PMID: 2449285.

6. Medzhitov R, Preston-Hurlburt P, Janeway CA, Jr. A human homologue of the Drosophila Toll protein signals activation of adaptive immunity. Nature. 1997;388(6640):394-7. Epub 1997/07/24. doi: 10.1038/41131. PubMed PMID: 9237759.

7. Simpson ME, Petri WA, Jr. TLR2 as a Therapeutic Target in Bacterial Infection. Trends Mol Med. 2020;26(8):715-7. Epub 2020/06/22. doi: 10.1016/j.molmed.2020.05.006. PubMed PMID: 32563557; PubMed Central PMCID: PMCPMC7845793.

8. Gopalakrishnan A, Salgame P. Toll-like receptor 2 in host defense against Mycobacterium tuberculosis: to be or not to be-that is the question. Curr Opin Immunol. 2016;42:76-82. Epub 2016/10/30. doi: 10.1016/j.coi.2016.06.003. PubMed PMID: 27326654; PubMed Central PMCID: PMCPMC5086274.

9. Oliveira-Nascimento L, Massari P, Wetzler LM. The Role of TLR2 in Infection and Immunity. Front Immunol. 2012;3:79. Epub 2012/05/09. doi: 10.3389/fimmu.2012.00079. PubMed PMID: 22566960; PubMed Central PMCID: PMCPMC3342043.

10. Moles A, Murphy L, Wilson CL, Chakraborty JB, Fox C, Park EJ, et al. A TLR2/S100A9/CXCL-2 signaling network is necessary for neutrophil recruitment in acute and chronic liver injury in the mouse. J Hepatol. 2014;60(4):782-91. Epub 2013/12/18. doi: 10.1016/j.jhep.2013.12.005. PubMed PMID: 24333183; PubMed Central PMCID: PMCPMC3960359.

11. Chen L, DiPietro LA. Toll-Like Receptor Function in Acute Wounds. Adv Wound Care (New Rochelle). 2017;6(10):344-55. Epub 2017/10/25. doi: 10.1089/wound.2017.0734. PubMed PMID: 29062591; PubMed Central PMCID: PMCPMC5649397.

12. Di Lorenzo A, Bolli E, Tarone L, Cavallo F, Conti L. Toll-Like Receptor 2 at the Crossroad between Cancer Cells, the Immune System, and the Microbiota. Int J Mol Sci. 2020;21(24). Epub 2020/12/17. doi: 10.3390/ijms21249418. PubMed PMID: 33321934; PubMed Central PMCID: PMCPMC7763461.

13. Rada I, Deldicque L, Francaux M, Zbinden-Foncea H. Toll like receptor expression induced by exercise in obesity and metabolic syndrome: A systematic review. Exerc Immunol Rev. 2018;24:60-71. Epub 2018/02/21. PubMed PMID: 29461969.

14. Mahfoud S, Petrova TV. The double life of TLR2. Sci Signal. 2021;14(666). doi: ARTN eabf4701

10.1126/scisignal.abf4701. PubMed PMID: WOS:000609622000004.

15. Li Y, Li Y, Cao X, Jin X, Jin T. Pattern recognition receptors in zebrafish provide functional and evolutionary insight into innate immune signaling pathways. Cell Mol Immunol. 2017;14(1):80-9. Epub 2016/10/11. doi: 10.1038/cmi.2016.50. PubMed PMID: 27721456; PubMed Central PMCID: PMCPMC5214946.

16. Takeuchi O, Akira S. Pattern recognition receptors and inflammation. Cell. 2010;140(6):805-20. Epub 2010/03/23. doi: 10.1016/j.cell.2010.01.022. PubMed PMID: 20303872.

17. Lemaitre B, Nicolas E, Michaut L, Reichhart JM, Hoffmann JA. The dorsoventral regulatory gene cassette spatzle/Toll/cactus controls the potent antifungal response in Drosophila adults. Cell. 1996;86(6):973-83. Epub 1996/09/20. doi: 10.1016/s0092-8674(00)80172-5. PubMed PMID: 8808632.

18. Sahoo BR. Structure of fish Toll-like receptors (TLR) and NOD-like receptors (NLR). Int J Biol Macromol. 2020;161:1602-17. Epub 2020/08/07. doi: 10.1016/j.ijbiomac.2020.07.293. PubMed PMID: 32755705; PubMed Central PMCID: PMCPMC7396143.

19. Imler JL, Hoffmann JA. Toll receptors in Drosophila: a family of molecules regulating development and immunity. Curr Top Microbiol Immunol. 2002;270:63-79. Epub 2002/12/07. doi: 10.1007/978-3-642-59430-4_4. PubMed PMID: 12467244.

20. Satake H, Sekiguchi T. Toll-like receptors of deuterostome invertebrates. Front Immunol. 2012;3:34. Epub 2012/05/09. doi: 10.3389/fimmu.2012.00034. PubMed PMID: 22566918; PubMed Central PMCID: PMCPMC3342246.

21. Meijer AH, Gabby Krens SF, Medina Rodriguez IA, He S, Bitter W, Ewa Snaar-Jagalska B, et al. Expression analysis of the Toll-like receptor and TIR domain adaptor families of zebrafish. Mol Immunol. 2004;40(11):773-83. Epub 2003/12/23. doi: 10.1016/j.molimm.2003.10.003. PubMed PMID: 14687934.

22. Blasius AL, Beutler B. Intracellular toll-like receptors. Immunity. 2010;32(3):305-15. Epub 2010/03/30. doi: 10.1016/j.immuni.2010.03.012. PubMed PMID: 20346772.

23. Pifer R, Benson A, Sturge CR, Yarovinsky F. UNC93B1 is essential for TLR11 activation and IL-12-dependent host resistance to Toxoplasma gondii. J Biol Chem. 2011;286(5):3307-14. Epub 2010/11/26. doi: 10.1074/jbc.M110.171025. PubMed PMID: 21097503; PubMed Central PMCID: PMCPMC3030336.

24. Rock FL, Hardiman G, Timans JC, Kastelein RA, Bazan JF. A family of human receptors structurally related to Drosophila Toll. Proc Natl Acad Sci U S A. 1998;95(2):588-93. Epub 1998/01/22. doi: 10.1073/pnas.95.2.588. PubMed PMID: 9435236; PubMed Central PMCID: PMCPMC18464.

25. Basto AP, Leitao A. Targeting TLR2 for vaccine development. J Immunol Res. 2014;2014:619410. Epub 2014/07/25. doi: 10.1155/2014/619410. PubMed PMID: 25057505; PubMed Central PMCID: PMCPMC4098989.

26. Eriksson EM, Jackson DC. Recent advances with TLR2-targeting lipopeptide-based vaccines. Curr Protein Pept Sci. 2007;8(4):412-7. Epub 2007/08/19. doi: 10.2174/138920307781369436. PubMed PMID: 17696872.

27. Tjarnlund A, Guirado E, Julian E, Cardona PJ, Fernandez C. Determinant role for Toll-like receptor signalling in acute mycobacterial infection in the respiratory tract. Microbes Infect. 2006;8(7):1790-800. Epub 2006/07/04. doi: 10.1016/j.micinf.2006.02.017. PubMed PMID: 16815067.

28. Thoma-Uszynski S, Stenger S, Takeuchi O, Ochoa MT, Engele M, Sieling PA, et al. Induction of direct antimicrobial activity through mammalian toll-like receptors. Science. 2001;291(5508):1544-7. Epub 2001/02/27. doi: 10.1126/science.291.5508.1544. PubMed PMID: 11222859.

29. Santos-Sierra S, Deshmukh SD, Kalnitski J, Kuenzi P, Wymann MP, Golenbock DT, et al. Mal connects TLR2 to PI3Kinase activation and phagocyte polarization. EMBO J. 2009;28(14):2018-27. Epub 2009/07/04. doi: 10.1038/emboj.2009.158. PubMed PMID: 19574958; PubMed Central PMCID: PMCPMC2718282.

30. O'Neill LA, Bowie AG. The family of five: TIR-domain-containing adaptors in Toll-like receptor signalling. Nat Rev Immunol. 2007;7(5):353-64. Epub 2007/04/26. doi: 10.1038/nri2079. PubMed PMID: 17457343.

31. McClure R, Massari P. TLR-Dependent Human Mucosal Epithelial Cell Responses to Microbial Pathogens. Front Immunol. 2014;5:386. Epub 2014/08/28. doi: 10.3389/fimmu.2014.00386. PubMed PMID: 25161655; PubMed Central PMCID: PMCPMC4129373.

32. Kawai T, Akira S. Toll-like receptors and their crosstalk with other innate receptors in infection and immunity. Immunity. 2011;34(5):637-50. Epub 2011/05/28. doi: 10.1016/j.immuni.2011.05.006. PubMed PMID: 21616434.

33. Kang SS, Sim JR, Yun CH, Han SH. Lipoteichoic acids as a major virulence factor causing inflammatory responses via Toll-like receptor 2. Arch Pharm Res. 2016;39(11):1519-29. Epub 2016/08/09. doi: 10.1007/s12272-016-0804-y. PubMed PMID: 27498542.

34. Akira S, Uematsu S, Takeuchi O. Pathogen recognition and innate immunity. Cell. 2006;124(4):783-801. Epub 2006/02/25. doi: 10.1016/j.cell.2006.02.015. PubMed PMID: 16497588.

35. Mukherjee S, Karmakar S, Babu SP. TLR2 and TLR4 mediated host immune responses in major infectious diseases: a review. Braz J Infect Dis. 2016;20(2):193-204. Epub 2016/01/19. doi: 10.1016/j.bjid.2015.10.011. PubMed PMID: 26775799.

36. Jimenez-Dalmaroni MJ, Xiao N, Corper AL, Verdino P, Ainge GD, Larsen DS, et al. Soluble CD36 ectodomain binds negatively charged diacylglycerol ligands and acts as a co-receptor for TLR2. PLoS One. 2009;4(10):e7411. Epub 2009/10/23. doi: 10.1371/journal.pone.0007411. PubMed PMID: 19847289; PubMed Central PMCID: PMCPMC2760212.

37. Uematsu S, Akira S. Toll-Like receptors (TLRs) and their ligands. Handb Exp Pharmacol. 2008;(183):1-20. Epub 2007/12/12. doi: 10.1007/978-3-540-72167-3_1. PubMed PMID: 18071652.

38. Gong T, Liu L, Jiang W, Zhou R. DAMP-sensing receptors in sterile inflammation and inflammatory diseases. Nat Rev Immunol. 2020;20(2):95-112. Epub 2019/09/29. doi: 10.1038/s41577-019-0215-7. PubMed PMID: 31558839.

39. Yu L, Wang L, Chen S. Endogenous toll-like receptor ligands and their biological significance. J Cell Mol Med. 2010;14(11):2592-603. Epub 2010/07/16. doi: 10.1111/j.1582-4934.2010.01127.x. PubMed PMID: 20629986; PubMed Central PMCID: PMCPMC4373479.

40. Soehnlein O, Lindbom L. Phagocyte partnership during the onset and resolution of inflammation. Nat Rev Immunol. 2010;10(6):427-39. Epub 2010/05/26. doi: 10.1038/nri2779. PubMed PMID: 20498669.

41. Bianchi ME. HMGB1 loves company. J Leukoc Biol. 2009;86(3):573-6. Epub 2009/05/06. doi: 10.1189/jlb.1008585. PubMed PMID: 19414536.

42. Brightbill HD, Libraty DH, Krutzik SR, Yang RB, Belisle JT, Bleharski JR, et al. Host defense mechanisms triggered by microbial lipoproteins through toll-like receptors. Science. 1999;285(5428):732-6. Epub 1999/07/31. doi: 10.1126/science.285.5428.732. PubMed PMID: 10426995.

43. Mogensen TH. Pathogen recognition and inflammatory signaling in innate immune defenses. Clin Microbiol Rev. 2009;22(2):240-73, Table of Contents. Epub 2009/04/16. doi: 10.1128/CMR.00046-08. PubMed PMID: 19366914; PubMed Central PMCID: PMCPMC2668232.

44. Hossain MM, Norazmi MN. Pattern recognition receptors and cytokines in Mycobacterium tuberculosis infection--the double-edged sword? Biomed Res Int. 2013;2013:179174. Epub 2013/12/19. doi: 10.1155/2013/179174. PubMed PMID: 24350246; PubMed Central PMCID: PMCPMC3844256.

45. Cook DN, Pisetsky DS, Schwartz DA. Toll-like receptors in the pathogenesis of human disease. Nat Immunol. 2004;5(10):975-9. Epub 2004/09/30. doi: 10.1038/ni1116. PubMed PMID: 15454920.

46. Pradhan VD, Das S, Surve P, Ghosh K. Toll-like receptors in autoimmunity with special reference to systemic lupus erythematosus. Indian J Hum Genet. 2012;18(2):155-60. Epub 2012/11/20. doi: 10.4103/0971-6866.100750. PubMed PMID: 23162288; PubMed Central PMCID: PMCPMC3491286.

47. Netea MG, Van der Meer JW, Kullberg BJ. Toll-like receptors as an escape mechanism from the host defense. Trends Microbiol. 2004;12(11):484-8. Epub 2004/10/19. doi: 10.1016/j.tim.2004.09.004. PubMed PMID: 15488388.

48. Dasu MR, Thangappan RK, Bourgette A, DiPietro LA, Isseroff R, Jialal I. TLR2 expression and signaling-dependent inflammation impair wound healing in diabetic mice. Lab Invest. 2010;90(11):1628-36. Epub 2010/08/25. doi: 10.1038/labinvest.2010.158. PubMed PMID: 20733560.

49. Caplan IF, Maguire-Zeiss KA. Toll-Like Receptor 2 Signaling and Current Approaches for Therapeutic Modulation in Synucleinopathies. Front Pharmacol. 2018;9:417. Epub 2018/05/22. doi: 10.3389/fphar.2018.00417. PubMed PMID: 29780321; PubMed Central PMCID: PMCPMC5945810.

50. Landen NX, Li D, Stahle M. Transition from inflammation to proliferation: a critical step during wound healing. Cell Mol Life Sci. 2016;73(20):3861-85. Epub 2016/05/18. doi: 10.1007/s00018-016-2268-0. PubMed PMID: 27180275; PubMed Central PMCID: PMCPMC5021733.

51. Kondo T, Kawai T, Akira S. Dissecting negative regulation of Toll-like receptor signaling. Trends Immunol. 2012;33(9):449-58. Epub 2012/06/23. doi: 10.1016/j.it.2012.05.002. PubMed PMID: 22721918.

52. Yang L, Seki E. Toll-like receptors in liver fibrosis: cellular crosstalk and mechanisms. Front Physiol. 2012;3:138. Epub 2012/06/05. doi: 10.3389/fphys.2012.00138. PubMed PMID: 22661952; PubMed Central PMCID: PMCPMC3357552.

53. LeBouder E, Rey-Nores JE, Rushmere NK, Grigorov M, Lawn SD, Affolter M, et al. Soluble forms of Toll-like receptor (TLR)2 capable of modulating TLR2 signaling are present in human plasma and breast milk. J

Immunol. 2003;171(12):6680-9. Epub 2003/12/10. doi: 10.4049/jimmunol.171.12.6680. PubMed PMID: 14662871.

54. Iwami KI, Matsuguchi T, Masuda A, Kikuchi T, Musikacharoen T, Yoshikai Y. Cutting edge: naturally occurring soluble form of mouse Toll-like receptor 4 inhibits lipopolysaccharide signaling. J Immunol. 2000;165(12):6682-6. Epub 2000/12/20. doi: 10.4049/jimmunol.165.12.6682. PubMed PMID: 11120784.

55. Jeong E, Lee JY. Intrinsic and extrinsic regulation of innate immune receptors. Yonsei Med J. 2011;52(3):379-92. Epub 2011/04/14. doi: 10.3349/ymj.2011.52.3.429

10.3349/ymj.2011.52.3.379. PubMed PMID: 21488180; PubMed Central PMCID: PMCPMC3101043.

56. Trengove MC, Ward AC. SOCS proteins in development and disease. Am J Clin Exp Immunol. 2013;2(1):1-29. Epub 2013/07/26. PubMed PMID: 23885323; PubMed Central PMCID: PMCPMC3714205.

57. Ahmed S, Maratha A, Butt AQ, Shevlin E, Miggin SM. TRIF-mediated TLR3 and TLR4 signaling is negatively regulated by ADAM15. J Immunol. 2013;190(5):2217-28. Epub 2013/02/01. doi: 10.4049/jimmunol.1201630. PubMed PMID: 23365087.

58. Lee HJ, Chung KC. PINK1 positively regulates IL-1beta-mediated signaling through Tollip and IRAK1 modulation. J Neuroinflammation. 2012;9:271. Epub 2012/12/19. doi: 10.1186/1742-2094-9-271. PubMed PMID: 23244239; PubMed Central PMCID: PMCPMC3533909.

59. Zhang G, Ghosh S. Negative regulation of toll-like receptor-mediated signaling by Tollip. J Biol Chem. 2002;277(9):7059-65. Epub 2001/12/26. doi: 10.1074/jbc.M109537200. PubMed PMID: 11751856.

60. Kobayashi K, Hernandez LD, Galan JE, Janeway CA, Jr., Medzhitov R, Flavell RA. IRAK-M is a negative regulator of Toll-like receptor signaling. Cell. 2002;110(2):191-202. Epub 2002/08/02. doi: 10.1016/s0092-8674(02)00827-9. PubMed PMID: 12150927.

61. Shio MT, Hassani K, Isnard A, Ralph B, Contreras I, Gomez MA, et al. Host cell signalling and leishmania mechanisms of evasion. J Trop Med. 2012;2012:819512. Epub 2011/12/02. doi: 10.1155/2012/819512. PubMed PMID: 22131998; PubMed Central PMCID: PMCPMC3216306.

62. Kim EJ, Lee SM, Suk K, Lee WH. CD300a and CD300f differentially regulate the MyD88 and TRIF-mediated TLR signalling pathways through activation of SHP-1 and/or SHP-2 in human monocytic cell lines. Immunology. 2012;135(3):226-35. Epub 2011/11/03. doi: 10.1111/j.1365-2567.2011.03528.x. PubMed PMID: 22043923; PubMed Central PMCID: PMCPMC3311045.

63. Liu Y, Yin H, Zhao M, Lu Q. TLR2 and TLR4 in autoimmune diseases: a comprehensive review. Clin Rev Allergy Immunol. 2014;47(2):136-47. Epub 2013/12/20. doi: 10.1007/s12016-013-8402-y. PubMed PMID: 24352680.

64. Skaug B, Chen J, Du F, He J, Ma A, Chen ZJ. Direct, noncatalytic mechanism of IKK inhibition by A20. Mol Cell. 2011;44(4):559-71. Epub 2011/11/22. doi: 10.1016/j.molcel.2011.09.015. PubMed PMID: 22099304; PubMed Central PMCID: PMCPMC3237303.

65. Whitmore MM, Iparraguirre A, Kubelka L, Weninger W, Hai T, Williams BR. Negative regulation of TLR-signaling pathways by activating transcription factor-3. J Immunol. 2007;179(6):3622-30. Epub 2007/09/06. doi: 10.4049/jimmunol.179.6.3622. PubMed PMID: 17785797.

66. Kuwata H, Matsumoto M, Atarashi K, Morishita H, Hirotani T, Koga R, et al. IkappaBNS inhibits induction of a subset of Toll-like receptor-dependent genes and limits inflammation. Immunity. 2006;24(1):41-51. Epub 2006/01/18. doi: 10.1016/j.immuni.2005.11.004. PubMed PMID: 16413922.

67. Carmody RJ, Ruan Q, Palmer S, Hilliard B, Chen YH. Negative regulation of toll-like receptor signaling by NF-kappaB p50 ubiquitination blockade. Science. 2007;317(5838):675-8. Epub 2007/08/04. doi: 10.1126/science.1142953. PubMed PMID: 17673665.

68. Koch BEV, Yang S, Lamers G, Stougaard J, Spaink HP. Intestinal microbiome adjusts the innate immune setpoint during colonization through negative regulation of MyD88. Nat Commun. 2018;9(1):4099. Epub 2018/10/07. doi: 10.1038/s41467-018-06658-4. PubMed PMID: 30291253; PubMed Central PMCID: PMCPMC6173721.

69. Harding E. WHO global progress report on tuberculosis elimination (vol 8, pg 19, 2020). Lancet Resp Med. 2020;8(1):E3-E. doi: 10.1016/S2213-2600(19)30421-7. PubMed PMID: WOS:000503397100003.

70. Chakaya J, Khan M, Ntoumi F, Aklillu E, Fatima R, Mwaba P, et al. Global Tuberculosis Report 2020 - Reflections on the Global TB burden, treatment and prevention efforts. Int J Infect Dis. 2021. Epub 2021/03/16. doi: 10.1016/j.ijid.2021.02.107. PubMed PMID: 33716195.

71. Hoefsloot W, van Ingen J, Andrejak C, Angeby K, Bauriaud R, Bemer P, et al. The geographic diversity of nontuberculous mycobacteria isolated from pulmonary samples: an NTM-NET collaborative study. Eur Respir J. 2013;42(6):1604-13. Epub 2013/04/20. doi: 10.1183/09031936.00149212. PubMed PMID: 23598956.

72. Prevots DR, Marras TK. Epidemiology of human pulmonary infection with nontuberculous mycobacteria: a review. Clin Chest Med. 2015;36(1):13-34. Epub 2015/02/14. doi: 10.1016/j.ccm.2014.10.002. PubMed PMID: 25676516; PubMed Central PMCID: PMCPMC4332564.

73. Saxena S, Spaink HP, Forn-Cuni G. Drug Resistance in Nontuberculous Mycobacteria: Mechanisms and Models. Biology (Basel). 2021;10(2). Epub 2021/02/13. doi: 10.3390/biology10020096. PubMed PMID: 33573039; PubMed Central PMCID: PMCPMC7911849.

74. Kilinc G, Saris A, Ottenhoff THM, Haks MC. Host-directed therapy to combat mycobacterial infections. Immunol Rev. 2021;301(1):62-83. Epub 2021/02/11. doi: 10.1111/imr.12951. PubMed PMID: 33565103; PubMed Central PMCID: PMCPMC8248113.

75. Harding CV, Boom WH. Regulation of antigen presentation by Mycobacterium tuberculosis: a role for Toll-like receptors. Nat Rev Microbiol. 2010;8(4):296-307. Epub 2010/03/18. doi: 10.1038/nrmicro2321. PubMed PMID: 20234378; PubMed Central PMCID: PMCPMC3037727.

76. Saraav I, Singh S, Sharma S. Outcome of Mycobacterium tuberculosis and Toll-like receptor interaction: immune response or immune evasion? Immunol Cell Biol. 2014;92(9):741-6. Epub 2014/07/02. doi: 10.1038/icb.2014.52. PubMed PMID: 24983458.

77. Pennini ME, Pai RK, Schultz DC, Boom WH, Harding CV. Mycobacterium tuberculosis 19-kDa lipoprotein inhibits IFN-gamma-induced chromatin remodeling of MHC2TA by TLR2 and MAPK signaling. J Immunol. 2006;176(7):4323-30. Epub 2006/03/21. doi: 10.4049/jimmunol.176.7.4323. PubMed PMID: 16547269.

78. Pai RK, Convery M, Hamilton TA, Boom WH, Harding CV. Inhibition of IFN-gamma-induced class II transactivator expression by a 19-kDa lipoprotein from Mycobacterium tuberculosis: a potential mechanism for

immune evasion. J Immunol. 2003;171(1):175-84. Epub 2003/06/21. doi: 10.4049/jimmunol.171.1.175. PubMed PMID: 12816996.

79. Drage MG, Pecora ND, Hise AG, Febbraio M, Silverstein RL, Golenbock DT, et al. TLR2 and its co-receptors determine responses of macrophages and dendritic cells to lipoproteins of Mycobacterium tuberculosis. Cell Immunol. 2009;258(1):29-37. Epub 2009/04/14. doi: 10.1016/j.cellimm.2009.03.008. PubMed PMID: 19362712; PubMed Central PMCID: PMCPMC2730726.

80. Gehring AJ, Dobos KM, Belisle JT, Harding CV, Boom WH. Mycobacterium tuberculosis LprG (Rv1411c): a novel TLR-2 ligand that inhibits human macrophage class II MHC antigen processing. J Immunol. 2004;173(4):2660-8. Epub 2004/08/06. doi: 10.4049/jimmunol.173.4.2660. PubMed PMID: 15294983.

81. Texereau J, Chiche JD, Taylor W, Choukroun G, Comba B, Mira JP. The importance of Toll-like receptor 2 polymorphisms in severe infections. Clin Infect Dis. 2005;41 Suppl 7:S408-15. Epub 2005/10/21. doi: 10.1086/431990. PubMed PMID: 16237639.

82. Ogus AC, Yoldas B, Ozdemir T, Uguz A, Olcen S, Keser I, et al. The Arg753GLn polymorphism of the human toll-like receptor 2 gene in tuberculosis disease. Eur Respir J. 2004;23(2):219-23. Epub 2004/02/26. doi: 10.1183/09031936.03.00061703. PubMed PMID: 14979495.

83. Pattabiraman G, Panchal R, Medvedev AE. The R753Q polymorphism in Toll-like receptor 2 (TLR2) attenuates innate immune responses to mycobacteria and impairs MyD88 adapter recruitment to TLR2. J Biol Chem. 2017;292(25):10685-95. Epub 2017/04/27. doi: 10.1074/jbc.M117.784470. PubMed PMID: 28442574; PubMed Central PMCID: PMCPMC5481573.

84. Sanchez D, Lefebvre C, Rioux J, Garcia LF, Barrera LF. Evaluation of Toll-like receptor and adaptor molecule polymorphisms for susceptibility to tuberculosis in a Colombian population. Int J Immunogenet. 2012;39(3):216-23. Epub 2012/01/10. doi: 10.1111/j.1744-313X.2011.01077.x. PubMed PMID: 22221660.

85. Jafari M, Nasiri MR, Sanaei R, Anoosheh S, Farnia P, Sepanjnia A, et al. The NRAMP1, VDR, TNF-alpha, ICAM1, TLR2 and TLR4 gene polymorphisms in Iranian patients with pulmonary tuberculosis: A case-control study. Infect Genet Evol. 2016;39:92-8. Epub 2016/01/18. doi: 10.1016/j.meegid.2016.01.013. PubMed PMID: 26774366.

86. Yim JJ, Kim HJ, Kwon OJ, Koh WJ. Association between microsatellite polymorphisms in intron II of the human Toll-like receptor 2 gene and nontuberculous mycobacterial lung disease in a Korean population. Hum Immunol. 2008;69(9):572-6. Epub 2008/07/08. doi: 10.1016/j.humimm.2008.06.003. PubMed PMID: 18602432.

87. Feng CG, Scanga CA, Collazo-Custodio CM, Cheever AW, Hieny S, Caspar P, et al. Mice lacking myeloid differentiation factor 88 display profound defects in host resistance and immune responses to Mycobacterium avium infection not exhibited by Toll-like receptor 2 (TLR2)- and TLR4-deficient animals. J Immunol. 2003;171(9):4758-64. Epub 2003/10/22. doi: 10.4049/jimmunol.171.9.4758. PubMed PMID: 14568952.

88. Reiling N, Holscher C, Fehrenbach A, Kroger S, Kirschning CJ, Goyert S, et al. Cutting edge: Toll-like receptor (TLR)2- and TLR4-mediated pathogen recognition in resistance to airborne infection with Mycobacterium tuberculosis. J Immunol. 2002;169(7):3480-4. Epub 2002/09/24. doi: 10.4049/jimmunol.169.7.3480. PubMed PMID: 12244136.

89. Drennan MB, Nicolle D, Quesniaux VJ, Jacobs M, Allie N, Mpagi J, et al. Toll-like receptor 2-deficient mice succumb to Mycobacterium tuberculosis infection. Am J Pathol. 2004;164(1):49-57. Epub 2003/12/26. doi: 10.1016/S0002-9440(10)63095-7. PubMed PMID: 14695318; PubMed Central PMCID: PMCPMC1602241.

90. Carlos D, Frantz FG, Souza-Junior DA, Jamur MC, Oliver C, Ramos SG, et al. TLR2-dependent mast cell activation contributes to the control of Mycobacterium tuberculosis infection. Microbes Infect. 2009;11(8-9):770-8. Epub 2009/05/16. doi: 10.1016/j.micinf.2009.04.025. PubMed PMID: 19442756.

91. McBride A, Konowich J, Salgame P. Host defense and recruitment of Foxp3(+) T regulatory cells to the lungs in chronic Mycobacterium tuberculosis infection requires toll-like receptor 2. PLoS Pathog. 2013;9(6):e1003397. Epub 2013/06/21. doi: 10.1371/journal.ppat.1003397. PubMed PMID: 23785280; PubMed Central PMCID: PMCPMC3681744.

92. Konowich J, Gopalakrishnan A, Dietzold J, Verma S, Bhatt K, Rafi W, et al. Divergent Functions of TLR2 on Hematopoietic and Nonhematopoietic Cells during Chronic Mycobacterium tuberculosis Infection. J Immunol. 2017;198(2):741-8. Epub 2016/12/07. doi: 10.4049/jimmunol.1601651. PubMed PMID: 27920273; PubMed Central PMCID: PMCPMC5224966.

93. Bafica A, Scanga CA, Feng CG, Leifer C, Cheever A, Sher A. TLR9 regulates Th1 responses and cooperates with TLR2 in mediating optimal resistance to Mycobacterium tuberculosis. J Exp Med. 2005;202(12):1715-24. Epub 2005/12/21. doi: 10.1084/jem.20051782. PubMed PMID: 16365150; PubMed Central PMCID: PMCPMC2212963.

94. Sugawara I, Yamada H, Li C, Mizuno S, Takeuchi O, Akira S. Mycobacterial infection in TLR2 and TLR6 knockout mice. Microbiol Immunol. 2003;47(5):327-36. Epub 2003/06/27. doi: 10.1111/j.1348-0421.2003.tb03404.x. PubMed PMID: 12825894.

95. BoseDasgupta S, Pieters J. Macrophage-microbe interaction: lessons learned from the pathogen Mycobacterium tuberculosis. Semin Immunopathol. 2018;40(6):577-91. Epub 2018/10/12. doi: 10.1007/s00281-018-0710-0. PubMed PMID: 30306257.

96. Kramarska E, Squeglia F, De Maio F, Delogu G, Berisio R. PE_PGRS33, an Important Virulence Factor of Mycobacterium tuberculosis and Potential Target of Host Humoral Immune Response. Cells. 2021;10(1). Epub 2021/01/21. doi: 10.3390/cells10010161. PubMed PMID: 33467487; PubMed Central PMCID: PMCPMC7830552.

97. Bocchino M, Galati D, Sanduzzi A, Colizzi V, Brunetti E, Mancino G. Role of mycobacteria-induced monocyte/macrophage apoptosis in the pathogenesis of human tuberculosis. Int J Tuberc Lung Dis. 2005;9(4):375-83. Epub 2005/04/16. PubMed PMID: 15830742.

98. Sanchez D, Rojas M, Hernandez I, Radzioch D, Garcia LF, Barrera LF. Role of TLR2- and TLR4-mediated signaling in Mycobacterium tuberculosis-induced macrophage death. Cell Immunol. 2010;260(2):128-36. Epub 2009/11/19. doi: 10.1016/j.cellimm.2009.10.007. PubMed PMID: 19919859.

99. Lin J, Chang Q, Dai X, Liu D, Jiang Y, Dai Y. Early secreted antigenic target of 6-kDa of Mycobacterium tuberculosis promotes caspase-9/caspase-3-mediated apoptosis in macrophages. Mol Cell Biochem. 2019;457(1-2):179-89. Epub 2019/03/27. doi: 10.1007/s11010-019-03522-x. PubMed PMID: 30911956.

100. Ghorpade DS, Leyland R, Kurowska-Stolarska M, Patil SA, Balaji KN. MicroRNA-155 is required for Mycobacterium bovis BCG-mediated apoptosis of macrophages. Mol Cell Biol. 2012;32(12):2239-53. Epub

2012/04/05. doi: 10.1128/MCB.06597-11. PubMed PMID: 22473996; PubMed Central PMCID: PMCPMC3372268.

101. Ayelign B, Workneh M, Molla MD, Dessie G. Role Of Vitamin-D Supplementation In TB/HIV Co-Infected Patients. Infect Drug Resist. 2020;13:111-8. Epub 2020/02/06. doi: 10.2147/IDR.S228336. PubMed PMID: 32021325; PubMed Central PMCID: PMCPMC6959508.

102. Krutzik SR, Hewison M, Liu PT, Robles JA, Stenger S, Adams JS, et al. IL-15 links TLR2/1-induced macrophage differentiation to the vitamin D-dependent antimicrobial pathway. J Immunol. 2008;181(10):7115-20. Epub 2008/11/05. doi: 10.4049/jimmunol.181.10.7115. PubMed PMID: 18981132; PubMed Central PMCID: PMCPMC2678236.

103. Rivas-Santiago B, Hernandez-Pando R, Carranza C, Juarez E, Contreras JL, Aguilar-Leon D, et al. Expression of cathelicidin LL-37 during Mycobacterium tuberculosis infection in human alveolar macrophages, monocytes, neutrophils, and epithelial cells. Infect Immun. 2008;76(3):935-41. Epub 2007/12/28. doi: 10.1128/IAI.01218-07. PubMed PMID: 18160480; PubMed Central PMCID: PMCPMC2258801.

104. Lasunskaia EB, Campos MN, de Andrade MR, Damatta RA, Kipnis TL, Einicker-Lamas M, et al. Mycobacteria directly induce cytoskeletal rearrangements for macrophage spreading and polarization through TLR2-dependent PI3K signaling. J Leukoc Biol. 2006;80(6):1480-90. Epub 2006/09/29. doi: 10.1189/jlb.0106066. PubMed PMID: 17005905.

105. Eum SY, Kong JH, Hong MS, Lee YJ, Kim JH, Hwang SH, et al. Neutrophils are the predominant infected phagocytic cells in the airways of patients with active pulmonary TB. Chest. 2010;137(1):122-8. Epub 2009/09/15. doi: 10.1378/chest.09-0903. PubMed PMID: 19749004; PubMed Central PMCID: PMCPMC2803122.

106. Borkute RR, Woelke S, Pei G, Dorhoi A. Neutrophils in Tuberculosis: Cell Biology, Cellular Networking and Multitasking in Host Defense. Int J Mol Sci. 2021;22(9). Epub 2021/05/06. doi: 10.3390/ijms22094801. PubMed PMID: 33946542; PubMed Central PMCID: PMCPMC8125784.

107. Hook JS, Cao M, Weng K, Kinnare N, Moreland JG. Mycobacterium tuberculosis Lipoarabinomannan Activates Human Neutrophils via a TLR2/1 Mechanism Distinct from Pam3CSK4. J Immunol. 2020;204(3):671-81. Epub 2019/12/25. doi: 10.4049/jimmunol.1900919. PubMed PMID: 31871022.

108. Gopalakrishnan A, Dietzold J, Verma S, Bhagavathula M, Salgame P. Toll-like Receptor 2 Prevents Neutrophil-Driven Immunopathology during Infection with Mycobacterium tuberculosis by Curtailing CXCL5 Production. Infect Immun. 2019;87(3). Epub 2018/12/19. doi: 10.1128/IAI.00760-18. PubMed PMID: 30559223; PubMed Central PMCID: PMCPMC6386542.

109. Andersson M, Lutay N, Hallgren O, Westergren-Thorsson G, Svensson M, Godaly G. Mycobacterium bovis bacilli Calmette-Guerin regulates leukocyte recruitment by modulating alveolar inflammatory responses. Innate Immun. 2012;18(3):531-40. Epub 2011/11/08. doi: 10.1177/1753425911426591. PubMed PMID: 22058091; PubMed Central PMCID: PMCPMC3548393.

110. Wieland CW, Knapp S, Florquin S, de Vos AF, Takeda K, Akira S, et al. Non-mannose-capped lipoarabinomannan induces lung inflammation via toll-like receptor 2. Am J Respir Crit Care Med. 2004;170(12):1367-74. Epub 2004/09/28. doi: 10.1164/rccm.200404-525OC. PubMed PMID: 15447943.

111. Tyne AS, Chan JGY, Shanahan ER, Atmosukarto I, Chan HK, Britton WJ, et al. TLR2-targeted secreted proteins from Mycobacterium tuberculosis are protective as powdered pulmonary vaccines. Vaccine. 2013;31(40):4322-9. doi: 10.1016/j.vaccine.2013.07.022. PubMed PMID: WOS:000324510500010.

112. Mangtani P, Abubakar I, Ariti C, Beynon R, Pimpin L, Fine PEM, et al. Protection by BCG Vaccine Against Tuberculosis: A Systematic Review of Randomized Controlled Trials. Clinical Infectious Diseases. 2014;58(4):470-80. doi: 10.1093/cid/cit790. PubMed PMID: WOS:000331097800005.

113. Tran V, Liu J, Behr MA. BCG Vaccines. Microbiol Spectr. 2014;2(1):MGM2-0028-2013. Epub 2014/02/01. doi: 10.1128/microbiolspec.MGM2-0028-2013. PubMed PMID: 26082111.

114. Simpson ME, Petri WA. TLR2 as a Therapeutic Target in Bacterial Infection. Trends in Molecular Medicine. 2020;26(8):715-7. doi: 10.1016/j.molmed.2020.05.006. PubMed PMID: WOS:000561576400003.

115. Ahmed A, Dolasia K, Mukhopadhyay S. Mycobacterium tuberculosis PPE18 Protein Reduces Inflammation and Increases Survival in Animal Model of Sepsis. Journal of Immunology. 2018;200(10):3587-98. doi: 10.4049/jimmunol.1602065. PubMed PMID: WOS:000442364400028.

116. Nakajima H, Chiba A, Fukumoto M, Morooka N, Mochizuki N. Zebrafish Vascular Development: General and Tissue-Specific Regulation. J Lipid Atheroscler. 2021;10(2):145-59. Epub 2021/06/08. doi: 10.12997/jla.2021.10.2.145. PubMed PMID: 34095009; PubMed Central PMCID: PMCPMC8159758.

117. van der Vaart M, Spaink HP, Meijer AH. Pathogen recognition and activation of the innate immune response in zebrafish. Adv Hematol. 2012;2012:159807. Epub 2012/07/20. doi: 10.1155/2012/159807. PubMed PMID: 22811714; PubMed Central PMCID: PMCPMC3395205.

118. Li S, Yeo KS, Levee TM, Howe CJ, Her ZP, Zhu S. Zebrafish as a Neuroblastoma Model: Progress Made, Promise for the Future. Cells. 2021;10(3). Epub 2021/04/04. doi: 10.3390/cells10030580. PubMed PMID: 33800887; PubMed Central PMCID: PMCPMC8001113.

119. Torraca V, Mostowy S. Zebrafish Infection: From Pathogenesis to Cell Biology. Trends Cell Biol. 2018;28(2):143-56. Epub 2017/11/28. doi: 10.1016/j.tcb.2017.10.002. PubMed PMID: 29173800; PubMed Central PMCID: PMCPMC5777827.

120. Patton EE, Zon LI, Langenau DM. Zebrafish disease models in drug discovery: from preclinical modelling to clinical trials. Nat Rev Drug Discov. 2021. Epub 2021/06/13. doi: 10.1038/s41573-021-00210-8. PubMed PMID: 34117457.

121. Sieber S, Grossen P, Bussmann J, Campbell F, Kros A, Witzigmann D, et al. Zebrafish as a preclinical in vivo screening model for nanomedicines. Adv Drug Deliv Rev. 2019;151-152:152-68. Epub 2019/01/08. doi: 10.1016/j.addr.2019.01.001. PubMed PMID: 30615917.

122. Meijer AH, Spaink HP. Host-pathogen interactions made transparent with the zebrafish model. Curr Drug Targets. 2011;12(7):1000-17. Epub 2011/03/04. doi: 10.2174/138945011795677809. PubMed PMID: 21366518; PubMed Central PMCID: PMCPMC3319919.

123. Torraca V, Cui C, Boland R, Bebelman JP, van der Sar AM, Smit MJ, et al. The CXCR3-CXCL11 signaling axis mediates macrophage recruitment and dissemination of mycobacterial infection. Dis Model Mech. 2015;8(3):253-69. Epub 2015/01/13. doi: 10.1242/dmm.017756. PubMed PMID: 25573892; PubMed Central PMCID: PMCPMC4348563.

124. Hosseini R, Lamers GE, Soltani HM, Meijer AH, Spaink HP, Schaaf MJ. Efferocytosis and extrusion of leukocytes determine the progression of early mycobacterial pathogenesis. J Cell Sci. 2016;129(18):3385-95. Epub 2016/07/30. doi: 10.1242/jcs.135194. PubMed PMID: 27469488.

125. Clay H, Davis JM, Beery D, Huttenlocher A, Lyons SE, Ramakrishnan L. Dichotomous role of the macrophage in early Mycobacterium marinum infection of the zebrafish. Cell Host Microbe. 2007;2(1):29-39. Epub 2007/11/17. doi: 10.1016/j.chom.2007.06.004. PubMed PMID: 18005715; PubMed Central PMCID: PMCPMC3115716.

126. Yang CT, Cambier CJ, Davis JM, Hall CJ, Crosier PS, Ramakrishnan L. Neutrophils exert protection in the early tuberculous granuloma by oxidative killing of mycobacteria phagocytosed from infected macrophages. Cell Host Microbe. 2012;12(3):301-12. Epub 2012/09/18. doi: 10.1016/j.chom.2012.07.009. PubMed PMID: 22980327; PubMed Central PMCID: PMCPMC3638950.

127. Bernut A, Mai NC, Halloum I, Herrmann JL, Lutfalla G, Kremer L. Mycobacterium abscessus-Induced Granuloma Formation Is Strictly Dependent on TNF Signaling and Neutrophil Trafficking. Plos Pathogens. 2016;12(11). doi: ARTN e1005986

10.1371/journal.ppat.1005986. PubMed PMID: WOS:000392193200021.

128. Pecora ND, Gehring AJ, Canaday DH, Boom WH, Harding CV. Mycobacterium tuberculosis LprA is a lipoprotein agonist of TLR2 that regulates innate immunity and APC function. J Immunol. 2006;177(1):422-9. Epub 2006/06/21. doi: 10.4049/jimmunol.177.1.422. PubMed PMID: 16785538.

129. Su H, Zhu S, Zhu L, Huang W, Wang H, Zhang Z, et al. Recombinant Lipoprotein Rv1016c Derived from Mycobacterium tuberculosis Is a TLR-2 Ligand that Induces Macrophages Apoptosis and Inhibits MHC II Antigen Processing. Front Cell Infect Microbiol. 2016;6:147. Epub 2016/12/06. doi: 10.3389/fcimb.2016.00147. PubMed PMID: 27917375; PubMed Central PMCID: PMCPMC5114242.

130. Jung SB, Yang CS, Lee JS, Shin AR, Jung SS, Son JW, et al. The mycobacterial 38-kilodalton glycolipoprotein antigen activates the mitogen-activated protein kinase pathway and release of proinflammatory cytokines through Toll-like receptors 2 and 4 in human monocytes. Infect Immun. 2006;74(5):2686-96. Epub 2006/04/20. doi: 10.1128/IAI.74.5.2686-2696.2006. PubMed PMID: 16622205; PubMed Central PMCID: PMCPMC1459749.

131. Chen ST, Li JY, Zhang Y, Gao X, Cai H. Recombinant MPT83 derived from Mycobacterium tuberculosis induces cytokine production and upregulates the function of mouse macrophages through TLR2. J Immunol. 2012;188(2):668-77. Epub 2011/12/17. doi: 10.4049/jimmunol.1102177. PubMed PMID: 22174456.

132. Das S, Bhattacharjee O, Goswami A, Pal NK, Majumdar S. Arabinosylated lipoarabinomannan (Ara-LAM) mediated intracellular mechanisms against tuberculosis infection: involvement of protein kinase C (PKC) mediated signaling. Tuberculosis (Edinb). 2015;95(2):208-16. Epub 2014/12/30. doi: 10.1016/j.tube.2014.11.007. PubMed PMID: 25544312.

133. Shukla S, Richardson ET, Drage MG, Boom WH, Harding CV. Mycobacterium tuberculosis Lipoprotein and Lipoglycan Binding to Toll-Like Receptor 2 Correlates with Agonist Activity and Functional Outcomes. Infect Immun. 2018;86(10). Epub 2018/07/25. doi: 10.1128/IAI.00450-18. PubMed PMID: 30037791; PubMed Central PMCID: PMCPMC6204744.

134. Gilleron M, Nigou J, Nicolle D, Quesniaux V, Puzo G. The acylation state of mycobacterial lipomannans modulates innate immunity response through toll-like receptor 2. Chem Biol. 2006;13(1):39-47. Epub 2006/01/24. doi: 10.1016/j.chembiol.2005.10.013. PubMed PMID: 16426970.

135. Gilleron M, Quesniaux VF, Puzo G. Acylation state of the phosphatidylinositol hexamannosides from Mycobacterium bovis bacillus Calmette Guerin and mycobacterium tuberculosis H37Rv and its implication in Toll-like receptor response. J Biol Chem. 2003;278(32):29880-9. Epub 2003/05/31. doi: 10.1074/jbc.M303446200. PubMed PMID: 12775723.

136. Bowdish DM, Sakamoto K, Kim MJ, Kroos M, Mukhopadhyay S, Leifer CA, et al. MARCO, TLR2, and CD14 are required for macrophage cytokine responses to mycobacterial trehalose dimycolate and Mycobacterium tuberculosis. PLoS Pathog. 2009;5(6):e1000474. Epub 2009/06/13. doi: 10.1371/journal.ppat.1000474. PubMed PMID: 19521507; PubMed Central PMCID: PMCPMC2688075.

137. Bulut Y, Michelsen KS, Hayrapetian L, Naiki Y, Spallek R, Singh M, et al. Mycobacterium tuberculosis heat shock proteins use diverse Toll-like receptor pathways to activate pro-inflammatory signals. J Biol Chem. 2005;280(22):20961-7. Epub 2005/04/06. doi: 10.1074/jbc.M411379200. PubMed PMID: 15809303.

138. Saraav I, Singh S, Pandey K, Sharma M, Sharma S. Mycobacterium tuberculosis MymA is a TLR2 agonist that activate macrophages and a TH1 response. Tuberculosis (Edinb). 2017;106:16-24. Epub 2017/08/15. doi: 10.1016/j.tube.2017.05.005. PubMed PMID: 28802400.

139. Palucci I, Camassa S, Cascioferro A, Sali M, Anoosheh S, Zumbo A, et al. PE_PGRS33 Contributes to Mycobacterium tuberculosis Entry in Macrophages through Interaction with TLR2. PLoS One. 2016;11(3):e0150800. Epub 2016/03/16. doi: 10.1371/journal.pone.0150800. PubMed PMID: 26978522; PubMed Central PMCID: PMCPMC4792380.

140. Zumbo A, Palucci I, Cascioferro A, Sali M, Ventura M, D'Alfonso P, et al. Functional dissection of protein domains involved in the immunomodulatory properties of PE_PGRS33 of Mycobacterium tuberculosis. Pathog Dis. 2013;69(3):232-9. Epub 2013/10/10. doi: 10.1111/2049-632X.12096. PubMed PMID: 24106104.

141. Pattanaik KP, Ganguli G, Naik SK, Sonawane A. Mycobacterium tuberculosis EsxL induces TNF-alpha secretion through activation of TLR2 dependent MAPK and NF-kappaB pathways. Mol Immunol. 2021;130:133-41. Epub 2021/01/10. doi: 10.1016/j.molimm.2020.11.020. PubMed PMID: 33419561.

142. Nair S, Pandey AD, Mukhopadhyay S. The PPE18 protein of Mycobacterium tuberculosis inhibits NF-kappaB/rel-mediated proinflammatory cytokine production by upregulating and phosphorylating suppressor of cytokine signaling 3 protein. J Immunol. 2011;186(9):5413-24. Epub 2011/04/01. doi: 10.4049/jimmunol.1000773. PubMed PMID: 21451109.

143. Nair S, Ramaswamy PA, Ghosh S, Joshi DC, Pathak N, Siddiqui I, et al. The PPE18 of Mycobacterium tuberculosis interacts with TLR2 and activates IL-10 induction in macrophage. J Immunol. 2009;183(10):6269-81. Epub 2009/11/03. doi: 10.4049/jimmunol.0901367. PubMed PMID: 19880448.

144. Su H, Kong C, Zhu L, Huang Q, Luo L, Wang H, et al. PPE26 induces TLR2-dependent activation of macrophages and drives Th1-type T-cell immunity by triggering the cross-talk of multiple pathways involved in the host response. Oncotarget. 2015;6(36):38517-37. Epub 2015/10/07. doi: 10.18632/oncotarget.5956. PubMed PMID: 26439698; PubMed Central PMCID: PMCPMC4770718.

145. Deng W, Li W, Zeng J, Zhao Q, Li C, Zhao Y, et al. Mycobacterium tuberculosis PPE family protein Rv1808 manipulates cytokines profile via co-activation of MAPK and NF-kappaB signaling pathways. Cell Physiol Biochem. 2014;33(2):273-88. Epub 2014/02/15. doi: 10.1159/000356668. PubMed PMID: 24525621.

146. Xu Y, Yang E, Huang Q, Ni W, Kong C, Liu G, et al. PPE57 induces activation of macrophages and drives Th1-type immune responses through TLR2. J Mol Med (Berl). 2015;93(6):645-62. Epub 2015/01/15. doi: 10.1007/s00109-014-1243-1. PubMed PMID: 25586105.

147. Liu Y, Li JY, Chen ST, Huang HR, Cai H. The rLrp of Mycobacterium tuberculosis inhibits proinflammatory cytokine production and downregulates APC function in mouse macrophages via a TLR2-mediated PI3K/Akt pathway activation-dependent mechanism. Cell Mol Immunol. 2016;13(6):729-46. Epub 2015/07/15. doi: 10.1038/cmi.2015.58. PubMed PMID: 26166760; PubMed Central PMCID: PMCPMC5101441.

148. Sweet L, Zhang W, Torres-Fewell H, Serianni A, Boggess W, Schorey J. Mycobacterium avium glycopeptidolipids require specific acetylation and methylation patterns for signaling through toll-like receptor 2. J Biol Chem. 2008;283(48):33221-31. Epub 2008/10/01. doi: 10.1074/jbc.M805539200. PubMed PMID: 18824550; PubMed Central PMCID: PMCPMC2586276.

149. Bhatnagar S, Schorey JS. Exosomes released from infected macrophages contain Mycobacterium avium glycopeptidolipids and are proinflammatory. J Biol Chem. 2007;282(35):25779-89. Epub 2007/06/27. doi: 10.1074/jbc.M702277200. PubMed PMID: 17591775; PubMed Central PMCID: PMCPMC3636815.

150. Sweet L, Schorey JS. Glycopeptidolipids from Mycobacterium avium promote macrophage activation in a TLR2- and MyD88-dependent manner. J Leukoc Biol. 2006;80(2):415-23. Epub 2006/06/09. doi: 10.1189/jlb.1205702. PubMed PMID: 16760377.

151. Le Moigne V, Roux AL, Jobart-Malfait A, Blanc L, Chaoui K, Burlet-Schiltz O, et al. A TLR2-Activating Fraction From Mycobacterium abscessus Rough Variant Demonstrates Vaccine and Diagnostic Potential. Front Cell Infect Microbiol. 2020;10:432. Epub 2020/09/29. doi: 10.3389/fcimb.2020.00432. PubMed PMID: 32984067; PubMed Central PMCID: PMCPMC7481331.

152. Roux AL, Ray A, Pawlik A, Medjahed H, Etienne G, Rottman M, et al. Overexpression of proinflammatory TLR-2-signalling lipoproteins in hypervirulent mycobacterial variants. Cell Microbiol. 2011;13(5):692-704. Epub 2010/12/15. doi: 10.1111/j.1462-5822.2010.01565.x. PubMed PMID: 21143571.

153. Briken V, Porcelli SA, Besra GS, Kremer L. Mycobacterial lipoarabinomannan and related lipoglycans: from biogenesis to modulation of the immune response. Mol Microbiol. 2004;53(2):391-403. Epub 2004/07/02. doi: 10.1111/j.1365-2958.2004.04183.x. PubMed PMID: 15228522.

Chapter 2

Infection and RNA-seq analysis of a zebrafish *tlr2* mutant shows a broad function of this Toll-like receptor in transcriptional and metabolic control and defense to *Mycobacterium marinum* infection

Wanbin Hu*, Shuxin Yang*, Yasuhito Shimada, Magnus Münch, Rubén Marín-Juez, Annemarie H. Meijer, Herman P. Spaink

*These authors contributed equally

Published in ***BMC genomics*** 20.1 (2019): 1-18. DOI: 10.1186/s12864-019-6265-1

2

Abstract

The function of Toll-like receptor 2 (TLR2) in host defense against pathogens, especially *Mycobacterium tuberculosis* (Mtb) is poorly understood. To investigate the role of TLR2 during mycobacterial infection, we analyzed the response of *tlr2* zebrafish mutant larvae to infection with *Mycobacterium marinum* (Mm), a close relative to Mtb, as a model for tuberculosis. We measured infection phenotypes and transcriptome responses using RNA deep sequencing in mutant and control larvae. *Tlr2* mutant embryos at 2 dpf do not show differences in numbers of macrophages and neutrophils compared to control embryos. However, we found substantial changes in gene expression in these mutants, particularly in metabolic pathways, when compared with the heterozygote $tlr2^{+/-}$ control. At 4 days after Mm infection, the total bacterial burden and the presence of extracellular bacteria were higher in $tlr2^{-/-}$ larvae than in $tlr2^{+/-}$, or $tlr2^{+/+}$ larvae, whereas granuloma numbers were reduced, showing a function of Tlr2 in zebrafish host defense. RNAseq analysis of infected $tlr2^{-/-}$ versus $tlr2^{+/-}$ shows that the number of up-regulated and down-regulated genes in response to infection was greatly diminished in *tlr2* mutants by at least 2 fold and 10 fold, respectively. Analysis of the transcriptome data and qPCR validation shows that Mm infection of *tlr2* mutants leads to decreased mRNA levels of genes involved in inflammation and immune responses, including *il1b*, *tnfb*, *cxcl11aa/ac*, *fosl1a*, and *cebpb*. Furthermore, RNAseq analyses revealed that the expression of genes for Maf family transcription factors, vitamin D receptors, and Dicps proteins is altered in *tlr2* mutants with or without infection. In addition, the data indicate a function of Tlr2 in the control of induction of cytokines and chemokines, such as the CXCR3-CXCL11 signaling axis. The transcriptome and infection burden analyses show a function of Tlr2 as a protective factor against mycobacteria. Transcriptome analysis revealed *tlr2*-specific pathways involved in Mm infection, which are related to responses to Mtb infection in human macrophages. Considering its dominant function in control of transcriptional processes that govern defense responses and metabolism, the TLR2 protein can be expected to be also of importance for other infectious diseases and interactions with the microbiome.

Introduction

Mycobacterium tuberculosis (Mtb) is the causative agent of tuberculosis (TB), which infects nearly 23% of the world's population, and kills about 1.6 million people annually (WHO Global Tuberculosis Report 2018). TB is characterized by the formation of granulomas, aggregates of infected macrophages and other immune cells, not only in the lung but also in other tissues and organs [1]. The formation of granulomas is the result of a concerted action of host innate and adaptive immunity [2-4].

Innate immune responses play a critical role in defense against TB infection in the host, and for a major part these processes are mediated by Toll-like receptors (TLRs), a conserved family of pattern recognition receptors. TLR2 is one of the most widely reported members of the TLR family to be involved in defense against Mtb by virtue of its recognition of cell wall-associated components associated with this pathogen [5-7]. Following mycobacterial infection in human cell cultures, TLR2 dimerizes with TLR1 or TLR6, and recognizes mycobacterial components such as cell wall glycolipids LAM and LM [8], 38-kDa and 19-kDa mycobacterial glycoprotein (LpqH) [9-11], phosphatidylinositol mannoside (PIM) [12], and triacylated (TLR2/TLR1) [13, 14] or diacylated (TLR2/TLR6) lipoproteins [15, 16]. Then, these heterodimers recruit the MYD88 and TIRAP (MAL) proteins to activate the IRAK (1 and 4)/TRAF6/IKK (α or β) cascade, which subsequently leads to the ubiquitination of IκBα and the activation of transcription factor NF-κB or AP-1 to induce the expression of host defense genes and cytokine and chemokine responses [17, 18]. Once released after further processing, these cytokines and chemokines attract migration of macrophages and neutrophils to the infection site and activate the microbicidal functions of these cells.

TLR2 has been shown to be important for granuloma formation in Mtb infection in mouse infection model [19]. Other studies have reported that *Tlr2*$^{-/-}$ mice lose control to high dose infection of Mtb delivered by aerosol administration and show higher susceptibility to Mtb infection compared to the wild type [20, 21]. However, using lower doses of infection of 100 bacteria, there are controversial results as to the function of TLR2 in defense to Mtb in rodent models [20-22]. Furthermore, the function of TLR2 in susceptibility to Mtb is still unclear because several independent studies have reported polymorphisms of TLR2 (TLR1 and TLR6) in humans that have been linked with TB susceptibility, whereas others have been unable to find such links [23, 24].

Several studies suggest that the interaction between TLR2 and Mtb or other pathogens does not always promote the killing of bacteria, but can in fact be part of the pathogens's strategy to evade the immune system [25-27]. TLR2 has been reported to inhibit MHC-II expression on the surface of murine macrophages, thereby preventing presentation of Mtb antigens, which may allow intracellular Mtb to evade immune surveillance and maintain chronic infection [11, 28]. Furthermore, LprG from Mtb was reported to inhibit human macrophage class II MHC antigen processing through TLR signaling [25]. In other infection systems, *Tlr2* mutant mice have an increased resistance against infection of *Candida albicans* [29] and *Yersinia pestis* [30]. It has been proposed that this phenotype is the result of Tlr2-dependent induction of the anti-inflammatory cytokine IL-10 [30]. Furthermore, TLR2 activation inhibits the release of IL-12 via activation of the cFos transcription factor. It also has been shown that IFN-γ or IFN-γ-induced signals [31] are inhibited after infection of murine macrophages in a Tlr2-dependent fashion [32]. These effects show that TLR2 activation can yield a bias to T helper Type 2 (Th2) cells [33], and by breaking the Th1/Th2 balance can lead to less Th1 type responses and reducing the killing of intracellular pathogens. However, most of the molecular mechanisms underlying TLR2 functions remain unknown and a better understanding of the TLR2-mediated immune response and immune evasion can help in planning prevention and therapy strategies against Mtb infection.

Animal models have shown their power in studies of the mechanisms of interaction of host and TB pathogens, and discovering new anti-TB drugs. Zebrafish adult and larvae models have become a useful complement for rodent studies, for three important reasons. First, zebrafish have a 3-4 weeks separation stage between development of innate and adaptive immunity after fertilization [34, 35], which gives the possibility to study the host innate immune response to infection in the absence of adaptive immune responses. Second, zebrafish can be infected by *Mycobacterium marinum* (Mm), a natural pathogen of cold-blooded vertebrates and a close relative of Mtb, which can induce granuloma formation in zebrafish, similar to human TB [36, 37]. Third, the transparent larvae are ideal for imaging the early steps of the infection process in real time. Hence, zebrafish has earned its place of being a versatile tuberculosis model [1, 38, 39]. Although zebrafish has no lungs and therefore the route of infection is through other tissues, it has been shown that the parasitism of immune cells and the aggregation of infected cells into granulomatous aggregates are highly similar to that in mammals [40]. Nevertheless, there are some notable difference with the progression of the tuberculosis infection processes in mice [41].

The TLR signaling pathway in zebrafish appears to be highly conserved with that in mammals [42]. The zebrafish *tlr2* gene and the genes encoding its adaptor proteins are highly similar in sequence to those of mammals and mutation of the down-stream signaling gene *myd88* leads to phenotypes that correlate with those seen in rodent and human cell culture studies [43, 44]. In our previous study, we demonstrated that the mammalian TLR2 ligand Pam3CSK4, a synthetic triacylated lipopeptide that mimics the triacylated lipoprotein of mycobacteria, could also specifically activate the zebrafish Tlr2 pathway, inducing *fosl1a* and *cebpb* gene upregulation [45]. In the current study, to further explore the involvement of Tlr2 in Mm infection, we conducted infection studies using *tlr2* mutant zebrafish. We found that a *tlr2* mutation led to an overall increased Mm bacterial burden, corresponding with reduced presence of macrophages in the granulomatous aggregates and more extracellular growth. These results indicate that Tlr2 plays an important role in protecting the host during the early stage of mycobacterial infection. In addition, we performed RNA deep sequencing (RNAseq) and determined a Tlr2-specific gene list for the response to Mm infection. This analysis revealed that most of transcriptional downregulation caused by Mm infection in control animals was abrogated by *tlr2* mutation, in addition to a dampening effect on the upregulation of transcription factors and inflammatory genes.

Results

Characterization of a *tlr2* mutant zebrafish line

The *tlr2*^{sa19423} mutant (*tlr2*$^{-/-}$) carries a thymine to adenine point mutation that creates a premature stop codon (Fig. 1A), which is located in the sequence coding for the C-terminus of the leucine-rich repeat (LRR) domain. This leads to a truncated protein without the Toll/IL-1 receptor (TIR) domain, which is required for the interaction with Myd88 and Tirap (Mal) [46, 47].

To confirm whether *tlr2* mutation blocks its downstream pathway, we analyzed the gene expression profiles of zebrafish treated with the TLR2 agonist, Pam3CSK4 similarly as in our previous work [48], now also including the heterozygote mutant (*tlr2*$^{+/-}$). Pam3CSK4 was injected into the blood island of zebrafish embryos at 27 hours post fertilization (hpf). One hour after injection (hpi), we collected samples and performed qPCR to analyze the expression levels

of CCAAT/enhancer-binding protein beta (*cebpb*) and FOS Like Antigen 1a (*fosl1a*), previously shown to be specific targets of Tlr2 signaling [45]. In wild-type siblings and *tlr2*$^{+/sa19423}$ heterozygotes (*tlr2*$^{+/-}$), the expression levels of *cebpb* and *fosl1a*, as well as the inflammatory gene *il1b* were significantly induced upon Pam3CSK4 injection, whereas *tlr2*$^{-/-}$ showed no significant response (Fig. 1B-D). *tlr2*$^{+/-}$ animals showed a lower induction of these marker genes than the wild-types, indicating that there is an effect of the *tlr2* mutation even in the heterozygote. To confirm that these results are specific to the Tlr2 pathway, we injected flagellin, a Tlr5 agonist, into 27 hpf embryos. Flagellin induced *il1b* expression, but not *cebpb* and *fosl1a* expression in wild-type siblings, *tlr2*$^{+/-}$ and *tlr2*$^{-/-}$ larvae (Fig. 1E-G). Overall, these data show that *tlr2* mutation specifically blocks the Tlr2 downstream pathways.

To determine if immune cell development was affected by *tlr2* mutation, we used the double-transgenic line *tlr2*$^{+/+}$ *Tg*(*mpeg1:mCherry-F);TgBAC(mpx:EGFP)* and *tlr2*$^{-/-}$ *Tg*(*mpeg1:mCherry-F);TgBAC(mpx:EGFP)* to count the number of macrophages and neutrophils at 2 dpf. The results show that there is no significant difference in the number of macrophages and neutrophils at 2 dpf between the wild type and mutant (Fig. 1J, K).

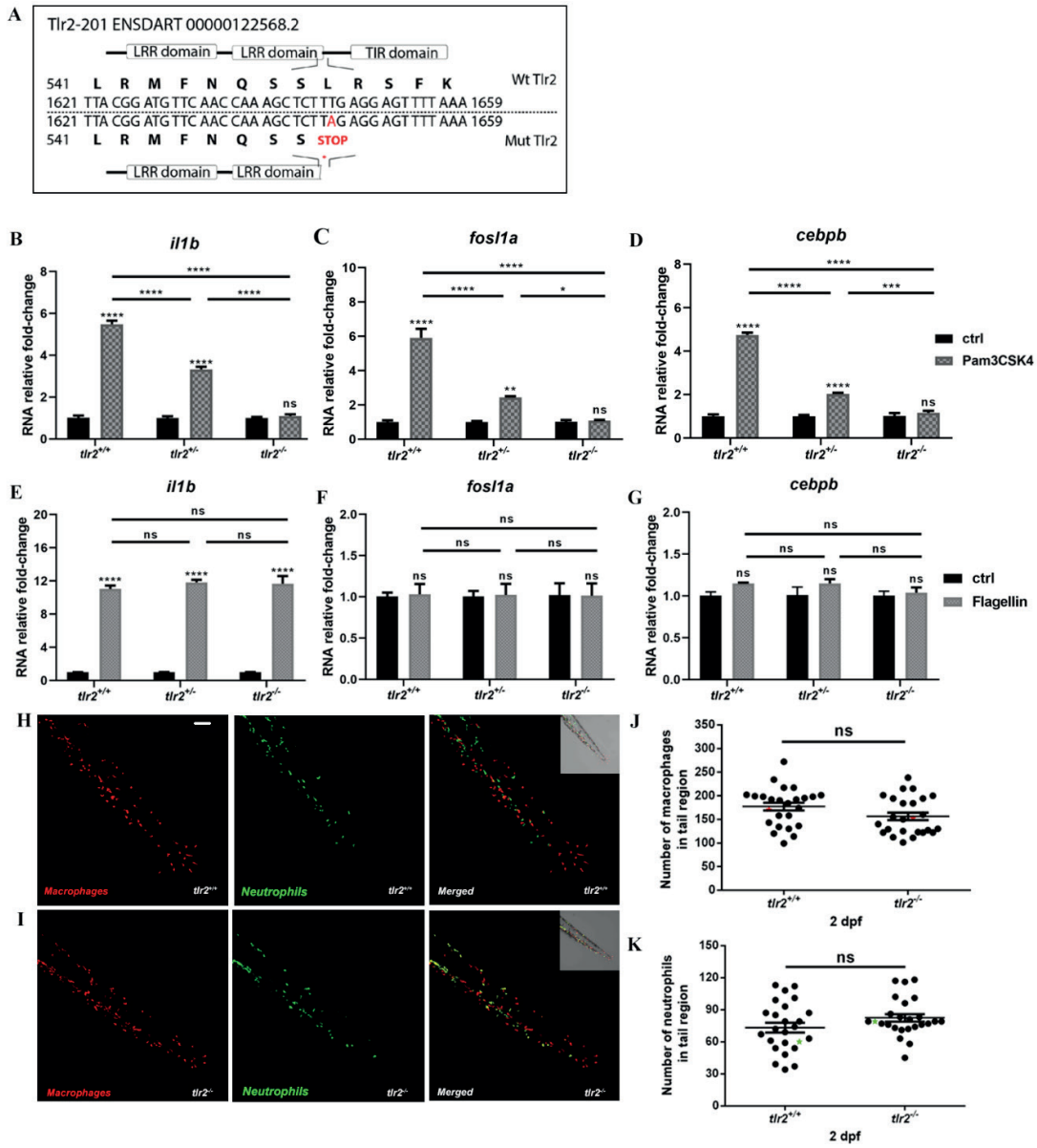

Figure 1 Characterization of the Tlr2 mutant. (A) mutant DNA and protein sequence. A point mutation (T to A) in the C-terminal of the second LRR domain of zebrafish Tlr2 introduces a premature stop codon. The predicted truncated protein lacks the whole TIR domain. Nucleotide and amino acid positions are indicated with respect to the translation start codon. *tlr2*$^{+/+}$, *tlr2*$^{+/-}$ and *tlr2*$^{-/-}$ embryos were injected at 27 hpf with 1 ng Pam3CSK4 (B-D) or 0.1ng flagellin (E-G) and expression levels of *il1b*, *fosl1a* and *cebpb* were determined at 1 hour post injection by qPCR. Data (mean ± SEM) are combined from three biological replicates (n=10 embryos per group) and expressed relative to their corresponding mock injection (water) control (ctrl), which is set at 1. Statistical significance of differences between ctrl and PAMPs injection groups was determined by two-way ANOVA with Tukey's Multiple Comparison method as a post-hoc test (B-G), ns, non-significant; *, $P<0.05$; ***, $P<0.001$; ****, $P<0.0001$. (H, I). Representative Stereo images of the caudal hematopoietic tissue of *tlr2*$^{+/+}$ *Tg(mpeg1:mCherry-F);TgBAC(mpx:EGFP)* (H) and *tlr2*$^{-/-}$ *Tg(mpeg1:mCherry-F);TgBAC(mpx:EGFP)* (I) were taken at 2 dpf for quantification of macrophages and neutrophils numbers. At 2 dpf, numbers of mCherry-labeled macrophages (J) and GFP-labeled neutrophils (K) were counted using Leica TCS SP8 confocal laser scanning microscopy (CLSM) of transgenic lines. Data (mean ± SEM) were combined from two independent experiments. No significant differences (ns) in the number of macrophages (J) and neutrophils (K) was detected with a t-test.

Comparison of gene expression profiles of *tlr2* homozygote and heterozygote mutants in the absence of infection

In order to investigate the systemic effects of the *tlr2* mutation we compared basal levels of gene expression in the absence of infection between *tlr2* homozygote and heterozygote mutants (Fig. 2). We chose to use the heterozygote $tlr2^{+/-}$ line as a control since these are genetically as comparable as possible, considering the fact that random ENU mutations could still contaminate our background even after 3 generations of outcrossing and the use of sibling lines. To further minimize the effect of polymorphisms, we pooled 10 larvae in each of our samples. These results show that there is a large group of genes that are expressed differently even at extremely stringent false discovery rate (FDR) adjusted *p*-value of 10^{-10} (Fig. 2). Since the results of the DEseq2 analyses showed such a surprisingly large number of significant differences we also used another statistical method for analyses, called edgeR, that differs in normalization and estimation of the dispersion parameters [49]. EdgeR analyses confirmed the statistical significance of the differences between the homozygote and heterozygote mutants (Fig. 2A and 2B). While no differences in numbers of mpeg-positive macrophages were detected (Fig. 1J, K), the RNAseq analysis showed that the *mpeg1* gene is expressed approximately 2 fold higher in the $tlr2^{+/-}$ control than in the $tlr2^{-/-}$ mutant (Supplementary Table 1). This was confirmed by pixel count measurements in the transgenic line $tlr2^{+/+}$ *Tg*(*mpeg1:mCherry-F);TgBAC(mpx:EGFP)* and $tlr2^{-/-}$ *Tg*(*mpeg1:mCherry-F);TgBAC(mpx:EGFP)* (Fig. S1 A, B). These results showed lower fluorescence of the mCherry *mpeg1* reporter as compared to the wild-type siblings at 2 dpf (Fig. S1 A) whereas no difference was detected for the eGFP *mpx* reporter (Fig. S1 B). Therefore these *in vivo* results confirm the RNAseq data. We also examined the expression levels of the *tlr2* gene in the homozygote and heterozygote mutants in the RNAseq data (Fig. S2). The results show that, although *tlr2* is very lowly expressed, there is no difference in expression levels between the homozygote and heterozygote mutants, indicating that there is no non-sense mediated mRNA decay (NMD).

To investigate whether the basal expression level differences of genes might be relevant to the Tlr2 pathway, we performed GO analysis of a set of genes that were expressed differently with the very low FDR adjust *P* value of 10^{-10} (Supplementary Table 2). Gene ontology analyses of the gene sets that differ with an FDR of 10^{-10} in both analyses show that there is a large enrichment of genes belonging to the GO terms related to neural development (Supplementary

Table 2). In addition, we have also analyzed differences with a fold change criterion of two and FDR of 0.05. These analyses indicated that under the GO category "Transcription factor genes" only two categories of genes including the c-Maf transcription factor were present (Supplementary Table 3). Pathway analysis shows that genes that function in glucose metabolism are differentially expressed in the *tlr2* homozygote versus heterozygote mutant (Fig. S3).

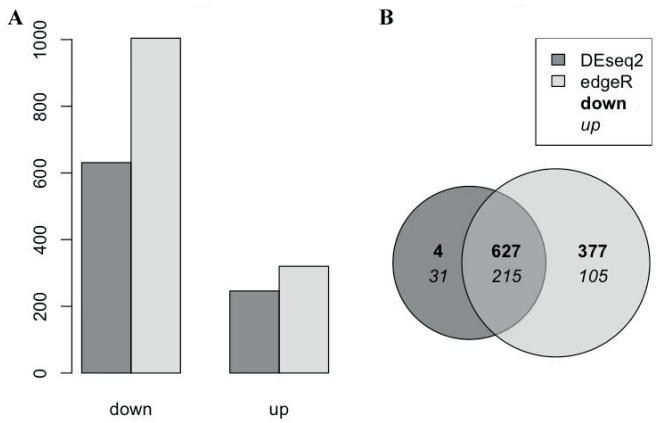

Figure 2 Gene expression in the absence of infection between Tlr2 mutants. (A) a number of down- and up-regulated genes per method (edgeR and DEseq2) and (B) a Venn diagram that compares the down-, up- and non-differentially expressed genes per method at a significance level of 10^{-10} in the edgeR and DEseq2 analyses methods. Down-regulated means that a gene is less expressed in the *tlr2*$^{+/-}$ compared to the *tlr2*$^{-/-}$ strain.

Tlr2-specific gene expression profiles after Mm infection

To study the role of Tlr2 in Mm infection we tested the *tlr2* mutant line in comparison with the heterozygote and wild-type sibling controls (Fig. 3). No differences in bacterial burden were observed at 3 dpi (Fig. 3D). However, we found that bacterial burden was significantly higher in *tlr2*$^{-/-}$ than in *tlr2*$^{+/-}$ and wild-type larvae at 4 dpi (Fig. 3E). There was no significant difference in bacterial infection burden between the heterozygote mutant strain (*tlr2*$^{+/-}$) and the wild-type siblings (*tlr2*$^{+/+}$). At 4 dpi, *tlr2*$^{-/-}$ larvae showed a significantly decreased percentage of survival compared with *tlr2*$^{+/-}$ and wild-type larvae (Fig. 3F). There was no significant difference in percentage of survival between *tlr2*$^{+/-}$ and wild-type larvae at 4 dpi. For further analysis of the infection phenotype we performed confocal laser scanning microscopy (CLSM)

in the *tlr2*$^{+/+}$ *Tg(mpeg1:EGFP)*, *tlr2*$^{+/-}$ *Tg(mpeg1:EGFP)* and *tlr2*$^{-/-}$ *Tg(mpeg1:EGFP)* transgenic lines in which macrophages are fluorescently labelled (Fig. 4A, B and Fig. S4). The results using fluorescent automated pixel count analyses showed that in the *tlr2* mutant the number of bacteria that were not present within macrophages was significantly higher than in the heterozygote and wild-type sibling controls (Fig. 4C). We also observed by manual counting that in the *tlr2* mutant a significantly higher number of bacteria in large extracellular clusters (Fig. 4D), indicative for cording structures [50]. Manual counting of infected macrophage clusters showed a significantly lower number of granulomas in the *tlr2* mutant (Fig. 4E). However, the percentage of larvae with at least one granuloma was not different from the heterozygote and wild-type sibling controls (Fig. 4F). These results show that the *tlr2* mutation results in a defect in the defense response against mycobacteria at 4 dpi.

Figure 3 Quantification of bacterial burden and survival after *M. marinum* infection. *tlr2*$^{+/+}$ (A), *tlr2*$^{+/-}$ (B) and *tlr2*$^{-/-}$ (C) embryos were infected with mCherry-labeled *M. marinum* strain Mma20 at a dose of ~150 CFU by caudal vein infection at 28 hpf. Representative images for bacterial pixel count in *tlr2*$^{+/+}$ (A), *tlr2*$^{+/-}$ (B) and *tlr2*$^{-/-}$ (C) were taken at 4 dpi. Bacterial burden of *tlr2*$^{+/+}$, *tlr2*$^{+/-}$ and *tlr2*$^{-/-}$ were also quantified at 3 dpi (D) and 4 dpi (E). Bacterial burdens were quantified by using bacterial fluorescence pixels. Red stars in (E) indicate the data for the representative images shown in (A-C). In (D, E), data (mean ± SEM) were combined from two independent experiments. Statistical significance of differences was determined by one-way ANOVA with Tukey's Multiple Comparison method as a post-hoc test for comparison between more than two groups (D, E). Percent of survival curves for *tlr2*$^{+/+}$ (n= 47), *tlr2*$^{+/-}$ (n= 49) and *tlr2*$^{-/-}$ (n= 49) (F) are based on two independent experiments. Statistical significance of difference was determined by a log-rank (Mantel-Cox) test. ns, non-significant; *, P<0.05, **, P<0.01, ****, P<0.0001.

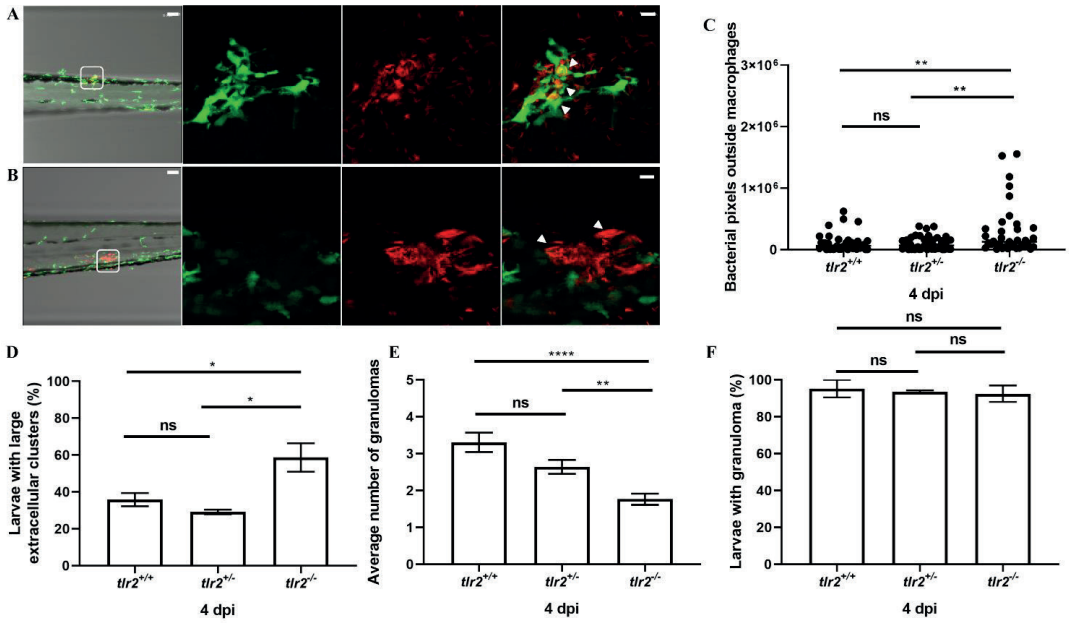

Figure 4. Quantification of Mma20 infection phenotype in the *tlr2* mutant. Embryos were infected at 28 hpf with ~150 CFU *M. marinum* Mma20 strain. Confocal images of green fluorescent macrophages and red fluorescent bacteria in a granuloma of *tlr2*$^{+/+}$ *Tg(mpeg1:EGFP)* larva (A) and extracellular bacteria in *tlr2*$^{-/-}$ *Tg(mpeg1:EGFP)* larva (B) was conducted at 4 dpi with 10 (A, B, bright view images) and 63 (A, B, fluorescent view images) times magnification objectives. White arrowheads indicates a granuloma (A) and extracellular bacteria (B). In the bright view images of (A, B), the scale bar represents 50 µm. In the fluorescent view images of (A, B), the scale bar represents 10 µm. For quantification of bacteria outside macrophages by pixel count (C) large extracellular clusters of at least 8 micrometer diameter (D) and average number of granulomas in the CHT region (E) three groups of at least 37 embryos of *tlr2*$^{+/+}$ *Tg(mpeg1:EGFP)*, *tlr2*$^{+/-}$ *Tg(mpeg1:EGFP)* and *tlr2*$^{-/-}$ *Tg(mpeg1:EGFP)* embryos were analysed at 4 dpi in the CHT region. For these CLSM analyses, 20 times magnification was used (Fig. S4 gives representative images). In panel f the percentage of embryos with at least one granuloma in the CHT region is shown. Statistical significance of differences was determined by one-way ANOVA with Tukey's Multiple Comparison method as a post-hoc test for comparison between more than two groups (C-F). ns, non-significant; * $P< 0.05$; ** $P< 0.01$, **** $P< 0.0001$.

Next, we set out to assess the general inflammation and specific immune responses in *tlr2* mutants. We analyzed these parameters at 4 dpi to correlate transcriptional responses with the first microscopically measured effect of the mutation on the progression of infection process as measured by bacterial burden (Fig. 3E). For this, genes that were shown previously to be specifically or aspecifically responding to Pam3CSK4 [45] were analyzed by qPCR of *tlr2*$^{-/-}$ and *tlr2*$^{+/-}$ larvae upon Mm (strain Mma20) infection at 4 dpi: *tlr2*-aspecific response genes *il1b*, *tnfa*, *tnfb*, *irg1l*, and *tlr2*-specific response genes *fosl1a* and *cebpb*. Our results show that the induction levels of *il1b*, *tnfb, fosl1a* and *cebpb* in *tlr2*$^{-/-}$ larvae were significantly reduced when compared to the heterozygotes in the infected condition (Fig. 5). The induction levels of *irg1l* and *tnfa* were less clearly affected. *tlr2*$^{-/-}$ larvae failed to upregulate *fosl1a* and *cebpb* expression

in response to Mm administration (Fig. 5E, F). In our previous work, we showed that Cxcl11-like chemokines expressed in macrophages play a crucial role in granuloma formation upon Mm infection [51, 52]. We therefore conducted qPCR to assess the expression levels of *cxcl11-like* genes, previously shown to be induced by infection [51], including *cxcl11aa* and *cxcl11ac* (Fig. 5G, H). The expression levels of *cxcl11aa* and *cxcl11ac* was significantly higher in *tlr2*$^{+/-}$ larvae than in *tlr2*$^{-/-}$ upon Mm infection (Fig. 5G, H). These results indicate that *tlr2* mutation results in a defective immune or inflammatory response to Mm infection.

To further study the function of *tlr2* in defense against mycobacterial infection, we performed RNAseq of *tlr2*$^{+/-}$ and *tlr2*$^{-/-}$ larvae at 4 dpi with *M. marinum* strain (strain Mma20) and PBS as control. We summarized the number of differential expressed genes (DEGs) according to *P*-value (Fig. 6A, B) and in volcano plots (Fig. S5). The number of DEGs in *tlr2*$^{+/-}$ infected with Mm was higher than those in *tlr2*$^{-/-}$ at any given *P*-value or false discovery rate less than 0.05, or any given fold-change with a *P*-value less than 0.05. These data also show that most of the genes downregulated by the Mm infection in the control remained unchanged in *tlr2* mutants (Fig. 6A, B). To further analyze these RNAseq data, we chose the genes with a threshold of a *P*-value less than 0.05 in *tlr2*$^{+/-}$ with Mm infection (1102 up- and 827 down-regulated genes, Fig. 6A). Then, for these genes, we calculated the fold-change ratio of *tlr2*$^{+/-}$ versus *tlr2*$^{-/-}$, and genes with ratios greater than 2 or less than 0.5 were selected for further analysis (Fig. 6C). As a result, 97 and 92 genes were scored as *tlr2* specific up- and down-regulated genes, respectively. Next, we conducted GO analysis (Fig. 6D, E) showing that genes grouped into the immune system category are the most prominently deregulated (36%) in the whole *tlr2* up-regulated 97-gene set (Fig. 6D). Within this category we found genes involved in lysosome, chemotaxis, transcription regulation, diverse immunoglobulin domain-containing proteins (*dicps*) and other immune processes (Fig. 6D and 7A-E). For other categories, many up-regulated genes fell in the categories oxidation-reduction process, DNA repair, transcription regulation and apoptotic process regulation (Fig. S6). In the *tlr2* down-regulated 92-gene set, the immune related genes also were the largest portion (15%; Fig. 6E, 7F). Many of these genes are poorly annotated and include genes encoding cysteine proteases, a *nitr* gene, a *mafb* transcription factor gene and *hsp70*. Categories encompassing non-immune related genes are listed in Fig. S7. These results show that, upon infection with Mm, *tlr2* mutants show a dampened response of immune genes.

To show the relationship between DEGs, we constructed networks based on common expression targets in the 97 up- and 92 down-regulated genes [53]. The involved networks with

the up-regulated genes contain *lipc*, *nr0b2*, *hmgcr*, *itln1*, *fgf23*, *vdr*, *irak3* and *tlr8* (Fig. S8). In *tlr2*$^{+/-}$ controls we observed positively regulated *hmgcr*, *fgf23*, *vdr* and *tlr8*, and negatively regulated *nr0b2*, whereas *tlr2*$^{-/-}$ showed an opposite regulation for most of these genes. However, *lipc* and *irak3*, were positively regulated in both *tlr2*$^{+/-}$ and *tlr2*$^{-/-}$. For the 92 downregulated genes, a network containing *nr0b2* and *mafb* was constructed (Fig. S9). *nr0b2* and *mafb* were positively regulated in *tlr2*$^{-/-}$ zebrafish and down regulated in *tlr2*$^{+/-}$.

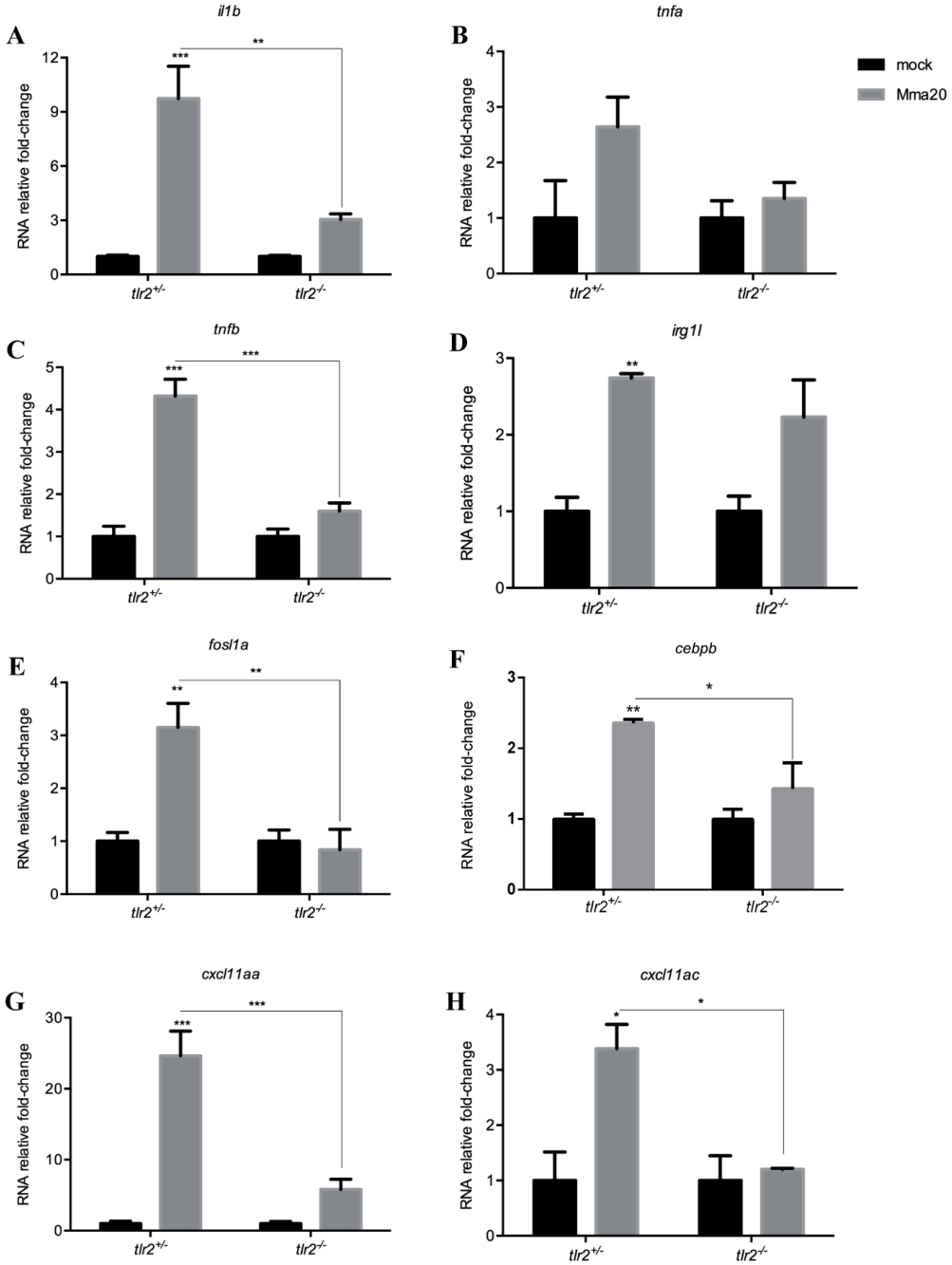

Figure 5 Immune genes expression in *tlr2*$^{+/-}$ and *tlr2*$^{-/-}$ fish lines infected with Mm. The expression levels of *il1b* (A), *tnfa* (B), *tnfb* (C), *irg1l* (D), *fosl1a* (E), *cebpb* (F), *cxcl11aa* (G) and *cxcl11ac* (H) were determined at 4dpi by qPCR. Data (mean ± SEM) are derived from at least three biological replicates (n = 10 embryos per group) and expressed relative to their corresponding mock injection (PBS) control, which is set at 1. Statistical significance of differences was determined by two-way ANOVA with Tukey's Multiple Comparison test as a post-hoc test. **P*<0.05, ***P*<0.01, ****P*<0.001

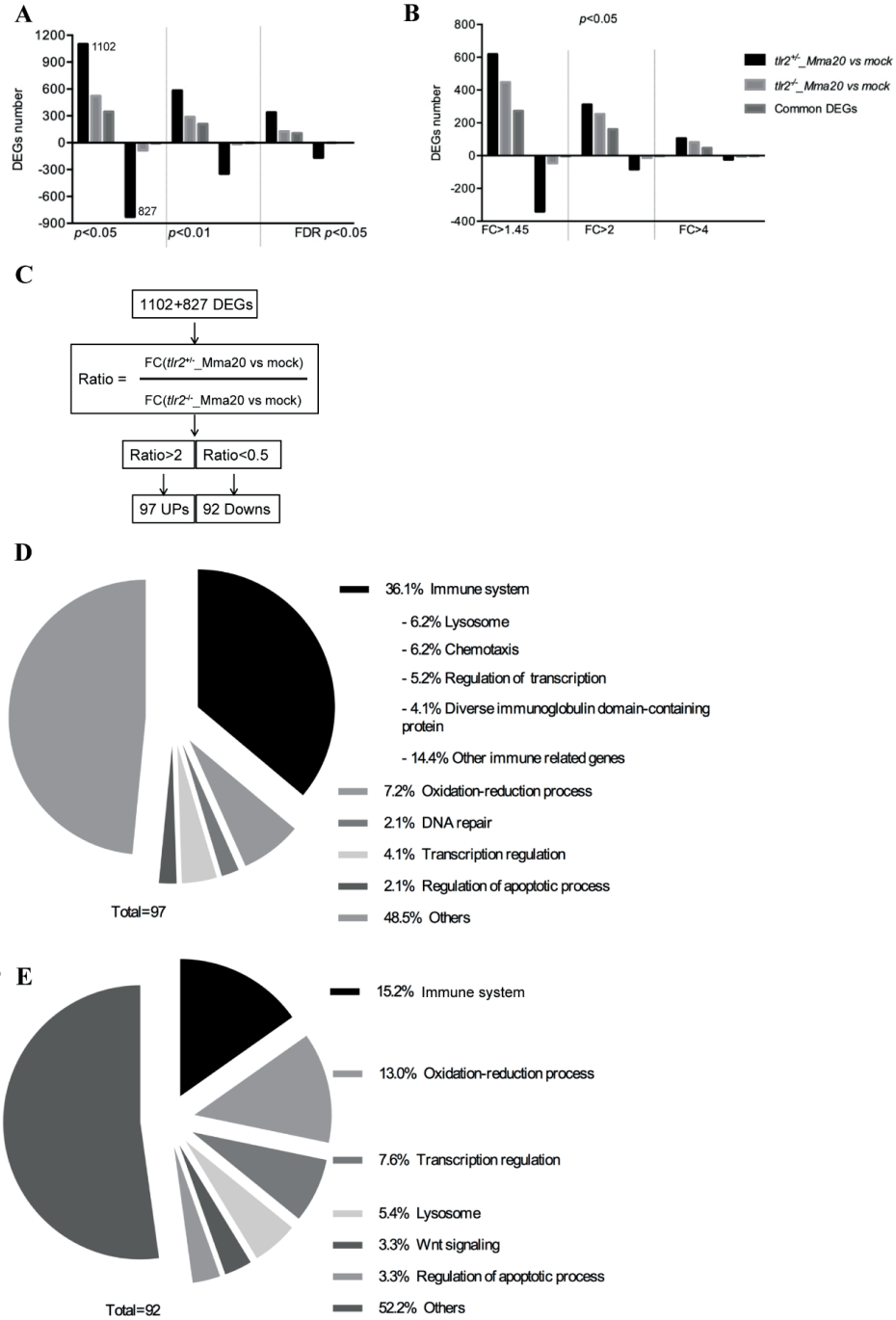

Figure 6 Overview of RNAseq results. (A, B) the number of DEGs of *tlr2*$^{+/-}$ and *tlr2*$^{-/-}$ strains infected with Mm compared to the control at different *p*-value and fold change. (C), the work flow of screening genes of which the regulation by infection is dependent on *tlr2*. (D), GO analysis of the 97 upregulated genes. (E), GO analysis of the 92 down-regulated genes. FC, fold-change.

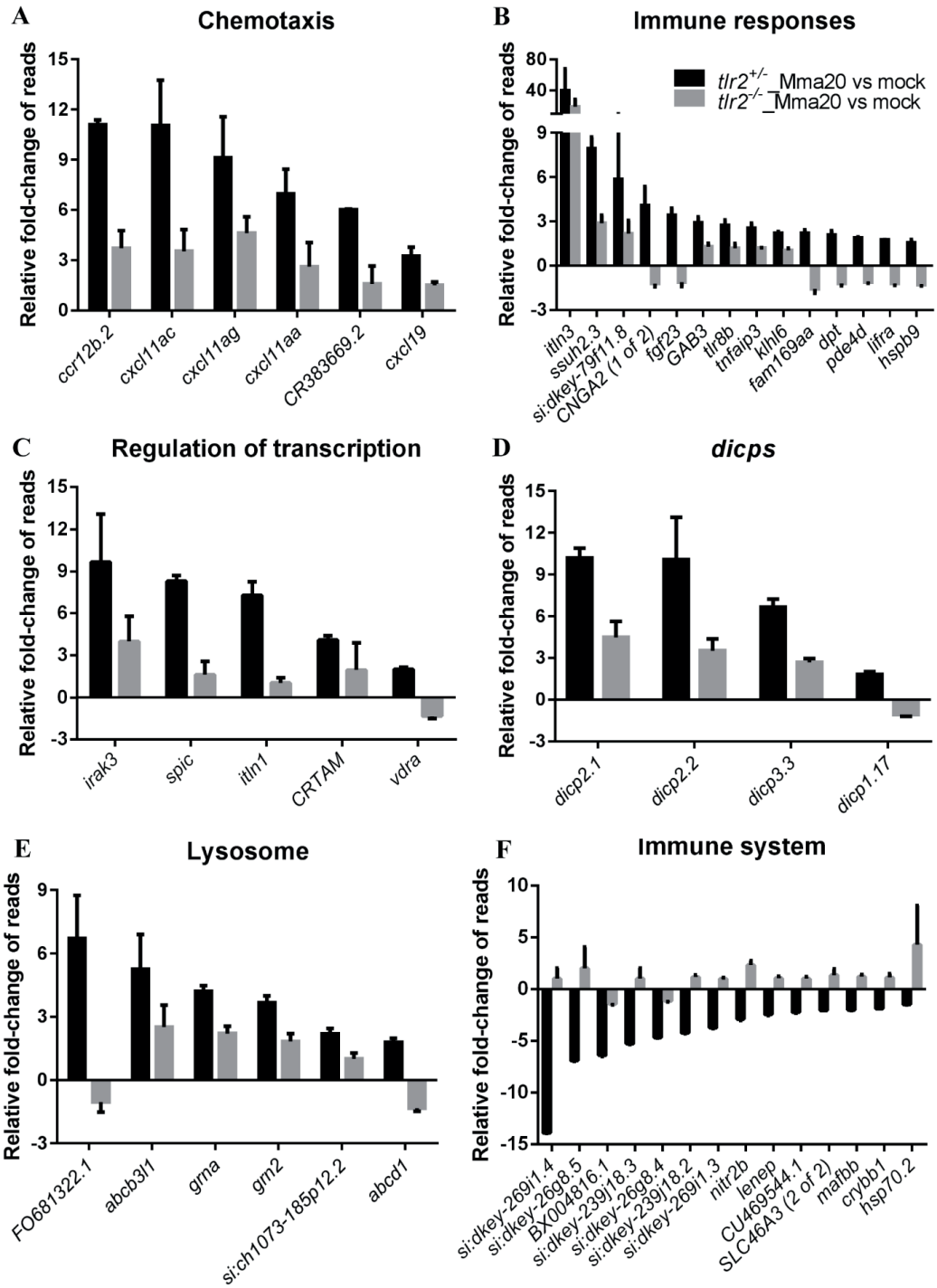

Figure 7 Overview of fold changes of representative genes selected from the gene categories resulting from GO-term analysis. (A-E): *tlr2*-dependent genes with up regulation corresponding to Fig. 6D. (F): *tlr2* specific genes with down regulation corresponding to Fig. 6E.

Enrichment analysis of Tlr2 specific genes after Mm infection

To link our data to gene sets defined based on prior biological knowledge (including GO), we conducted Gene-Set Enrichment Analysis (GSEA) of the differently expressed genes. This method derives its power by focusing on gene sets, that is, groups of genes that share common biological function, chromosomal location, or regulation [54]. Because the number of predicted gene sets were too large for our analysis method (more than 1,000 with $P < 0.05$), we focused on the gene sets related to metabolic, immunological and inflammation pathways. GSEA predicted 61 pathways in *tlr2*$^{+/-}$ and 67 pathways in *tlr2*$^{-/-}$ zebrafish responsive to Mm infection (Supplementary Table 4A and 4B). Interestingly, most of these pathways are common in *tlr2*$^{+/-}$ and *tlr2*$^{-/-}$, however some of them are detected as being anti-correlated in regulation, including some pathways underlying natural killer cell functions and omega-6-fatty acid metabolism (Supplementary Table 4C). We also performed Sub-Network Enrichment Analysis (SNEA) [55] to identify possible key genes that are responsible for the difference in response of the *tlr2*$^{+/-}$ and *tlr2*$^{-/-}$ group to Mm infection ($P < 0.05$). SNEA predicted 565 and 503 pathways for *tlr2*$^{+/-}$ and *tlr2*$^{-/-}$ zebrafish that are linked to the response to infection, respectively (Supplementary Table 4D and 4E), and 264 and 202 of them are specific for the response in *tlr2*$^{+/-}$ and *tlr2*$^{-/-}$ fish, respectively (Supplementary Table 4F). Since the RNAseq was conducted with the total RNA from whole body of zebrafish, it is not possible to define which pathways are involved in macrophage functions related to *tlr2* expression. Therefore, we analyzed previously published DNA microarray data (GDS4781) of human macrophages transfected with *Mtb* from Gene Expression Omnibus [56]. SNEA analysis of human macrophages shows that 659 pathways are linked to Mtb infection (Supplementary Table 4G). By comparing the human SNEA result to *tlr2*$^{+/-}$ specific pathways in zebrafish, 56 pathways were defined as *tlr2*$^{+/-}$-specific (Supplementary Table 4H). Of these, the pathway of TLR8, which has the lowest *P*-value in both zebrafish and human enrichment (Supplementary Table 4H), and its network is depicted as example in Figure S10. Overall, these analyses show that *tlr2*$^{-/-}$ mutants have a strongly altered immune response of which many pathways that are linked to human tuberculosis are differently responding.

Discussion

TLR2 has been shown to play a role in host defense against Mtb in several rodent studies but its role in host innate immunity during infection is still not clear. Moreover, little is known about the systemic regulation of down-stream signaling of TLR receptors in animal models. As part of this study we generated a *tlr2* zebrafish mutant to study Tlr2 function in the innate immune system during mycobacterial infection. Our results show a function of Tlr2 in defense against mycobacterial infection. This function is apparent by a larger number of extracellular bacteria and a lower number of granulomas in the *tlr2* mutant compared to the controls. This result is in agreement with *in vivo* studies in mice infected with tuberculosis bacteria that show a defect in granuloma formation in a Tlr2 mutant [19]. To obtain explanations and genetic markers for further studies of the effect of the *tlr2* mutation on infection we performed deep RNA sequencing to study the whole transcriptome profile in our mycobacterial infection model at the systems level. There are only a few RNA sequencing results of tuberculosis studies in rodents [57, 58], human serum [59], human pulmonary epithelial cells [60], and bovine systems.

To characterize the effect of *tlr2* mutation in the absence of infection, we compared the transcriptome of homozygous mutant larvae with that of heterozygote larvae, thereby excluding the effect of non-dominant background polymorphisms that might have resulted from ENU mutagenesis. The results show large differences between these genotypes, for instance in genes involved in glycolysis (Fig. S3). In accordance, a previous study in human peripheral blood mononuclear cells and an *in vivo* mouse model for tuberculosis showed a switch in host cellular metabolism toward aerobic glycolysis after mycobacterial infection that is dependent on TLR2 [61]. In agreement, our previous results in zebrafish larvae suggested a role in metabolism also for Myd88, the adaptor in TLR signaling [48]. The largest category of genes that was significantly affected in *tlr2* homozygous mutants was “neurological system process” (Supplementary table 2). Many recent studies show that a mutation in Tlr2 in mice resulted in effects of neuronal development and responses to injury [62, 63]. Some of these studies show a connection of Tlr2 deficiency to neuronal defects that could be related to Il10 function and autophagy [64, 65]. When focusing on the signaling pathways that could be involved, we observed that there was a significant effect in the GO category of transcription factors, namely the c-Maf factors that totals up to 546 representatives that were affected (Supplementary Table 3). The members of the Maf family of transcription factors, c-Maf and Mafb are specifically expressed in monocyte and macrophage lineages [66, 67], and in addition, c-Maf is also

expressed in T helper cells [67]. c-Maf was also reported to directly regulate IL-10 expression induced by LPS in macrophages [68]. Double deficiency of Mafb/c-Maf promotes self-renewal of differentiated macrophages [69]. We did not detect differences in macrophage numbers between *tlr2* mutants and controls, but it remains to be further investigated if macrophage differentiation is altered as a result of Tlr2 deficiency.

Recently, we have shown that Tlr2 and its adaptor MyD88 are important for the response of the zebrafish host to the microbiome [48]. Therefore, it is very well possible that the transcriptional differences we find in the *tlr2* mutant versus the controls are due to an aberrant response to the microbiome. Similarly, we have found that mutation in *myd88* leads to a large difference in the zebrafish gene expression profile, even in the absence of pathogenic infection[48]. This difference appeared to be dependent on the presence of a microbiome. In future work we therefore aim to study the transcriptome response of the *tlr2* mutant under germfree conditions and in the presence of a microbiome under gnotobiotic conditions and investigate whether the dysregulation of neural development pathways in *tlr2* mutants might be linked to control of the gut-brain axis [70-74]. Such studies could also show whether the composition of the microbiome affects the progression of mycobacterial infection. This could be clinically relevant, considering that recent studies show a correlation of the occurrence of tuberculosis with aberrations of the microbiome in human patients [75].

The analysis of differential gene expression during infection showed that there is a very pronounced effect of mutation of the *tlr2* gene. However, the expression of many genes is independent of *tlr2* as expected, since also other TLR receptors play a role in recognition of mycobacterial infections [76-79]. With respect to the number of genes affected, the strongest effect was observed in genes that are down regulated during infection, since this category was strongly diminished in the *tlr*2 mutant (Fig. 6A, B and Fig. S5). This observation suggests that Tlr2 has an important function in anti-inflammatory responses, in line with previous reports of studies in mice that showed a strongly decreased anti-inflammatory response in *Tlr2* knockouts [77, 78]. In a further analysis of the quantitative effects on the differences in expression levels of genes in both the up regulated and down regulated groups, we selected a number of genes that were most significantly affected in GO analysis (Fig. 6D, E). This GO analysis showed many groups to be affected with the immune response as the biggest group. We also performed GSEA and SNEA analyses (Fig. S8, S9, S10 and Supplementary Table 4) showing that the *tlr2* mutant has a very different immune response than heterozygote controls. Furthermore, we show

that many signaling pathways that have been reported to be linked to tuberculosis infection in humans are differentially regulated in our data set. Most significantly, activation of the Tlr8 pathway was strongly affected (Fig. S10). This evidence suggests that the Tlr2 signaling is strongly connected with Tlr8 function. *TLR8* mutations (polymorphisms) increase susceptibility to mycobacteria in the human population [79, 80]. Recently it was shown that TLR8 is a sensor of various bacteria in human primary monocytes [81]. This indication that TLR8 is a more important sensor in the antibacterial defense system than previously known might explain our SNEA results. In addition, our analysis revealed differential expression of three other interesting categories of immune genes, discussed below.

The vitamin D receptor pathway genes that are normally up-regulated during infection in zebrafish larvae were down regulated in the *tlr2* mutant. Furthermore, pathway analysis (Fig. S8 and S10) also implicated the expression of the Tlr8 pathway connected to vitamin D signaling as being strongly affected in the *tlr2* mutant. Vitamin D has been shown to be an important regulatory factor during tuberculosis [82] and has been linked previously to TLR2 function in studies in cell cultures [83]. Therefore, aberrant vitamin D signaling could be a major contributing factor to the hyper-susceptibility phenotype of *tlr2* mutants in Mm infection.

Tlr2 has been shown to be essential for the up-regulation of a group of genes that encode the Diverse Immunoglobulin Domain-Containing Proteins (DICPS) (Fig. 6D). This group is as novel multigene family encoding diversified immune receptors. Haire *et al*. [84] reported that recombinant DICP Ig domains bind lipids and lipid extracts of different bacteria, including Mtb and Mm, a property shared by mammalian CD300 and TREM family members. In the down-regulated set also several DICP members appear to be dependent on Tlr2, such as *dicp1.17*, *dicp3.3*, that are linked to the GO term insulin-like growth factor binding. These correlations might relate to functions of Tlr2 in other processes such as the control of diabetes type II by gut microbiota. However, the DICP gene family lacks easily recognizable genetic homologs in mammals, making a translation to a function in mammalian tuberculosis and other diseases currently not yet possible [85].

Another highly relevant category of genes of which the induction or repression during infection is dependent on Tlr2 includes the chemokines. In a previous study of our laboratory, Torraca *et al*. demonstrated the function of the Cxcr3-Cxcl11 axis in macrophage recruitment to infection foci and showed that disruption of this axis by *cxcr3.2* mutation increases the resistance to

mycobacterial infection [51]. Furthermore, by Fluorescence-activated cell sorting (FACS) of Mm-infected cells, we recently showed that *cxcl11a* is a robust marker of infected macrophages [52]. The infection induced expression of this chemokine is dependent on Myd88, the common adaptor of the majority of Tlrs, including *tlr2* [52]. In agreement, the *tlr2* mutant shows a significant lower expression of *cxcl11aa* and also of an related chemokine, *cxcl11ac,* during Mm infection (Fig. 5). Considering the large number of other chemokines that are controlled by Tlr2 during infection, it is clear that the integrative network of connections cannot yet be understood from these expression studies and need more detailed functional analyses, e.g. by combinations of different mutations or directed studies on responses to chemokines as shown by Torraca *et al* [51]. However, we can state that the phenotype of the *tlr2* mutant, at the infection level, and the level of transcriptional control such as the mentioned effects on regulation of MafB/c-Maf and chemokines shows a clear connection with macrophage chemotaxis. These evidences do not exclude that Tlr2 has many other functions during infection such as phagocytosis. For instance, Blander *et al*. [86] and Rahman *et al*. [87] showed that phagocytosis of bacteria and phagosome maturation are impaired in the absence of TLR signaling. Therefore, the large number of unannotated genes of which the expression during infection is dependent on Tlr2 is also worth studying in more detail in future studies.

Conclusion

Our study shows that Tlr2, as a part of innate immunity, plays an important role in controlling mycobacterial infection as observed on the transcriptome and infection level. This function may be mediated by several mechanisms, including a general attenuation of the inflammatory response, reduced mycobacterial dissemination by dampening of CXCR3-CXCL11 signaling, and anti-mycobacterial effects like vitamin D signaling. Our results show that Tlr2 is a major Tlr family member upstream of Myd88 that activates the CXCR3-CXCL11 signaling axis. The *tlr2* mutant is therefore a valuable model for further studies using published infection models for other pathogens and the study of the interactions with gut microbiota in zebrafish larvae.

Materials and Methods

Zebrafish husbandry

All zebrafish were handled in compliance with the local animal welfare regulations and maintained according to standard protocols (zfin.org). Larvae were raised in egg water (60 g/ml Instant Ocean sea salts) at 28.5 °C. For the duration of bacterial injections, larvae were kept under anesthesia in egg water containing 0.02% buffered 3-aminobenzoic acid ethyl ester (Tricaine, Sigma-Aldrich, the Netherlands). The culture of zebrafish with mutations in immune genes was approved by the local animal welfare committee (DEC) of the University of Leiden (protocol 14198). All protocols adhered to the international guidelines specified by the EU Animal Protection Directive 2010/63/EU.

The *tlr2*^{sa19423} mutant line (ENU-mutagenized) was obtained from the Sanger Institute Zebrafish Mutation Resource (Hinxton, Cambridge, UK) and shipped by the Zebrafish Resource Center of the Karlsruhe Institute of Technology. The mutant allele was identified by sequencing. Heterozygous carriers of the mutation were outcrossed three times against wild type (*AB* strain), and were subsequently incrossed three times. Heterozygous fish of the resulting family were used to produce embryos. Homozygous mutants were outcrossed to the *Tg*(*mpeg1:mCherry-F);TgBAC(mpx:EGFP)* double transgenic line [88, 89], and the offspring with GFP and mCherry fluorescence were subsequently incrossed to produce the *Tg*(*mpeg1:mCherry-F);TgBAC(mpx:EGFP)* line.

Bacterial strain preparation

The bacterial strain, *Mycobacterium marinum* m20 (Mma20) expressing mCherry fluorescent protein [90], was used in this study. For the infection to zebrafish larvae, the bacteria were prepared as previously described [91]. The infection inoculum was prepared in 2% polyvinylpyrrolidone40 solution (Calbiochem, the Netherlands), and 150 colony-forming units (CFU) of bacteria were injected into the blood stream at 28 hours post fertilization (hpf) as previously described [92].

Ligands injection

Purified Pam3CSK4 (InvivoGen, France) and flagellin from *S. typhimurium* (Flagellin FliC VacciGrade™, Invitrogen, France) were diluted in 1 mg/ml and 100 µg/ml in sterile water,

respectively. For injection, 1 nl of the ligand solutions were injected into the blood stream at 28 hpf. Sterile water was injected as a control experiment. Injections were performed using a FemtoJet microinjector (Eppendorf, the Netherlands) equipped with a capillary glass needle.

Bacterial burden imaging and quantification

Pools of 20 larvae were collected at 3- and 4-day post infection (dpi) and imaged by using the Leica MZ16FA Fluorescence Stereo Microscope (Leica Microsystems, Wetzlar Germany) equipped with the DFC420C color camera (Leica Microsystems). Bacterial loads were analyzed using dedicated pixel counting software as previously described [93].

Confocal laser scanning microscopy imaging and image quantification

Larvae (2 dpf) were embedded in 1% low melting point agarose (Sigma Aldrich), and image acquisition was performed by using a Leica TCS SP8 confocal microscope (Leica Microsystems) with a 10 times magnification objective (N.A. 0.40). Acquisition settings and area of imaging (in the caudal vein region) were kept the same across the groups for macrophages and neutrophils number counting (Fig. 1 J, K) and pixel counting (Fig. S1). Experiments were performed in two independent series. Double fluorescent lines *tlr2*$^{+/+}$ *Tg*(*mpeg1:mCherry-F);TgBAC(mpx:EGFP)* and *tlr2*$^{-/-}$ *Tg*(*mpeg1:mCherry-F);TgBAC(mpx:EGFP)* were used for macrophages and neutrophils number counting. Macrophage and neutrophil cell counting was either performed manually or by using the plugin Find Maxima in Fiji (http://imagej.nih.gov/ij/docs/menus/ process.html#find-maxima) (Fig. 1 J, K) using projections of the z-series. 25 individual larvae for each group were used for counting and representative images are given in Fig. 1H, I. With manual counting the z-series data was examined in cases when it was unclear whether the fluorescent pixels presented one or multiple cells. The result of manual cell counting (Fig. S11) is comparable with the result of automated cell counting using Fiji. Pixel counting of the double transgenic lines (Fig. 1S A, B) was performed using dedicated pixel counting software as well as previously described [93]. For CLSM analysis of progression of infection of Fig. 4 we used Fiji software. To quantify the number of bacteria outside macrophages, total bacteria pixel count was quantified by Fiji software and followed by subtracting this number with the number of co-localised pixels. Co-localisation of macrophage and bacterial pixels was performed using a custom made script written in Java. For this experiment we used three objectives: 10x (N.A. 0.40), 20x (N.A. 0.75), 63x (oil immersion, N.A. 1.40) magnification.

RNA isolation, cDNA synthesis and qPCR

Total RNAs were extracted using TRIzol Reagent (Life Technologies) and purified using RNeasy MinElute Cleanup Kit (Qiagen, the Netherlands). The concentration and quality of RNAs were evaluated by NanoDrop 2000 (Thermo Scientific, the Netherlands). cDNAs were synthesized from 1 μg total RNAs and qPCR were performed by using the iScript™ cDNA Synthesis Kit (BioRad, the Netherlands) and iQ™ SYBR Green Supermix (BioRad) and normalized against the expression of *ppial* as a housekeeping gene [94]. Results were analyzed using the ΔΔCt method [95]. Primer sequences are described in Supplementary Table 5.

Deep sequencing and data analysis

Triplicates of 10 larvae of *tlr2*$^{+/-}$ and *tlr2*$^{-/-}$ with PBS (as control) or Mma20 injection, were homogenized in 300ul of TRIzol reagent, and total RNAs were purified as described above. RNAseq was performed using Illumina Hi-Seq 2500 as previously described [96]. The raw data is available in the NCBI GEO database under accession number GSE102766. The RNAseq data were mapped on the zebrafish genome (version GRCz10) and tag counts were performed by Bowtie 2 using GeneTiles software (http://www. genetiles. com) [97]. Then, we performed normalization and gene expression analysis using the R package and DESeq2 [98]. After statistical tests, we performed further bioinformatics analyses Gene-Set Enrichment Analysis [54], Sub-Network Enrichment Analysis [55] and Pathway Enrichment Analysis [99]. For creating gene networks based on common regulatory targets, we used Pathway Studio 9.0 (Elsevier, Amsterdam, the Netherlands) as previously described [53].

Comparison of edgeR and DEseq2: EdgeR and DEseq2 differ mainly in the aspects of normalization and estimation of the dispersion parameters. Normalization in edgeR is done via the trimmed mean of M values, while in DEseq2 this is done by comparing each library with a virtual library based on the relative log expressions. The dispersion parameters in edgeR are estimated by empirical Bayes and are therefore shrunken towards the overall mean of the estimates. Dispersion in DEseq2 is estimated by taking the maximum of the individual dispersions and the mean trend of the dispersions. As a consequence, edgeR tends to be more sensitive to outliers, while DEseq2 is less powerful [49].

Statistical analyses

Graphpad Prism software (Version 8.1.1; GraphPad Software, San Diego, CA, USA) was used for statistical analysis. All experiment data are shown as mean ± SEM. In the gene expression profiles of zebrafish treated with the TLR2 agonist (Fig. 1 B-G) and in immune gene expression in *tlr2*$^{+/-}$ and *tlr2*$^{-/-}$ fish lines infected with Mm (Fig. 5), statistical significance of differences was determined by two-way ANOVA with Tukey's Multiple Comparison test as a post-hoc test. The other experiments were analyzed by using unpaired, two-tailed t-tests for comparisons between two groups and one-way ANOVA with Tukey's multiple comparison methods as a post-hoc test for comparisons between more than two groups. For percent survival analysis (Fig. 3 F), statistical significance of difference was determined by a log-rank (Mantel-Cox) test. (ns, no significant difference; *p<0.05; **p<0.01; ***p<0.001; ****p<0.0001).

Acknowledgments

We thank all members of the fish facility team for fish caretaking. We would like to thank our colleagues from Leiden University: Lanpeng Chen and Gerda E.M. Lamers for assistance with confocal laser scanning imaging and Joost J. Willemse for providing microscopic analysis programs. We also thank Vincenzo Torraca (London School of Hygiene & Tropical Medicine) for helpful discussions and the qPCR primers of *cxcl11*-like genes. The zebrafish *tlr2* mutant was obtained from the Sanger Institute Zebrafish Mutation Resource (ZF-MODELS Integrated Project funded by the European Commission; contract number LSHG-CT-2003-503496), also sponsored by the Welcome Trust [grant number WT 077047/Z/05/Z].

References

1. Ramakrishnan L. The zebrafish guide to tuberculosis immunity and treatment. Cold Spring Harbor symposia on quantitative biology. 2013;78:179-92. Epub 2014/03/20. doi: 10.1101/sqb.2013.78.023283. PubMed PMID: 24643219.

2. Co DO, Hogan LH, Kim SI, Sandor M. Mycobacterial granulomas: keys to a long-lasting host-pathogen relationship. Clin Immunol. 2004;113(2):130-6. Epub 2004/09/29. doi: 10.1016/j.clim.2004.08.012. PubMed PMID: 15451467.

3. Salgame P. Host innate and Th1 responses and the bacterial factors that control Mycobacterium tuberculosis infection. Curr Opin Immunol. 2005;17(4):374-80. Epub 2005/06/21. doi: 10.1016/j.coi.2005.06.006. PubMed PMID: 15963709.

4. Ramakrishnan L. Revisiting the role of the granuloma in tuberculosis. Nature reviews Immunology. 2012;12(5):352-66. Epub 2012/04/21. doi: 10.1038/nri3211. PubMed PMID: 22517424.

5. Jo EK, Yang CS, Choi CH, Harding CV. Intracellular signalling cascades regulating innate immune responses to Mycobacteria: branching out from Toll-like receptors. Cell Microbiol. 2007;9(5):1087-98. Epub 2007/03/16. doi: 10.1111/j.1462-5822.2007.00914.x. PubMed PMID: 17359235.

6. Tapping RI, Tobias PS. Mycobacterial lipoarabinomannan mediates physical interactions between TLR1 and TLR2 to induce signaling. J Endotoxin Res. 2003;9(4):264-8. Epub 2003/08/26. doi: 10.1179/096805103225001477. PubMed PMID: 12935358.

7. Means TK, Jones BW, Schromm AB, Shurtleff BA, Smith JA, Keane J, et al. Differential effects of a Toll-like receptor antagonist on Mycobacterium tuberculosis-induced macrophage responses. J Immunol. 2001;166(6):4074-82. Epub 2001/03/10. PubMed PMID: 11238656.

8. Quesniaux VJ, Nicolle DM, Torres D, Kremer L, Guerardel Y, Nigou J, et al. Toll-like receptor 2 (TLR2)-dependent-positive and TLR2-independent-negative regulation of proinflammatory cytokines by mycobacterial lipomannans. J Immunol. 2004;172(7):4425-34. Epub 2004/03/23. PubMed PMID: 15034058.

9. Jung SB, Yang CS, Lee JS, Shin AR, Jung SS, Son JW, et al. The mycobacterial 38-kilodalton glycolipoprotein antigen activates the mitogen-activated protein kinase pathway and release of proinflammatory cytokines through Toll-like receptors 2 and 4 in human monocytes. Infect Immun. 2006;74(5):2686-96. Epub 2006/04/20. doi: 10.1128/iai.74.5.2686-2696.2006. PubMed PMID: 16622205; PubMed Central PMCID: PMCPMC1459749.

10. Brightbill HD, Libraty DH, Krutzik SR, Yang RB, Belisle JT, Bleharski JR, et al. Host defense mechanisms triggered by microbial lipoproteins through toll-like receptors. Science. 1999;285(5428):732-6. Epub 1999/07/31. PubMed PMID: 10426995.

11. Noss EH, Pai RK, Sellati TJ, Radolf JD, Belisle J, Golenbock DT, et al. Toll-like receptor 2-dependent inhibition of macrophage class II MHC expression and antigen processing by 19-kDa lipoprotein of Mycobacterium tuberculosis. J Immunol. 2001;167(2):910-8. Epub 2001/07/07. PubMed PMID: 11441098.

12. Gilleron M, Quesniaux VF, Puzo G. Acylation state of the phosphatidylinositol hexamannosides from Mycobacterium bovis bacillus Calmette Guerin and mycobacterium tuberculosis H37Rv and its implication in Toll-like receptor response. J Biol Chem. 2003;278(32):29880-9. Epub 2003/05/31. doi: 10.1074/jbc.M303446200. PubMed PMID: 12775723.

13. Gilleron M, Nigou J, Nicolle D, Quesniaux V, Puzo G. The acylation state of mycobacterial lipomannans modulates innate immunity response through toll-like receptor 2. Chem Biol. 2006;13(1):39-47. Epub 2006/01/24. doi: 10.1016/j.chembiol.2005.10.013. PubMed PMID: 16426970.

14. Takeuchi O, Sato S, Horiuchi T, Hoshino K, Takeda K, Dong Z, et al. Cutting edge: role of Toll-like receptor 1 in mediating immune response to microbial lipoproteins. J Immunol. 2002;169(1):10-4. Epub 2002/06/22. PubMed PMID: 12077222.

15. Takeuchi O, Kawai T, Mühlradt PF, Morr M, Radolf JD, Zychlinsky A, et al. Discrimination of bacterial lipoproteins by Toll-like receptor 6. International Immunology. 2001;13(7):933-40. doi: 10.1093/intimm/13.7.933.

16. Marinho FAV, de Paula RR, Mendes AC, de Almeida LA, Gomes MTR, Carvalho NB, et al. Toll-like receptor 6 senses Mycobacterium avium and is required for efficient control of mycobacterial infection. European Journal of Immunology. 2013;43(9):2373-85. doi: 10.1002/eji.201243208.

17. Basu J, Shin DM, Jo EK. Mycobacterial signaling through toll-like receptors. Front Cell Infect Microbiol. 2012;2:145. Epub 2012/11/29. doi: 10.3389/fcimb.2012.00145. PubMed PMID: 23189273; PubMed Central PMCID: PMCPMC3504976.

18. Underhill DM, Ozinsky A, Smith KD, Aderem A. Toll-like receptor-2 mediates mycobacteria-induced proinflammatory signaling in macrophages. Proc Natl Acad Sci U S A. 1999;96(25):14459-63. Epub 1999/12/10. PubMed PMID: 10588727; PubMed Central PMCID: PMCPMC24458.

19. Carlos D, Frantz FG, Souza-Junior DA, Jamur MC, Oliver C, Ramos SG, et al. TLR2-dependent mast cell activation contributes to the control of Mycobacterium tuberculosis infection. Microbes Infect. 2009;11(8-9):770-8. Epub 2009/05/16. doi: 10.1016/j.micinf.2009.04.025. PubMed PMID: 19442756.

20. Reiling N, Holscher C, Fehrenbach A, Kroger S, Kirschning CJ, Goyert S, et al. Cutting edge: Toll-like receptor (TLR)2- and TLR4-mediated pathogen recognition in resistance to airborne infection with Mycobacterium tuberculosis. J Immunol. 2002;169(7):3480-4. Epub 2002/09/24. PubMed PMID: 12244136.

21. Drennan MB, Nicolle D, Quesniaux VJ, Jacobs M, Allie N, Mpagi J, et al. Toll-like receptor 2-deficient mice succumb to Mycobacterium tuberculosis infection. Am J Pathol. 2004;164(1):49-57. Epub 2003/12/26. doi: 10.1016/s0002-9440(10)63095-7. PubMed PMID: 14695318; PubMed Central PMCID: PMCPMC1602241.

22. McBride A, Konowich J, Salgame P. Host defense and recruitment of Foxp3(+) T regulatory cells to the lungs in chronic Mycobacterium tuberculosis infection requires toll-like receptor 2. PLoS Pathog. 2013;9(6):e1003397. Epub 2013/06/21. doi: 10.1371/journal.ppat.1003397. PubMed PMID: 23785280; PubMed Central PMCID: PMCPMC3681744.

23. Ogus AC, Yoldas B, Ozdemir T, Uguz A, Olcen S, Keser I, et al. The Arg753GLn polymorphism of the human toll-like receptor 2 gene in tuberculosis disease. Eur Respir J. 2004;23(2):219-23. PubMed PMID: 14979495.

24. Biswas D, Gupta SK, Sindhwani G, Patras A. TLR2 polymorphisms, Arg753Gln and Arg677Trp, are not associated with increased burden of tuberculosis in Indian patients. BMC research notes. 2009;2:162. Epub 2009/08/19. doi: 10.1186/1756-0500-2-162. PubMed PMID: 19686607; PubMed Central PMCID: PMCPMC2732632.

25. Gehring AJ, Dobos KM, Belisle JT, Harding CV, Boom WH. Mycobacterium tuberculosis LprG (Rv1411c): a novel TLR-2 ligand that inhibits human macrophage class II MHC antigen processing. J Immunol. 2004;173(4):2660-8. Epub 2004/08/06. PubMed PMID: 15294983.

26. Saraav I, Singh S, Sharma S. Outcome of Mycobacterium tuberculosis and Toll-like receptor interaction: immune response or immune evasion? Immunol Cell Biol. 2014;92(9):741-6. Epub 2014/07/02. doi: 10.1038/icb.2014.52. PubMed PMID: 24983458.

27. Netea MG, Van der Meer JW, Kullberg BJ. Toll-like receptors as an escape mechanism from the host defense. Trends Microbiol. 2004;12(11):484-8. Epub 2004/10/19. doi: 10.1016/j.tim.2004.09.004. PubMed PMID: 15488388.

28. Noss EH, Harding CV, Boom WH. Mycobacterium tuberculosis inhibits MHC class II antigen processing in murine bone marrow macrophages. Cell Immunol. 2000;201(1):63-74. Epub 2000/05/12. doi: 10.1006/cimm.2000.1633. PubMed PMID: 10805975.

29. Netea MG, Sutmuller R, Hermann C, Van der Graaf CA, Van der Meer JW, van Krieken JH, et al. Toll-like receptor 2 suppresses immunity against Candida albicans through induction of IL-10 and regulatory T cells. J Immunol. 2004;172(6):3712-8. Epub 2004/03/09. PubMed PMID: 15004175.

30. Sing A, Rost D, Tvardovskaia N, Roggenkamp A, Wiedemann A, Kirschning CJ, et al. Yersinia V-antigen exploits toll-like receptor 2 and CD14 for interleukin 10-mediated immunosuppression. J Exp Med. 2002;196(8):1017-24. Epub 2002/10/23. PubMed PMID: 12391013; PubMed Central PMCID: PMCPMC2194041.

31. Gehring AJ, Rojas RE, Canaday DH, Lakey DL, Harding CV, Boom WH. The Mycobacterium tuberculosis 19-kilodalton lipoprotein inhibits gamma interferon-regulated HLA-DR and Fc gamma R1 on human macrophages through Toll-like receptor 2. Infect Immun. 2003;71(8):4487-97. Epub 2003/07/23. PubMed PMID: 12874328; PubMed Central PMCID: PMCPMC166015.

32. Alvarez GR, Zwilling BS, Lafuse WP. Mycobacterium avium inhibition of IFN-gamma signaling in mouse macrophages: Toll-like receptor 2 stimulation increases expression of dominant-negative STAT1 beta by mRNA stabilization. J Immunol. 2003;171(12):6766-73. Epub 2003/12/10. PubMed PMID: 14662881.

33. Agrawal S, Agrawal A, Doughty B, Gerwitz A, Blenis J, Van Dyke T, et al. Cutting edge: different Toll-like receptor agonists instruct dendritic cells to induce distinct Th responses via differential modulation of extracellular signal-regulated kinase-mitogen-activated protein kinase and c-Fos. J Immunol. 2003;171(10):4984-9. Epub 2003/11/11. PubMed PMID: 14607893.

34. Lam SH, Chua HL, Gong Z, Lam TJ, Sin YM. Development and maturation of the immune system in zebrafish, Danio rerio: a gene expression profiling, in situ hybridization and immunological study. Dev Comp Immunol. 2004;28(1):9-28. Epub 2003/09/10. PubMed PMID: 12962979.

35. Willett CE, Cortes A, Zuasti A, Zapata AG. Early hematopoiesis and developing lymphoid organs in the zebrafish. Developmental dynamics : an official publication of the American Association of Anatomists. 1999;214(4):323-36. Epub 1999/04/23. doi: 10.1002/(sici)1097-0177(199904)214:4<323::aid-aja5>3.0.co;2-3. PubMed PMID: 10213388.

36. Swaim LE, Connolly LE, Volkman HE, Humbert O, Born DE, Ramakrishnan L. Mycobacterium marinum Infection of Adult Zebrafish Causes Caseating Granulomatous Tuberculosis and Is Moderated by

Adaptive Immunity. Infection and Immunity. 2006;74(11):6108-17. doi: 10.1128/IAI.00887-06. PubMed PMID: PMC1695491.

37. Davis JM, Clay H, Lewis JL, Ghori N, Herbomel P, Ramakrishnan L. Real-time visualization of mycobacterium-macrophage interactions leading to initiation of granuloma formation in zebrafish embryos. Immunity. 2002;17(6):693-702. Epub 2002/12/14. PubMed PMID: 12479816.

38. Meijer AH. Protection and pathology in TB: learning from the zebrafish model. Semin Immunopathol. 2016;38(2):261-73. Epub 2015/09/02. doi: 10.1007/s00281-015-0522-4. PubMed PMID: 26324465; PubMed Central PMCID: PMCPMC4779130.

39. Cronan MR, Tobin DM. Fit for consumption: zebrafish as a model for tuberculosis. Disease models & mechanisms. 2014;7(7):777-84. Epub 2014/06/29. doi: 10.1242/dmm.016089. PubMed PMID: 24973748; PubMed Central PMCID: PMCPMC4073268.

40. Lesley R, Ramakrishnan L. Insights into early mycobacterial pathogenesis from the zebrafish. Current opinion in microbiology. 2008;11(3):277-83.

41. Arora G, Misra R, Sajid A. Model Systems for Pulmonary Infectious Diseases: Paradigms of Anthrax and Tuberculosis. Curr Top Med Chem. 2017;17(18):2077-99. Epub 2017/02/01. doi: 10.2174/1568026617666170130111324. PubMed PMID: 28137237.

42. Kanwal Z, Wiegertjes GF, Veneman WJ, Meijer AH, Spaink HP. Comparative studies of Toll-like receptor signalling using zebrafish. Developmental & Comparative Immunology. 2014;46(1):35-52.

43. van der Vaart M, Korbee CJ, Lamers GE, Tengeler AC, Hosseini R, Haks MC, et al. The DNA damage-regulated autophagy modulator DRAM1 links mycobacterial recognition via TLR-MYD88 to autophagic defense. Cell host & microbe. 2014;15(6):753-67.

44. van der Vaart M, van Soest JJ, Spaink HP, Meijer AH. Functional analysis of a zebrafish myd88 mutant identifies key transcriptional components of the innate immune system. Disease models & mechanisms. 2013;6(3):841-54.

45. Yang S, Marin-Juez R, Meijer AH, Spaink HP. Common and specific downstream signaling targets controlled by Tlr2 and Tlr5 innate immune signaling in zebrafish. BMC Genomics. 2015;16:547. Epub 2015/07/26. doi: 10.1186/s12864-015-1740-9. PubMed PMID: 26208853; PubMed Central PMCID: PMCPMC4514945.

46. Medzhitov R, Preston-Hurlburt P, Kopp E, Stadlen A, Chen C, Ghosh S, et al. MyD88 is an adaptor protein in the hToll/IL-1 receptor family signaling pathways. Mol Cell. 1998;2(2):253-8. Epub 1998/09/12. PubMed PMID: 9734363.

47. Fitzgerald KA, Palsson-McDermott EM, Bowie AG, Jefferies CA, Mansell AS, Brady G, et al. Mal (MyD88-adapter-like) is required for Toll-like receptor-4 signal transduction. Nature. 2001;413(6851):78-83. Epub 2001/09/07. doi: 10.1038/35092578. PubMed PMID: 11544529.

48. Koch BEV, Yang S, Lamers G, Stougaard J, Spaink HP. Intestinal microbiome adjusts the innate immune setpoint during colonization through negative regulation of MyD88. Nat Commun. 2018;9(1):4099. Epub 2018/10/07. doi: 10.1038/s41467-018-06658-4. PubMed PMID: 30291253; PubMed Central PMCID: PMCPMC6173721.

49. Anders S, McCarthy DJ, Chen Y, Okoniewski M, Smyth GK, Huber W, et al. Count-based differential expression analysis of RNA sequencing data using R and Bioconductor. Nature protocols. 2013;8(9):1765-86. Epub 2013/08/27. doi: 10.1038/nprot.2013.099. PubMed PMID: 23975260.

50. Clay H, Volkman HE, Ramakrishnan L. Tumor necrosis factor signaling mediates resistance to mycobacteria by inhibiting bacterial growth and macrophage death. Immunity. 2008;29(2):283-94. Epub 2008/08/12. doi: 10.1016/j.immuni.2008.06.011. PubMed PMID: 18691913; PubMed Central PMCID: PMCPMC3136176.

51. Torraca V, Cui C, Boland R, Bebelman JP, van der Sar AM, Smit MJ, et al. The CXCR3-CXCL11 signaling axis mediates macrophage recruitment and dissemination of mycobacterial infection. Disease models & mechanisms. 2015;8(3):253-69. Epub 2015/01/13. doi: 10.1242/dmm.017756. PubMed PMID: 25573892; PubMed Central PMCID: PMCPMC4348563.

52. Rougeot J, Torraca V, Zakrzewska A, Kanwal Z, Jansen HJ, Sommer F, et al. RNAseq Profiling of Leukocyte Populations in Zebrafish Larvae Reveals a cxcl11 Chemokine Gene as a Marker of Macrophage Polarization During Mycobacterial Infection. Frontiers in Immunology. 2019;10. doi: ARTN 832

10.3389/fimmu.2019.00832. PubMed PMID: WOS:000465045400003.

53. Nikitin A, Egorov S, Daraselia N, Mazo I. Pathway studio--the analysis and navigation of molecular networks. Bioinformatics. 2003;19(16):2155-7. PubMed PMID: 14594725.

54. Subramanian A, Tamayo P, Mootha VK, Mukherjee S, Ebert BL, Gillette MA, et al. Gene set enrichment analysis: a knowledge-based approach for interpreting genome-wide expression profiles. Proc Natl Acad Sci U S A. 2005;102(43):15545-50. doi: 10.1073/pnas.0506580102. PubMed PMID: 16199517; PubMed Central PMCID: PMCPMC1239896.

55. Kotelnikova E, Yuryev A, Mazo I, Daraselia N. Computational approaches for drug repositioning and combination therapy design. J Bioinform Comput Biol. 2010;8(3):593-606. PubMed PMID: 20556864.

56. Verway M, Bouttier M, Wang TT, Carrier M, Calderon M, An BS, et al. Vitamin D induces interleukin-1beta expression: paracrine macrophage epithelial signaling controls M. tuberculosis infection. PLoS Pathog. 2013;9(6):e1003407. Epub 2013/06/14. doi: 10.1371/journal.ppat.1003407. PubMed PMID: 23762029; PubMed Central PMCID: PMCPMC3675149.

57. Leisching G, Pietersen RD, Mpongoshe V, van Heerden C, van Helden P, Wiid I, et al. The Host Response to a Clinical MDR Mycobacterial Strain Cultured in a Detergent-Free Environment: A Global Transcriptomics Approach. PLoS One. 2016;11(4):e0153079. Epub 2016/04/08. doi: 10.1371/journal.pone.0153079. PubMed PMID: 27055235; PubMed Central PMCID: PMCPMC4824497.

58. Kubler A, Larsson C, Luna B, Andrade BB, Amaral EP, Urbanowski M, et al. Cathepsin K Contributes to Cavitation and Collagen Turnover in Pulmonary Tuberculosis. J Infect Dis. 2016;213(4):618-27. Epub 2015/09/30. doi: 10.1093/infdis/jiv458. PubMed PMID: 26416658; PubMed Central PMCID: PMCPMC4721912.

59. Zhang H, Sun Z, Wei W, Liu Z, Fleming J, Zhang S, et al. Identification of serum microRNA biomarkers for tuberculosis using RNA-seq. PLoS One. 2014;9(2):e88909. Epub 2014/03/04. doi: 10.1371/journal.pone.0088909. PubMed PMID: 24586438; PubMed Central PMCID: PMCPMC3930592.

60. Mvubu NE, Pillay B, Gamieldien J, Bishai W, Pillay M. Canonical pathways, networks and transcriptional factor regulation by clinical strains of Mycobacterium tuberculosis in pulmonary alveolar epithelial cells. Tuberculosis (Edinb). 2016;97:73-85. Epub 2016/03/17. doi: 10.1016/j.tube.2015.12.002. PubMed PMID: 26980499.

61. Lachmandas E, Beigier-Bompadre M, Cheng SC, Kumar V, van Laarhoven A, Wang X, et al. Rewiring cellular metabolism via the AKT/mTOR pathway contributes to host defence against Mycobacterium tuberculosis in human and murine cells. Eur J Immunol. 2016;46(11):2574-86. Epub 2016/11/05. doi: 10.1002/eji.201546259. PubMed PMID: 27624090; PubMed Central PMCID: PMCPMC5129526.

62. Ziegler G, Freyer D, Harhausen D, Khojasteh U, Nietfeld W, Trendelenburg G. Blocking TLR2 in vivo protects against accumulation of inflammatory cells and neuronal injury in experimental stroke. J Cereb Blood Flow Metab. 2011;31(2):757-66. Epub 2010/09/16. doi: 10.1038/jcbfm.2010.161. PubMed PMID: 20842165; PubMed Central PMCID: PMCPMC3049529.

63. Hoffmann O, Braun JS, Becker D, Halle A, Freyer D, Dagand E, et al. TLR2 mediates neuroinflammation and neuronal damage. J Immunol. 2007;178(10):6476-81. Epub 2007/05/04. PubMed PMID: 17475877.

64. Gu Y, Zhang Y, Bi Y, Liu J, Tan B, Gong M, et al. Mesenchymal stem cells suppress neuronal apoptosis and decrease IL-10 release via the TLR2/NFkappaB pathway in rats with hypoxic-ischemic brain damage. Mol Brain. 2015;8(1):65. Epub 2015/10/18. doi: 10.1186/s13041-015-0157-3. PubMed PMID: 26475712; PubMed Central PMCID: PMCPMC4609057.

65. Kim C, Rockenstein E, Spencer B, Kim HK, Adame A, Trejo M, et al. Antagonizing Neuronal Toll-like Receptor 2 Prevents Synucleinopathy by Activating Autophagy. Cell Rep. 2015;13(4):771-82. Epub 2015/10/23. doi: 10.1016/j.celrep.2015.09.044. PubMed PMID: 26489461; PubMed Central PMCID: PMCPMC4752835.

66. Moriguchi T, Hamada M, Morito N, Terunuma T, Hasegawa K, Zhang C, et al. MafB is essential for renal development and F4/80 expression in macrophages. Mol Cell Biol. 2006;26(15):5715-27. Epub 2006/07/19. doi: 10.1128/mcb.00001-06. PubMed PMID: 16847325; PubMed Central PMCID: PMCPMC1592773.

67. Bauquet AT, Jin H, Paterson AM, Mitsdoerffer M, Ho IC, Sharpe AH, et al. The costimulatory molecule ICOS regulates the expression of c-Maf and IL-21 in the development of follicular T helper cells and TH-17 cells. Nat Immunol. 2009;10(2):167-75. doi: 10.1038/ni.1690.

68. Cao S, Liu J, Song L, Ma X. The protooncogene c-Maf is an essential transcription factor for IL-10 gene expression in macrophages. J Immunol. 2005;174(6):3484-92. Epub 2005/03/08. PubMed PMID: 15749884; PubMed Central PMCID: PMCPMC2955976.

69. Aziz A, Soucie E, Sarrazin S, Sieweke MH. MafB/c-Maf deficiency enables self-renewal of differentiated functional macrophages. Science. 2009;326(5954):867-71. Epub 2009/11/07. doi: 10.1126/science.1176056. PubMed PMID: 19892988.

70. Smith PA. The tantalizing links between gut microbes and the brain. Nature. 2015;526(7573):312-4. Epub 2015/10/16. doi: 10.1038/526312a. PubMed PMID: 26469024.

71. Davis DJ, Bryda EC, Gillespie CH, Ericsson AC. Microbial modulation of behavior and stress responses in zebrafish larvae. Behav Brain Res. 2016;311:219-27. Epub 2016/05/25. doi: 10.1016/j.bbr.2016.05.040. PubMed PMID: 27217102.

72. de Abreu MS, Giacomini A, Zanandrea R, Dos Santos BE, Genario R, de Oliveira GG, et al. Psychoneuroimmunology and immunopsychiatry of zebrafish. Psychoneuroendocrinology. 2018;92:1-12. Epub 2018/04/03. doi: 10.1016/j.psyneuen.2018.03.014. PubMed PMID: 29609110.

73. Phelps D, Brinkman NE, Keely SP, Anneken EM, Catron TR, Betancourt D, et al. Microbial colonization is required for normal neurobehavioral development in zebrafish. Sci Rep. 2017;7(1):11244. Epub 2017/09/13. doi: 10.1038/s41598-017-10517-5. PubMed PMID: 28894128; PubMed Central PMCID: PMCPMC5593827.

74. Borrelli L, Aceto S, Agnisola C, De Paolo S, Dipineto L, Stilling RM, et al. Probiotic modulation of the microbiota-gut-brain axis and behaviour in zebrafish. Sci Rep. 2016;6:30046. Epub 2016/07/16. doi: 10.1038/srep30046. PubMed PMID: 27416816; PubMed Central PMCID: PMCPMC4945902.

75. Naidoo CC, Nyawo GR, Wu BG, Walzl G, Warren RM, Segal LN, et al. The microbiome and tuberculosis: state of the art, potential applications, and defining the clinical research agenda. Lancet Respir Med. 2019;7(10):892-906. Epub 2019/03/27. doi: 10.1016/S2213-2600(18)30501-0. PubMed PMID: 30910543.

76. Abdallah AM, Savage ND, van Zon M, Wilson L, Vandenbroucke-Grauls CM, van der Wel NN, et al. The ESX-5 secretion system of Mycobacterium marinum modulates the macrophage response. J Immunol. 2008;181(10):7166-75. Epub 2008/11/05. doi: 10.4049/jimmunol.181.10.7166. PubMed PMID: 18981138.

77. Richardson ET, Shukla S, Sweet DR, Wearsch PA, Tsichlis PN, Boom WH, et al. Toll-like receptor 2-dependent extracellular signal-regulated kinase signaling in Mycobacterium tuberculosis-infected macrophages drives anti-inflammatory responses and inhibits Th1 polarization of responding T cells. Infect Immun. 2015;83(6):2242-54. Epub 2015/03/18. doi: 10.1128/iai.00135-15. PubMed PMID: 25776754; PubMed Central PMCID: PMCPMC4432743.

78. Piermattei A, Migliara G, Di Sante G, Foti M, Hayrabedyan SB, Papagna A, et al. Toll-Like Receptor 2 Mediates In Vivo Pro- and Anti-inflammatory Effects of Mycobacterium Tuberculosis and Modulates Autoimmune Encephalomyelitis. Front Immunol. 2016;7:191. Epub 2016/06/03. doi: 10.3389/fimmu.2016.00191. PubMed PMID: 27252700; PubMed Central PMCID: PMCPMC4878199.

79. Davila S, Hibberd ML, Hari Dass R, Wong HE, Sahiratmadja E, Bonnard C, et al. Genetic association and expression studies indicate a role of toll-like receptor 8 in pulmonary tuberculosis. PLoS Genet. 2008;4(10):e1000218. Epub 2008/10/18. doi: 10.1371/journal.pgen.1000218. PubMed PMID: 18927625; PubMed Central PMCID: PMCPMC2568981.

80. Lai YF, Lin TM, Wang CH, Su PY, Wu JT, Lin MC, et al. Functional polymorphisms of the TLR7 and TLR8 genes contribute to Mycobacterium tuberculosis infection. Tuberculosis (Edinb). 2016;98:125-31. Epub 2016/05/10. doi: 10.1016/j.tube.2016.03.008. PubMed PMID: 27156628.

81. Moen SH, Ehrnström B, Kojen JF, Beckwith KS, Afset JE, Damås JK, et al. Human Toll-like receptor 8 (TLR8) is an important sensor of pyogenic bacteria, and is attenuated by cell surface TLR signaling. Frontiers in Immunology. 2019;10:1209.

82. Reeme AE, Robinson RT. Dietary Vitamin D3 Suppresses Pulmonary Immunopathology Associated with Late-Stage Tuberculosis in C3HeB/FeJ Mice. J Immunol. 2016;196(3):1293-304. Epub 2016/01/06. doi: 10.4049/jimmunol.1500931. PubMed PMID: 26729807.

83. Liu PT, Stenger S, Li H, Wenzel L, Tan BH, Krutzik SR, et al. Toll-like receptor triggering of a vitamin D-mediated human antimicrobial response. Science. 2006;311(5768):1770-3. Epub 2006/02/25. doi: 10.1126/science.1123933. PubMed PMID: 16497887.

84. Haire RN, Cannon JP, O'Driscoll ML, Ostrov DA, Mueller MG, Turner PM, et al. Genomic and functional characterization of the diverse immunoglobulin domain-containing protein (DICP) family. Genomics. 2012;99(5):282-91. Epub 2012/03/06. doi: 10.1016/j.ygeno.2012.02.004. PubMed PMID: 22386706; PubMed Central PMCID: PMCPMC3351558.

85. Rodriguez-Nunez I, Wcisel DJ, Litman GW, Yoder JA. Multigene families of immunoglobulin domain-containing innate immune receptors in zebrafish: deciphering the differences. Dev Comp Immunol. 2014;46(1):24-34. doi: 10.1016/j.dci.2014.02.004. PubMed PMID: 24548770; PubMed Central PMCID: PMC4028400.

86. Blander JM, Medzhitov R. Regulation of Phagosome Maturation by Signals from Toll-Like Receptors. Science. 2004;304(5673):1014-8. doi: 10.1126/science.1096158.

87. Rahman MJ, Chuquimia OD, Petursdottir DH, Periolo N, Singh M, Fernandez C. Impact of toll-like receptor 2 deficiency on immune responses to mycobacterial antigens. Infect Immun. 2011;79(11):4649-56. Epub 2011/08/17. doi: 10.1128/iai.05724-11. PubMed PMID: 21844233; PubMed Central PMCID: PMCPMC3257930.

88. Bernut A, Herrmann JL, Kissa K, Dubremetz JF, Gaillard JL, Lutfalla G, et al. Mycobacterium abscessus cording prevents phagocytosis and promotes abscess formation. Proc Natl Acad Sci U S A. 2014;111(10):E943-52. Epub 2014/02/26. doi: 10.1073/pnas.1321390111. PubMed PMID: 24567393; PubMed Central PMCID: PMCPMC3956181.

89. Renshaw SA, Loynes CA, Trushell DM, Elworthy S, Ingham PW, Whyte MK. A transgenic zebrafish model of neutrophilic inflammation. Blood. 2006;108(13):3976-8. Epub 2006/08/24. doi: 10.1182/blood-2006-05-024075. PubMed PMID: 16926288.

90. van der Sar AM, Spaink HP, Zakrzewska A, Bitter W, Meijer AH. Specificity of the zebrafish host transcriptome response to acute and chronic mycobacterial infection and the role of innate and adaptive immune components. Molecular immunology. 2009;46(11–12):2317-32. doi: http://dx.doi.org/10.1016/j.molimm.2009.03.024.

91. Benard EL, van der Sar AM, Ellett F, Lieschke GJ, Spaink HP, Meijer AH. Infection of zebrafish embryos with intracellular bacterial pathogens. Journal of visualized experiments : JoVE. 2012;(61):2.

92. Stockhammer OW, Zakrzewska A, Hegedus Z, Spaink HP, Meijer AH. Transcriptome profiling and functional analyses of the zebrafish embryonic innate immune response to Salmonella infection. J Immunol. 2009;182(9):5641-53. Epub 2009/04/22. doi: 10.4049/jimmunol.0900082. PubMed PMID: 19380811.

93. Stoop EJM, Schipper T, Rosendahl Huber SK, Nezhinsky AE, Verbeek FJ, Gurcha SS, et al. Zebrafish embryo screen for mycobacterial genes involved in the initiation of granuloma formation reveals a newly identified ESX-1 component. Disease models & mechanisms. 2011;4(4):526-36. doi: 10.1242/dmm.006676.

94. van Soest JJ, Stockhammer OW, Ordas A, Bloemberg GV, Spaink HP, Meijer AH. Comparison of static immersion and intravenous injection systems for exposure of zebrafish embryos to the natural pathogen Edwardsiella tarda. BMC Immunol. 2011;12:58. Epub 2011/10/19. doi: 10.1186/1471-2172-12-58. PubMed PMID: 22003892; PubMed Central PMCID: PMC3206475.

95. Livak KJ, Schmittgen TD. Analysis of relative gene expression data using real-time quantitative PCR and the 2(-Delta Delta C(T)) Method. Methods. 2001;25(4):402-8. Epub 2002/02/16. doi: 10.1006/meth.2001.1262. PubMed PMID: 11846609.

96. Marin-Juez R, Jong-Raadsen S, Yang S, Spaink HP. Hyperinsulinemia induces insulin resistance and immune suppression via Ptpn6/Shp1 in zebrafish. The Journal of endocrinology. 2014. Epub 2014/06/07. doi: 10.1530/joe-14-0178. PubMed PMID: 24904114.

97. Veneman W, de Sonneville J, van der Kolk KJ, Ordas A, Al-Ars Z, Meijer A, et al. Analysis of RNAseq datasets from a comparative infectious disease zebrafish model using GeneTiles bioinformatics. Immunogenetics. 2015;67(3):135-47. doi: 10.1007/s00251-014-0820-3. PubMed PMID: WOS:000349370100001.

98. Love MI, Huber W, Anders S. Moderated estimation of fold change and dispersion for RNA-seq data with DESeq2. Genome Biol. 2014;15(12):550. doi: 10.1186/s13059-014-0550-8. PubMed PMID: 25516281; PubMed Central PMCID: PMCPMC4302049.

99. Kotelnikova E, Shkrob MA, Pyatnitskiy MA, Ferlini A, Daraselia N. Novel approach to meta-analysis of microarray datasets reveals muscle remodeling-related drug targets and biomarkers in Duchenne muscular dystrophy. PLoS Comput Biol. 2012;8(2):e1002365. doi: 10.1371/journal.pcbi.1002365. PubMed PMID: 22319435; PubMed Central PMCID: PMCPMC3271016.

Supplementary materials

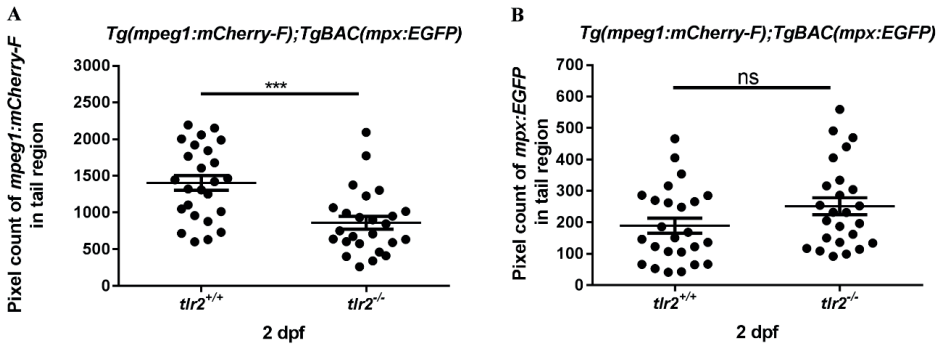

Supplementary figure 1 Pixel count analysis for double transgenic lines *Tg*(*mpeg1:mCherry-F);TgBAC(mpx:EGFP)* of 2 dpf *tlr2*$^{+/+}$ and *tlr2*$^{-/-}$ embryos. A: mCherry reporter, B, EGFP reporter.

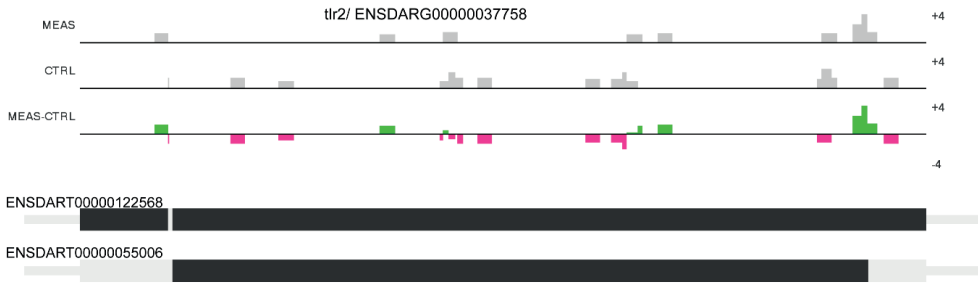

Supplementary figure 2 RNAseq read counts of *tlr2* transcripts in heterozygotes (*tlr2*$^{+/-}$) control versus *tlr2* mutant (*tlr2*$^{-/-}$) larvae. RNAseq data comparing reads mapped to *tlr2* transcript (ENSDART0000012256). Heterozygotes and mutant reads are mapped to the entire length of the mutant transcript indicating that the mutant transcript is not subjected to nonsense mediated decay. Mutant data (MEAS) and heterozygotes (CTRL) data have been submitted to the NCBI gene expression Omnibus database, accession number is GSE102766.

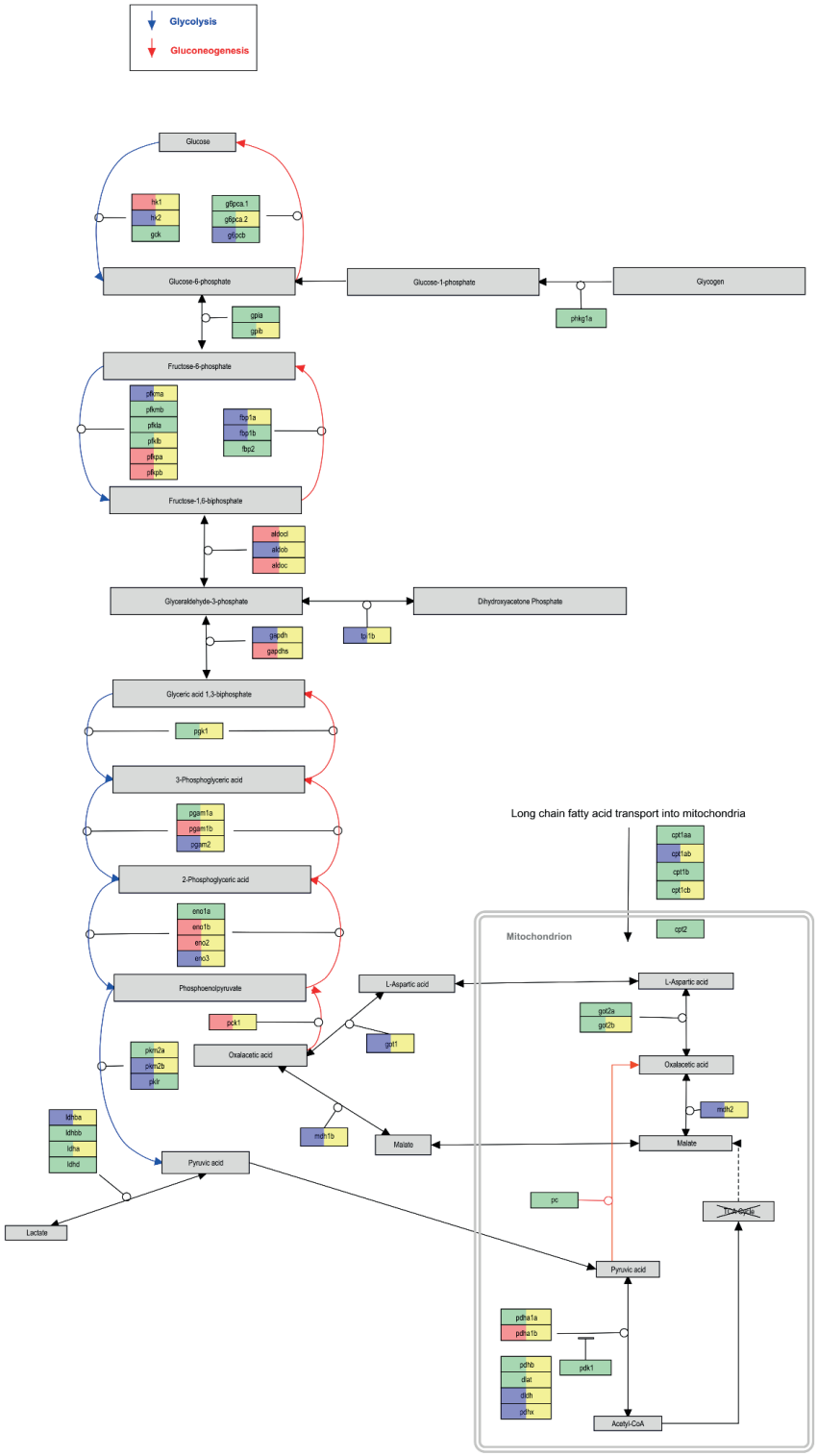
Glycolysis
Gluconeogenesis
Glucose
hk1
hk2
gck
g6pca.1
g6pca.2
g6pcb
Glucose-6-phosphate
Glucose-1-phosphate
Glycogen
phkg1a
gpia
gpib
Fructose-6-phosphate
pfkma
pfkmb
pfkla
pfklb
pfkpa
pfkpb
fbp1a
fbp1b
fbp2
Fructose-1,6-biphosphate
aldocl
aldob
aldoc
Glyceraldehyde-3-phosphate
Dihydroxyacetone Phosphate
gapdh
gapdhs
tpi1b
Glyceric acid 1,3-biphosphate
pgk1
3-Phosphoglyceric acid
pgam1a
pgam1b
pgam2
2-Phosphoglyceric acid
eno1a
eno1b
eno2
eno3
Phosphoenolpyruvate
pck1
pkm2a
pkm2b
pklr
Oxalacetic acid
got1
L-Aspartic acid
ldhba
ldhbb
ldha
ldhd
mdh1b
Malate
Pyruvic acid
Lactate
Long chain fatty acid transport into mitochondria
cpt1aa
cpt1ab
cpt1b
cpt1cb
cpt2
Mitochondrion
L-Aspartic acid
got2a
got2b
Oxalacetic acid
mdh2
Malate
pc
TCA cycle
Pyruvic acid
pdha1a
pdha1b
pdhb
dlat
dldh
pdhx
pdk1
Acetyl-CoA

Supplementary figure 3 Analysis of differential expression of genes functioning in glycolysis and gluconeogenesis between uninfected *tlr2*$^{+/-}$ and *tlr2*$^{-/-}$. The red boxes represent up regulated genes (FC >2); blue boxes represent down regulated genes (FC<-2); yellow boxes represent the genes that are differentially expressed with a *P* value lower than 0.05; green represent not-significantly differentially expressed genes.

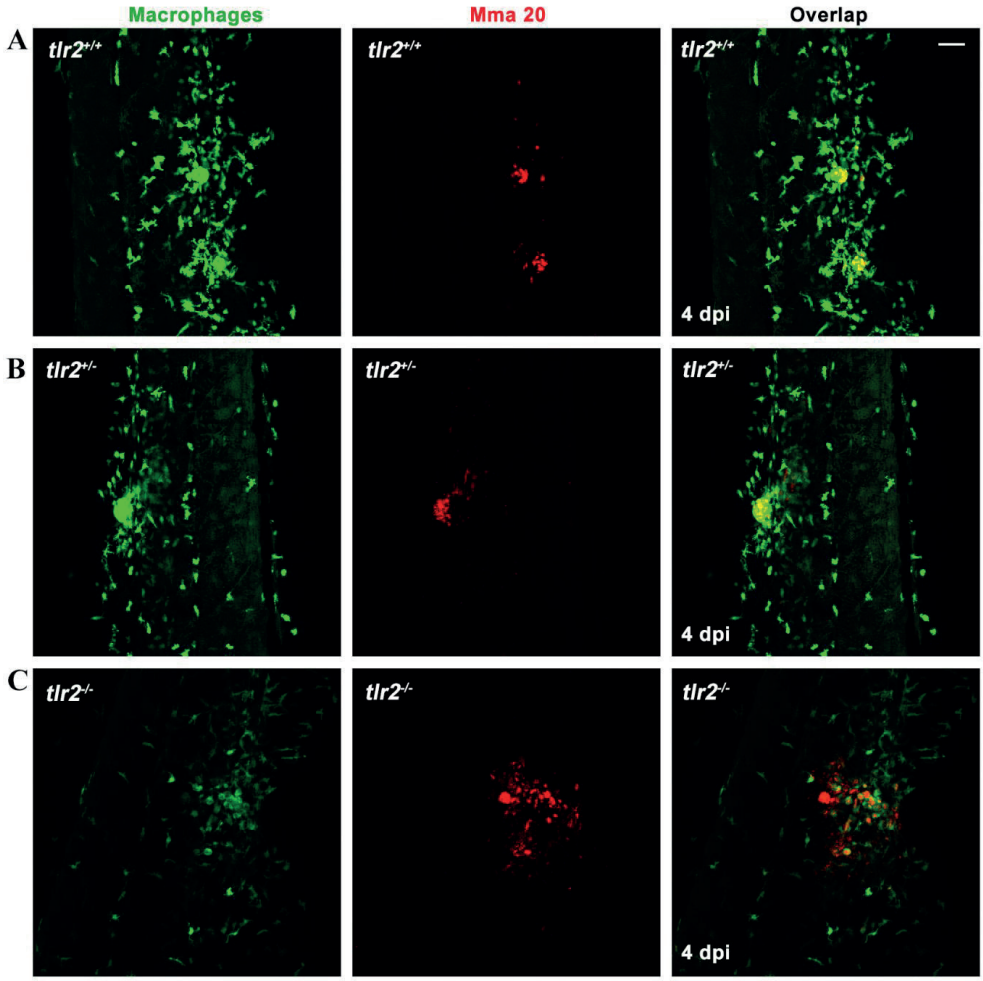

Supplementary Figure 4 Representative images of the quantification of Mma20 infection phenotype in the *tlr2* mutant, heterozygote and wild type siblings. One representative picture is shown for the entire sets of 38, 47 and 37 larvae were analyzed for the *tlr2* mutant, the heterozygote and the wild-type, respectively. Macrophages are in green and bacteria are in red. The scale bar represents 50 μm.

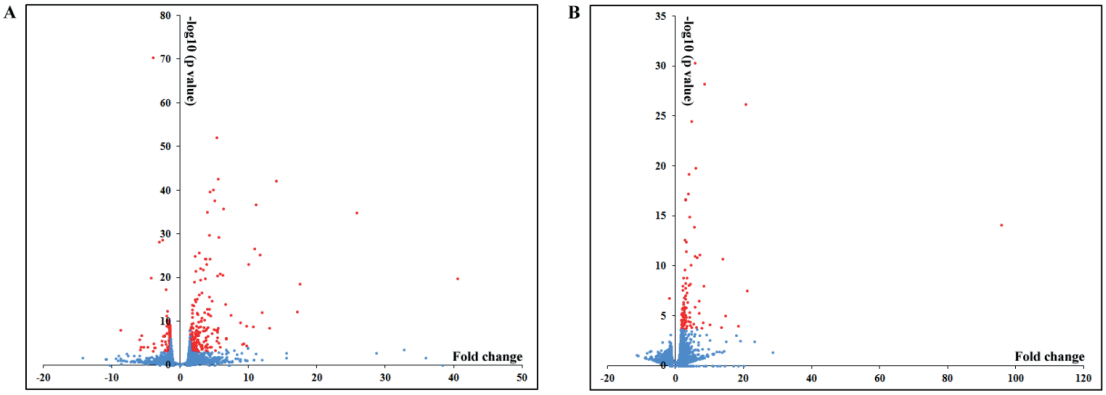

Supplementary Figure 5 Volcano plots showing the significance cutoff applied to *tlr2*$^{+/-}$ infected with strain Mma20 versus control with PBS (A) and *tlr2*$^{-/-}$ infected with strain Mma20 versus control with PBS (B). In these volcano plots, the transcripts were considered significant (red) or non-significant (blue) by the conditions of |fold change| ≥ 1,45 and adjusted *P* value threshold ≤ 0,05. Fold changes for each transcript was plotted on the X-axis against -log10 transformed p-values on the Y-axis.

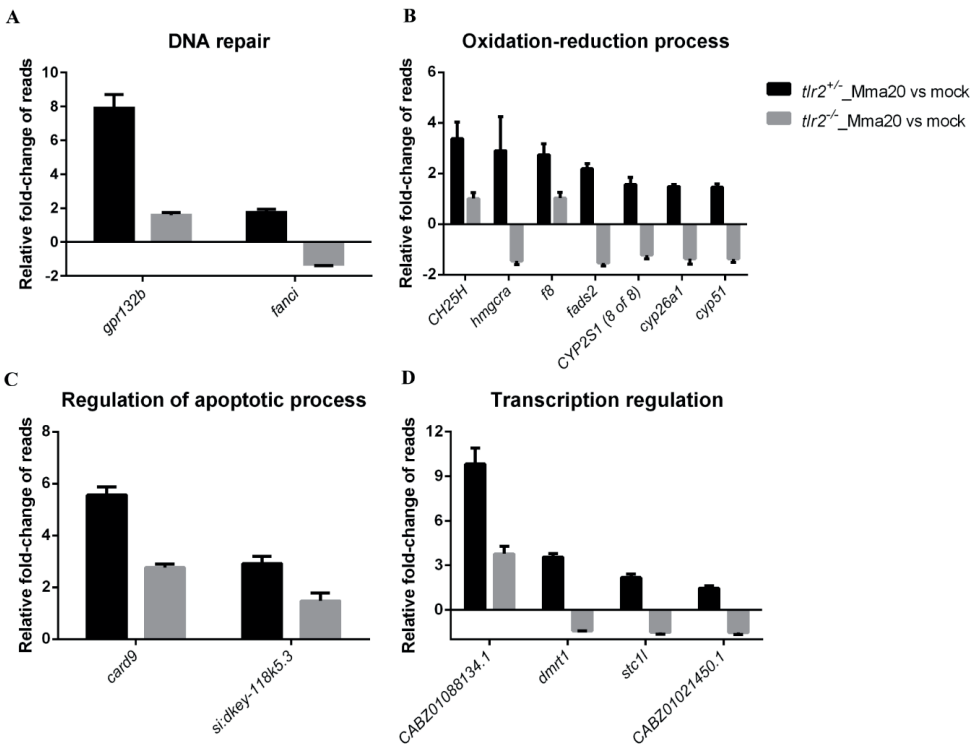

Supplementary figure 6 *tlr2*-dependent up regulation of genes with various GO terms.

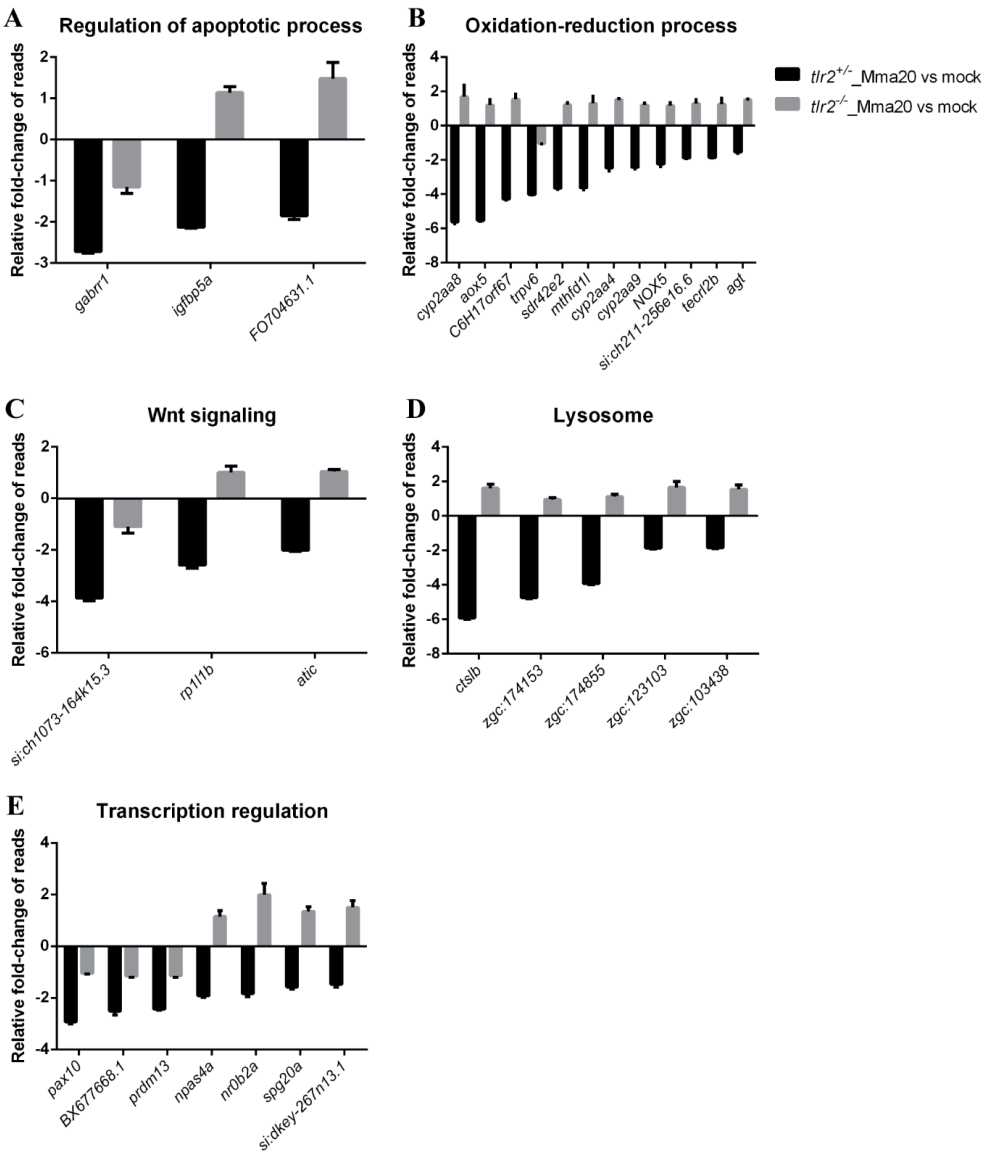

Supplementary figure 7 *tlr2*-dependent down regulation of genes with various GO terms.

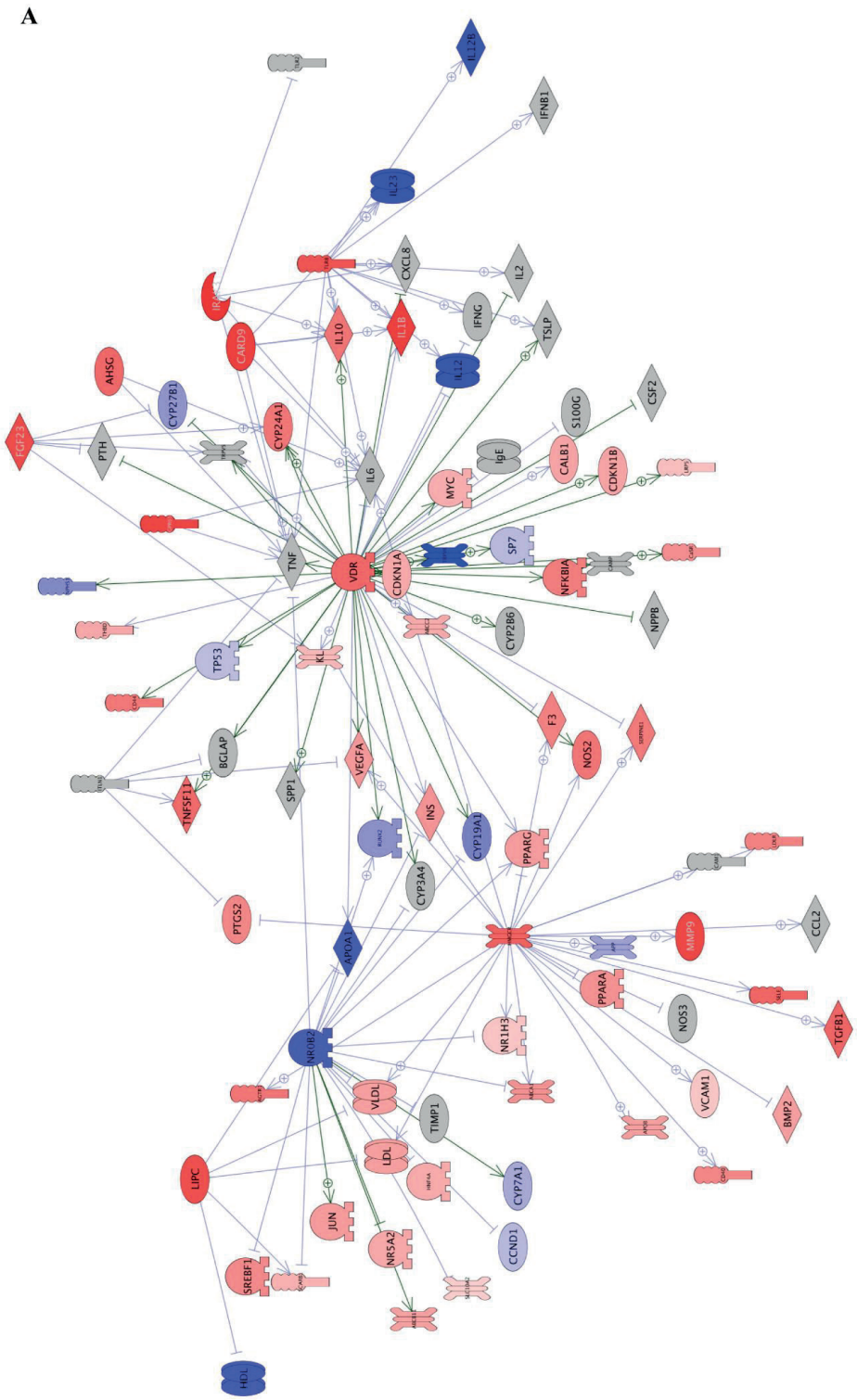
A
IL23
IFNB1
IL23
CXCL8
IL2
IFNG
TSLP
IL10
IL1B
IL12
CARD9
AHSG
CYP27B1
CYP24A1
FGF23
PTH
IL6
S100G
CSF2
IgE
CALB1
CDKN1B
MYC
TNF
VDR
CDKN1A
SP7
NFKBIA
NPPB
CYP2B6
TP53
KL
F3
NOS2
BGLAP
VEGFA
SPP1
TNFSF11
INS
CYP19A1
PPARG
CYP3A4
PTGS2
APOA1
CCL2
MMP9
PPARA
NOS3
TGFB1
VCAM1
BMP2
NR1H3
NR0B2
VLDL
LDL
TIMP1
LIPC
CYP7A1
JUN
NR5A2
CCND1
SREBF1
HDL

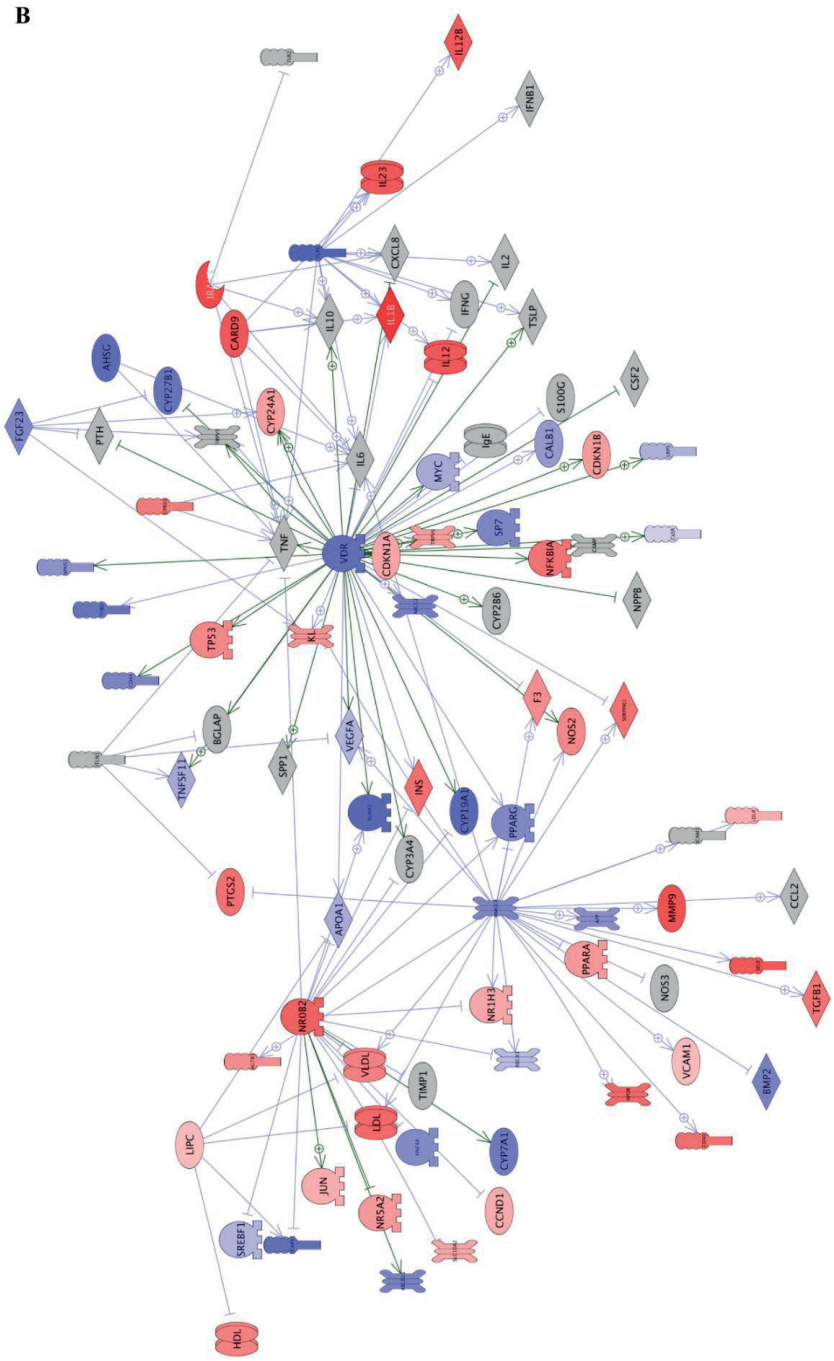

Supplementary figure 8 Sub-network enrichment analysis. Networks of common targets of the 97 up regulated genes (Fig. 6D) in *tlr2*$^{+/-}$ (A) and *tlr2*$^{-/-}$ (B) with Mma20 infection. Red represents up regulation, blue represents down regulation and grey represents genes for which no expression was detected.

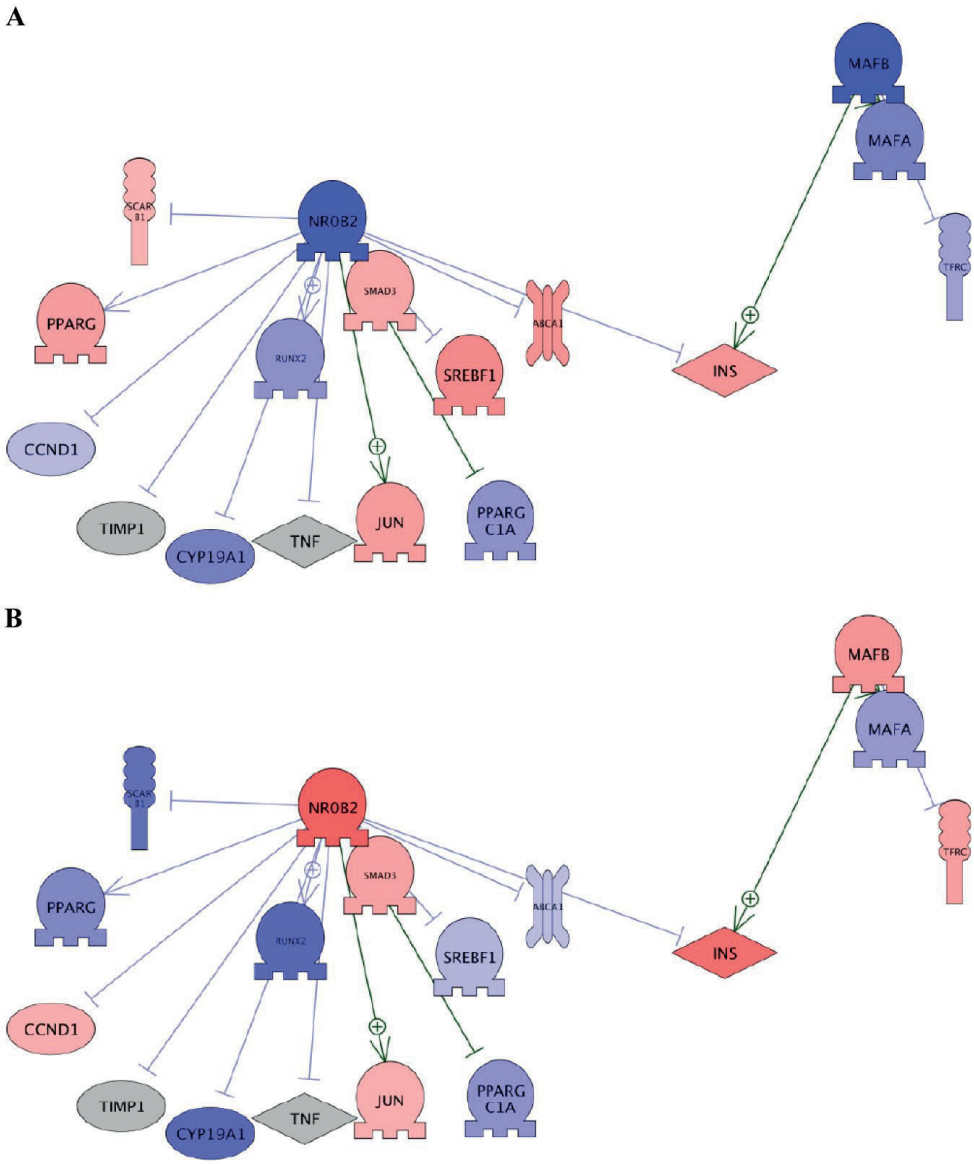

Supplementary figure 9 Sub-network enrichment analysis. The networks of common targets of the 92 down regulated genes (Fig. 6E) in *tlr2*$^{+/-}$ (A) and *tlr2*$^{-/-}$ (B) with Mma20 infection. Red represents up-regulation, blue represents down-regulation and grey represents genes for which no expression was detected.

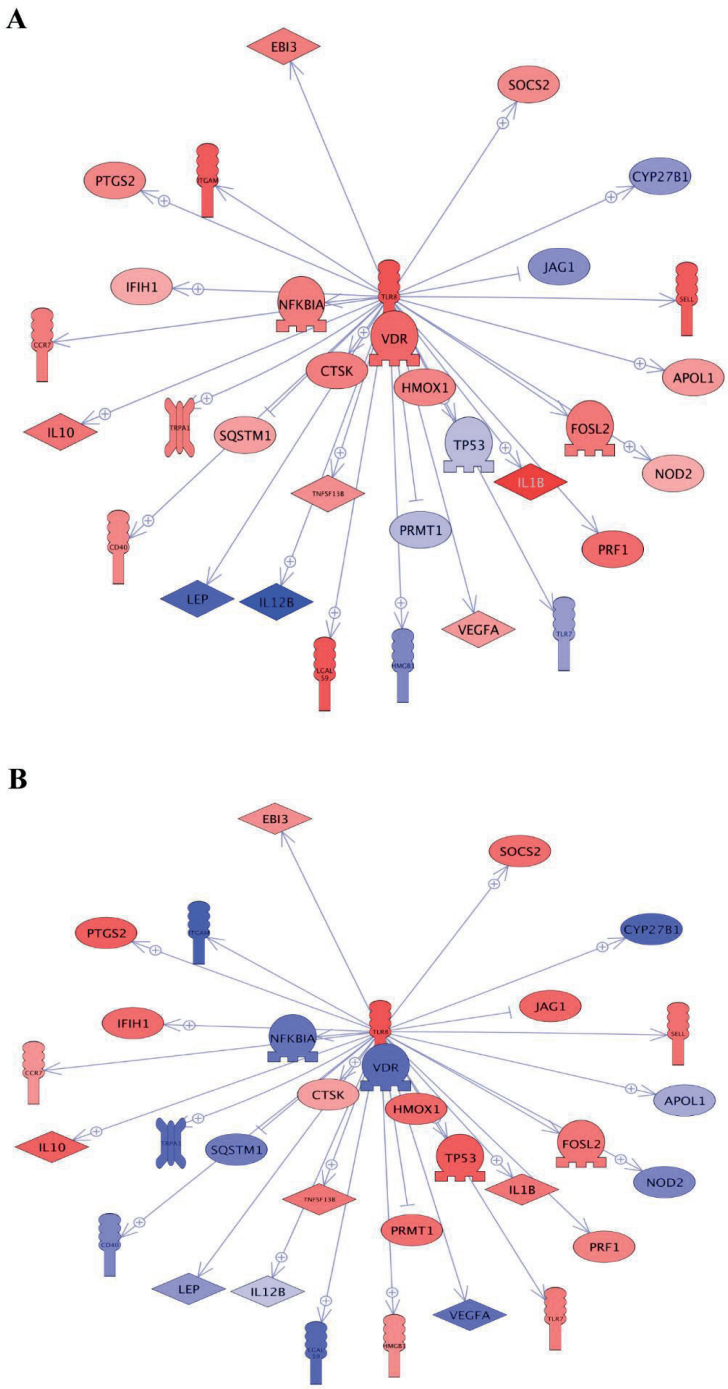

Supplementary figure 10 Sub-network enrichment analysis between zebrafish and human. The Tlr8 pathway in zebrafish (A) with Mm infection and human macrophages (B) with Mtb infection. Red represents up-regulation, blue represents down-regulation.

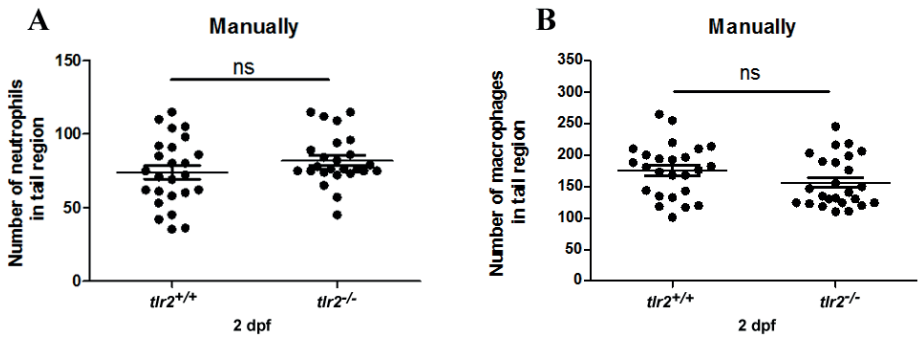

Supplementary figure 11 Manual counting analysis for *Tg(mpeg1:mCherry-F);TgBAC(mpx:EGFP)* of neutrophils (A) and macrophages (B) in 2 dpf *tlr2*$^{+/+}$ and *tlr2*$^{-/-}$ embryos.

Availability of data and materials

The raw data of the RNAseq experiments is available in the NCBI GEO database under accession number GSE102766.

Supplementary Tables are available online:
https://bmcgenomics.biomedcentral.com/articles/10.1186/s12864-019-6265-1

2

Chapter 3

A novel function of TLR2 and MyD88 in the regulation of leukocyte cell migration behavior during wounding in zebrafish larvae

Wanbin Hu, Leonie van Steijn, Chen Li, Fons J. Verbeek, Lu Cao, Roeland M.H. Merks, Herman P. Spaink

Published in ***Frontiers in cell and developmental biology*** 9 (2021). DOI: 10.3389/fcell.2021.624571

3

Abstract

Toll-like receptor (TLR) signaling via myeloid differentiation factor 88 protein (MyD88) has been indicated to be involved in the response to wounding. It remains unknown whether the putative role of MyD88 in wounding responses is due to a control of leukocyte cell migration. The aim of this study was to explore *in vivo* whether TLR2 and MyD88 are involved in modulating neutrophil and macrophage cell migration behavior upon zebrafish larval tail wounding. Live cell imaging of tail-wounded larvae was performed in *tlr2* and *myd88* mutants and their corresponding wild type siblings. In order to visualize cell migration following tissue damage, we constructed double transgenic lines with fluorescent markers for macrophages and neutrophils in all mutant and sibling zebrafish lines. Three days post fertilization (dpf), tail-wounded larvae were studied using confocal laser scanning microscopy (CLSM) to quantify the number of recruited cells at the wounding area. We found that in both *tlr2*$^{-/-}$ and *myd88*$^{-/-}$ groups the recruited neutrophil and macrophage numbers are decreased compared to their wild type sibling controls. Through analyses of neutrophil and macrophage migration patterns, we demonstrated that both *tlr2* and *myd88* control the migration direction of distant neutrophils upon wounding. Furthermore, in both the *tlr2* and the *myd88* mutants, macrophages migrated more slowly towards the wound edge. Taken together, our findings show that *tlr2* and *myd88* are involved in responses to tail wounding by regulating the behavior and speed of leukocyte migration *in vivo*.

Introduction

Acute inflammation is characterized by the directed migration of leukocytes, which can be triggered by tissue damage [1, 2]. The function of directed leukocyte migration is to eliminate cell debris and invading pathogens, with the aim of maintaining homeostasis upon tissue damage [3]. Neutrophils and macrophages are the two crucial immune cells that engage in this process [2, 4]. Neutrophils are the first cells to rapidly respond to the site of injury, and produce cytokines and chemokines to mediate the recruitment of other cells [4, 5]. However, persisting neutrophil recruitment can release toxic granule contents to further damage tissue, and thereby is a hallmark of chronic inflammatory disease [3, 6, 7]. In comparison, distant macrophages move slower and accumulate later at the wounded area and are considered to play a role in eliminating the debris of apoptotic cells and assist in regeneration of wounded tissue [2, 4, 8, 9]. Leukocyte migration must be tightly regulated to avoid negative effects on tissue repair or further damage. Despite myriad studies on leukocyte migration in response to wounding, the underlying mechanisms are not yet completely understood [10].

Neutrophils and macrophages depend on membrane-localized pattern recognition receptors (PRRs) to sense invading microbes and associated tissue damage [11]. PRRs play a crucial role to recognize pathogen associated molecular patterns (PAMPs) of invading microbes in open wounds and damage associated molecular patterns (DAMPs) released by lysing cells [12, 13]. Toll-like receptors (TLRs) are prominent recognition factors for PAMPs and DAMPs to regulate inflammatory responses [14, 15]. Extensive studies have demonstrated that cellular distribution is different for each TLR. TLRs recognize different classes of PAMPs and trigger the production of cytokines and chemokines during infection. Two typical examples are TLR2, which senses bacterial lipoproteins [16], and TLR4, which recognizes bacterial lipopolysaccharide (LPS) [17]. Accumulating evidence shows that high-mobility group box 1 protein (HMGB1), which is the best well known endogenous danger signal, activates inflammation by forming complexes with other DAMPs (such as single-stranded DNA, nucleosomes and LPS) to be recognized by IL-1R as well as TLR2, TLR4 and TLR9 to induce inflammatory responses [2, 18, 19]. After interacting with these PAMPs and DAMPs, TLRs initiate downstream signaling cascades that ultimately result in producing cytokines and chemokines. Importantly, the activation of downstream signaling pathway by HMGB1 has been shown to be dependent on the TLR down-stream signaling mediated by myeloid differentiation factor 88 protein (MyD88) [2, 20].

TLR2 is one of the best known PRRs and acts as a heterodimer with TLR1 or TLR6 to recognize gram positive bacteria including mycobacteria, presumably based on the specific binding to their cell wall components, such as glycolipids and glycoproteins [16, 21]. TLR2 is expressed and activated after tissue injury even in the absence of infections, like in acute ischemic injury as well as in acute liver and kidney injury [22-25]. In the study of Mojumdar *et al.* (2016), it was shown that macrophage infiltration was reduced into normal muscle following acute injury in TLR2 deficiency mice [26]. In addition, Kim et al. demonstrated that TLR2 contributes to macrophage infiltration in the dorsal root ganglia after peripheral nerve injury in mice [27]. Such injury-induced TLR2 expression and activation has therefore been hypothesized to be important for human health [24, 28, 29]. Following ischemic injury in mice, TLR2 activation promotes cell permeability, lymphocyte invasion and endothelial cell migration and mediates the release of TNF-α and IL-6 [23]. TLR2-deficient mice have a defective ability to recruit neutrophils to an injured liver and fail to induce the neutrophil chemokine CXCL-2 [24]. Additionally, TLR2 contributes to chronic liver disease in a mouse model by mediating MAPK and NF-κB signaling pathways [30]. However, there is little knowledge of the function of Toll-like receptor signaling in cell migration of myeloid cells to epithelial wounding sites [31].

MyD88 is an essential adaptor protein for all TLRs, except TLR3 [32, 33]. MyD88 is responsible for activating downstream signaling through binding to the TIR domain of TLRs [32, 33]. A few studies have shown changes in MyD88 expression after tissue injury. Similar to *Tlr2*, the gene expression of *Myd88* is upregulated following ischemic injury in mice [34]. Moreover, the expression of *Myd88* and *Tlr2* is significantly increased in diabetic wounded mice [35]. In addition, some evidence indicate that Myd88 is involved in the modulation of wound healing [36, 37], but the underlying mechanism is still unclear. Although TLR signaling is important for chemokine production, little is known about the role of MyD88 in leukocyte migratory responses to tissue injuries in the absence of pathogenic infections.

In this paper we use zebrafish larvae as a model for studying leukocyte cell migration after tail wounding. The zebrafish model has become an important vertebrate model for studying human diseases. The small size and transparency of their larvae are useful characteristics for the screening and imaging of transgenic reporter lines [38]. Zebrafish larvae are a popular model for studying functions involved in wound repair [39-44]. The availability of mutants in Toll-like receptor signaling genes *tlr2* and *myd88* make it possible to study their roles in leukocyte migratory behavior upon tail wounding in zebrafish [41, 42, 45-47]. Tlr2 and Myd88 show a

highly conserved structure in mammals and zebrafish [48]. In a previous study, we demonstrated the conserved role of *tlr2* in zebrafish as a PRR to recognize the mammalian TLR2 ligand Pam3CSK4, and identified a set of genes that are specifically expressed genes by activation of the downstream pathway of zebrafish *tlr2* [49]. Moreover, He et al., confirmed that *tlr2* gene expression can be upregulated upon wounding in zebrafish larvae which is consistent with previous studies in mice [50]. In addition, the study of Sommer et al., suggests that *myd88* is required for induction of chemokine gene expression, such as *ccl2* and *cxcl11aa,* following tail wounding [51].

In the present study, live fluorescent imaging was used to investigate the effect of the *tlr2* mutation and the *myd88* mutation on leukocyte migration upon tail wounding. We found reduced numbers of recruited neutrophils and macrophages at the wounding area in both *tlr2* mutants and *myd88* mutants, compared to their sibling controls. Leukocyte migration of the *tlr2* and *myd88* mutations upon wounding was analyzed using quantitative analyses of cell migration tracks. Our results demonstrate that the *tlr2* and the *myd88* mutations affect distant neutrophil migration upon wounding by negatively affecting their directional persistence, but not their migration speed. Not only the directional persistence of distant macrophage was significantly decreased in the *tlr2* and the *myd88* mutants, but also their migration speed. This study shows for the first time that TLR signaling is directly involved in controlling behavior of cell migration of neutrophils and macrophages during wounding, stimulating further studies also in other model systems.

Results

Tlr2 and myd88 mutations do not affect development and basal motility of leukocytes.

To determine the leukocyte development in *tlr2* and *myd88* mutants, the double-transgenic line *tlr2*$^{+/+}$ *Tg (mpeg1:mCherry-F);TgBAC (mpx: EGFP)*, *tlr2*$^{-/-}$ *Tg (mpeg1:mCherry-F);TgBAC (mpx: EGFP), myd88*$^{+/+}$ *Tg (mpeg1:mCherry-F);TgBAC (mpx: EGFP)* and *myd88*$^{-/-}$ *Tg (mpeg1:mCherry-F);TgBAC (mpx: EGFP)* were constructed. The lines were imaged at 3 dpf to count the number of macrophages and neutrophils in their tail region, and then compared with their wild type siblings (Fig. 1A). Embryos of the *tlr2* and *myd88* mutants showed similar numbers of macrophages and neutrophils as their wild type siblings (Fig. 1B- E). This result is consistent with our previous studies of the same *myd88* mutant at 3 dpf and the *tlr2* mutant at 2

dpf [45, 47]. With the aim of investigating the importance of the *tlr2* and the *myd88* mutations for leukocyte behavior under unchallenged condition, the CHT region was analyzed in the double transgenic lines of *tlr2* and *myd8*8 using CLSM by taking time-lapse images (Fig. 1A). No significant effect was observed on leukocyte basal motility in the CHT tissue in the *tlr2* and *myd88* mutants compared with their wild type sibling control (Fig. 1F-M). Representative images are shown in Fig. S2, 3.

Tlr2 and myd88 regulate neutrophil recruitment to a tail wound

To study the effect of the *tlr2* and *myd88* mutations on the recruitment of neutrophils towards a site of injury, a tail wound method was used in 3 dpf zebrafish larvae as a model for inflammation. To quantify the number of recruited neutrophils to the wound, we counted the number of neutrophils that were located in a range closer than 200 μm from the wound edge of the tail at 1, 2, 4 and 6 hpw (Fig. 2A). Our results show that the *tlr2* mutation had a significant negative effect on the recruitment of neutrophils after 2, 4 and 6 hpw (Fig. 2B, C). However, there is no significant difference in recruited neutrophil numbers between wild type and *tlr2*$^{-/-}$ at 1 hpw (Fig. 2B, C). Notably, a significant difference of recruited neutrophil numbers was already observed at 1 hpw in *myd88* zebrafish larvae and remained significant until 6 hpw (Fig. 2D, E).

Tlr2 and myd88 regulate macrophage recruitment to a tail wound

To assess the role of the *tlr2* and *myd88* mutations in regulating the recruitment of macrophages to a site of the tail wound, we counted the recruited macrophage numbers by the same method as for measuring the neutrophil recruitment to the wound (Fig. 3A). Both *tlr2*$^{-/-}$ and *myd88*$^{-/-}$ mutant zebrafish larvae displayed diminished macrophage responses upon wounding (Fig. 3). Significantly decreased numbers of recruited macrophages toward the injury were measured in the *tlr2*$^{-/-}$ group at 2, 4 and 6 hpw (Fig. 3B, C). Similarly, there is no significant difference in recruited macrophage numbers between wild type and *tlr2*$^{-/-}$ at 1 hpw (Fig. 3C). A significant difference of recruited macrophage numbers was already observed from 1 hpw in *myd88* zebrafish larvae, the same as was observed with neutrophil recruitment (Fig. 3D ,E).

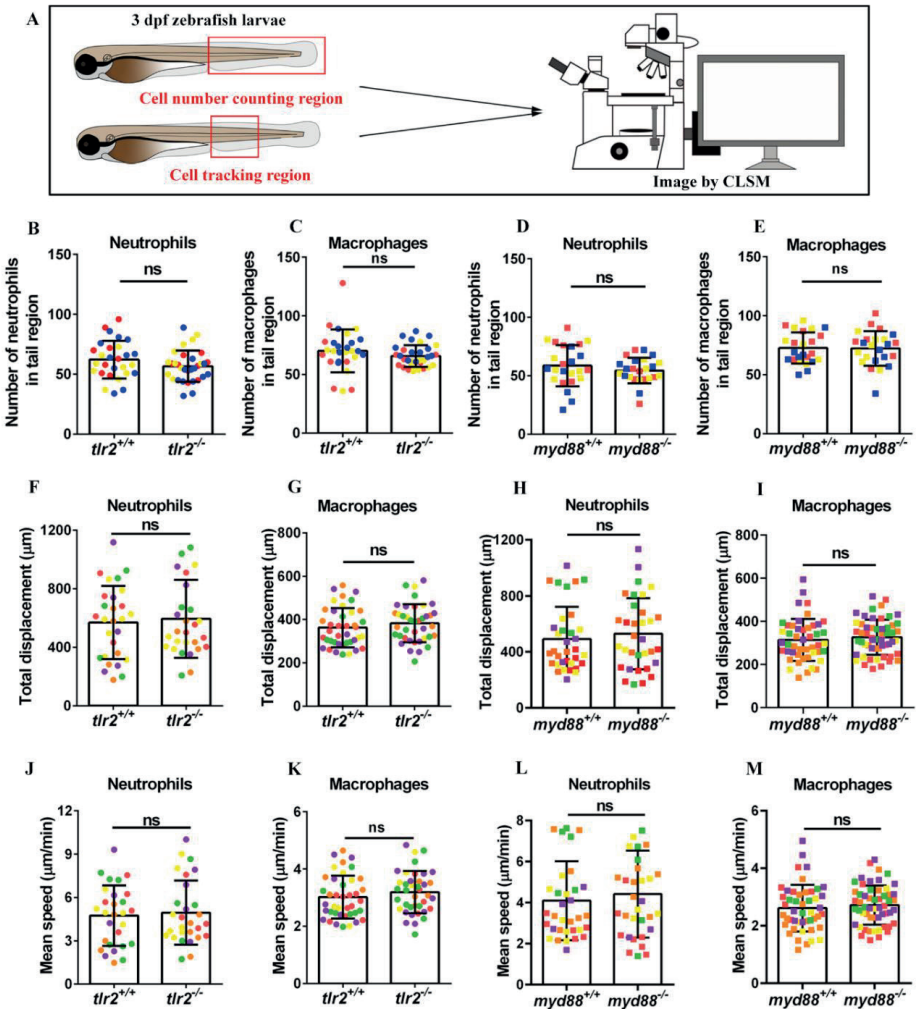

Figure 1 Quantification of macrophage and neutrophil numbers and their basal migratory capability in the 3 dpf *tlr2 and myd88* mutants and wild sibling controls larvae. (A) Experimental scheme. At 3 dpf, numbers and basal migratory capability of GFP-labeled neutrophils and mCherry-labeled macrophages in tail region were quantified using Leica TCS SP8 confocal laser scanning microscopy (CLSM). Red boxes show the area in which cells were counted or tracked. (B- E) The quantification of neutrophil and macrophage numbers in tail region by using *tlr2* and *myd88* zebrafish larvae. Data (mean ± SD) are combined from three pools of zebrafish larvae. No significant differences (ns) in the number of neutrophils (B, D) and macrophages (C, E) was detected with an unpaired, two-tailed t-test. Each point represents one larva and different colors represent different pools. Sample size (n): 28, 32 (B, C); 24, 24 (D, E). (F- G, J- K) Quantification of basal migratory capability in 3 dpf *tlr2* zebrafish. The total displacement and mean speed of individual neutrophils (F, J) and macrophages (G, K) were quantified by using a manual tracking plugin. Data (mean ± SD) are combined from 5 larvae of *tlr2*$^{+/+}$ *Tg (mpeg1:mCherry-F);TgBAC (mpx: EGFP)* and *tlr2*$^{-/-}$ *Tg (mpeg1:mCherry-F);TgBAC (mpx: EGFP)* larvae respectively. Each color indicates a different larva. No significant differences (ns) in the total displacement and mean speed of neutrophils (F, J) and macrophages (G, K) were detected with an unpaired, two-tailed t-test. Sample size (n): 28, 28 (F, J); 40, 39 (G, K). Cell tracking movies are shown in Supplementary Movie S1-4). (H- I, L- M) Quantification of basal migratory capability in 3 dpf *myd88* zebrafish. The total displacement and mean speed of individual neutrophils (H, L) and macrophages (I, M) were quantified by using a manual tracking plugin. Data (mean ± SD) are combined from 5 larvae of *myd88*$^{+/+}$ *Tg (mpeg1:mCherry-F);TgBAC (mpx: EGFP)* and *myd88*$^{-/-}$ *Tg (mpeg1:mCherry-F);TgBAC (mpx: EGFP)* larvae respectively. Each color indicates a different larva. No significant differences (ns) in the total displacement and mean speed of neutrophils (H, L) and macrophages (I, M) were detected with an unpaired, two-tailed t-test. Sample size (n): 34, 33 (H, L); 47, 55 (I, M). Cell tracking movies are shown in Supplementary Movie S5-8).

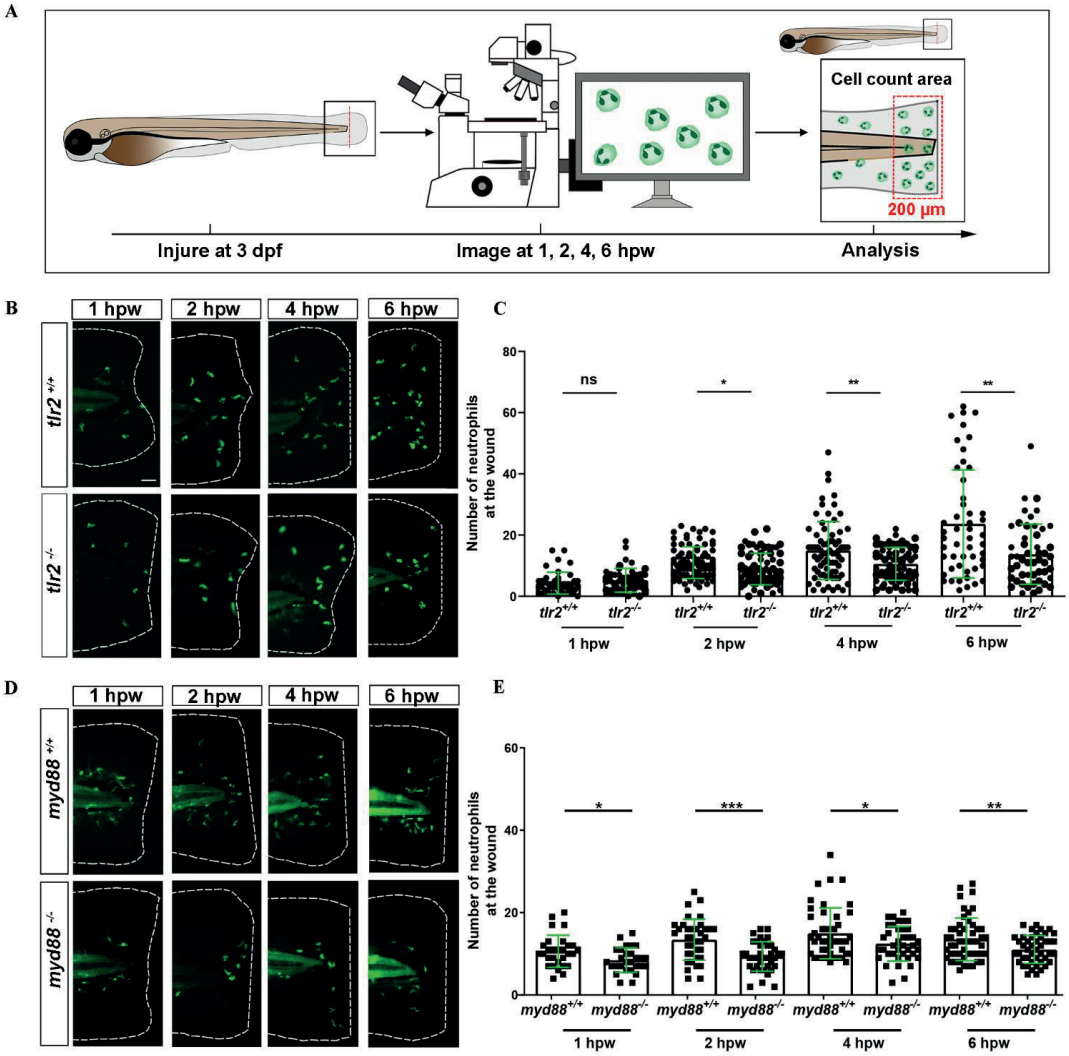

Figure 2 The number of neutrophils recruited to the wounded area in the *tlr2* and *myd88* mutants and wild type sibling controls larvae. (A) Experimental scheme. *Tlr2* and *myd88* homozygous mutants and sibling control larvae were wounded at 3 dpf. Their tails were wounded to the tip of the notochord. The red dashed line shows the site of wounding. Recruited neutrophils at the wound were imaged at 1, 2, 4 and 6 hpw by using CLSM. For recruited cell counting analysis, cells localized within an area of 200 µm from the wounding edge toward the body trunk were counted as recruited cells. The red dashed box shows the area where neutrophils were counted as recruited neutrophils. (B, D) Representative images of 3 dpf larvae at 1, 2, 4 and 6 hours post-wounding (hpw). Scale bar: 50 µm. (C) Quantification of recruited neutrophil numbers to the wounded area at 1, 2, 4 and 6 hpw in 3 dpf *tlr2*$^{+/+}$ and *tlr2*$^{-/-}$ larvae. Each point represents a different larva. Sample size (n): 45, 46, 82, 72, 74, 68, 50, 50. (E) Quantification of recruited neutrophil numbers to the wounded area at 1, 2, 4 and 6 hpw in 3 dpf *myd88*$^{+/+}$ and *myd88*$^{-/-}$ larvae. Each point represents a different larva. Sample size (n): 29, 28, 37, 38, 45, 39, 51, 45. In all cases, statistical analyses were done from 3 independent experiments. An unpaired, two-tailed t-test was used to assess significance (ns, no significant difference, *$P < 0.05$, **$P < 0.01$, ***$P < 0.001$) and data are shown as mean± SD.

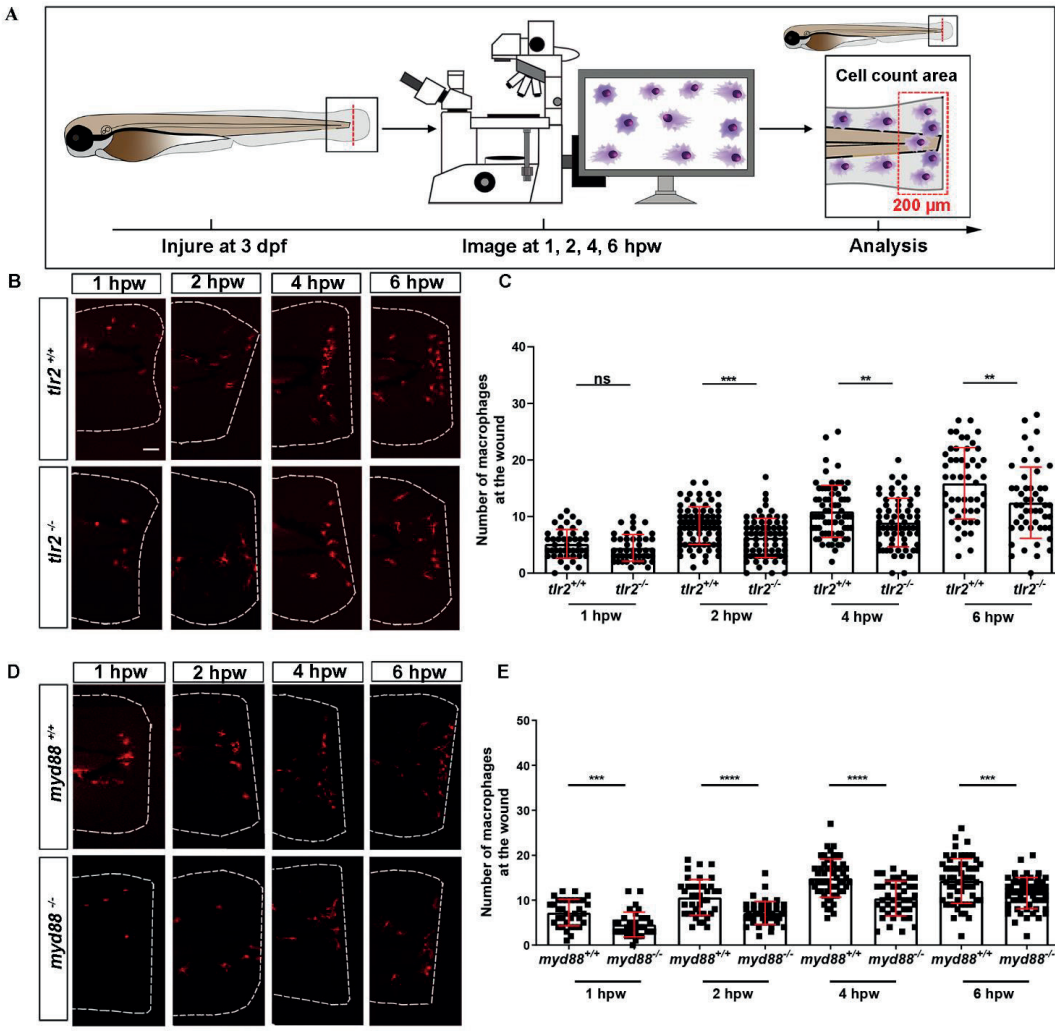

Figure 3 The number of macrophages recruited to the wounded area in the *tlr2* and *myd88* mutants and wild type sibling controls larvae. (A) Experimental scheme. *Tlr2* and *myd88* homozygous mutants and sibling control larvae were wounded at 3 dpf. Their tails were wounded to the tip of the notochord. The red dashed line shows the site of wounding. Recruited macrophages at the wound were imaged at 1, 2, 4 and 6 hpw by using CLSM. For recruited cell counting analysis, cells localized within an area of 200 µm from the wounding edge toward the body trunk were counted as recruited cells. The red dashed box shows the area where macrophages were counted as recruited macrophages. (B, D) Representative images of 3 dpf larvae at 1, 2, 4 and 6 hpw. Scale bar: 50 µm. (C) The quantification of recruited macrophage numbers to the wounded area at 1, 2, 4 and 6 hpw in 3 dpf $tlr2^{+/+}$ and $tlr2^{-/-}$ larvae. Each point represents a different larva. Sample size (n): 45, 45, 82, 71, 69, 68, 51, 50. (E) The quantification of recruited macrophage numbers to the wounded area at 1, 2, 4 and 6 hpw in 3 dpf $myd88^{+/+}$ and $myd88^{-/-}$ larvae. Each point represents a different larva. Sample size (n): 35, 34, 40, 43, 56, 42, 60, 58. In all cases, statistical analyses were done with data of 3 independent experiments. An unpaired, two-tailed t-test was used to assess significance (ns, no significant difference, $^{**}P < 0.01$, $^{***}P < 0.001$, $^{****}P < 0.0001$) and data are shown as mean± SD.

Live imaging reveals that the *tlr2* and *myd88* mutations affect distant neutrophil directional persistence, but not migration speed upon tail wounding

To investigate how neutrophils migrate in the absence of *tlr2* or *myd88* after tail wounding, a time-lapse microscopy experiment was performed by using CLSM between 1 hpw to 3 hpw (Fig. 5, 6). The definition of distant and local resident neutrophils was shown in panel A of Fig. 5-6 and Fig. S4-5. Neutrophils located closer than 200μm to the wound were defined as local resident neutrophils and further than 200μm were defined as distant neutrophils. Measurement of the distance to the wound over time of all distant neutrophils in the *tlr2*$^{-/-}$ group indicated a trend of impaired infiltration towards the wound (Fig. 5B,C up panel). In total, the group of distant neutrophils in the *tlr2*$^{+/+}$ group that arrived at the wound edge and stayed within a distance of 20 μm to the wound comprises 84 % of a total of 25 tracked neutrophils (Fig. 5C up panel). The local resident neutrophils in this group all remained at the wound (Fig. S4B, C up panel). In contrast, the group of the distant neutrophils in the *tlr2*$^{-/-}$ group that arrived at the wound within 2 h time-lapse cell tracking comprises only approximately 36 % (Fig. 5B,C bottom panel). Moreover, approximately 33 % of local resident neutrophils in the *tlr2*$^{-/-}$ group already migrated away from the wound edge within 3 hpw (Fig. S4B,C bottom panel).

In general, distant neutrophils in the *myd88*$^{+/+}$ group showed more chemotaxis to the wound compared to *myd88*$^{-/-}$ neutrophils (Fig. 6B,C). Approximately 96.7% distant neutrophils arrived at the wound (within a distance of 20 μm to the wound) in the *myd88*$^{+/+}$ group in total (Fig. 6C up panel). However, only 86.4% distant neutrophils arrived to the wound (within a distance of 20 μm to the wound) in the *myd88*$^{-/-}$ group. (Fig. 6C bottom panel). The local resident neutrophils in this group all remained at the wound except for a few outliers (Fig S5C). In summary, the general trend of distant neutrophils migration in the *myd88* mutant and sibling zebrafish groups was consistent with the result in the *tlr2* mutant and sibling zebrafish groups, respectively (Fig 6C).

To quantify differences in neutrophil migration behavior between *tlr2* and *myd88* mutants and their wild type siblings, we first analyzed whether the deficiency of *tlr2* and *myd88* can affect neutrophil mean migration speed upon wounding. The results showed that the *tlr2* and the *myd88* mutations do not affect the mean speed of both distant and local resident neutrophils upon the wounding (Fig. 5D; Fig. 6D; Fig. S4D and Fig. S5D). In addition to manual cell tracking analysis we also performed automatic 3D cell tracking by using a Viterbi Algorithm [52]. The results, shown in Fig. S8, confirm that there is no difference in mean speed between

mutant and sibling neutrophils. However, automatic tracking of living cells showed to be very challenging due to the complex leukocyte cell behaviors. Since in the automated method there are cell disappearing and appearing leading to gaps in the time series images it is currently still outperformed by manual tracking.

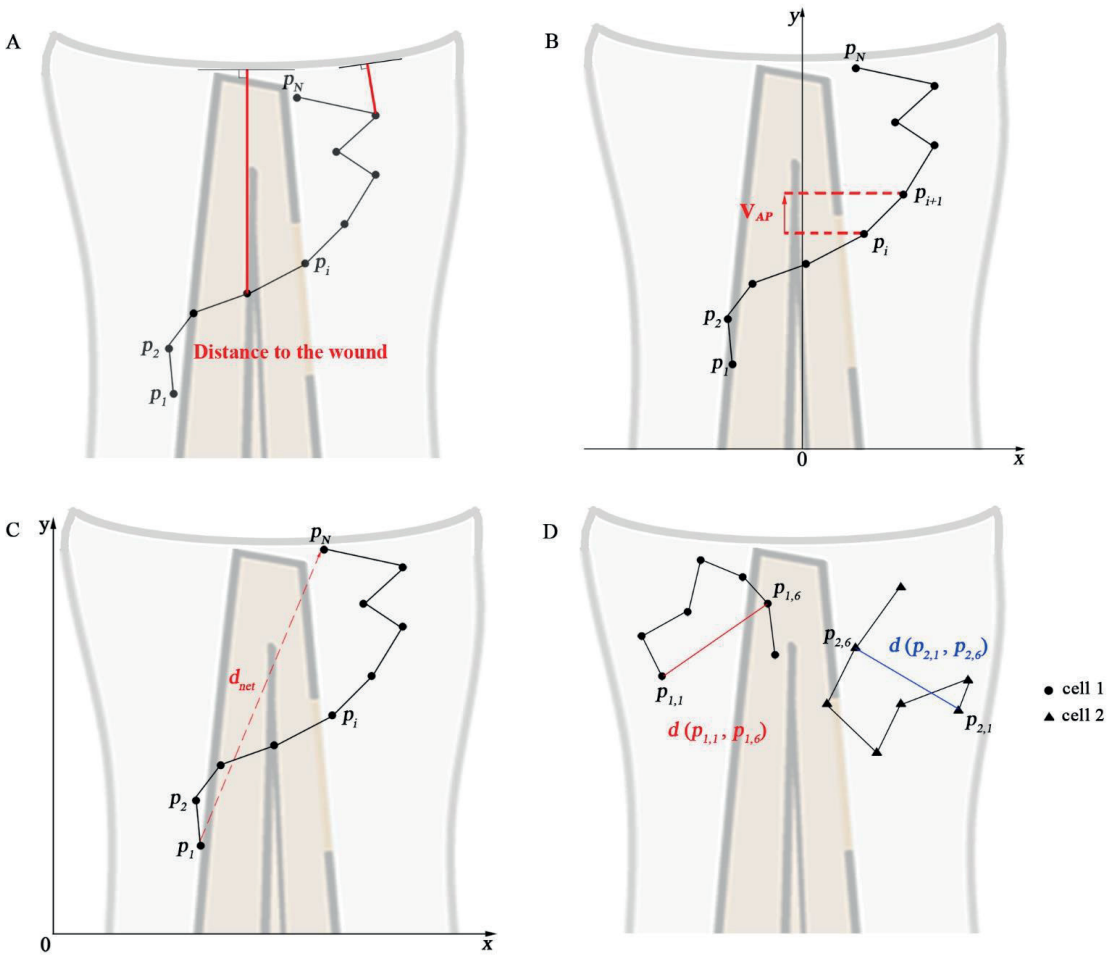

Figure 4 Calculated track measures.
(A) Depiction of distance to the wound. It measured for each frame as the shortest distance from the cell's current position to the entire line of the wound, i.e. the orthogonal projection to the wound.
(B) Depiction of V_{AP}: velocity in anteroposterior axis direction. The visible part of the spine is taken as the y-axis.
(C) Depiction of the net displacement, total displacement, meandering index and mean speed: the net displacement is the distance of the cell between the first and final time frame. Total displacement is the sum of the net displacement between 2 successive frames. Meandering index corresponds to the net displacement divided by the total displacement. Mean speed is the total displacement divided by traveled time. Formulas show in Table 1. (Eq. 1-4).
(D) Depiction of the construction of the mean squared displacement: the displacement between the first time frame and time frame t from all cells is squared and averaged, see Table 1. (Eq. 5).

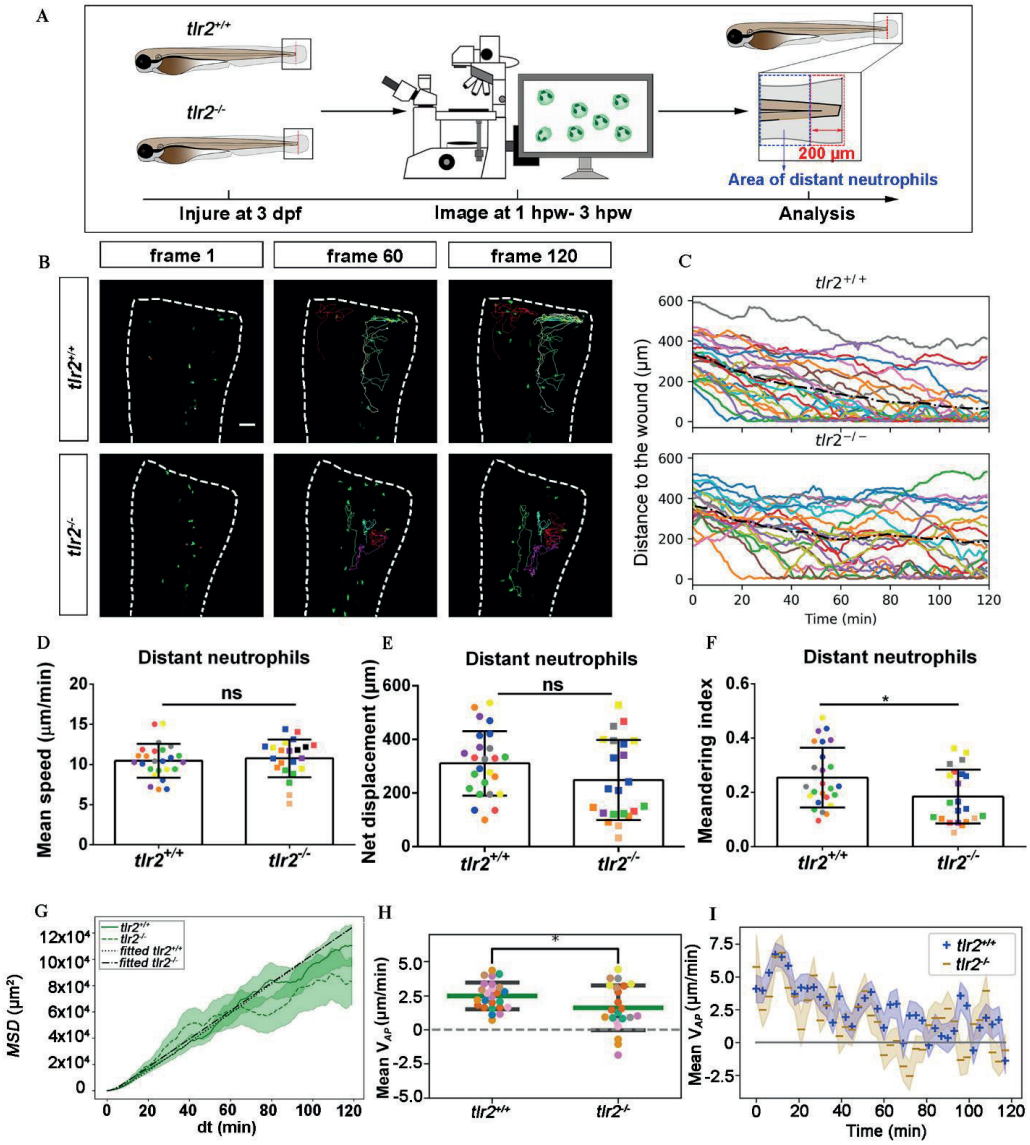

Figure 5 Quantification of distant neutrophils behavior in wounded *tlr2* mutant and sibling control larvae. (A) Experimental scheme. *Tlr2*$^{+/+}$ and *tlr2*$^{-/-}$ larvae were wounded at 3 dpf. The red dashed line shows the site of wounding. Neutrophils of wounded zebrafish larvae were tracked for 2 h and images were taken every 1 min by using CLSM. For cell tracking analysis, cells localized outside an area of 200 µm from the wounding edge toward the body trunk were counted as distant cells. Blue dashed box shows the area where distant neutrophils were tracked. (B) Representative images of distant neutrophil tracks in the wounded tail fin of 3 dpf *tlr2*$^{+/+}$ or *tlr2*$^{-/-}$ larvae at frame 1, frame 60 and frame 120. Time interval between two successive frames is 1 min. Each color track represents an individual neutrophil. Cell tracking movies are shown in Supplementary Movie S9-10). Scale bar: 50 µm. (C) Distance to the wound. Black dash line represents average distance to the wound. Each color line represents one cell. (D-I) Quantification of distant neutrophil tracks. In panel D-F and H, each color indicates a different larva. There was no significant difference between the groups in terms of mean speed (D), net displacement (E) and MSD (green) and fitted MSD (black) (G). However, meandering index (F) and mean V_{AP} (H) of neutrophils at the wound in *tlr2*$^{+/+}$ is greater than in *tlr2*$^{-/-}$ larvae. The fitted MSD (G, black) was fitted for $dt < 80$ min. The shaded regions in MSD (G) and mean V_{AP} over time (I) indicate standard error of the mean. Statistical analyses were done with 7 and 8 fish respectively for each group. An unpaired, two-tailed t-test was used to assess significance (ns, non-significance, $*P < 0.05$) and data are shown as mean± SD. Sample size (n): 25, 22 (D, E, F, H).

We also tested the effect of the *tlr2* and the *myd88* mutations on the movement direction of neutrophils upon wounding by the quantification of net displacement, whose definition is shown in Fig. 4 and Table 1. We observed that the net displacement of distant neutrophils had a decreased trend in the $tlr2^{-/-}$ group compared to the $tlr2^{+/+}$ group (Fig. 5E). Moreover, cell diffusivity determined by the fitting Eq. 6 to the MSD curve (Table 1.) did not differ much between the $tlr2^{-/-}$ group (277 μm^2/min) and the $tlr2^{+/+}$ group (268 μm^2/min) (Fig. 5G). A significant decrease in net displacements was consistently observed in the *myd88* mutant group (Fig. 6E). Also, $myd88^{-/-}$ neutrophils have lower diffusivity (274 μm^2/min) than $myd88^{+/+}$ neutrophils (412 μm^2/min) as measured from the slopes of the MSD plots (Fig. 6G). As the cell speed of $myd88^{-/-}$ neutrophils does not differ from that of $myd88^{+/+}$ neutrophils (Fig. 6D), the reduced diffusivity may be due to more frequent or sharper changes of direction of the $myd88^{-/-}$ neutrophils. As neutrophils reach the wound edge, their diffusivity is limited in space. This is also visible in the flattening of the MSD at later time frames. Hence, fitting Eq. 6 to the MSD curve was limited to $dt < 80$.

To further study the effect of the *tlr2* and *myd88* mutations on the neutrophil migration direction, we determined the meandering index and mean V_{AP} (Fig. 5F,H and Fig. 6F,H). The meandering index and mean V_{AP} are all significantly decreased in the distant neutrophils of both $tlr2^{-/-}$ and $myd88^{-/-}$ mutants compared to their wild type sibling controls (Fig. 5F,H and Fig. 6F,H). However, no significant difference of meandering index was found in local resident neutrophils of the $tlr2^{-/-}$ and $myd88^{-/-}$ mutants compared to the wild type siblings (Fig. S4F and Fig. S5F). The mean V_{AP} over time qualitatively shows again the impaired chemotaxis of $tlr2^{-/-}$ and $myd88^{-/-}$ neutrophils compared to the $tlr2^{+/+}$ and $myd88^{+/+}$ neutrophils, respectively (Fig. 5I and Fig. 6I). As more and more neutrophils approach the wound (Fig. 5C, 6C), the mean V_{AP} drops. For almost every time point, mean V_{AP} of $tlr2^{+/+}$ exceeds mean V_{AP} of $tlr2^{-/-}$ (Fig. 5I). Similar results were observed for $myd88^{+/+}$ and $myd88^{-/-}$ distant neutrophils (Fig. 6I).

Live imaging reveals that the *tlr2* and *myd88* mutations affect distant macrophage migration speed and directional persistence upon tail wounding

To study the effect of the *tlr2* and *myd88* mutations on macrophage migration upon wounding, we compared macrophage behavior with their wild type siblings. The definition of distant macrophage and local resident macrophage was shown in panel A of Fig. 7-8 and Fig. S6-7. Macrophages located closer than 200μm to the wound were defined as local resident

macrophages and further than 200μm were defined as distant macrophages. In contrast to neutrophils, the majority of macrophages do not reach the wound within the measured time period. By measuring their distance to the wound over time, we can see a trend that distant macrophages show less chemotaxis in the *tlr2*$^{-/-}$ and *myd88*$^{-/-}$ mutant groups compared to their wild type sibling groups (Fig. 7 B, C and Fig. 8B, C). Within 50 μm to the wound, the local resident macrophages all remained at the wound in both the *tlr2* and *myd88* mutants and their wild type sibling controls (Fig. S6B, C and Fig. S7B, C). Within a distance of 200 μm, but outside 50 μm to the wound, local resident macrophages tend to migrate to the wound direction (Fig. S6B, C and Fig. S7B, C).

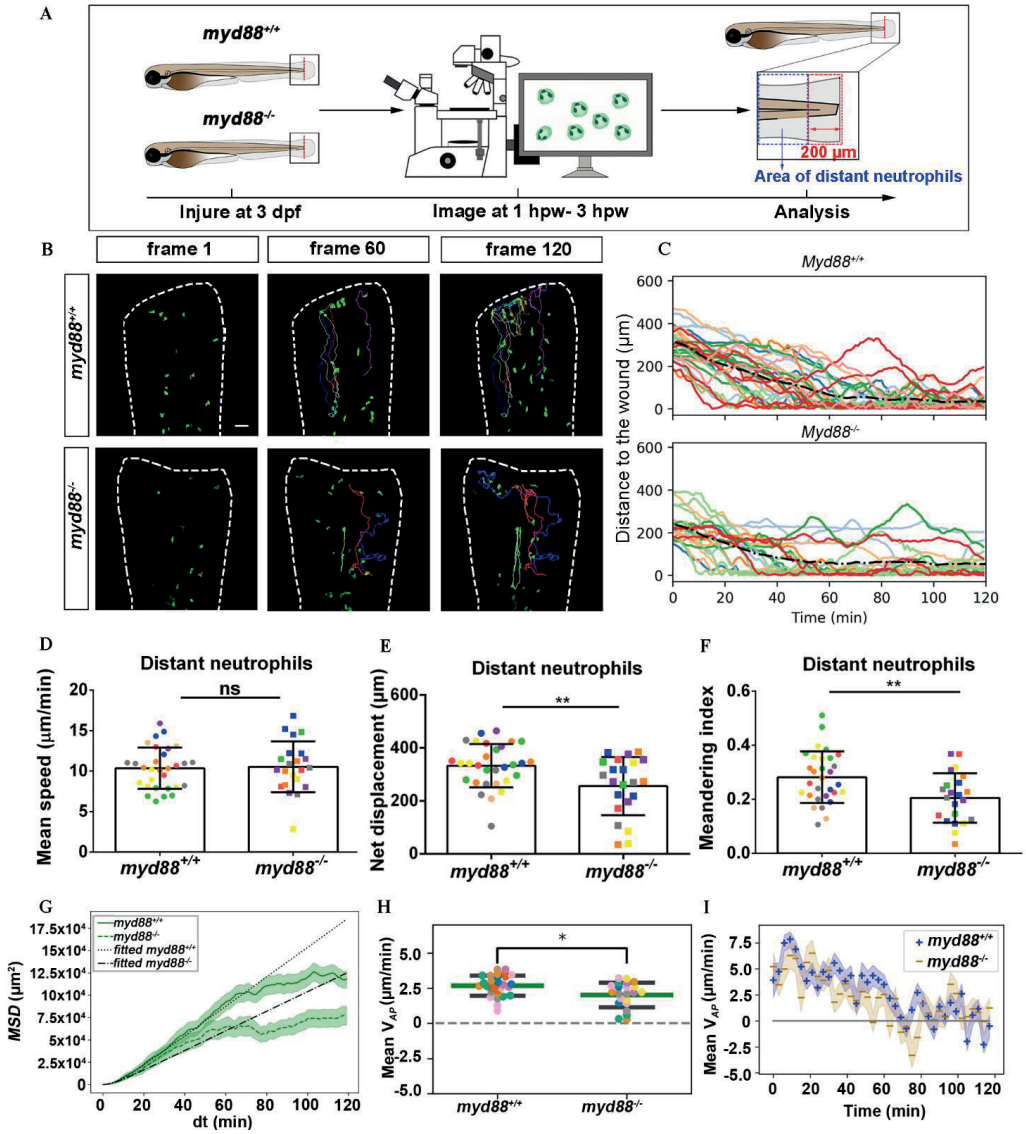

Figure 6 Quantification of distant neutrophils behavior in wounded *myd88* mutant and sibling control larvae. (A) Experimental scheme. *Myd88*$^{+/+}$ and *myd88*$^{-/-}$ larvae were wounded at 3 dpf. The red dashed line shows the site of wounding. Neutrophils of wounded *myd88* zebrafish larvae were tracked for 2 h and images were taken every 1 min by using CLSM. For cell tracking analysis, cells localized outside an area of 200 µm from the wounding edge toward the body trunk were counted as distant cells. Blue dashed box shows the area where distant neutrophils were tracked. (B) Representative images of distant neutrophil tracks in the wounded tail fin of 3 dpf *myd88*$^{+/+}$ or *myd88*$^{-/-}$ larvae at frame 1, frame 60 and frame 120. Time interval between two successive frames is 1 min. Each color track represents an individual neutrophil. Cell tracking movies are shown in Supplementary Movie S11-12). Scale bar: 50 µm. (C) Distance to the wound. Black dash line represents average distance to the wound. Each color line represents one cell. (D-I) Quantification of distant neutrophil tracks. In panel D-F and H, each color indicates a different larva. There was no significant difference between the groups in terms of mean speed (D). However, the net displacement (E), meandering index (F),), MSD (green) and fitted MSD (black) (G) and mean V_{AP} (H) of neutrophils at the wound in *myd88*$^{+/+}$ is greater than in *myd88*$^{-/-}$ larvae. The shaded regions MSD (G) and in mean V_{AP} over time (I) indicate standard error of the mean. The fitted MSD (G, black) was fitted for $dt < 80$ min. Statistical analyses were done with 8 and 7 fish respectively for each group. An unpaired, two-tailed t-test was used to assess significance (ns, non-significance, $^{**}P < 0.01$) and data are shown as mean± SD. Sample size (n): 30, 22 (D, E, F, H).

To quantify differences in macrophage migration behavior between *tlr2* and *myd88* mutants and their wild type siblings, we first analyzed whether the deficiency of *tlr2* and *myd88* can affect macrophage mean migration speed upon wounding. Following tail wounding, both distant and local resident macrophages migrate more slowly in the $tlr2^{-/-}$ and $myd88^{-/-}$ mutant groups than in the wild type sibling controls (Fig. 7D; Fig. 8D; Fig. S6D; Fig. S7D). In addition to manual cell tracking analysis we also performed automatic cell tracking by using a Viterbi Algorithm [52] (Fig. S8). The results from this automated 3D cell tracking confirm the significant difference in mean speed between mutant and sibling macrophages (Fig. S8).

Subsequently, we studied the directional persistence of macrophage migration upon wounding. To this end, we quantified the net displacement, meandering index and mean V_{AP} in the *tlr2* and *myd88* mutants and siblings. The net displacement of the distant macrophages (Table 1. Eq. 1) was reduced in the $tlr2^{-/-}$ and $myd88^{-/-}$ mutants compared to the controls (Fig. 7E; Fig. 8E). The meandering index (Table 1. Eq. 3) and mean V_{AP} of distant macrophages were also significantly decreased in the $tlr2^{-/-}$ and $myd88^{-/-}$ groups (Fig. 7F,H and Fig. 8F,H). However, no significant differences in net displacement were found in local resident *tlr2* and *myd88* macrophage groups (Fig. S6E and Fig. S7E). The trend of mean V_{AP} over time is similar to the one observed for distant neutrophils, in that $tlr2^{+/+}$ and $myd88^{+/+}$ macrophages have a higher mean V_{AP} than $tlr2^{-/-}$ and $myd88^{-/-}$ macrophages during the entire tracking period. The mean V_{AP} of macrophages is positive for a longer period of time compared to the neutrophils, as the majority of macrophages have not reached the wound site during the 2h time span.

The differences in speed and directionality also became apparent from the differences in MSD between the $tlr2^{+/+}$ and $myd88^{+/+}$ distant macrophages versus the $tlr2^{-/-}$ and $myd88^{-/-}$ distant macrophages (Fig. 7G,8G). The MSD (Table 1. Eq. 5) is lower for the $tlr2^{-/-}$ and $myd88^{-/-}$ macrophages, which can reflect a speed reduction and/or a lowered directional persistence. A decreased directional persistence can also be seen through the shape of the MSD curve. For $tlr2^{+/+}$ and $myd88^{+/+}$ distant macrophages, the MSD curve, especially at short time intervals dt, has a parabolic shape, indicating straight cell trajectories. For $tlr2^{-/-}$ and $myd88^{-/-}$, however, the MSD curve has a more linear shape, indicating random cell motility. Finally, the cell diffusivity D is also decreased in the $tlr2^{-/-}$ (38 μm^2/min) and $myd88^{-/-}$ (221 μm^2/min) macrophage groups compared to the $tlr2^{+/+}$ (132 μm^2/min) and $myd88^{+/+}$ (284 μm^2/min) macrophage groups. In summary, the data show that both *tlr2* and *myd88* mutations affect distant macrophage migration speed and directional persistence upon tail wounding.

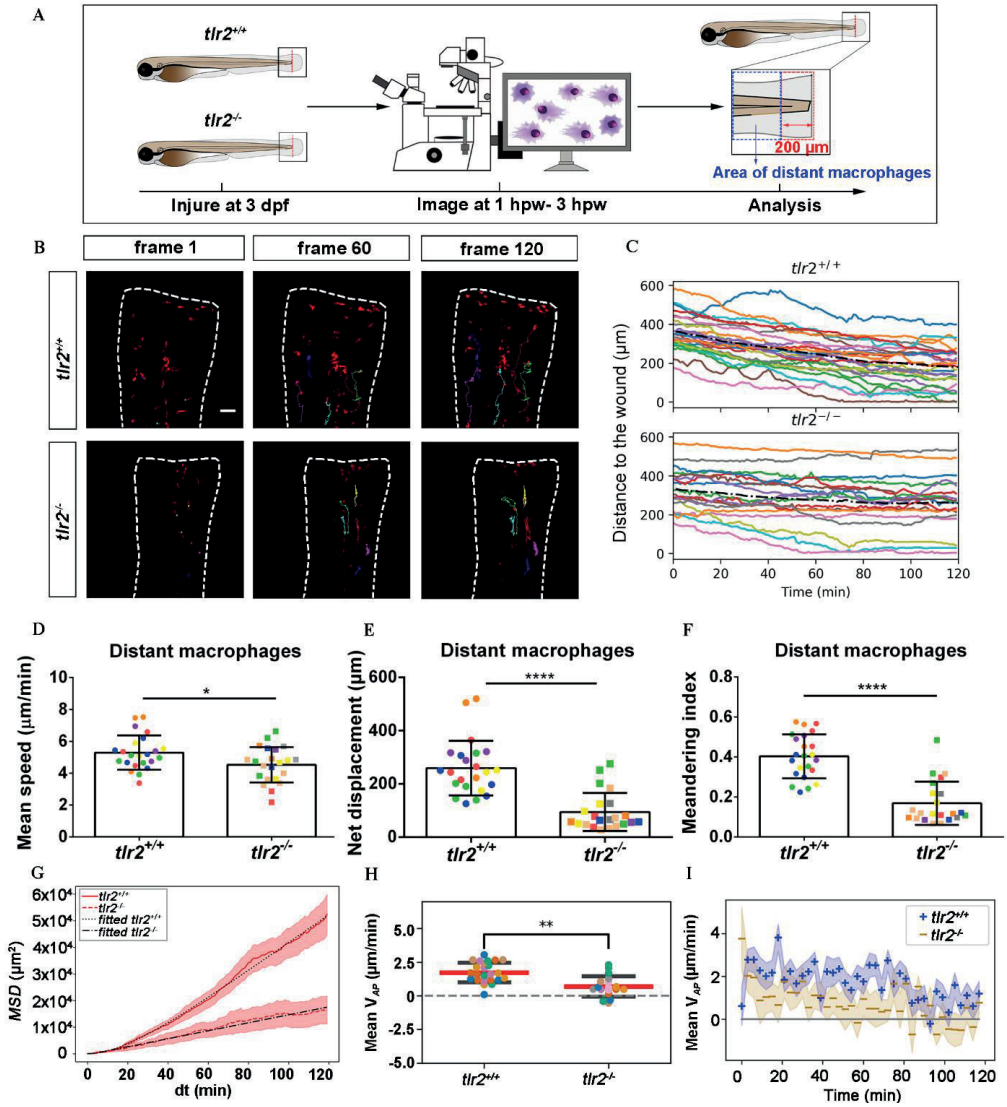

Figure 7 Quantification of distant macrophage behavior in wounded *tlr2* mutant and sibling control larvae. (A) Experimental scheme. *Tlr2*$^{+/+}$ and *tlr2*$^{-/-}$ larvae were wounded at 3 dpf. The red dashed line shows the site of wounding. Macrophages of wounded *tlr2* zebrafish larvae were tracked for 2 h and images were taken every 1 min by using CLSM. For cell tracking analysis, cells localized outside an area of 200 µm from the wounding edge toward the body trunk were counted as distant cells. Blue dashed box shows the area where distant macrophages were tracked. (B) Representative images of distant macrophage tracks in the wounded tail fin of 3 dpf *tlr2*$^{+/+}$ or *tlr2*$^{-/-}$ larvae at frame 1, frame 60 and frame 120. Time interval between two successive frames is 1 min. Each color track represents an individual macrophage. Cell tracking movies are shown in Supplementary Movie S13-14). Scale bar: 50 µm. (C) Distance to the wound. Black dash line represents average distance to the wound. Each color line represents one cell. (D-I) Quantification of distant macrophage tracks. In panel D-F and H, each color indicates a different larva. There was a significant difference between the groups in terms of mean speed (D), net displacement (E), meandering index (F),), MSD (red) and fitted MSD (black) (G) and mean V_{AP} (H) of macrophages. The shaded regions in MSD (G) and mean V_{AP} over time (I) indicate standard error of the mean. Statistical analyses were done with 6 and 8 fish respectively for each group. An unpaired, two-tailed t-test was used to assess significance (ns, non-significance, $*P < 0.05$, $**P < 0.01$, $****P < 0.0001$) and data are shown as mean± SD. Sample size (n): 23, 22 (D, E, F, H).

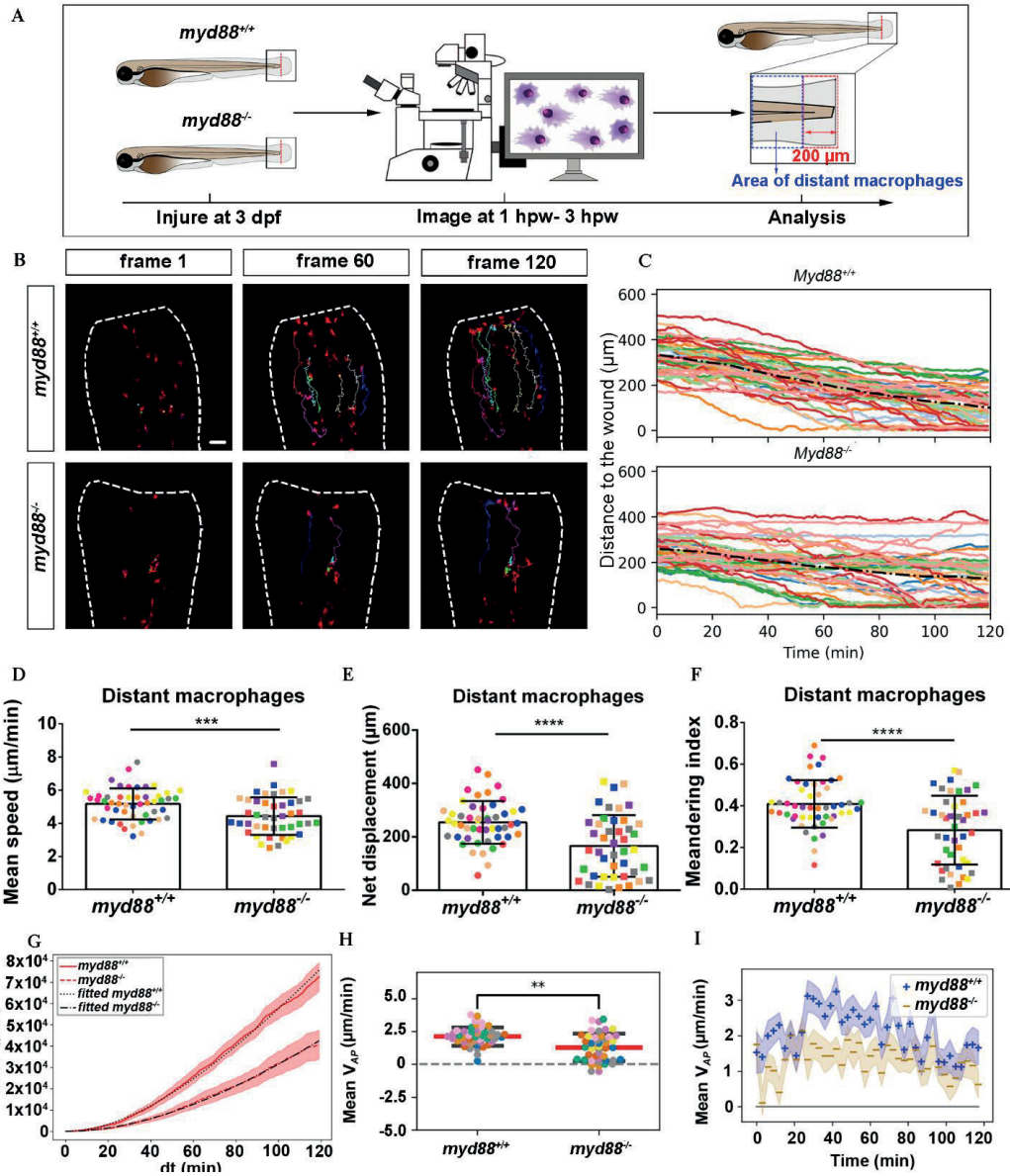

Figure 8 Quantification of distant macrophages behavior in wounded *myd88* mutant and sibling control larvae. (A) Experimental scheme. *Myd88*$^{+/+}$ and *myd88*$^{-/-}$ larvae were wounded at 3 dpf. The red dashed line shows the site of wounding. Macrophages of wounded zebrafish larvae were tracked for 2 h and images were taken every 1 min by using CLSM. For cell tracking analysis, cells localized outside an area of 200 µm from the wounding edge toward the body trunk were counted as distant cells. Blue dashed box shows the area where distant macrophages were tracked. (B) Representative images of distant macrophage tracks in the wounded tail fin of 3 dpf *myd88*$^{+/+}$ or *myd88*$^{-/-}$ larvae at frame 1, frame 60 and frame 120. Time interval between two successive frames is 1 min. Each color track represents an individual macrophage. Cell tracking movies are shown in Supplementary Movie S15-16). Scale bar: 50 µm. (C) Distance to the wound. Black dash line represents average distance to the wound. Each color line represents one cell. (D-I) Quantification of distant macrophage tracks. In panel D-F and H, each color indicates a different larva. There was a significant difference between the groups in terms of mean speed (D), net displacement (E), meandering index (F), MSD (red) and fitted MSD (black) (G) and mean V_{AP} (H) of macrophages. Statistical analyses were done with 9 and 8 fish respectively for each group. The shaded regions in MSD (G) and mean V_{AP} over time (I) indicate standard error of the mean. An unpaired, two-tailed t-test was used to assess significance (ns, non-significance, $*P < 0.05$, $**P < 0.01$, $****P < 0.0001$) and data are shown as mean± SD. Sample size (n): 50, 44 (D, E, F, H).

Discussion

In this study we visualized cell migration in *tlr2* and *myd88* mutants using live-imaging in a zebrafish tail wounding model. Thereby we demonstrated that these genes play a crucial role to control the migration of both neutrophils and macrophages upon tissue wounding. Like in mammals, neutrophils and macrophages play a dominant role in the wounding response during the first several hours after zebrafish tail fin wounding [4, 42, 53]. In mice, it has been shown previously that TLR signaling plays a role in controlling infiltration of neutrophils and macrophages into injured tissue [22-25]. The function of TLR signaling in migration to epithelial wounds has only been studied so far in zebrafish larvae [31]. This study found that knock-down of *myd88* by morpholinos impairs the infiltration of neutrophils into the wound area, but the mechanisms underlying such reduced wound infiltration remained unknown. By using double transgenic lines, here we show that *tlr2* and *myd88* are both essential for directed migration of distant neutrophils and macrophages to the wounded tissue. The meandering index (Fig. 4 and Table 1. Eq. 3) of distant neutrophils and macrophages was significantly decreased in *tlr2* and *myd88* mutant larvae compared with wild type sibling control groups (Fig. 5F, 6F, 7F and 8F). Moreover, the migration speed of distant and local resident macrophages was decreased upon wounding in the *tlr2* and *myd88* mutants (Fig. 7D and 8D; Fig. 6D and 7D), but not in unchallenged larvae. In summary, our data suggest that TLR signaling regulates neutrophil and macrophage migration upon wounding by controlling their directional persistence and the migration speed of macrophages (Fig. 9).

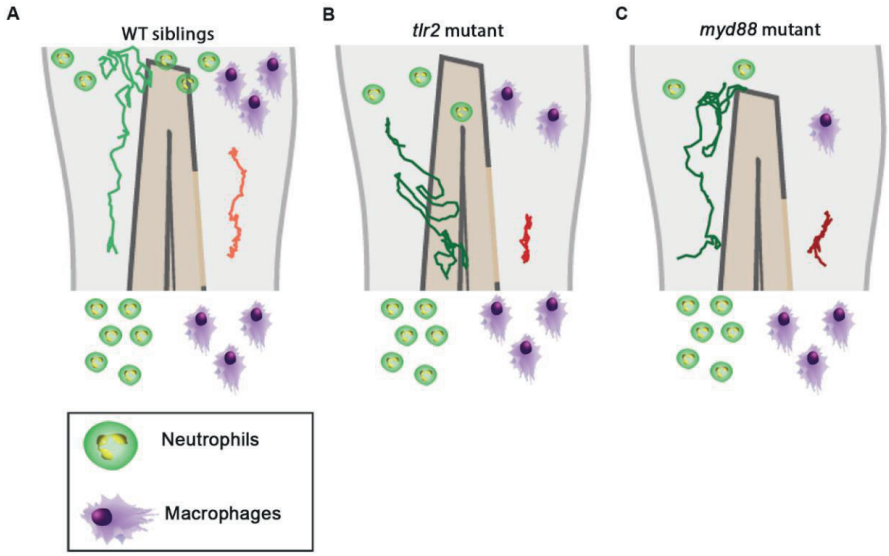

Figure 9 Graphic summary of the data of cell migration behavior in the *tlr2* and *myd88* mutants and wild type siblings.
(A) Cell migration behavior in the wild type siblings.
(B) Cell migration behavior in the *tlr2* mutant.
(C) Cell migration behavior in the *myd88* mutant.
In all cases, the green and red tracks are representative for the medians of the measured total displacements and net displacements in the anteroposterior axis of distant neutrophils and macrophages, respectively. The number of drawn leukocytes at the wound are only representing estimates of the relative numbers in the different genotypes. For the wild type sibling the *tlr2*$^{+/+}$ sibling was used as an example (A).

The difference in directional persistence of the distant neutrophils and macrophages in the mutant shows already within 3 hours post wounding, suggesting that TLR signaling is involved in direct sensing of signals from the wound at the post-transcriptional level. However, since TLRs have not been implied in sensing meandering gradients, we assume that this function involves other receptors. Tlr2 has been shown to be essential for the regulation of cytokines and chemokines expression in both mice and zebrafish [24, 45]. For instance, we have shown that *tlr2* mutant shows a significant lower expression of *cxcl11aa* and also of a related chemokine, *cxcl11ac*, during mycobacterial infection. The CXCR3-CXCL11 chemokine-signaling axis has been demonstrated to play an essential role not only in infection process and but also in inflammation process by regulating leukocyte trafficking [41, 54]. It is possible that an insufficient level of basal transcripts for chemokines at the time of wounding is responsible for the observed defects in leukocyte migration behavior. It is also possible that DAMPs released by dead cells around the wound do not lead to secretion of chemokines in the absence of TLR signaling. DAMPs are well known for activating PRRs and then activating downstream

chemokines and cytokines secretion [13]. Molecules that can function as DAMPs and associated recognition factors during tissue injury such as hyaluronic acid and HMGB1, have been shown to be directly recognized by TLRs in tissues [18, 55, 56]. Chemokines can be produced by leukocytes which are exposed to reactive oxygen species (ROS) produced by injury [2, 57]. Moreover, previous studies have demonstrated that ROS are required for leukocyte recruitment upon wounding in the zebrafish larval model showing its function in long range chemotaxis to arachidonic acid [40, 44]. It has been demonstrated that the generation of ROS is related to TLR signaling in inflammation and tissue injury [58]. For example, Shishido et al. found that TLR2 mediates the generation of ROS after vascular injury [59]. Thus, it is interesting to further study whether the generation of ROS may be altered in *tlr2* and *myd88* mutant zebrafish larvae. In addition, it is possible that the function of other TLRs can be affected in a TLR2 mutant upon tissue wounding. For example, the mRNA expression of TLR4 was decreased in TLR2-deficient mice, which indicated that TLR2 can cooperate with TLR4 to play a role upon tissue wounding [60, 61]. Taken together, these studies suggest that TLR signaling is implicated in the sensitivity to signaling molecules secreted by the wound, explaining why less infiltration of neutrophils and macrophages is observed in tail wounds of the *tlr2* and *myd88* mutants. Future research should be aimed at experiments investigating the cell autonomous nature of the function of TLR signaling in leukocyte cell migration behavior in response to wounding.

To study the mechanistic basis of the differences in cell migratory behavior, mathematical and computational models can also provide insights. Chemokine and ROS gradients can easily be modelled by partial differential equations (PDEs). These can also be incorporated into a cell chemotaxis models, such as random walk models, phase field models, or the Cellular Potts model, with varying degrees of cell resolution, to study the chemotaxis of leukocytes. Such models could provide quantitative insights into how chemokine and ROS gradients affect the migration behavior of the leukocytes, and how the cells change these gradients by binding or secretion of chemokines or absorption and metabolizing ROS (Dona et al., 2013) which is known to affect the robustness of chemotaxis (Tweedy et al., 2016). Using Bayesian inference on tracking data, one can infer a number of chemotaxis parameters, such as the flow rate, diffusion coefficient and production time of the chemoattractant (Manolopoulou et al., 2012). Furthermore, simulated tracks can be compared to experimentally derived tracks. Altogether, such quantitative approaches in close interaction with new experiments could help demonstrate that the chemokine or ROS gradients are affected by the *tlr2* and *myd88* mutations. For such

experiments we will need larger data sets than were currently obtained. This was partially due to the limitations of manual cell tracking. Therefore, in follow-up experiments with larger datasets, the tracking needs to be automated. Consequently, we plan to develop further optimized automatic tracking methods based on the used Viterbi algorithm to quantify larger data sets.

Better theoretical cell migration analysis methods will also be useful for studying subsequent phases of the inflammatory response after wounding [2]. This can assist us in future studies focused on examining the involvement of the TLR signaling in neutrophil reverse migration and in the repair of wounded tissue. Previously we have reported that *myd88* mutant larvae that were raised under germ-free conditions show increased macrophage and decreased neutrophil numbers in the gut [62]. This indicates that the function of TLR signaling in leukocyte migration is dependent on the gut microbiota. It will be highly interesting to test whether the response of leukocytes to tail wounding is also dependent on the microbiome.

Materials and methods

Zebrafish maintenance and strain construction

All animal experiments described in this study were performed at the University of Leiden according to standard protocols (zfin.org) and adhered to the international guidelines specified by the EU Animal Protection Directive 2010/63/EU. The culture of adult fish was approved by the local animal welfare committee (DEC) of the university (License number: protocol 14,198). No adult zebrafish were sacrificed for this study. All experiments were done on 3 days post fertilization (dpf) fish, therefore prior to the free-feeding stage and did not fall under animal experimentation law according to the EU Animal Protection Directive 2010/63/EU. Eggs and larvae were grown at 28.5˚C in egg water (60 g/ml Instant Ocean sea salts). For living imaging and tail wounding experiments, 3 dpf larvae were anesthetized with egg water containing 0.02% buffered 3-aminobenzoic acid ethyl ester (Tricaine, Sigma-Aldrich, the Netherlands).

The *tlr2*^{sa19423} mutant and *myd88*^{hu3568} mutant lines were identified by the sequencing of an ENU-mutagenized zebrafish library [45, 47]. To investigate the effect of the *tlr2* and the *myd88* mutations on leukocyte development, double fluorescent lines *tlr2*$^{+/+}$ *Tg (mpeg1:mCherry-F);TgBAC (mpx: EGFP)*, *tlr2*$^{-/-}$ *Tg (mpeg1:mCherry-F);TgBAC (mpx: EGFP), myd88*$^{+/+}$ *Tg (mpeg1:mCherry-F);TgBAC (mpx: EGFP)*, *myd88*$^{-/-}$ *Tg (mpeg1:mCherry-F);TgBAC (mpx:*

EGFP) were used. Both homozygous mutants were outcrossed with the double transgenic line *Tg (mpeg1:mCherry-F);TgBAC (mpx: EGFP)* [39, 63]. Subsequently, their heterozygous offspring with both positive GFP and mCherry fluorescence were imaged and then used for in-cross. F1 heterozygous in-cross offspring with both positive GFP and mCherry fluorescence were imaged blindly and genotyped post-imaging to produce the homozygous mutants and wild type siblings. In the present study, the double transgenic lines were used for the quantification of cell numbers, cell recruitment assays upon wounding and leukocyte living imaging experiments.

Tail wounding

In the present study, a caudal fin wounding model was applied as previously described [39, 42, 64]. 3 dpf *tlr2* zebrafish larvae were anesthetized with egg water containing 0.02% tricaine (Sigma Aldrich). Subsequently, the caudal fins of larvae were wounded by using a 1 mm sterile sapphire blade scalpel (World Precision Instruments) on a 2% agarose covered petri-dish. To avoid damaging the notochord and other tissues of zebrafish larvae, all of the wounding experiments were performed under a MZ16FA Fluorescence Stereo Microscope (Leica Microsystems, Wetzlar Germany) equipped with a DFC420C color camera (Leica Microsystems). After the wounding, the egg water with 0.02% tricaine was changed with untreated egg water. Wounded larvae were put back into an incubator at 28.5˚C. Subsequently, the wounded larvae were collected or fixed for follow up experiments.

Imaging and quantification

For the quantification of the recruited cell number upon wounding, the double transgenic *tlr2* and *myd88* larvae were wounded with the method described before. 1, 2, 4 and 6 hour post wounding (hpw), larvae were collected and fixed with 4% paraformaldehyde (PFA) in PBS overnight at 4˚C and washed with PBS the next day. The wounded tail area of fixed samples from each group were imaged by using a Leica MZ16FA fluorescence stereo microscope equipped with a DFC420C color camera. Cells localized within an area of 200 µm from the wounding edge toward the body trunk were counted as recruited cells. Analysis was performed by combining three independent experiments.

For detailed cell migration behavior analyses, larvae (3 dpf) were mounted into 1% low melting point agarose (Sigma Aldrich) with 0.02% tricaine and imaged under a Leica TCS SP8 confocal microscope (Leica Microsystems) with a 10× objective (N.A. 0.40). Data were saved as

maximum projection images for further cell counting. The number of neutrophils and macrophages in the tail region were manually quantified.

Live imaging

All time-lapse imaging was performed on 3 dpf larvae. Larvae for each condition (unchallenged/ wounded) were mounted in the method described before and visualized in the CLSM with 1 min time interval for 2 h image capture using a 20× objective (N.A. 0.75). For the manual cell tracking analysis, all time-lapse images were saved as maximum projection images.

We first defined the role of *tlr2* and *myd88* in leukocyte migration under the unchallenged condition. The caudal hematopoietic tissue (CHT) of double transgenic lines was imaged using the CLSM with unchallenged condition. To investigate the effect of the *tlr2* and *myd88* mutations on leukocyte migration upon wounding, the double transgenic line *Tg (mpeg1:mCherry-F);TgBAC (mpx: EGFP)* larvae in the *tlr2*, *myd88* mutant or their wild type background were wounded and performed for real time imaging from 1 hpw to 3 hpw.

Cell tracking and its quantification

The cell tracking of macrophages and neutrophils was either performed manually by using a manual tracking plug-in from Fiji [54, 65] or automatically by using automatic 3D cell tracking algorithms [66, 67]. In this paper, we applied a Viterbi Algorithm, proposed by Magnusson et al. for quantifying leukocyte migration speed [52]. The Viterbi Algorithm follows a global linking strategy which can find the optimal path based on a probabilistically motivated scoring function. The algorithm incorporates six different cell behaviors which include cell migration, migration into or out of image based on probability framework, and cell count, mitosis, apoptosis based on logistic regression. In our application, we did not take into account mitosis and apoptosis. An operation called “swaps” is applied in the Viterbi Algorithm. It can modify links in preexisting tracks if there is a better linking way during a creation of new tracks.

The distance to the wound, mean speed, net displacement, meandering index (M.I.), mean square displacement (MSD), cell diffusivity (D), velocity in anteroposterior direction (V_{AP}) and V_{AP} over time were calculated in different groups by manual tracking data. The calculation and explanation of the parameters are shown in Fig. 4. The distance to the wound is defined as the shortest Euclidean distance to the wound edge (Fig. 4A). For the velocity in the anteroposterior direction, tracks were rotated such that the spines of the larvae were aligned (Fig. 4B). Then,

for each cell the average velocity in the anteroposterior axis was calculated. For V_{AP} over time, the V_{AP} of all cells within a group was averaged over three consecutive time frames. Net displacement, total displacement, meandering index and mean speed are shown in Fig. 4C and Table 1 (Eq. 1-4). The net displacement is the distance of the cell between the first and final time frame (Fig. 4C), i.e., the Euclidian distance traveled being: $d_{net} = d(p_i, p_N)$ (Table 1. Eq. 1). The total displacement is the length of the total cell track, i.e., the sum of the net displacements between two successive frames ($d_{tot} = \sum_{i=1}^{N-1} d(p_i, p_{i+1})$) (Fig. 4C) (Table 1. Eq. 2). Cells can reorient between two frames, such that this measure may underestimate the actual distance traveled. However, we used the same frame rate of 1 min in all experiments, such that the results are comparable with one another. Meandering index is most simply defined as the net distance traveled divided by the total distance traveled (M.I $=\frac{d_{net}}{d_{tot}}$) [68] (Fig. 4C) (Table 1. Eq. 3). Mean speed is the total displacement divided by traveled time ($\bar{v} = \frac{1}{N-1}\sum_{i=1}^{N-1} v_i$) (Table 1. Eq. 4). The MSD at time t was calculated for each group by averaging the squared displacement from starting time t_1=1hpw to time t over all cells (K) within that group ($MSD\ (t) = \frac{1}{K}\sum_{i=1}^{K}\left(d\ (p_{i,1}\ , p_{i,1+t})\right)^2$) (Fig. 4D) (Table 1. Eq. 5). For persistent random walkers, an analytical expression for the MSD exists: $Fitted\ MSD\ (t) = 2v^2\ \tau t - 2(v\tau)^2\ (1 - e^{\frac{-t}{\tau}})$) (Table 1. Eq. 6), with v the intrinsic cell velocity and τ the persistent time, which can be fit to the MSD calculated from cell tracks [69]. The cell diffusivity constant D and MSD (t) at large t are related through $D = 1/2n\ \frac{dMSD(t)}{dt}$, with n=2 the dimension, which for persistent random walkers results in $D = 1/2\ v^2\ \tau$ (Table 1. Eq. 7). We assume that distant neutrophils and macrophages can behave like persistent random walkers during the time span of imaging [70]. We fit Eq. 6 to the MSD curve (Table 1. Eq. 5) using a non-linear least squares method. The obtained parameters v and τ are then used to compute the approximated cell diffusivity D. For distant neutrophils, the fit was performed on the first 80 min of tracking, for distant macrophages, the entire 2h tracking period was used.

The movement behavior of cells can change after they arrive at the wound edge (Fig. S1). To analyze the behavior of leukocyte tracks more accurately, we defined categories of distant and local resident cell movements based on their starting location in the first frame of the time lapse. Cells with a starting point of movements localized further than 200 µm from the wound edge toward to the trunk were categorized as distantly-localized cells (in brief called distant cells).

Cells with a starting point of movements localized within a distance of up to 200 µm from the wound edge toward to the trunk were categorized as wound-residing cells (in brief called local resident cells, Fig. S1A). Although there is no difference between distant neutrophils and local resident neutrophils in mean speed (Fig. S1C), net displacement and meandering index are significantly decreased in the local resident neutrophil groups compared to the distant neutrophil groups (Fig. S1D,E). Furthermore, mean speed, net displacement and meandering index are all significantly decreased in the local resident macrophage groups (Fig. S1F-H). Thus, the cell movement behavior is quantified by separating distant and local resident cell movements in this study.

Table 1. Formulas of calculated track measures and derived measures

Measure	Definition	No.
Net displacement (µm)	$d_{net} = d(p_i, p_N)$	Eq.1
Total displacement (µm)	$d_{tot} = \sum_{i=1}^{N-1} d(p_i, p_{i+1})$	Eq. 2
Meandering index	M.I. = d_{net}/d_{tot}	Eq. 3
Mean speed (µm/min)	$\bar{v} = \frac{1}{N-1}\sum_{i=1}^{N-1} v_i$	Eq. 4
Mean squared displacement (µm^2)	$MSD\ (t) = \frac{1}{K}\sum_{i=1}^{K}(d\ (p_{i,1}\ , p_{i,1+t}))^2$	Eq. 5
Fitted mean squared displacement (µm^2)	$MSD(t) = 2v^2\ \tau t - 2(v\tau)^2\ \left(1 - e^{\frac{-t}{\tau}}\right)$	Eq. 6
Cell diffusivity constant D (µm^2/min)	$D = 1/2\ v^2\ \tau$	Eq. 7

Statistical analysis

Graphpad Prism software (Version 8.1.1; GraphPad Software, San Diego, CA, USA) was used for statistical analysis. Computations of distance to the wound, MSD and V_{AP} were performed using a Python script including the SciPy stats library for statistical testing. Shaded regions of MSD and V_{AP} over time indicate standard error of mean, the other experiment data are shown as mean ± SD. Statistical significance of differences was determined by using an unpaired, two-tailed t-test for comparing the difference between wild type and *tlr2* and *myd88* mutant. (ns, no significant difference; *P < 0.05; **P < 0.01; ***P < 0.001; ****P < 0.0001).

Acknowledgments

We acknowledge Ulrike Nehrdich and Guus van der Velden for the assistance in adult zebrafish care.

Reference

1. Lieschke GJ, Oates AC, Crowhurst MO, Ward AC, Layton JE. Morphologic and functional characterization of granulocytes and macrophages in embryonic and adult zebrafish. Blood. 2001;98(10):3087-96. Epub 2001/11/08. doi: 10.1182/blood.v98.10.3087. PubMed PMID: 11698295.

2. Soehnlein O, Lindbom L. Phagocyte partnership during the onset and resolution of inflammation. Nat Rev Immunol. 2010;10(6):427-39. Epub 2010/05/26. doi: 10.1038/nri2779. PubMed PMID: 20498669.

3. Serhan CN, Brain SD, Buckley CD, Gilroy DW, Haslett C, O'Neill LA, et al. Resolution of inflammation: state of the art, definitions and terms. FASEB J. 2007;21(2):325-32. Epub 2007/02/03. doi: 10.1096/fj.06-7227rev. PubMed PMID: 17267386; PubMed Central PMCID: PMCPMC3119634.

4. Li L, Yan B, Shi YQ, Zhang WQ, Wen ZL. Live imaging reveals differing roles of macrophages and neutrophils during zebrafish tail fin regeneration. J Biol Chem. 2012;287(30):25353-60. Epub 2012/05/11. doi: 10.1074/jbc.M112.349126. PubMed PMID: 22573321; PubMed Central PMCID: PMCPMC3408142.

5. Nathan C. Neutrophils and immunity: challenges and opportunities. Nat Rev Immunol. 2006;6(3):173-82. Epub 2006/02/25. doi: 10.1038/nri1785. PubMed PMID: 16498448.

6. Weiss SJ. Tissue destruction by neutrophils. N Engl J Med. 1989;320(6):365-76. Epub 1989/02/09. doi: 10.1056/NEJM198902093200606. PubMed PMID: 2536474.

7. Brazil JC, Louis NA, Parkos CA. The role of polymorphonuclear leukocyte trafficking in the perpetuation of inflammation during inflammatory bowel disease. Inflamm Bowel Dis. 2013;19(7):1556-65. Epub 2013/04/20. doi: 10.1097/MIB.0b013e318281f54e. PubMed PMID: 23598816; PubMed Central PMCID: PMCPMC4110963.

8. Mescher AL. Macrophages and fibroblasts during inflammation and tissue repair in models of organ regeneration. Regeneration (Oxf). 2017;4(2):39-53. Epub 2017/06/16. doi: 10.1002/reg2.77. PubMed PMID: 28616244; PubMed Central PMCID: PMCPMC5469729.

9. Martin P, Leibovich SJ. Inflammatory cells during wound repair: the good, the bad and the ugly. Trends Cell Biol. 2005;15(11):599-607. Epub 2005/10/06. doi: 10.1016/j.tcb.2005.09.002. PubMed PMID: 16202600.

10. Hopkin SJ, Lewis JW, Krautter F, Chimen M, McGettrick HM. Triggering the Resolution of Immune Mediated Inflammatory Diseases: Can Targeting Leukocyte Migration Be the Answer? Front Pharmacol. 2019;10:184. Epub 2019/03/19. doi: 10.3389/fphar.2019.00184. PubMed PMID: 30881306; PubMed Central PMCID: PMCPMC6407428.

11. Hato T, Dagher PC. How the Innate Immune System Senses Trouble and Causes Trouble. Clin J Am Soc Nephrol. 2015;10(8):1459-69. Epub 2014/11/22. doi: 10.2215/CJN.04680514. PubMed PMID: 25414319; PubMed Central PMCID: PMCPMC4527020.

12. Janeway CA, Jr., Medzhitov R. Innate immune recognition. Annu Rev Immunol. 2002;20:197-216. Epub 2002/02/28. doi: 10.1146/annurev.immunol.20.083001.084359. PubMed PMID: 11861602.

13. Niethammer P. The early wound signals. Curr Opin Genet Dev. 2016;40:17-22. Epub 2016/06/09. doi: 10.1016/j.gde.2016.05.001. PubMed PMID: 27266971; PubMed Central PMCID: PMCPMC5278878.

14. Vijay K. Toll-like receptors in immunity and inflammatory diseases: Past, present, and future. Int Immunopharmacol. 2018;59:391-412. Epub 2018/05/08. doi: 10.1016/j.intimp.2018.03.002. PubMed PMID: 29730580; PubMed Central PMCID: PMCPMC7106078.

15. Yu L, Wang L, Chen S. Endogenous toll-like receptor ligands and their biological significance. J Cell Mol Med. 2010;14(11):2592-603. Epub 2010/07/16. doi: 10.1111/j.1582-4934.2010.01127.x. PubMed PMID: 20629986; PubMed Central PMCID: PMCPMC4373479.

16. Quesniaux VJ, Nicolle DM, Torres D, Kremer L, Guerardel Y, Nigou J, et al. Toll-like receptor 2 (TLR2)-dependent-positive and TLR2-independent-negative regulation of proinflammatory cytokines by mycobacterial lipomannans. J Immunol. 2004;172(7):4425-34. Epub 2004/03/23. doi: 10.4049/jimmunol.172.7.4425. PubMed PMID: 15034058.

17. Poltorak A, He X, Smirnova I, Liu MY, Van Huffel C, Du X, et al. Defective LPS signaling in C3H/HeJ and C57BL/10ScCr mice: mutations in Tlr4 gene. Science. 1998;282(5396):2085-8. Epub 1998/12/16. doi: 10.1126/science.282.5396.2085. PubMed PMID: 9851930.

18. Bianchi ME. HMGB1 loves company. J Leukoc Biol. 2009;86(3):573-6. Epub 2009/05/06. doi: 10.1189/jlb.1008585. PubMed PMID: 19414536.

19. Yanai H, Ban T, Wang Z, Choi MK, Kawamura T, Negishi H, et al. HMGB proteins function as universal sentinels for nucleic-acid-mediated innate immune responses. Nature. 2009;462(7269):99-103. Epub 2009/11/06. doi: 10.1038/nature08512. PubMed PMID: 19890330.

20. Teixeira HS, Zhao J, Kazmierski E, Kinane DF, Benakanakere MR. TLR3-Dependent Activation of TLR2 Endogenous Ligands via the MyD88 Signaling Pathway Augments the Innate Immune Response. Cells. 2020;9(8). Epub 2020/08/23. doi: 10.3390/cells9081910. PubMed PMID: 32824595; PubMed Central PMCID: PMCPMC7464415.

21. Oliveira-Nascimento L, Massari P, Wetzler LM. The Role of TLR2 in Infection and Immunity. Front Immunol. 2012;3:79. Epub 2012/05/09. doi: 10.3389/fimmu.2012.00079. PubMed PMID: 22566960; PubMed Central PMCID: PMCPMC3342043.

22. Schauber J, Dorschner RA, Coda AB, Buchau AS, Liu PT, Kiken D, et al. Injury enhances TLR2 function and antimicrobial peptide expression through a vitamin D-dependent mechanism. J Clin Invest. 2007;117(3):803-11. Epub 2007/02/10. doi: 10.1172/JCI30142. PubMed PMID: 17290304; PubMed Central PMCID: PMCPMC1784003.

23. Xu Y, Zhou Y, Lin H, Hu H, Wang Y, Xu G. Toll-like receptor 2 in promoting angiogenesis after acute ischemic injury. Int J Mol Med. 2013;31(3):555-60. Epub 2013/01/15. doi: 10.3892/ijmm.2013.1240. PubMed PMID: 23314218.

24. Moles A, Murphy L, Wilson CL, Chakraborty JB, Fox C, Park EJ, et al. A TLR2/S100A9/CXCL-2 signaling network is necessary for neutrophil recruitment in acute and chronic liver injury in the mouse. J Hepatol. 2014;60(4):782-91. Epub 2013/12/18. doi: 10.1016/j.jhep.2013.12.005. PubMed PMID: 24333183; PubMed Central PMCID: PMCPMC3960359.

25. Castoldi A, Braga TT, Correa-Costa M, Aguiar CF, Bassi EJ, Correa-Silva R, et al. TLR2, TLR4 and the MYD88 signaling pathway are crucial for neutrophil migration in acute kidney injury induced by sepsis. PLoS One. 2012;7(5):e37584. Epub 2012/06/02. doi: 10.1371/journal.pone.0037584. PubMed PMID: 22655058; PubMed Central PMCID: PMCPMC3360043.

26. Mojumdar K, Giordano C, Lemaire C, Liang F, Divangahi M, Qureshi ST, et al. Divergent impact of Toll-like receptor 2 deficiency on repair mechanisms in healthy muscle versus Duchenne muscular dystrophy. J Pathol. 2016;239(1):10-22. Epub 2016/01/23. doi: 10.1002/path.4689. PubMed PMID: 26800321.

27. Kim D, You B, Lim H, Lee SJ. Toll-like receptor 2 contributes to chemokine gene expression and macrophage infiltration in the dorsal root ganglia after peripheral nerve injury. Mol Pain. 2011;7:74. Epub 2011/09/29. doi: 10.1186/1744-8069-7-74. PubMed PMID: 21951975; PubMed Central PMCID: PMCPMC3192680.

28. Seki E, Park E, Fujimoto J. Toll-like receptor signaling in liver regeneration, fibrosis and carcinogenesis. Hepatol Res. 2011;41(7):597-610. Epub 2011/06/24. doi: 10.1111/j.1872-034X.2011.00822.x. PubMed PMID: 21696522; PubMed Central PMCID: PMCPMC3754784.

29. Miura K, Yang L, van Rooijen N, Brenner DA, Ohnishi H, Seki E. Toll-like receptor 2 and palmitic acid cooperatively contribute to the development of nonalcoholic steatohepatitis through inflammasome activation in mice. Hepatology. 2013;57(2):577-89. Epub 2012/09/19. doi: 10.1002/hep.26081. PubMed PMID: 22987396; PubMed Central PMCID: PMCPMC3566276.

30. Ji L, Xue R, Tang W, Wu W, Hu T, Liu X, et al. Toll like receptor 2 knock-out attenuates carbon tetrachloride (CCl4)-induced liver fibrosis by downregulating MAPK and NF-kappaB signaling pathways. FEBS Lett. 2014;588(12):2095-100. Epub 2014/05/13. doi: 10.1016/j.febslet.2014.04.042. PubMed PMID: 24815695.

31. Deng Q, Harvie EA, Huttenlocher A. Distinct signalling mechanisms mediate neutrophil attraction to bacterial infection and tissue injury. Cell Microbiol. 2012;14(4):517-28. Epub 2011/12/23. doi: 10.1111/j.1462-5822.2011.01738.x. PubMed PMID: 22188170; PubMed Central PMCID: PMCPMC3302966.

32. Chen L, Zheng L, Chen P, Liang G. Myeloid Differentiation Primary Response Protein 88 (MyD88): The Central Hub of TLR/IL-1R Signaling. J Med Chem. 2020. Epub 2020/09/16. doi: 10.1021/acs.jmedchem.0c00884. PubMed PMID: 32931267.

33. Takeda K, Akira S. Microbial recognition by Toll-like receptors. J Dermatol Sci. 2004;34(2):73-82. Epub 2004/03/23. doi: 10.1016/j.jdermsci.2003.10.002. PubMed PMID: 15033189.

34. Wagner N, Reinehr S, Palmhof M, Schuschel D, Tsai T, Sommer E, et al. Microglia Activation in Retinal Ischemia Triggers Cytokine and Toll-Like Receptor Response. J Mol Neurosci. 2020. Epub 2020/08/25. doi: 10.1007/s12031-020-01674-w. PubMed PMID: 32833183.

35. Dasu MR, Thangappan RK, Bourgette A, DiPietro LA, Isseroff R, Jialal I. TLR2 expression and signaling-dependent inflammation impair wound healing in diabetic mice. Lab Invest. 2010;90(11):1628-36. Epub 2010/08/25. doi: 10.1038/labinvest.2010.158. PubMed PMID: 20733560.

36. Macedo L, Pinhal-Enfield G, Alshits V, Elson G, Cronstein BN, Leibovich SJ. Wound healing is impaired in MyD88-deficient mice: a role for MyD88 in the regulation of wound healing by adenosine A2A receptors. Am J Pathol. 2007;171(6):1774-88. Epub 2007/11/03. doi: 10.2353/ajpath.2007.061048. PubMed PMID: 17974599; PubMed Central PMCID: PMCPMC2111102.

37. Houseright RA, Rosowski EE, Lam PY, Tauzin SJM, Mulvaney O, Dewey CN, et al. Cell type specific gene expression profiling reveals a role for complement component C3 in neutrophil responses to tissue damage. Sci Rep. 2020;10(1):15716. Epub 2020/09/26. doi: 10.1038/s41598-020-72750-9. PubMed PMID: 32973200; PubMed Central PMCID: PMCPMC7518243.

38. Meijer AH, Spaink HP. Host-pathogen interactions made transparent with the zebrafish model. Curr Drug Targets. 2011;12(7):1000-17. Epub 2011/03/04. doi: 10.2174/138945011795677809. PubMed PMID: 21366518; PubMed Central PMCID: PMCPMC3319919.

39. Renshaw SA, Loynes CA, Trushell DM, Elworthy S, Ingham PW, Whyte MK. A transgenic zebrafish model of neutrophilic inflammation. Blood. 2006;108(13):3976-8. Epub 2006/08/24. doi: 10.1182/blood-2006-05-024075. PubMed PMID: 16926288.

40. Niethammer P, Grabher C, Look AT, Mitchison TJ. A tissue-scale gradient of hydrogen peroxide mediates rapid wound detection in zebrafish. Nature. 2009;459(7249):996-9. Epub 2009/06/06. doi: 10.1038/nature08119. PubMed PMID: 19494811; PubMed Central PMCID: PMCPMC2803098.

41. Sommer F, Torraca V, Kamel SM, Lombardi A, Meijer AH. Frontline Science: Antagonism between regular and atypical Cxcr3 receptors regulates macrophage migration during infection and injury in zebrafish. J Leukoc Biol. 2020;107(2):185-203. Epub 2019/09/19. doi: 10.1002/JLB.2HI0119-006R. PubMed PMID: 31529512; PubMed Central PMCID: PMCPMC7028096.

42. Xie Y, Tolmeijer S, Oskam JM, Tonkens T, Meijer AH, Schaaf MJM. Glucocorticoids inhibit macrophage differentiation towards a pro-inflammatory phenotype upon wounding without affecting their migration. Dis Model Mech. 2019;12(5). Epub 2019/05/11. doi: 10.1242/dmm.037887. PubMed PMID: 31072958; PubMed Central PMCID: PMCPMC6550045.

43. Bernut A, Loynes CA, Floto RA, Renshaw SA. Deletion of cftr Leads to an Excessive Neutrophilic Response and Defective Tissue Repair in a Zebrafish Model of Sterile Inflammation. Front Immunol. 2020;11:1733. Epub 2020/08/28. doi: 10.3389/fimmu.2020.01733. PubMed PMID: 32849617; PubMed Central PMCID: PMCPMC7412881.

44. Katikaneni A, Jelcic M, Gerlach GF, Ma Y, Overholtzer M, Niethammer P. Lipid peroxidation regulates long-range wound detection through 5-lipoxygenase in zebrafish. Nat Cell Biol. 2020;22(9):1049-55. Epub 2020/09/02. doi: 10.1038/s41556-020-0564-2. PubMed PMID: 32868902.

45. Hu W, Yang S, Shimada Y, Munch M, Marin-Juez R, Meijer AH, et al. Infection and RNA-seq analysis of a zebrafish tlr2 mutant shows a broad function of this toll-like receptor in transcriptional and metabolic control and defense to Mycobacterium marinum infection. BMC Genomics. 2019;20(1):878. Epub 2019/11/22. doi: 10.1186/s12864-019-6265-1. PubMed PMID: 31747871; PubMed Central PMCID: PMCPMC6869251.

46. Henry KM, Loynes CA, Whyte MK, Renshaw SA. Zebrafish as a model for the study of neutrophil biology. J Leukoc Biol. 2013;94(4):633-42. Epub 2013/03/07. doi: 10.1189/jlb.1112594. PubMed PMID: 23463724.

47. van der Vaart M, van Soest JJ, Spaink HP, Meijer AH. Functional analysis of a zebrafish myd88 mutant identifies key transcriptional components of the innate immune system. Dis Model Mech. 2013;6(3):841-54. Epub 2013/03/09. doi: 10.1242/dmm.010843. PubMed PMID: 23471913; PubMed Central PMCID: PMCPMC3634667.

48. Meijer AH, Gabby Krens SF, Medina Rodriguez IA, He S, Bitter W, Ewa Snaar-Jagalska B, et al. Expression analysis of the Toll-like receptor and TIR domain adaptor families of zebrafish. Mol Immunol. 2004;40(11):773-83. Epub 2003/12/23. doi: 10.1016/j.molimm.2003.10.003. PubMed PMID: 14687934.

49. Yang S, Marin-Juez R, Meijer AH, Spaink HP. Common and specific downstream signaling targets controlled by Tlr2 and Tlr5 innate immune signaling in zebrafish. BMC Genomics. 2015;16:547. Epub 2015/07/26. doi: 10.1186/s12864-015-1740-9. PubMed PMID: 26208853; PubMed Central PMCID: PMCPMC4514945.

50. He M, Halima M, Xie YF, Schaaf MJM, Meijer AH, Wang M. Ginsenoside Rg1 Acts as a Selective Glucocorticoid Receptor Agonist with Anti-Inflammatory Action without Affecting Tissue Regeneration in Zebrafish Larvae. Cells. 2020;9(5). doi: 10.3390/cells9051107. PubMed PMID: WOS:000539340200041.

51. Sommer F, Ortiz Zacari As NV, Heitman LH, Meijer AH. Inhibition of macrophage migration in zebrafish larvae demonstrates in vivo efficacy of human CCR2 inhibitors. Dev Comp Immunol. 2020;116:103932. Epub 2020/11/26. doi: 10.1016/j.dci.2020.103932. PubMed PMID: 33238180.

52. Magnusson KEG, Jalden J, Gilbert PM, Blau HM. Global Linking of Cell Tracks Using the Viterbi Algorithm. Ieee Transactions on Medical Imaging. 2015;34(4):911-29. doi: 10.1109/Tmi.2014.2370951. PubMed PMID: WOS:000352533200008.

53. Gray C, Loynes CA, Whyte MK, Crossman DC, Renshaw SA, Chico TJ. Simultaneous intravital imaging of macrophage and neutrophil behaviour during inflammation using a novel transgenic zebrafish. Thromb Haemost. 2011;105(5):811-9. Epub 2011/01/13. doi: 10.1160/TH10-08-0525. PubMed PMID: 21225092.

54. Torraca V, Cui C, Boland R, Bebelman JP, van der Sar AM, Smit MJ, et al. The CXCR3-CXCL11 signaling axis mediates macrophage recruitment and dissemination of mycobacterial infection. Dis Model Mech. 2015;8(3):253-69. Epub 2015/01/13. doi: 10.1242/dmm.017756. PubMed PMID: 25573892; PubMed Central PMCID: PMCPMC4348563.

55. Jiang D, Liang J, Fan J, Yu S, Chen S, Luo Y, et al. Regulation of lung injury and repair by Toll-like receptors and hyaluronan. Nat Med. 2005;11(11):1173-9. Epub 2005/10/26. doi: 10.1038/nm1315. PubMed PMID: 16244651.

56. Komai K, Shichita T, Ito M, Kanamori M, Chikuma S, Yoshimura A. Role of scavenger receptors as damage-associated molecular pattern receptors in Toll-like receptor activation. Int Immunol. 2017;29(2):59-70. Epub 2017/03/25. doi: 10.1093/intimm/dxx010. PubMed PMID: 28338748.

57. Yamamoto S, Shimizu S, Kiyonaka S, Takahashi N, Wajima T, Hara Y, et al. TRPM2-mediated Ca2+influx induces chemokine production in monocytes that aggravates inflammatory neutrophil infiltration. Nat Med. 2008;14(7):738-47. Epub 2008/06/11. doi: 10.1038/nm1758. PubMed PMID: 18542050; PubMed Central PMCID: PMCPMC2789807.

58. Mittal M, Siddiqui MR, Tran K, Reddy SP, Malik AB. Reactive oxygen species in inflammation and tissue injury. Antioxid Redox Signal. 2014;20(7):1126-67. Epub 2013/09/03. doi: 10.1089/ars.2012.5149. PubMed PMID: 23991888; PubMed Central PMCID: PMCPMC3929010.

59. Shishido T, Nozaki N, Takahashi H, Arimoto T, Niizeki T, Koyama Y, et al. Central role of endogenous Toll-like receptor-2 activation in regulating inflammation, reactive oxygen species production, and subsequent neointimal formation after vascular injury. Biochem Biophys Res Commun. 2006;345(4):1446-53. Epub 2006/05/30. doi: 10.1016/j.bbrc.2006.05.056. PubMed PMID: 16730663.

60. Suga H, Sugaya M, Fujita H, Asano Y, Tada Y, Kadono T, et al. TLR4, rather than TLR2, regulates wound healing through TGF-beta and CCL5 expression. J Dermatol Sci. 2014;73(2):117-24. Epub 2013/11/21. doi: 10.1016/j.jdermsci.2013.10.009. PubMed PMID: 24252748.

61. Chen L, DiPietro LA. Toll-Like Receptor Function in Acute Wounds. Advances in Wound Care. 2017;6(10):344-55. doi: 10.1089/wound.2017.0734. PubMed PMID: WOS:000412015700004.

62. Koch BEV, Yang S, Lamers G, Stougaard J, Spaink HP. Author Correction: Intestinal microbiome adjusts the innate immune setpoint during colonization through negative regulation of MyD88. Nat Commun. 2019;10(1):526. Epub 2019/01/30. doi: 10.1038/s41467-019-08456-y. PubMed PMID: 30692545; PubMed Central PMCID: PMCPMC6349902.

63. Bernut A, Herrmann JL, Kissa K, Dubremetz JF, Gaillard JL, Lutfalla G, et al. Mycobacterium abscessus cording prevents phagocytosis and promotes abscess formation. Proc Natl Acad Sci U S A. 2014;111(10):E943-52. Epub 2014/02/26. doi: 10.1073/pnas.1321390111. PubMed PMID: 24567393; PubMed Central PMCID: PMCPMC3956181.

64. Chatzopoulou A, Heijmans JP, Burgerhout E, Oskam N, Spaink HP, Meijer AH, et al. Glucocorticoid-Induced Attenuation of the Inflammatory Response in Zebrafish. Endocrinology. 2016;157(7):2772-84. Epub 2016/05/25. doi: 10.1210/en.2015-2050. PubMed PMID: 27219276.

65. Meijering E, Dzyubachyk O, Smal I. Methods for cell and particle tracking. Methods Enzymol. 2012;504:183-200. Epub 2012/01/24. doi: 10.1016/B978-0-12-391857-4.00009-4. PubMed PMID: 22264535.

66. Tinevez JY, Perry N, Schindelin J, Hoopes GM, Reynolds GD, Laplantine E, et al. TrackMate: An open and extensible platform for single-particle tracking. Methods. 2017;115:80-90. Epub 2016/10/08. doi: 10.1016/j.ymeth.2016.09.016. PubMed PMID: 27713081.

67. Ulman V, Maska M, Magnusson KEG, Ronneberger O, Haubold C, Harder N, et al. An objective comparison of cell-tracking algorithms. Nat Methods. 2017;14(12):1141-52. Epub 2017/10/31. doi: 10.1038/nmeth.4473. PubMed PMID: 29083403; PubMed Central PMCID: PMCPMC5777536.

68. Stokes CL, Lauffenburger DA, Williams SK. Migration of individual microvessel endothelial cells: stochastic model and parameter measurement. J Cell Sci. 1991;99 (Pt 2):419-30. Epub 1991/06/01. PubMed PMID: 1885678.

69. Selmeczi D, Mosler S, Hagedorn PH, Larsen NB, Flyvbjerg H. Cell motility as persistent random motion: Theories from experiments. Biophysical Journal. 2005;89(2):912-31. doi: 10.1529/biophysj.105.061150. PubMed PMID: WOS:000230822200017.

70. Taylor HB, Liepe J, Barthen C, Bugeon L, Huvet M, Kirk PDW, et al. P38 and JNK have opposing effects on persistence of in vivo leukocyte migration in zebrafish. Immunology and Cell Biology. 2013;91(1):60-9. doi: 10.1038/icb.2012.57. PubMed PMID: WOS:000313549700010.

Supplementary Material

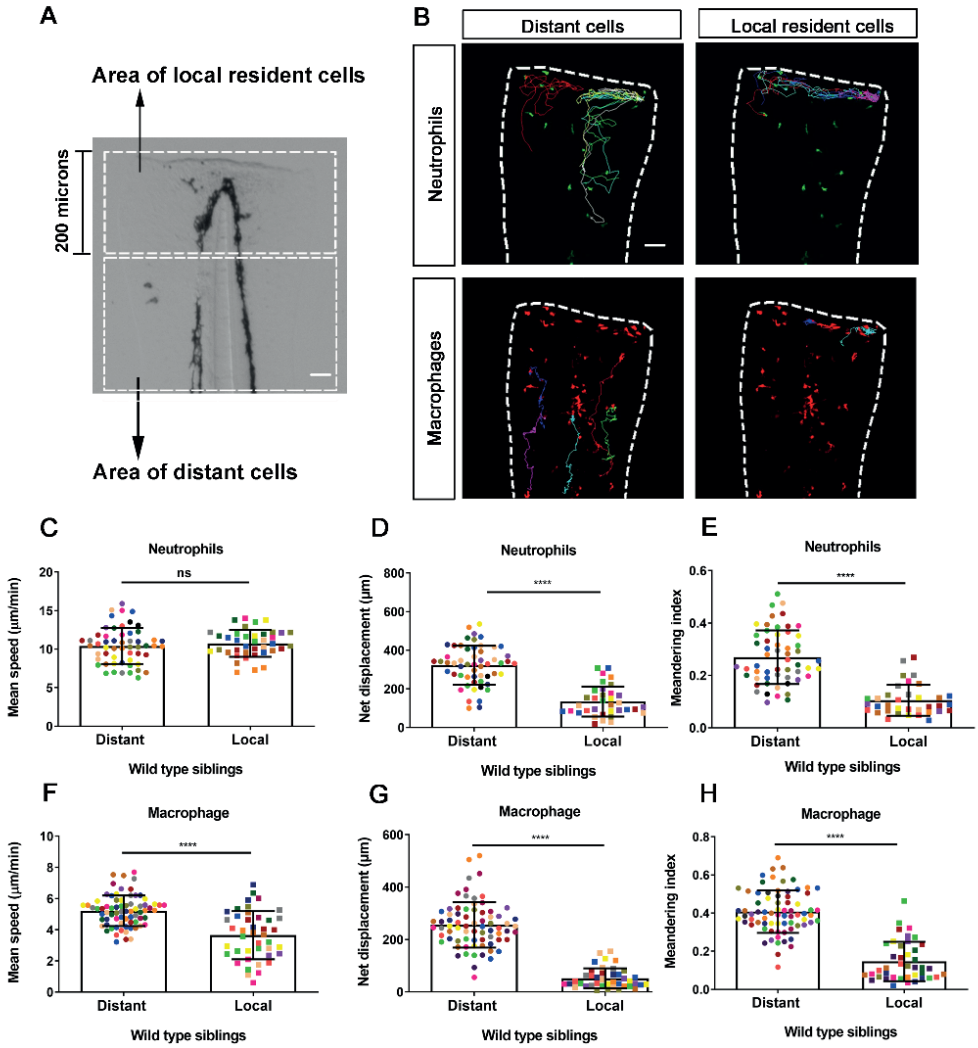

Supplementary Figure 1 (A) Schematic diagram of distant and local resident cell migration. (B) Representative images of the distant cell tracks and local resident cell tracks. (C-D) Quantification of the distant neutrophil tracks and the local resident neutrophil tracks. Statistical analyses were done with 15 and 13 fish, respectively, for each group. Sample size (n): 55, 39. (F-H) Quantification of the distant macrophage tracks and the local resident tracks. Statistical analyses were done with 15 fish for each group. Sample size (n): 73, 41. In all cases, each color indicates a different larva. An unpaired, two-tailed t-test was used to assess significance (ns, non-significance) and data are shown as mean± SD. Scale bar: 50 μm.

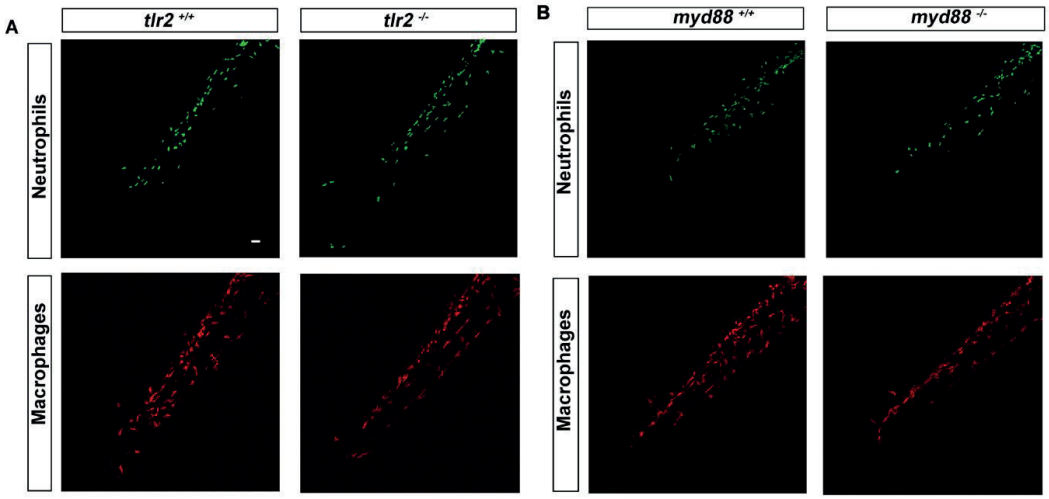

Supplementary Figure 2 Representative images of the quantification of cell numbers in tail region. The pictures of *tlr2*$^{+/+}$, *tlr2*$^{-/-}$ (A), *myd88*$^{+/+}$ and *myd88*$^{-/-}$ (B) zebrafish larvae were taken at 3 dpf for quantifying the number of neutrophils and macrophages.

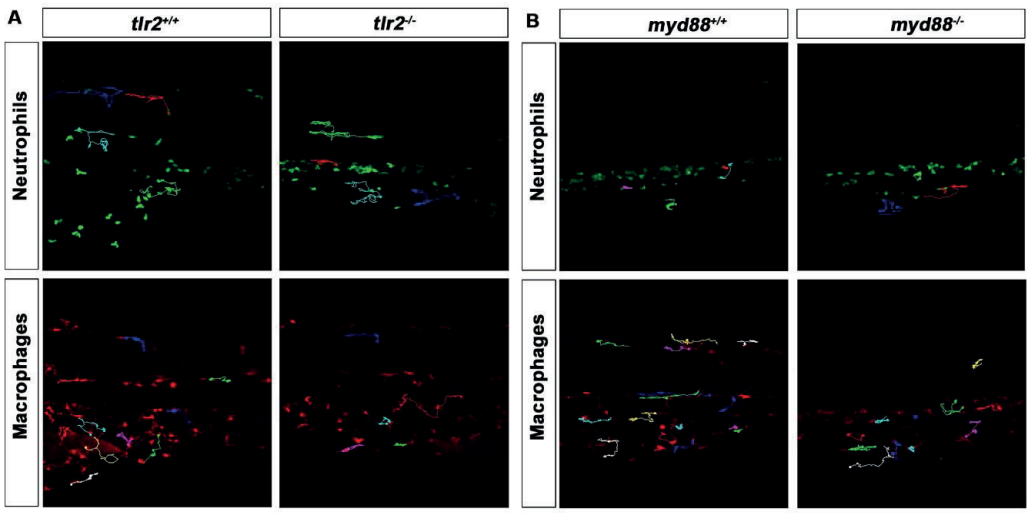

Supplementary Figure 3 Representative images of the neutrophil and macrophage basal migratory tracks in *tlr2* and *myd88* zebrafish. The cell tracks of 3 dpf *tlr2*$^{+/+}$, *tlr2*$^{-/-}$ (A), *myd88*$^{+/+}$ and *myd88*$^{-/-}$ (B) zebrafish larvae were tracked for 2 h and images were taken every 1 min by using a confocal microscope for quantifying cells basal migratory capability.

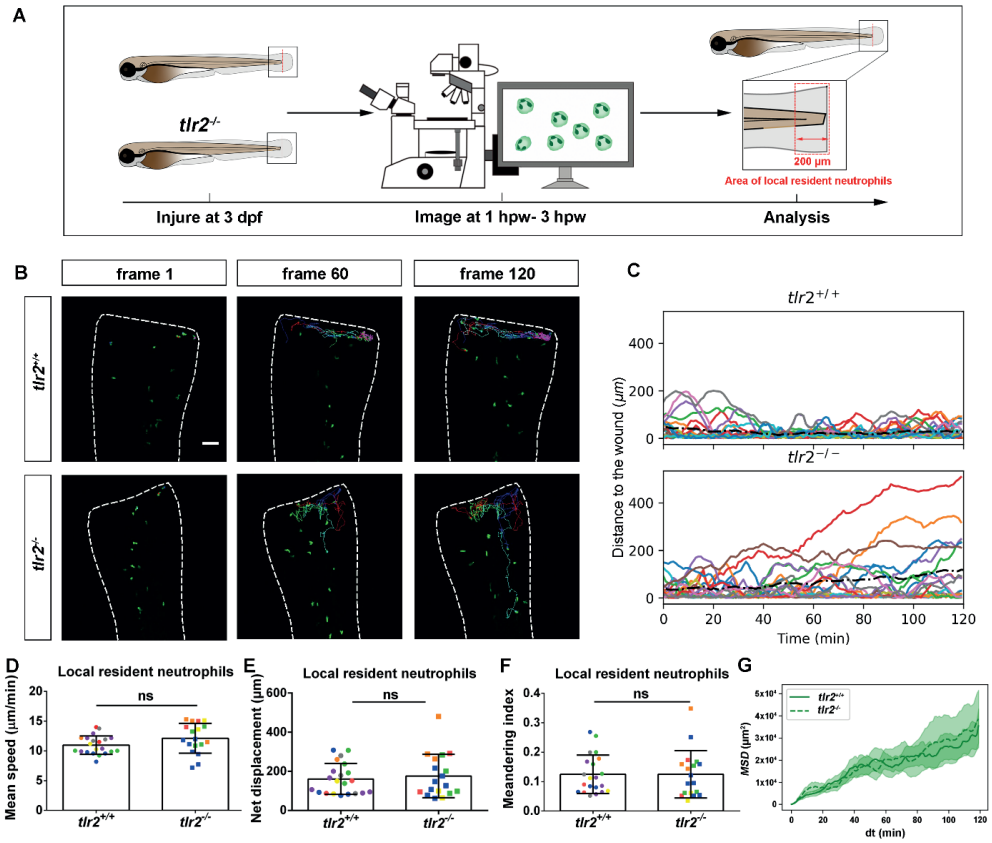

Supplementary Figure 4 Quantification of localized resident neutrophils behavior in wounded *tlr2* larvae. (A) Experimental scheme. (B) Representative images of local resident neutrophils tracks in the wounded tail fin of 3 dpf *tlr2*$^{+/+}$ or *tlr2*$^{-/-}$ larvae at frame 1, frame 60 and frame 120. Cell tracking movies are shown in Supplementary Movie S17-18). Scale bar: 50 µm. (C) Distance to the wound. Black dash line represents average distance to the wound. Each color line represents one cell. (D-I) Quantification of local resident neutrophil tracks, mean speed (D); net displacement (E); Meandering index (F); MSD (G). In panel D-F and H, each color indicates a different larva. Statistical analyses were done with 7 and 5 fish, respectively, for each group. An unpaired, two-tailed t-test was used to assess significance (ns, non-significance) and data are shown as mean± SD. Sample size (n): 21, 18.

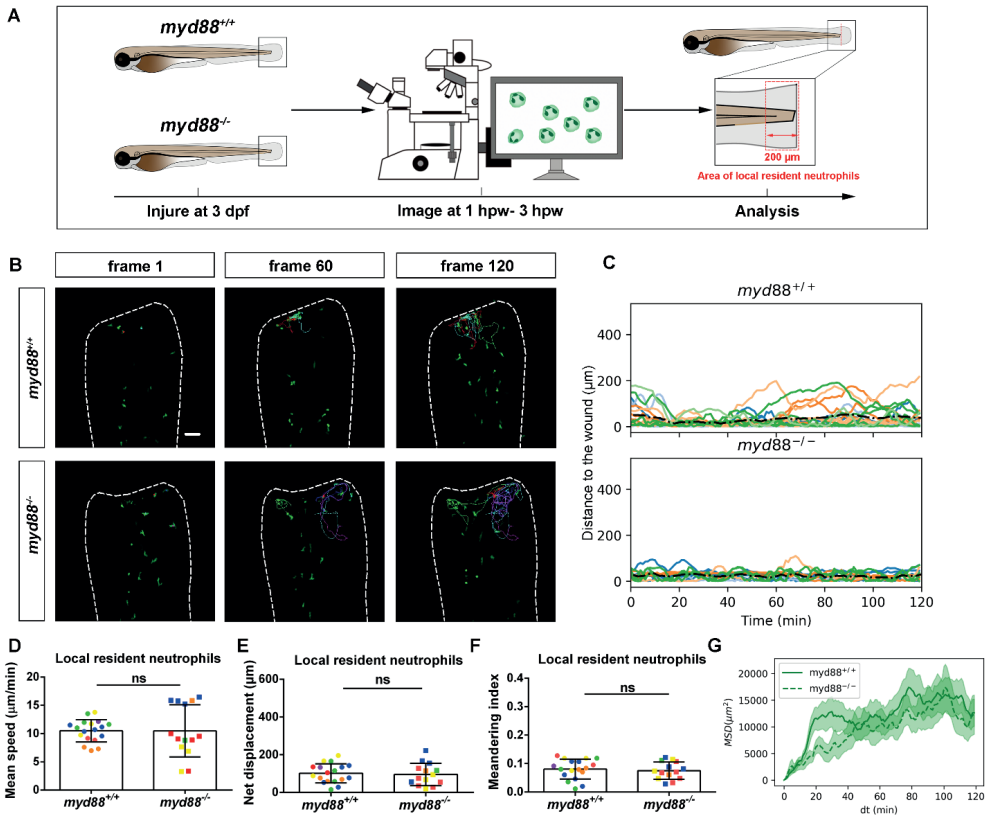

Supplementary Figure 5 Quantification of localized resident neutrophils behavior in wounded *myd88* larvae. (A) Experimental scheme. (B) Representative images of local resident neutrophils tracks in the wounded tail fin of 3 dpf *myd88*$^{+/+}$ or *myd88*$^{-/-}$ larvae at frame 1, frame 60 and frame 120. Cell tracking movies are shown in Supplementary Movie S19-20). Scale bar: 50 µm. (C) Distance to the wound. Black dash line represents average distance to the wound. Each color line represents one cell. (D-I) Quantification of local resident neutrophil tracks, mean speed (D); net displacement (E); Meandering index (F); MSD (G). In panel D-F and H, each color indicates a different larva. Statistical analyses were done with 6 and 5 fish, respectively, for each group. An unpaired, two-tailed t-test was used to assess significance (ns, non-significance) and data are shown as mean± SD. Sample size (n): 18, 14

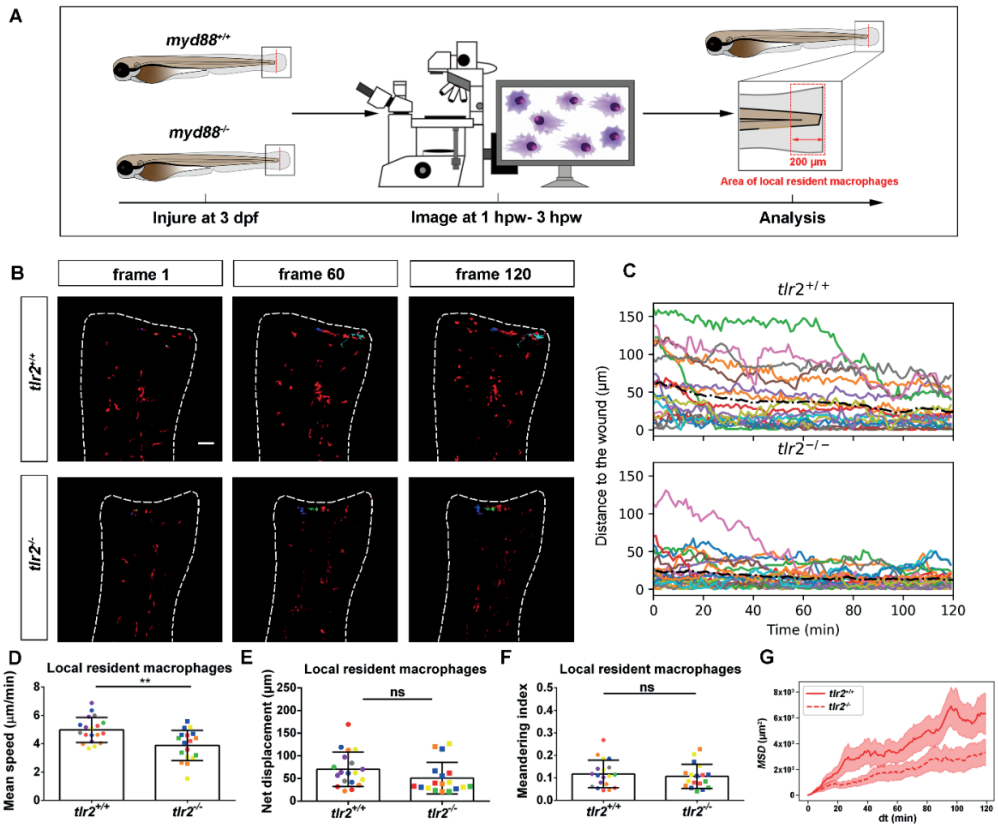

Supplementary Figure 6 Quantification of localized resident macrophages behavior in wounded *tlr2* larvae. (A) Experimental scheme. (B) Representative images of local resident macrophages tracks in the wounded tail fin of 3 dpf $tlr2^{+/+}$ or $tlr2^{-/-}$ larvae at frame 1, frame 60 and frame 120. Cell tracking movies are shown in Supplementary Movie S21-22). Scale bar: 50 µm. (C) Distance to the wound. Black dash line represents average distance to the wound. Each color line represents one cell. (D-I) Quantification of local resident macrophage tracks, mean speed (D); net displacement (E); Meandering index (F); MSD (G). In panel D-F and H, each color indicates a different larva. Statistical analyses were done with 7 and 5 fish, respectively, for each group. An unpaired, two-tailed t-test was used to assess significance (ns, non-significance) and data are shown as mean± SD. Sample size (n): 19, 18.

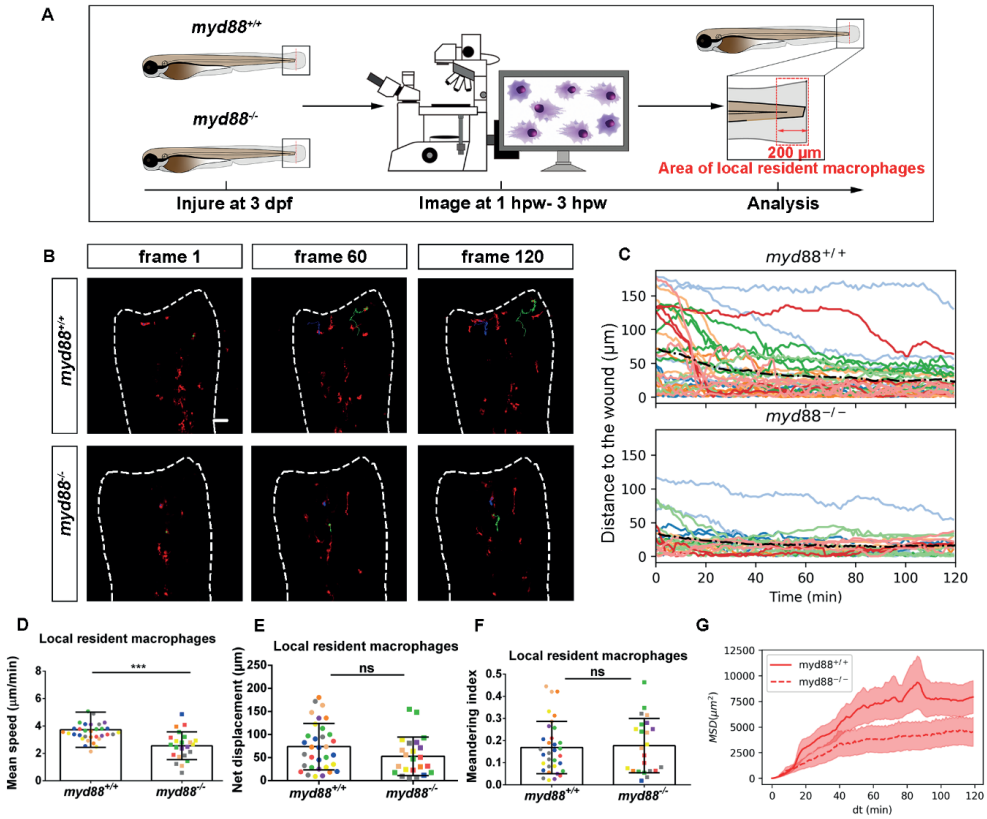

Supplementary Figure 7 Quantification of localized resident macrophages behavior in wounded *myd88* larvae. (A) Experimental scheme. (B) Representative images of local resident macrophages tracks in the wounded tail fin of 3 dpf *myd88*$^{+/+}$ or *myd88*$^{-/-}$ larvae at frame 1, frame 60 and frame 120. Scale bar: 50 µm. (C) Distance to the wound. Black dash line represents average distance to the wound. Each color line represents one cell. Cell tracking movies are shown in Supplementary Movie S23-24). (D-I) Quantification of local resident macrophage tracks, mean speed (D); net displacement (E); Meandering index (F); MSD (G). In panel D-F and H, each color indicates a different larva. Statistical analyses were done with 8 and 8 fish, respectively, for each group. An unpaired, two-tailed t-test was used to assess significance (ns, non-significance) and data are shown as mean± SD. Sample size (n): 33, 23.

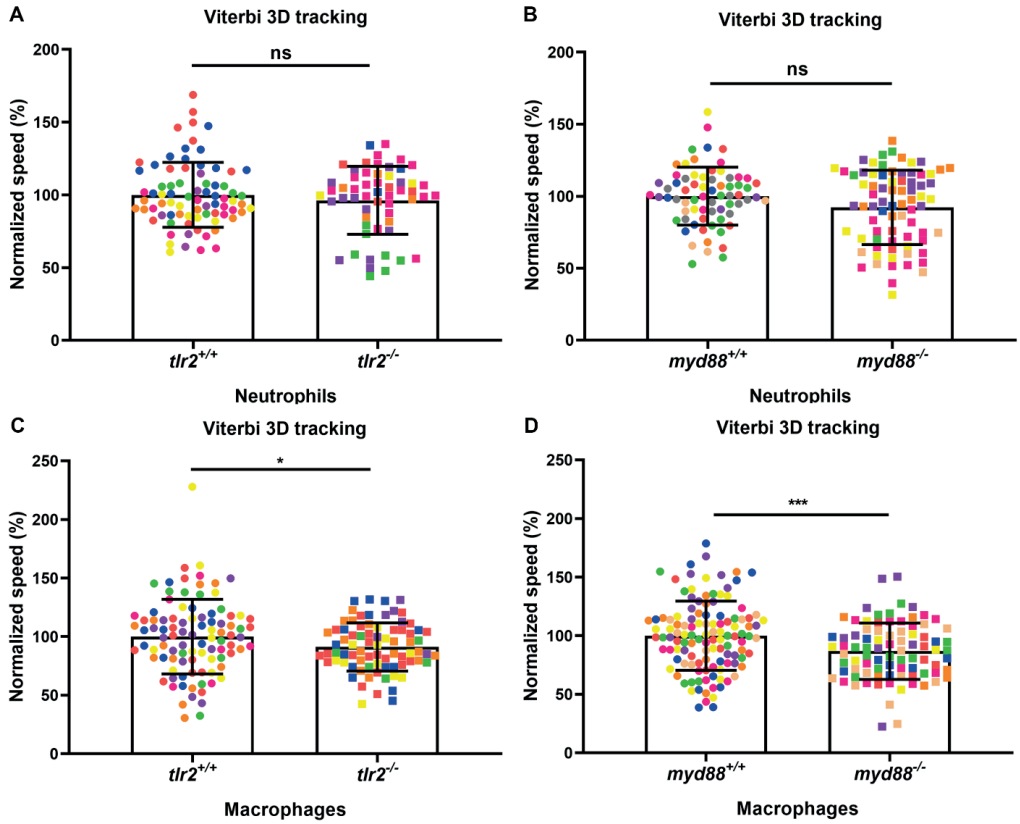

Supplementary Figure 8 Quantification of tracks using automatic Viterbi Algorithm. (A) Quantification of neutrophil behavior in wounded *tlr2* larvae. Statistical analyses were done with 7 fish, for each group. Sample size (n): 77, 56. (B) Quantification of neutrophil behavior in wounded *myd88* larvae. Statistical analyses were done with 9 or 8 fish, respectively, for each group. Sample size (n): 69, 76. (C) Quantification of macrophage behavior in wounded *tlr2* larvae. Statistical analyses were done with 7 fish, for each group. Sample size (n): 95, 78. (D) Quantification of macrophage behavior in wounded *myd88* larvae. Statistical analyses were done with 8 fish, for each group. Sample size (n): 119, 85.In all cases, an unpaired, two-tailed t-test was used to assess significance (ns, non-significance) and data are shown as mean± SD. To normalize the data, each value was divided by the average value of its wild type sibling group, which was set at 100 percent.

Availability of data and materials

Supplementary Movies are available online:
https://www.frontiersin.org/articles/10.3389/fcell.2021.624571/full

3

Chapter 4

Specificity of the innate immune responses to different classes of non-tuberculous mycobacteria using a zebrafish larval model

Wanbin Hu, Bjørn Koch, Gabriel Forn-Cuní, Herman P. Spaink

In preparation

4

Abstract

Mycobacterium avium is a slow growing nontuberculous mycobacterium which causes 80% of NTM infectious disease cases worldwide. However, there is neither a straightforward treatment regimen for the disease nor any effective animal models for investigating it. Here, we used zebrafish larvae and took advantage of their transparency and high throughput potential to establish a *M. avium* infectious model. We characterized the *M. avium* MAC 101 infection in larvae comparing it to that of a recognized model of tuberculosis infection, *Mycobacterium marinum* Mma20, in terms of bacterial burden, formation of granuloma-like clusters, gene expression profiles, function of *tlr2* and immune cell migratory behavior. We found that Mma20 is more virulent than MAC 101 in zebrafish larvae. MAC 101 has a distinct transcriptome response compared to Mma20, especially regarding cytokine and chemokines, autophagy regulators, and matrix remodeling. At the cellular level, our results demonstrate that macrophages play an important role in the response to both mycobacterial infections because more recruited macrophages were observed in the infected area. The migration speed of macrophages is faster to Mma20 infection. Interestingly, the MAC 101 infected larvae have a more closed granuloma-like cluster structure, while we observed higher bacterial burden outside macrophages in Mma20 infected larvae. In addition, we found that *tlr2* plays a conservative and protective role for the host upon mycobacterial infection, and is involved in the regulation of the migration of macrophages and neutrophils in response to the infection. Taken together, we characterized a new *M. avium* MAC 101 infection model in zebrafish that can be further used to study the interaction between the host and NTM bacteria.

Introduction

The infectious diseases caused by mycobacterial pathogens other than the *Mycobacterium tuberculosis* (Mtb) and *Mycobacterium leprae* (*M. leprae*) complexes, are collectively called nontuberculous mycobacteria (NTM) infections [1]. NTM include more than 150 species and are ubiquitously distributed in the environment, like soil, dust, and water [2, 3]. Currently, NTM infectious diseases have aroused wide attention because of the rise of its incidences globally [2]. Although there are existing treatments for NTM infectious diseases, the treatment regimens are long and have a high frequency of multi-drug resistant cases [4]. Thus, it is urgent to discover novel prevention and therapeutic strategies for patients infected with NTM. Currently, host-directed therapies (HDT) are one of the most promising strategies to combat NTM infectious diseases by making the NTM antibiotic treatment regimens more effective [5-7]. However, the current knowledge of the mechanisms underlying host-NTM bacteria interactions is limited and therefore more studies are highly needed.

The *Mycobacterium avium complex* (MAC), which consists of the *Mycobacterium intracellulare* (*M. intracellulare*) and *Mycobacterium avium* (*M. avium*) species, is one of the most common disease-causing NTM group [3, 8]. Although MAC bacteria are generally believed to be less virulent for primates than Mtb, they can cause pulmonary and extra-pulmonary disease in susceptible individuals, e.g. patients with acquired immunodeficiency syndrome (AIDS) or with a history of lung disease [9-11]. To be noted, Mtb infected patients can be dually infected with MAC bacteria. Unfortunately, there is no straightforward drug or treatment regime for the MAC infections available [12]. That is, among other reasons, because developing new drugs or treatment regime is challenging due to the limited research and sometimes results are contradictory between *in vitro* and mice *in vivo* studies [13, 14] or between studies using different subspecies of *M. avium*: *M. avium* has four subspecies, and it has been demonstrated that they cause different disease characteristics [15, 16]. A standardized MAC infectious disease animal model is therefore urgently needed to study the mechanism of MAC infection and test new drugs effectively. In previous studies, the *M. avium Chester* (also called MAC 101) infectious capacity has been evaluated in different mouse strains, including BALA/c, C57BL/6, nude, and beige mice, allowing for drug or treatment assessment [17, 18]. Thus, MAC 101 can be considered as a standard strain to investigate *M. avium* infection studies.

Zebrafish (*Danio rerio*) larvae are popular as a model to study human infectious disease because their innate immune system is highly similar to that of mammals and they are optically

accessible making the infectious agents and immune cells easy to track *in vivo* [19]. Furthermore, they enable investigation of innate immune function isolating from adaptive immunity [19-21]. Zebrafish larvae have been an effective model organism to study the mechanism of Mtb infection for over 15 years [22]. A majority of the studies have used *M. marinum* as the infectious agent because it is genetically closely related to Mtb, and has been shown to be the causing granuloma formation in zebrafish larvae at high frequency [23].

Immune cells, as an important part of the innate immune system, depend on pattern recognition receptors (PRRs) to initiate protective innate immune responses in the host [24]. Toll-like receptor 2 (TLR2) serves as one of the most important PRR to sense invaded microbial pathogens through pathogen-associated molecular patterns (PAMPs) [25]. Much progress has been made the last decades in revealing the function of TLR2 in defense against Mtb infection. It has been reported that TLR2 senses invading Mtb bacteria through the lipoproteins and glycolipids located on their cell wall [26, 27]. A profound pro-inflammatory response is triggered after the stimulation of TLR2, which is considered to promote bacterial clearances [28]. However, it has been shown that activation of TLR2 also activates anti-inflammatory responses [29]. The PRR feature of TLR2 makes it popular as a therapeutic target for TB [30]. However, there is little known about the involvement of TLR2 in *M. avium* infection.

In this study, we developed an innovative zebrafish larval infectious model for studying *M. avium* infection. Moreover, we compared the innate immune response of zebrafish larvae to infection with two different species of NTM, *M. marinum* Mma20 and *M. avium* MAC 101, specifically with regard to the bacterial burden, granuloma-like cluster formation, and transcriptomic gene expression profiles. Using this system, we analyzed the function of *tlr2* during the infection with both mycobacterial species with special attention to the responsive cell migration behavior.

Results

M. marinum is more virulent than *M. avium* in zebrafish larvae

To compare the virulence of *M. avium* MAC101 and *M. marinum* Mma20, we infected zebrafish larvae with increasing dosages of the two species of mycobacteria carrying fluorescent protein reporters. We infected the larvae systemically by injection into the caudal vein at 28 hours post fertilization (hpf) and monitored larval survival and infectious

development by fluorescent microscopy over the following 4 days. The representative images for the bacterial burden quantification are shown in Fig. 1A. The results clearly demonstrated that infection with Mma20 was drastically more lethal than with MAC 101 over the 4-day assessment period. Even at the highest infectious dose of 9000 colony forming units (CFU) of MAC101, 86.67% (26/30) of larvae survived until the end of the experiment, and with lower dosages of 4500 and 1000 CFU, the survival was higher than 90% (Fig. 1B). In contrast, 73.33% (22/30) of larvae infected with 500 CFU Mma20 survived until 4 days post infection (dpi) and only 16.13% (5/31) larvae survived in 1000 CFU Mma20 group (Fig. 1B), while the survival rate of the larvae infected with the dose of 250 CFU Mma20 was 96.67% (29/30). We subsequently assessed the infectious development of MAC 101 and Mma20 by microscopy-based analysis, using fluorescent signal derived from the injected bacteria as a proxy for the infectious status in the larvae. Larvae infected with 250 CFU Mma20 and 4500 and 9000 CFU MAC 101 all exhibited significant increases in the fluorescent signal at 4 dpi compared with 1 dpi (Fig. 1C, D and E), indicating a progressing infection despite the low overall mortality in these groups. Interestingly, while the fluorescent signal in Mma20 infected larvae rose steadily from 1 to 4 dpi, MAC 101 infected larvae exhibited a drop in fluorescent signal from 1 to 2 dpi, only to recover and grow at 3 and 4 dpi. This underscores the different dynamics of infection between these two species of mycobacteria. Taken together, these results show that Mma20 causes a more rapid disease development and higher mortality compared to MAC 101 which declines during the first days of the infection, but recovers and may cause mortality at later time points than what we could measure with this experimental setup. Having characterized these broad spanning CFU burdens, moving forward we focused only on two groups: 250 CFU for Mma20 and 4500 CFU for MAC 101, as these have similar mortality and measurable fluorescent signals.

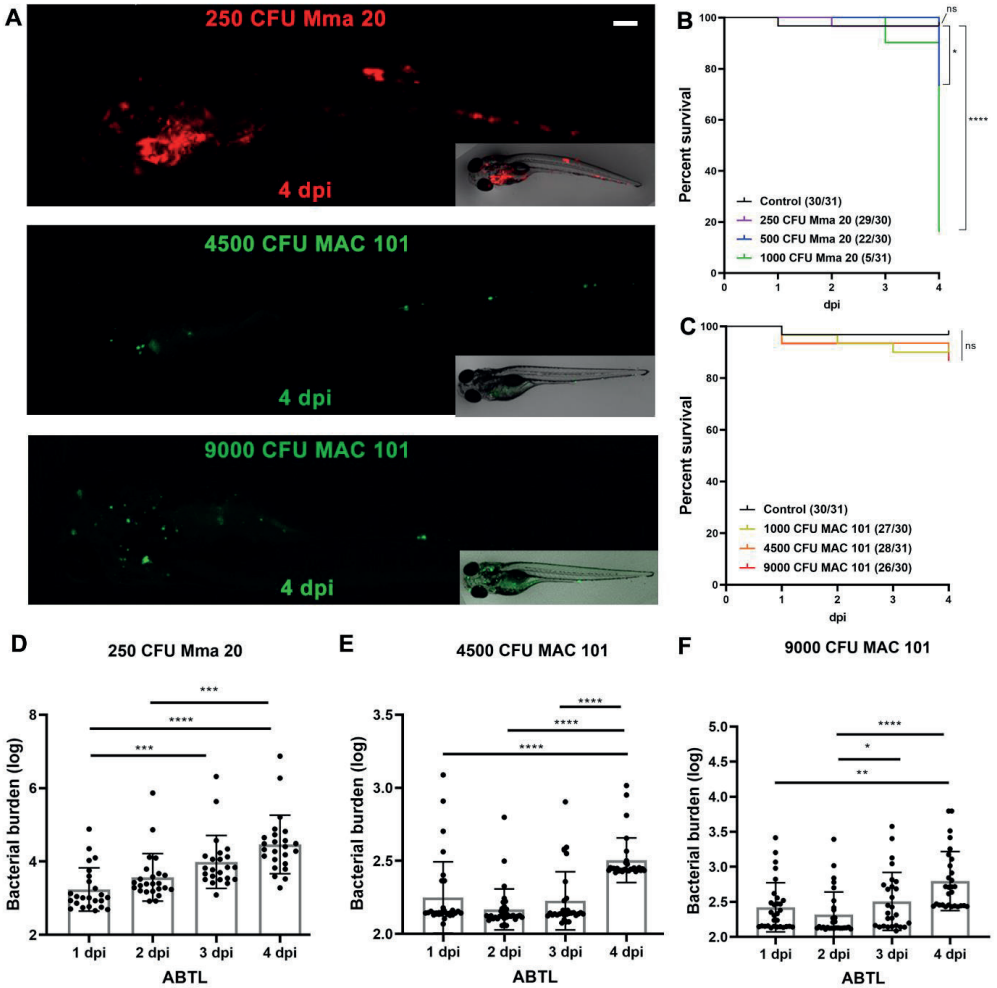

Figure 1 Quantification of bacterial burden and survival after *M. marinum* or *M. avium* infection. ABTL zebrafish larva infected with mCherry-labeled *M. marinum* Mma 20 at a dose of ~250 CFU and infected with wasabi-labeled *M. avium* MAC 101 at a dose of ~ 4500 CFU or 9000 CFU by caudal vein infection at 28 hpf. (A) Representative images for the bacterial burden quantification were taken at 4 dpi. (B, C) Percent of survival curves for ABTL zebrafish larva infected with a series of does *M. marinum* Mma20 or *M. avium* MAC 101. (D) Bacterial burden quantification of ABTL zebrafish larvae upon ~250 CFU Mma 20 infection. (E) Bacterial burden quantification of ABTL zebrafish larvae upon ~4500 CFU MAC 101 infection. (F) Bacterial burden quantification of ABTL zebrafish larvae upon ~9000 CFU MAC 101 infection. In (B, C) data were collected from three pools of zebrafish larvae. In (D, E, and F) data (mean ± SD) were combined from three pools of zebrafish larvae. Statistical significance of differences was determined by unpaired t-test for comparison between the *tlr2* mutant and its wild type sibling group. *, $P < 0.05$, **, $P < 0.01$, ***, $P < 0.001$, ****, $P < 0.0001$. Scale bar: 50 µm. Sample size (n): 24, 24, 23, 24 (C), 31, 33, 31, 30 (D), 30, 29, 27, 29 (E). Scale bar: 50 µm.

M. avium is persisting in macrophages that form granuloma-like clusters

Although granulomas are regarded as host-defensive structures historically, they can prevent drugs from penetrating the bacteria inside of them and make therapeutic treatment of NTM infection challenging [4]. It has been demonstrated that macrophages play a dominant role in initiating the granuloma formation at the early *M. marinum* infection stage in zebrafish embryos [19, 31]. However, the information about granuloma formation upon *M. avium* infection is limited. In order to investigate the role of macrophages in MAC 101 granuloma formation we used larvae of the *Tg(Mpeg1:EGFP)* zebrafish line, in which macrophages express EGFP. We infected the larvae in the same manner as before, with ~250 CFU *M. marinum* Mma20 or ~4500 CFU *M. avium* MAC 101 respectively, and observed the appearance of granuloma-like clusters (Fig. 2). While both infections exhibited clear overlap between bacteria and clusters of macrophages at 4 dpi, the Mma20 infection showed more extracellular bacteria and cording morphology (Fig. 2A), while larvae infected with MAC 101 exhibited more intracellular bacteria (Fig. 2B). This result suggests that the granuloma structures caused by *M. avium* infection are more sealed compared to the granulomas resulting from *M. marinum* infection.

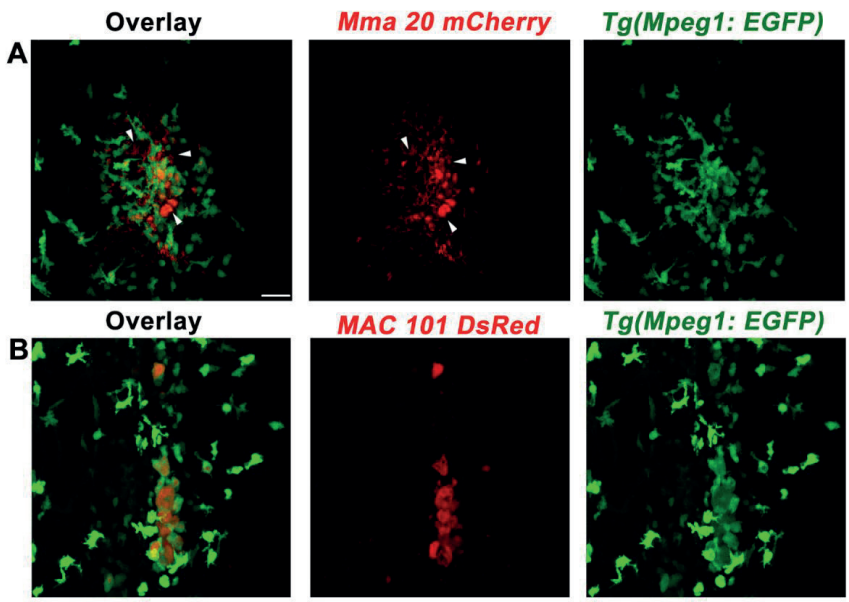

Figure 2 The comparison of granuloma-like cluster phenotypes in wild type transgenic line *Tg(Mpeg1: EGFP)* zebrafish larvae upon *M. marinum* Mma20 or *M. avium* MAC 101 infection. (A) A representative CLSM image of *Tg(Mpeg1: EGFP)* zebrafish larva infected with mCherry-labeled Mma20 strain. *Tg(Mpeg1: EGFP)* embryos were infected ~250 CFU Mma20 mCherry strain at 28 hpf. CLSM imaging was performed with the infected larvae at 4 dpi with 40 times magnification lens (oil immersion, N.A. 1.3). (B) A representative CLSM image of *Tg(Mpeg1: EGFP)* zebrafish larva infected with DsRed-labeled MAC 101 strain. ~4500 CFU MAC 101 DsRed strain was injected in 28 hpf *Tg(Mpeg1: EGFP)* zebrafish embryos. CLSM images were taken for the 4 dpi MAC 101 infected larvae by using 20 times magnification lens (oil immersion, N.A. 1.3). The white arrow represents the bacteria outside macrophages. Scale bar: 50 µm.

Transcriptional difference between *M. marinum* and *M. avium* infected zebrafish larvae

To gain a better understanding of the differences in host responses to Mma20 versus MAC 101 we performed transcriptome analysis of zebrafish larvae infected with MAC 101 by RNAseq. MAC 101 infected and PBS-injected control groups were collected for RNA isolation at 4 dpi and used to create RNAseq libraries. We compared the results to published RNAseq datasets of 4 dpi larvae infected with ~250 CFU *M. marinum* Mma20 versus PBS, from NCBI (GEO database accession for the RNASeq data: GSE76499) [32]. When comparing the previously published RNAseq data of 4 dpi Mma20 infection larvae to that of PBS-injected control group [32] , we found 1164 genes upregulated and 772 genes downregulated (Fig. 3A). A different response was observed when larvae were challenged with ~4500 CFU *M. avium* MAC 101, which exhibited 5244 upregulated genes and 4978 downregulated genes (Fig. 3A). To investigate the overlap of genes regulated by the two mycobacteria, we plotted three Venn diagrams. The results show that 1270 genes (12.4% in MAC 101 *vs* PBS group, 65.6% in Mma20 *vs* PBS group) are regulated by both Mma20 and MAC 101, 696 upregulated genes were shared, while only 410 common downregulated genes were found. For further analysis, we classified the differential regulated genes according to the KEGG pathway by using the online functional classification tool Database for Annotation, Visualization and Integrated Discovery (DAVID; http://david.abcc.ncifcrf.gov/summary.jsp). The analysis showed that most DEGs were enriched in metabolism-related pathways in MAC 101 vs PBS group (Fig. S1B). Moreover, we further compared the enriched pathways by using the Venn diagram. We found that there were 6 enriched pathways the same: ECM-receptor interaction; Focal adhesion; Glycine, serine and threonine metabolism; Glutathione metabolism; Arginine and proline metabolism and Tryptophan metabolism. These results indicate that zebrafish larvae have a different transcriptome response to MAC 101 infection.

Common and specific gene expression profiles in toll-like receptor signaling pathway after *M. marinum* and *M. avium* infection

Innate immune responses are important to protect the host from NTM infection, which is mainly mediated by the toll-like receptor (TLR) signaling pathway [33-35]. We wanted to compare the transcriptomic profiles of the host responses to the infections specifically in relation to TLR signaling. Thus, we visualized the DEGs that are characterized as being part of or downstream of TLR signaling pathways (Fig. S2 and Fig. 4) for the two mycobacterial infections.

In Fig. 4, the categories of Cytokines and chemokines; Cytokine and chemokine receptor; Autophagy regulators; Transcription factors; Blood factors; Complement cascade; Matrix remodeling and Mitochondrial were analyzed and visualized by the program Pathvisio. In each category, we summarized common regulated gene set, specific regulated gene set in Mma20 infection group, specific regulated gene set in MAC 101 infection group, and different regulated gene set. In the category of the Cytokines and chemokines, we found *tnfb*, *il1b*, *lepb*, *il12a*, *cxcl8b*, *cxcl8b.1*, *cxcl8a*, *ccl19a.1*, and *csf3b* were upregulated to respond to both Mma20 and MAC 101 infection. *Tnfa*, *cxcl19*, *cxcl19b*, *cxck20*, *ccl34b.8*, and *ccl34a.4* were specifically upregulated in Mma20 infection group. *Cxcl14*, *cxcl8b.3*, and *ccl25b* were specifically regulated, while *cxcl11.7*, *ccl36.1*, *cxcl12b*, *ccl33.3* were specifically downregulated in MAC 101 infection group. Interestingly, *ccl34b.1* was downregulated in Mma20 infection group but was upregulated in MAC 101 infection group. In the categories of Cytokine and chemokine receptors, Autophagy regulators and Matrix remodeling, we found that there were more genes only significantly responded to the MAC 101 infection. In the Blood factors category, *hp* was upregulated in Mma20 infection group. In contrast, *hp* was downregulated in MAC 101 infection group (Fig. 4).

Overall, the transcriptomic profile of genes characterized as functioning downstream of TLR signaling pathways showed divergences in all functional classes of genes, but particularly in cytokines and chemokines, autophagy regulators, and genes involved in matrix remodeling. This further underscores that the host immune response is different between Mma20 and MAC 101.

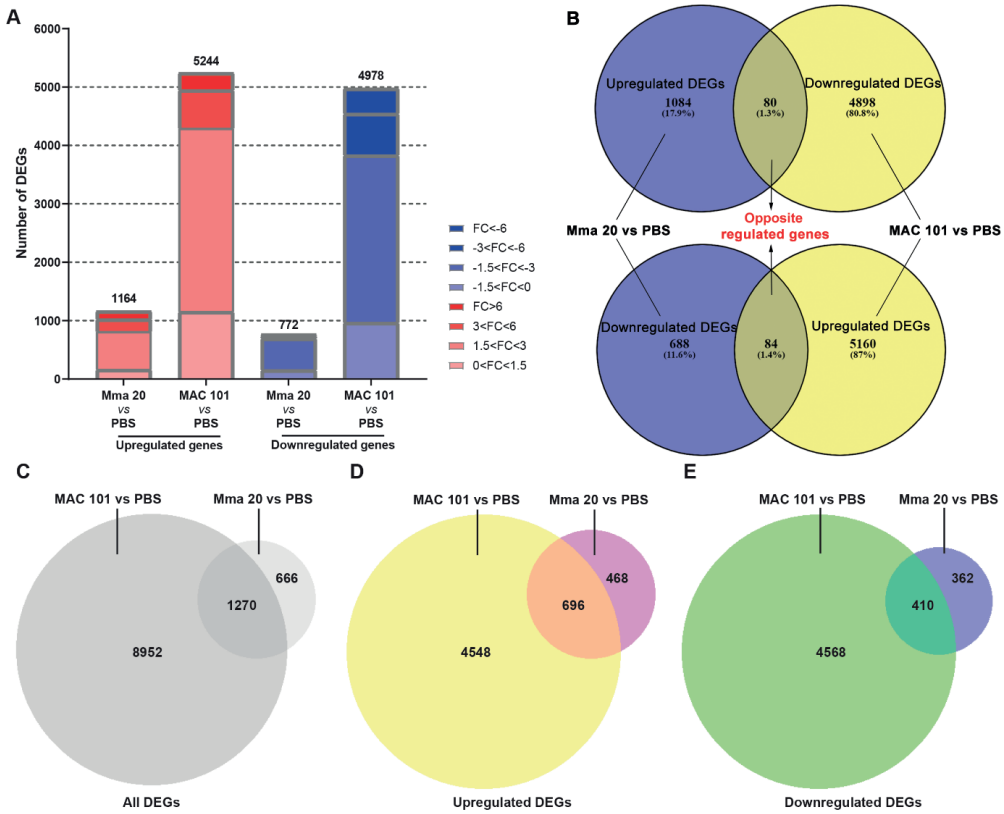

Figure 3 The global comparative analysis of the differential expressed genes (DEGs) in zebrafish larvae upon *M. marinum* Mma20 or *M. avium* MAC 101 infection. AB/TL zebrafish embryos were injected with ~250 CFU *M. marinum* Mma20 strain (GEO database accession for RNA-Seq: GSE76499 [32]) or ~4500 CFU *M. avium* MAC 101 strain at 28 hpf, respectively. The embryos in the control group were injected with PBS. The samples for RNAseq are taken from three independent sample sets with the infected larvae at 4 dpi. (A) Overview of the distribution of DEGs fold change in zebrafish larvae infected with Mma 20 or MAC 101. DEGs were assessed by FDR p-value < 0.05. Upregulated gene sets are shown in red and downregulated gene sets are shown in blue. The intensity of the color represents the fold change level. (B) Venn diagram shows the opposite regulated DEGs. (C- E) Venn diagram shows the common and specific gene numbers of all DEGs (C), upregulated DEGs (D), and downregulated DEGs (E) between Mma20 vs PBS and MAC 101 vs PBS groups. The Venn diagrams were made by the website: https://www.biovenn.nl/.

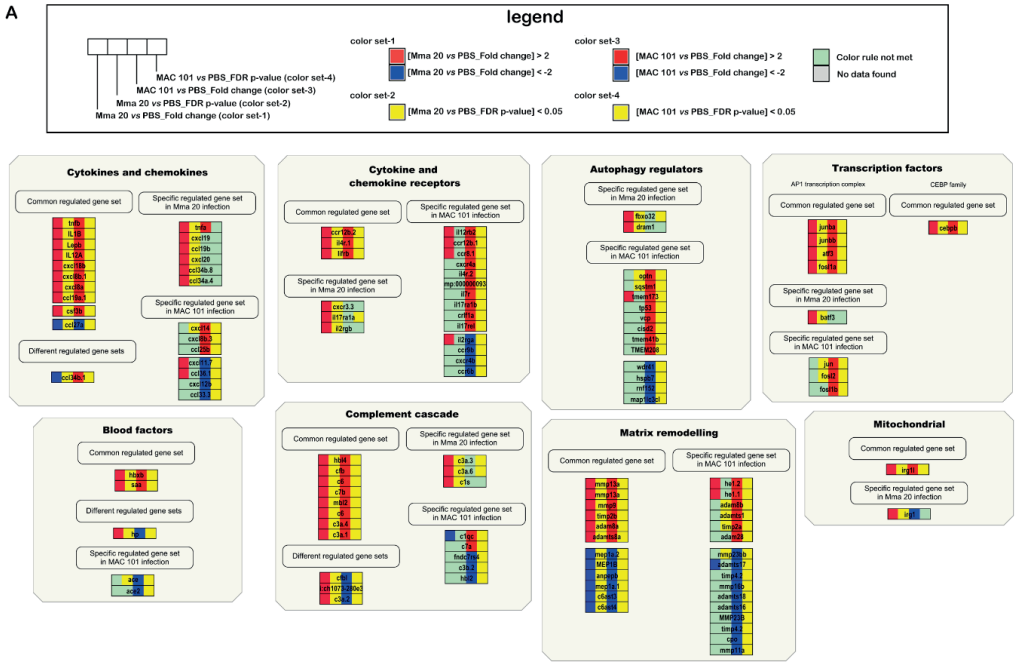

Figure 4 Inflammatory response genes in the transcriptome of larvae infected with *M. marinum* Mma20 or *M. avium* MAC 101. The pathway was adapted from the Wiki pathway. In the visualization, the gene expression in the comparison of Mma20 infection *vs* PBS and MAC 101 infection *vs* PBS are depicted by color (red, upregulated; blue, downregulated; yellow, FDR *p*-value < 0.05).

M. marinum and *M. avium* infection in *tlr2* mutant larvae

Having established that the TLR associated transcriptomic profiles of the host responses to the two mycobacterial infections differ, we wanted to address this in more detail. Previous studies by our group have demonstrated that *tlr2* is important for the ability of zebrafish larvae to control *M. marinum* infection, a phenomenon which can be explained by the effect on metabolic pathways and the presence of higher extracellular bacterial burden in the *tlr2* mutants [36]. To further explore the role of *tlr2* in the control mycobacterial infection, we investigated whether *tlr2* is also involved in the immune response to *M. avium* infection.

To compare the role of *tlr2* in *M. marinum* and *M. avium* infection, we injected ~250 CFU Mma20 or ~4500 CFU MAC 101 into *tlr2* loss-of-function mutants and their wild type siblings. Images of infected larvae were taken at 1 dpi and 4 dpi to assess the bacterial burden by integrated intensity. In both cases, the bacterial burden was significantly increased at 4 dpi in the *tlr2* deficient background (Fig. 5). This increased bacterial burden in the *tlr2* mutant could be caused by inability of macrophages to clear bacteria. To confirm this, we analyzed

macrophage behavior upon infection by confocal microscopy, using *tlr2*$^{+/+}$ *Tg (mpeg1:EGFP)* and *tlr2*$^{-/-}$ *Tg (mpeg1:EGFP)* infected *M. avium* MAC 101 strain (Fig. 6). Surprisingly, the bacterial pixel count within macrophages was significantly higher in the *tlr2* mutant. There was no statistically significant difference between *tlr2* mutants and WT siblings in the bacterial burden outside of macrophages. In previous work, we found that Mma20 bacterial fluorescent signal was significantly elevated outside of macrophages in *tlr2* mutants compared with its heterozygote and wild type sibling controls [36], but no significant difference was found in the intracellular bacterial pixel count (data are not shown). This finding indicates a *tlr2* related difference in the host response to MAC 101 compared to Mma20.

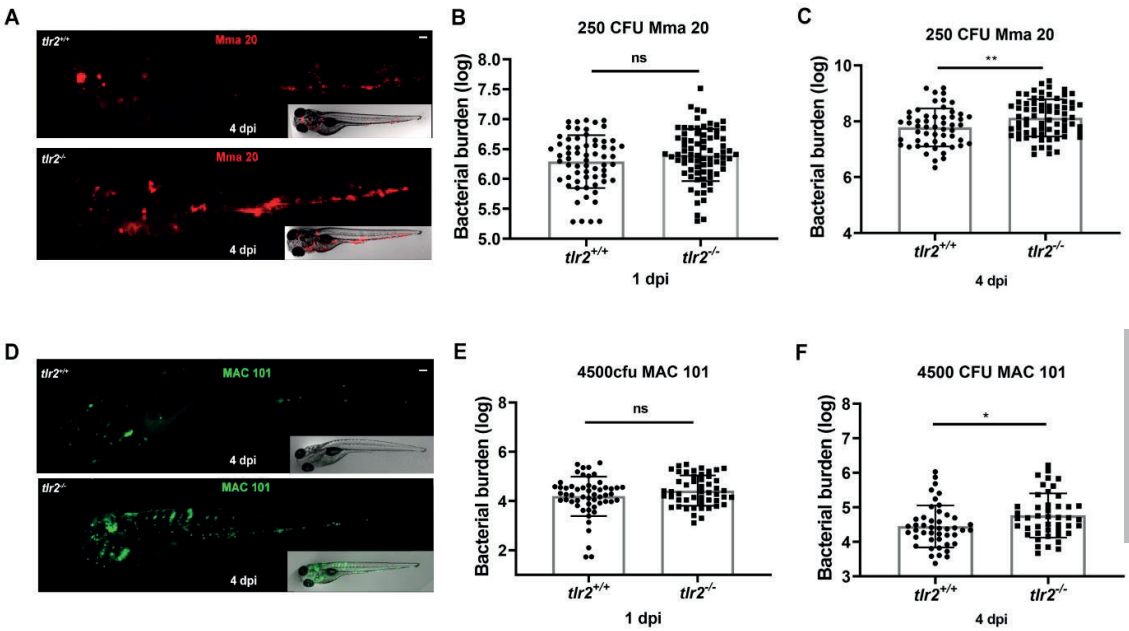

Figure 5 Quantification of bacterial burden in *tlr2* zebrafish larvae with *M. marinum* Mma20 or *M. avium* MAC 101 infection. *Tlr2*$^{+/+}$ and *tlr2*$^{-/-}$ embryos were infected at 28 hpf by caudal vein infection with mCherry-labeled *M. marinum* strain Mma20 at a dose of ~ 250 CFU, or infected with ~ 4500 CFU wasabi-labeled *M. avium* strain MAC 101. (A) Representative images of *tlr2*$^{+/+}$ and *tlr2*$^{-/-}$ embryos infected with mCherry-labeled *M. marinum* strain Mma20 at 4 dpi. (B) Quantification of bacterial burden of *tlr2*$^{+/+}$ and *tlr2*$^{-/-}$ upon Mma20 infection at 1 dpi. (C) Quantification of bacterial burden of *tlr2*$^{+/+}$ and *tlr2*$^{-/-}$ upon Mma20 infection at 4 dpi. (D) Representative images of *tlr2*$^{+/+}$ and *tlr2*$^{-/-}$ embryos infected with wasabi-labeled *M. avium* strain MAC 101 at 4 dpi. (E) The bacterial burden of *tlr2*$^{+/+}$ and *tlr2*$^{-/-}$ upon MAC 101 infection were quantified at 1 dpi. (F) The bacterial burden of *tlr2*$^{+/+}$ and *tlr2*$^{-/-}$ upon MAC 101 infection were quantified at 4 dpi. In (B, C, and E, F) data (mean ± SD) were combined from three independent experiments. Statistical significance of differences was determined by unpaired t-test for comparison between the *tlr2* mutant and its wild type sibling group. ns, non-significant; *, $P < 0.05$, **, $P < 0.01$. Scale bar: 50 µm. Sample size (n): 64, 78 (B), 54, 72 (C), 54 , 50 (E), and 45, 45 (F)

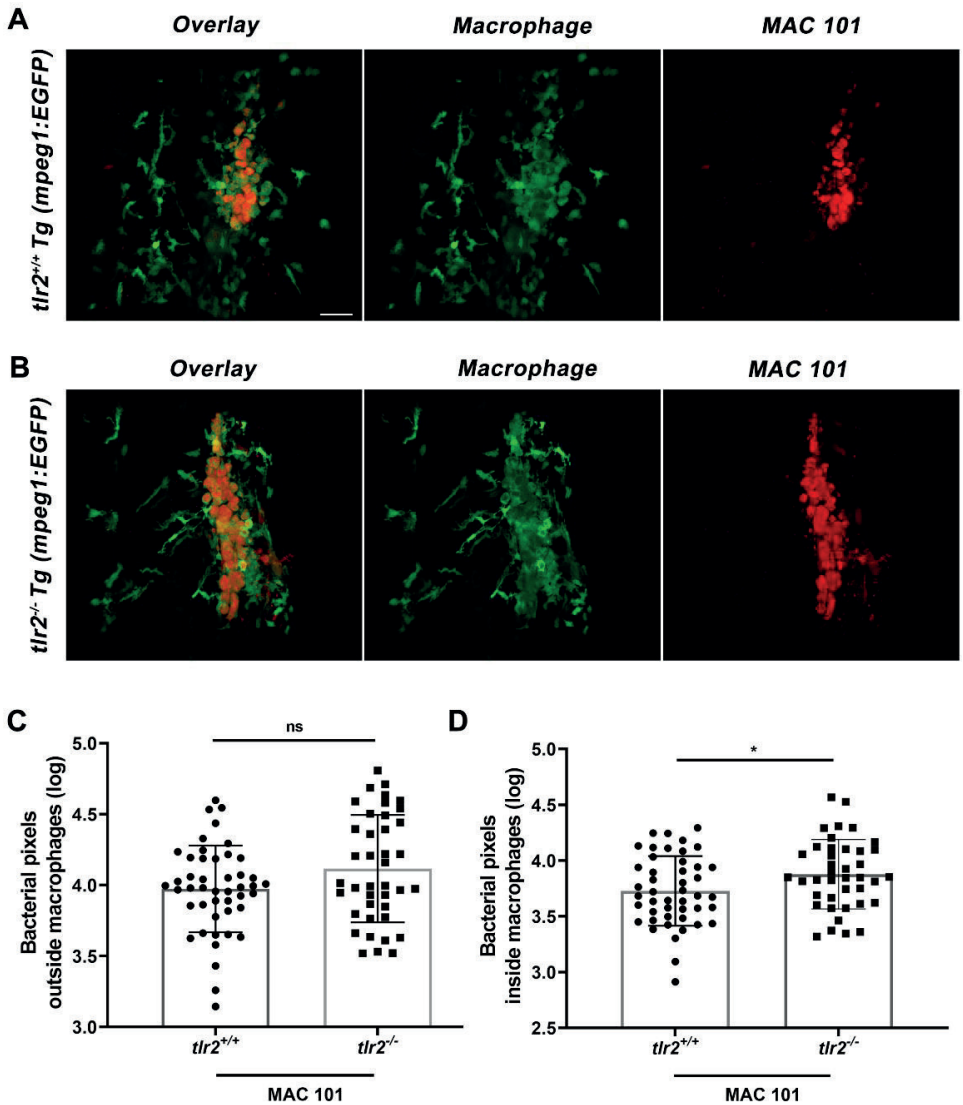

Figure 6 Quantification of the extracellular and intracellular bacterial burden in the *tlr2* mutant upon *M. avium* infection. *Tlr2*$^{+/+}$ *Tg(Mpeg1: EGFP)* and *tlr2*$^{-/-}$ *Tg(Mpeg1: EGFP)* zebrafish embryos were infected with ~4500 CFU MAC 101 DsRed strain at 28 hpf by caudal vein infection. (A, B) Representative CLSM images of *tlr2*$^{+/+}$ *Tg(Mpeg1: EGFP)* and *tlr2*$^{-/-}$ *Tg(Mpeg1: EGFP)* zebrafish larvae infected with DsRed-labeled *M. avium* MAC 101 strain. CLSM imaging was performed with the infected larvae at 4 dpi with 40 times magnification lens (oil immersion, N.A. 1.3). (C) Quantification of bacteria outside macrophages by pixel count. (D) Quantification of bacteria inside macrophages by pixel count. In (C and D) data (mean ± SD) were combined from two independent experiments. Statistical significance of differences was determined by unpaired t-test for comparison between the *tlr2* mutant and its wild type sibling group. ns, non-significant; *, $P < 0.05$. Sample size (n): 46, 40 (C, D). Scale bar: 30 µm.

Different migratory behavior of macrophages and neutrophils after *M. marinum* and *M. avium* infection in *tlr2* mutant larvae

Some studies have demonstrated that the migration of leukocytes during the infection process is important for bacterial clearance, containment, dissemination, and granuloma formation at the early mycobacterial infectious stage [37-40]. We have previously shown that *tlr2* is involved in regulating leukocyte migration in response to inflammatory signaling [29]. We hypothesized that *tlr2* could also be involved in the regulation of migratory behavior of macrophages and neutrophils to the sites of mycobacterial infection.

To test the hypothesis, we applied the tail fin infection model which was described before [37, 41]. This model has unique advantages in studying cell tracking. The tail fin of zebrafish larvae is a very thin tissue which contains mesenchymal cells, extracellular collagenous fibers, and an epidermis [42]. The thin tail fin makes it possible to set short time interval when the cell tracking was performed by CLSM, enabling high accuracy of tracing individual cells. Representative images of this tail fin infection model are shown in Fig. 7. mCherry labeled Mma20 or DsRed labeled MAC 101 were locally injected into the tail fin by using the 2 dpf zebrafish larvae. The region of the tail fin was imaged by using CLSM at 3 dpi.

To assess the role of *tlr2* mutation in regulating the recruitment of macrophages and neutrophils to the sites of the infection, Alexa Fluor dye stained Mma20 or MAC 101 were injected into 3 dpf *tlr2*$^{+/+}$ *Tg (mpeg1:mCherry-F);TgBAC (mpx: EGFP)* and *tlr2*$^{-/-}$ *Tg (mpeg1:mCherry-F);TgBAC (mpx: EGFP)* larvae. Time-lapse microscopy was performed by using CLSM between 1 hpi to 3 hpi. The time-lapse images were analyzed by Imaris to quantify the number, the speed of migration and meandering index of recruited leukocytes to the granuloma-like structures in the tail fin region (Fig. 8 and 9). We found that the recruited macrophages were fewer in numbers in the *tlr2* mutants upon Mma20 and MAC 101 infection compared with wild type sibling controls (Fig. 8 A-C). Interestingly, fewer macrophages were recruited to the MAC 101 site of infection in wild type sibling larvae compared to Mma20 wild type larvae (Fig. 8 A-C). We further quantified the speed and meandering index of the macrophages in the tail region. In the Mma20 infection group, macrophages in *tlr2*$^{-/-}$ group move significantly slower than the macrophages in it wild type sibling group, whereas no difference of meandering index was found (Fig. 8 D, E). In contrast, no significant difference was found in the speed of *tlr2*$^{+/+}$ macrophages and *tlr2*$^{-/-}$ macrophages after MAC 101 infection, while the meandering index of *tlr2*$^{-/-}$ macrophages is decreased after MAC 101 infection (Fig. 8 D, E). Interestingly, the mean

speed and meandering index of macrophages in Mma20 infection groups are always higher than the macrophages in their corresponding genotype MAC 101 infection groups (Fig. 8 D, E).

Comparing the behavior of neutrophils, we found that fewer neutrophils were recruited to the infected tail fin in Mma20 infected *tlr2*$^{+/+}$ group compared to the *tlr2*$^{-/-}$ at early time points (Fig. 9 A, C). In contrast, higher numbers of neutrophils were recruited in *tlr2*$^{+/+}$ compared to the *tlr2*$^{-/-}$ MAC101 infection group although the difference in the number of neutrophils becomes smaller in the later stage of the tracking among the four groups. We found that the mean speed and meandering index in the *tlr2*$^{-/-}$ neutrophils are decreased after Mma20 infection (Fig. 9 D, E). However, no difference in mean speed and the meandering index was observed between the *tlr2* mutant and its wild type siblings after MAC 101 infection (Fig. 9 D, E). The same to what we found in macrophages, the mean speed and meandering index of neutrophils in the Mma20 infection groups are always higher than of the neutrophils in the MAC 101 infection groups.

We found no difference in recruited leukocyte numbers, mean speed and meandering index of macrophages and neutrophils between *tlr2*$^{+/+}$ and *tlr2*$^{-/-}$ after PBS mock injection, which demonstrates that the differences observed above are depended on *tlr2* mutation and different mycobacteria, and not the damage of the injection (Fig. S3). To confirm the results we got from Imaris analysis, we used the Track Foci plug-in [43] (Fig. S4). The result of Track Foci, we found the overall mean speed of both macrophages and neutrophils is faster in the *tlr2*$^{+/+}$ Mma20 infection group compared to the *tlr2*$^{-/-}$ Mma20 infection group and *tlr2*$^{+/+}$ MAC 101 infection group respectively, which is consistent with what we observed by the Imaris analysis (Fig. S4). In conclusion, the results suggest that *tlr2* regulates the macrophages and neutrophils in different ways after different mycobacterial infections.

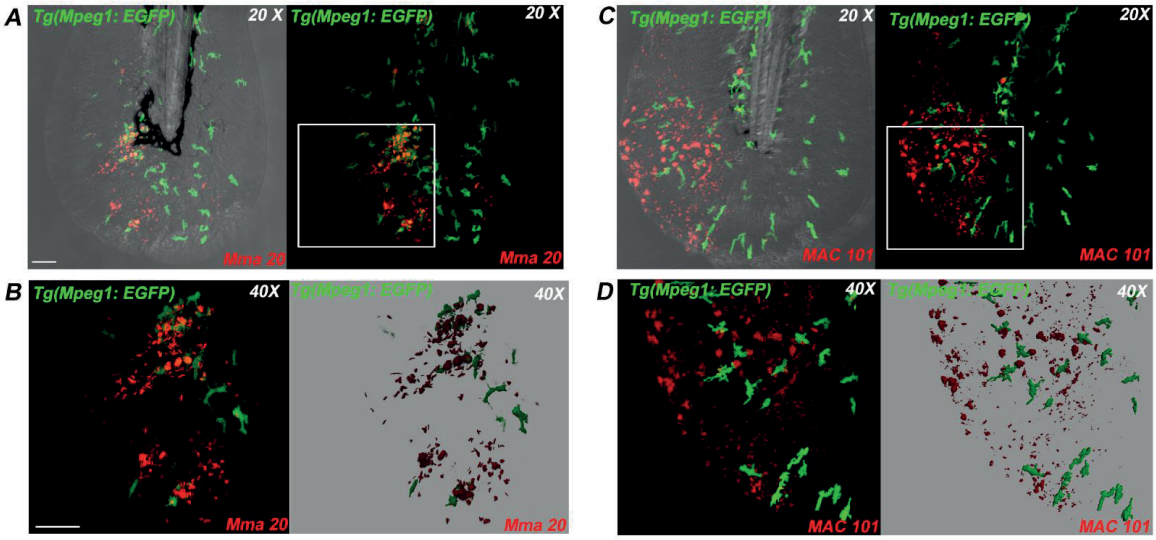

Figure 7 The tail fin infection model. (A, B) Representative images of *Tg (Mpeg1:EGFP)* larva infected with mCherry-labeled *M. marinum* strain Mma20 by tail fin injection. In A, The 3 dpi *Tg (Mpeg1:EGFP)* larva with tail fin Mma20 infection was imaged by using CLSM (20X, N.A. 0.75). The higher magnification image (40X, oil immersion, N.A. 1.3) in the white box area of (A) is shown in (B). (C, D) DsRed-labeled *M. avium* strain MAC 101 tail fin infected *Tg (Mpeg1:EGFP)* larva was imaged at 3 dpi in the tail fin region by using CLSM (20X, N.A. 0.75). A higher magnification image (40X, oil immersion, N.A. 1.3) in the white box area of (C) is shown in (D). In (A, C), the right panel is the image without a bright field. In (B, D), the right panel images are the 3D version of the left panel built by Imaris x64 7.4. Scale bar: 50 µm.

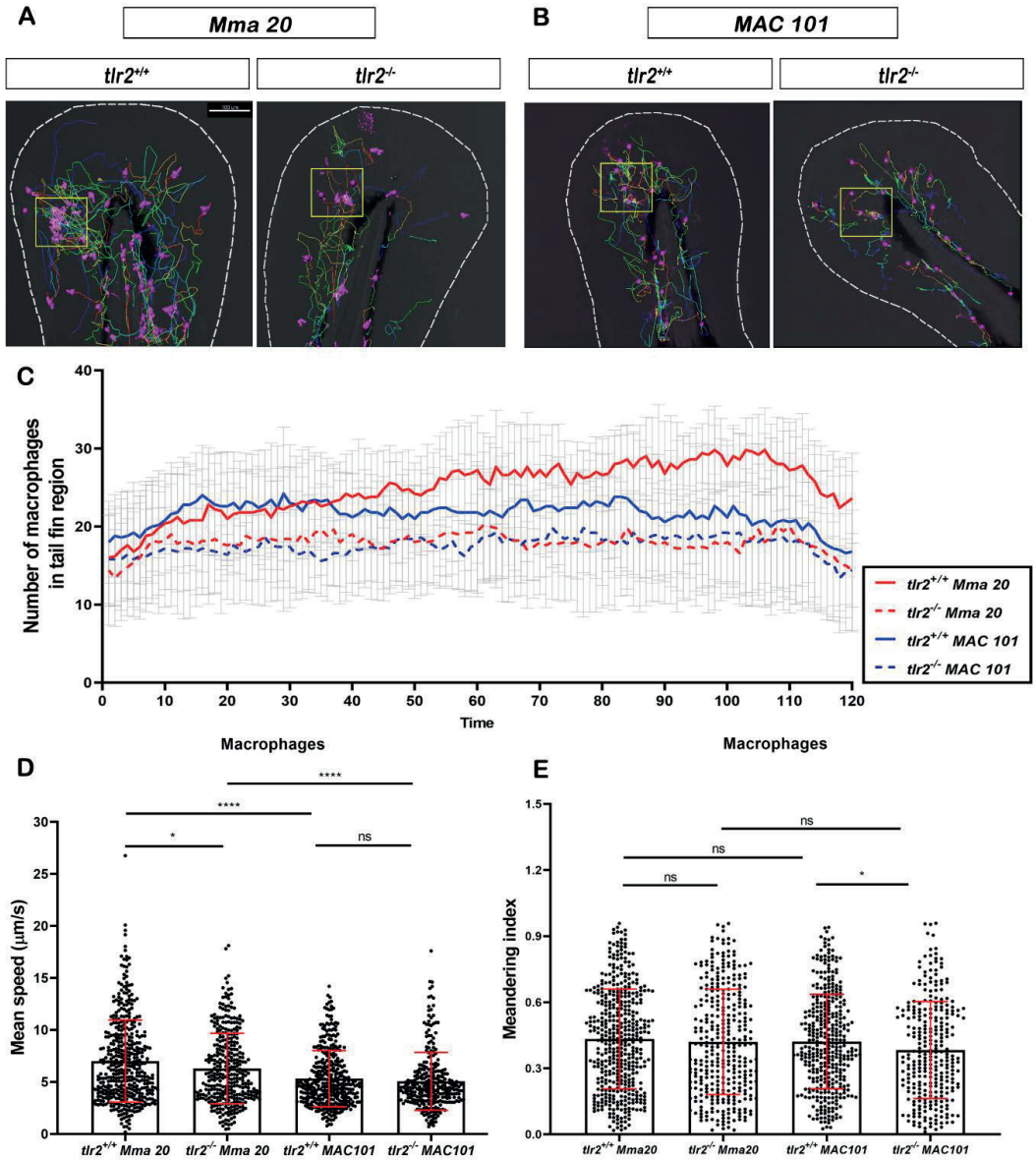

Figure 8 Quantification of macrophages behavior in *tlr2* mutant and sibling control larvae after *M. marinum* Mma20 or *M. avium* MAC 101 tail fin infection. (A) Representative images of macrophage tracks in $tlr2^{+/+}$ or $tlr2^{-/-}$ larvae with Mma20 tail fin infected. (B) Representative images of macrophage tracks in $tlr2^{+/+}$ or $tlr2^{-/-}$ larvae with MAC 101 tail fin infected. In (A, B), the magenta balls represent the tracked macrophages, the yellow box indicates the infected area. (C) The number of recruited macrophages to the tail fin region upon Mma20 or MAC 101 infection. The curves represent the mean value of the recruited neutrophil numbers at different time points. (D) The mean speed of tracked macrophages in infected tail fin region. (E) The meandering index of tracked macrophages in infected tail fin region. In (D, E) data (mean ± SD) were combined from three independent experiments with 5 fish in each group. An unpaired, two-tailed t-test was used to assess significance. ns, non-significant; *, $P < 0.05$, ****, $P < 0.0001$. Scale bar: 100 μm; Sample size (n): 447, 343, 372, 290 (D, E).

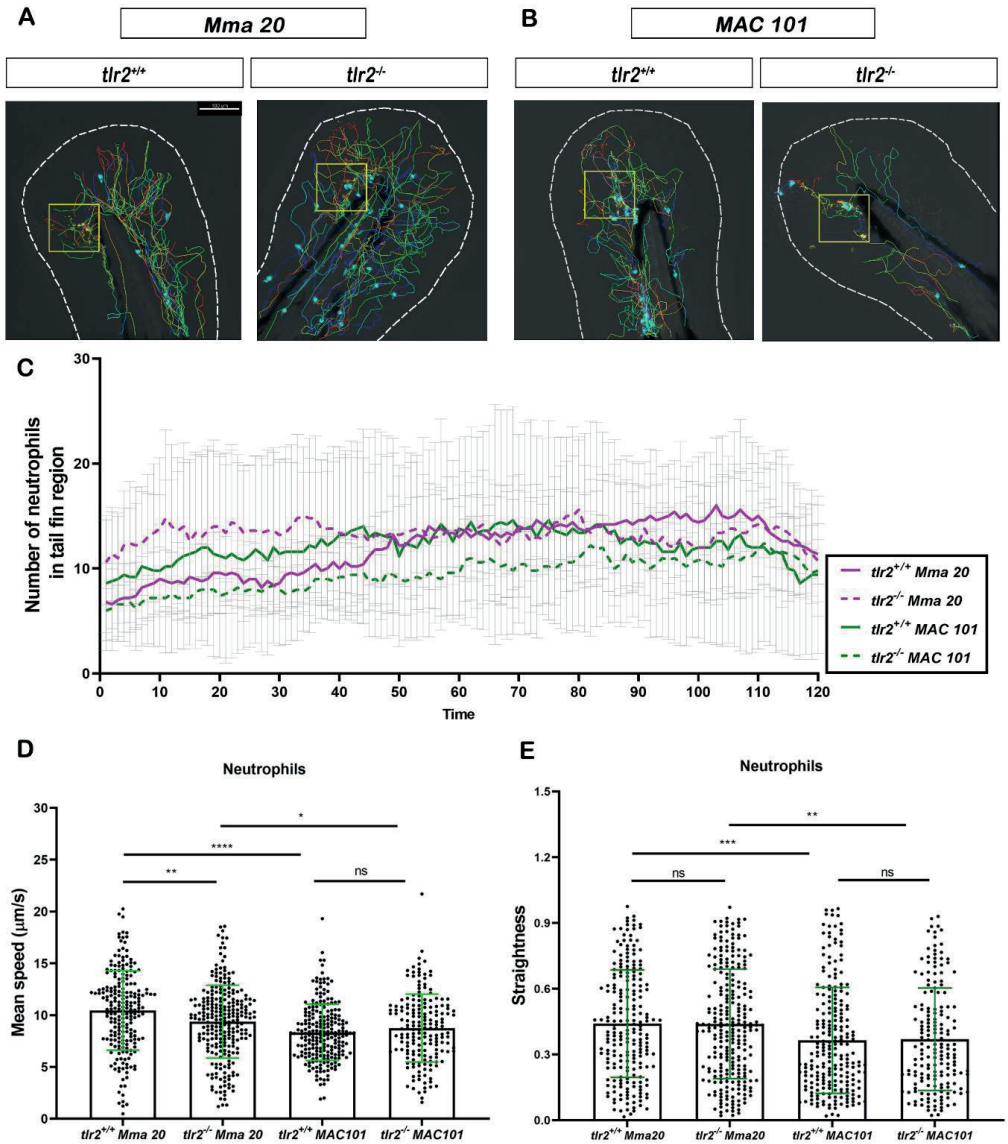

Figure 9 Quantification of neutrophils behavior in *tlr2* mutant and sibling control larvae after *M. marinum* Mma20 or *M. avium* MAC 101 tail fin infection. (A) Representative images of neutrophil tracks in *tlr2*$^{+/+}$ or *tlr2*$^{-/-}$ larvae with Mma20 tail fin infected. (B) Representative images of neutrophil tracks in *tlr2*$^{+/+}$ or *tlr2*$^{-/-}$ larvae with MAC 101 tail fin infected. In (A, B), the cyan balls represent the tracked neutrophils, the yellow box indicates the infected area. (C) The number of recruited neutrophils to the tail fin region upon Mma20 or MAC 101 infection. The curves represent the mean value of the recruited neutrophil numbers at different time points. (D) The mean speed of tracked neutrophils in infected tail fin region. (E) The meandering index of tracked neutrophils in infected tail fin region. In (D, E) data (mean ± SD) were combined from three independent experiments with 5 fish in each group. An unpaired, two-tailed t-test was used to assess significance. ns, non-significant; *, $P < 0.05$, ****, $P < 0.0001$. Scale bar: 100 μm; Sample size (n): 217, 254, 228, 179 (D, E)

Discussion

The investigation of the infectious diseases caused by nontuberculous mycobacteria (NTM) is receiving increasing attention because the disease prevalence has been increasing sharply since 2000 [44]. The bacteria belonging to the *M. avium* complex (MAC) are the most important pathogens for NTM infectious disease, accounting for 80% of NTM infectious disease cases [45, 46]. However, our understanding of the MAC infection mechanism is incomplete. *M. marinum*, that is genetically close related to the *M. tuberculosis* complex is widely utilized to model human tuberculosis *in vivo* [47]. Many new insights have been obtained in the last decades in our understanding of tuberculosis disease progression by using *M. marinum* infection in a zebrafish model [21, 22]. It could help us further uncover the pathobiology of MAC infectious diseases by comparing *M. avium* infection with *M. marinum* infection. In this study, we applied the zebrafish infection model to study the formation of granuloma-like cluster by CLSM imaging and investigate the host response to the infection through RNAseq analysis. In the first place we compared the difference between the *M. marinum* Mma20 and *M. avium* MAC 101 infection processes. Secondly, we focused on the function of toll-like receptor signaling after Mma20 and MAC 101 infection to compare the function of Tlr2 in infection with two different bacteria.

M. marinum Mma20 is more virulent than *M. avium* MAC 101

NTM are intracellular pathogens and macrophages are the first responders to defend against NTM at the early infection stage [48]. In this study, we found that MAC 101 is persisting in the macrophages with less extracellular cording compared to Mma20 (Fig. 2). Extracellular cording is a morphology of mycobacteria accompanied by necrotic macrophages and extracellularly replicating bacteria which prevent phagocytosis because of the size of the clusters [49, 50]. Bacterial cording is a pathogenic feature associated with hyper-virulence in *M. tuberculosis*, *M. marinum*, *M. abscessus*, *M. fortuitum*, and *M. chelonae* [49, 51-54]. Thus, Mma20 infected larvae presenting more extracellular cords may be a feature of the higher lethality and bacterial growth in Mma20 infection (Fig. 1 and 2). It is widely believed that macrophages play a protective role during mycobacterium infection. Macrophages execute a series of functions including recognizing mycobacteria, forming granulomas, and eliminating bacteria [48]. However, mycobacteria have evolved the ability to evade the immune system by using macrophages as a safe haven [55, 56]. This safe haven in the form of a granuloma affects drug delivery into the mycobacteria inside it and then makes them drug-tolerant [4]. Moreover,

granulomas can also provide a favorable environment for mycobacteria to survive longer inside the host [57]. Thus, more closed granuloma-like clusters in MAC 101 infection might contribute to a slower disease progression in MAC infectious diseases and the difficulties in treatment. The MAC 101 zebrafish infection model is therefore suitable to be further applied to study the host-mediated mechanism of drug tolerance in macrophages.

Different transcriptome responses to infection by *M. avium* MAC 101 and *M. marinum* Mma20

In general, we found that *M. avium* MAC 101 infection induced more innate immune responses, including a higher number of significantly regulated genes from the categories of cytokines, chemokines, and their receptors, autophagy regulators, blood factors, complement cascade and matrix remodeling. It should, however, be noted that as the transcriptomic dataset of the Mma20 response has been reanalyzed from a previous publication [32], and therefore a number of technical factors may have contributed to the apparent difference in the magnitude of the host transcriptomic response. In the category of cytokines, chemokines and their receptors, we found more genes were downregulated specifically in the MAC 101infection group, e.g. *il1rga*, *ccr9b*, *cxcr4b*, *ccr6b*, *cxcl11.7*, *ccl36.1*, *cxcl12.b* and *ccl33.3* (Fig. 4). Interestingly, we found that Cxcr4b/Cxcl12 signaling was downregulated in the MAC 101 infection group. CXCR4 signaling is well known to relate to HIV pathogenesis, tumor-sustained angiogenesis and mycobacteria-induced angiogenesis [58-60]. Deficiency of *cxcr4b* has been shown to delay *M. marinum* growth in zebrafish larvae through effects on granuloma-associated angiogenesis [60]. Additionally, Doncker et al. reported that AIDS patients with disseminated MAC infection are associated with CXCR4 dysfunction, which seriously affected the internalization promoted by CXCL12, but with normal membrane CXCR4 expression on the leukocytes surface [61]. In contrast, *cxcr4a* was upregulated in zebrafish larvae upon MAC 101 infection, which indicates that *cxcr4a* and *cxcr4b* may have antagonistic functions to mycobacterial infection (Fig. 4). These studies suggest that CXCR4 signaling play a role during MAC 101 infection. However, the function of CXCR4 upon MAC infection is still not clear and merits further studies. Furthermore, it has been demonstrated that CXCR4/CXCL12 signaling sustains leukocytes trafficking to inflammatory sites as well as CXCL11 signaling which mediates the recruitment of macrophages upon mycobacterial infection [62, 63]. Thus, we hypothesize that the macrophage and neutrophil migration behavior can be different in zebrafish larvae after infection with different NTM. The cell tracking experiments in this report (Fig. 8 and Fig. 9)

confirmed this hypothesis. Lower numbers of recruited macrophages were observed in MAC 101 infection regions compared to Mma20 infection regions, while the number of recruited neutrophils was not different. The migration speed of neutrophils to infection regions was decreased (Fig. 7 and 8). This will be discussed further below.

The complement system is a critical part of the innate immune system and plays a role in mediating the leukocyte function upon mycobacterial infection. For example, mycobacteria can utilize complement receptors, like the complement receptor types 1, 3 and 4 (CR1, CR3 ,CR4) to enter the macrophages [64]. In this study, we found several complement components regulated in different ways in response to different mycobacterial infections, e.g. *c3b.2* which specifically responded to MAC 101 (Fig. 4). It has been demonstrated by Schorey et al. that pathogenic mycobacteria including *M. tuberculosis*, *M. leprae*, and *M. avium* share the same macrophage invasion mechanism [65, 66]. The generation of C3b is induced upon mycobacterial infection to promote the uptake of the invading mycobacteria by macrophages [65]. These results also indicated that C3b was the predominant *M. avium* opsonin, which provides a link with our results [65]. However, the research of the link between the complement system and *M. avium* infection still has some contradictory points. Bohlson et al. found that the induction of TNF-α in C3 deficient mice was of a similar level as in C3 wild type mice and there was no difference in bacterial burden, which indicates that the major effector function of complement is not necessary to control *M. avium* infection [13]. On the contrary, Irani et al. reported that the synthesis of TNF-α in *M. avium*-infected mice macrophages is C3-dependent [14]. Considering that it is likely that the main reason for the difference between these reports is that they used different subtypes of *M. avium*, the link between MAC infection and the complement system, needs to be further confirmed.

Tlr2 plays a role in defense against different mycobacterial species

In the present study, we found that *tlr2*$^{-/-}$ zebrafish larvae showed a higher bacterial burden compared to their wild type sibling controls after either *M. marinum* Mma20 or *M. avium* MAC 101 infection. The results with Mma20 are consistent with what we have shown in our previous study with Mma20 infection in *tlr2*$^{-/-}$ zebrafish larvae [36]. Moreover, it has been demonstrated that mice deficient in TLR2 show increased susceptibility to *M. tuberculosis* infection [67, 68]. In agreement, Feng et al. reported that *Tlr2*$^{-/-}$ mice showed increased susceptibility to *M. avium*-infection compared with their wild type counterparts [69]. Interestingly, the bacterial growth in *Myd88*$^{-/-}$ mice infected with *M. avium* far exceeded that of *Tlr2*$^{-/-}$ and C57BL/6 mice. *M. avium*-

infected *Myd88*$^{-/-}$ mice died at 9-14 weeks post infection [69]. In contrast, no pronounced difference was observed in *M. avium*-infected *Tlr4*$^{-/-}$ mice and infected C57BL/6 mice [69]. In addition, TLR2 plays a role in active macrophages by recognition of *M. avium* biofilms on their surface [70]. Sweet et al. showed that TLR2 and MyD88, but not TLR4, activate macrophages through the glycopeptidolipids (GPLs) expressed on the surface of *M. avium* that are related to biofilm formation [70]. The studies suggest that TLR2, but not TLR4, plays a crucial protective role in mycobacterial infection. However, TLR2 is not the only member from the Toll-like receptor family that can respond to *M. avium* infection and trigger an immune response. TLR6 and TLR9 have also been shown to be required to effectively control *M. avium* growth in mice [71, 72]. In this study, we found that *tlr5a* and *tlr5b* were significantly upregulated in response to both *M. marinum* Mma20 and *M. avium* MAC 101 infection, while *myd88* was only significantly upregulated in the *M. avium* infection group (Fig. S2). It indicates that *tlr5a* and *tlr5b* are also involved in the process of the host response to *M. avium* infection and the role of *myd88* may be very important in this process. The function of *myd88*, *tlr5a*, and *tlr5b* in the NTM infection process are very interesting to be further investigated.

Tlr2 functions in defense against different mycobacterial species by regulating leukocyte cell migration

Although *tlr2* plays a protective role in the host defense against different NTM species, the underlying mechanisms may be different in infections by different mycobacterial species. We observed higher MAC 101 burdens inside *tlr2*$^{-/-}$ macrophages compared to *tlr2*$^{+/+}$ macrophages. This suggests that the bacterial clearance ability is impaired in the *tlr2* mutant upon MAC 101 infection. The antimicrobial function of TLR2 in macrophages has been previously demonstrated. In both mouse and human macrophages, the clearance of intracellular *M. tuberculosis* bacteria is dependent on TLR2 activation, although the mechanism of the antimicrobial activity is distinct between mouse and human macrophages [73]. In mouse macrophages, direct antimicrobial activity triggered by TLR2 is nitric oxide-dependent, however, this process is nitric oxide-independent in human macrophages [73, 74]. Liu et al. reported that human macrophage activation by TLR2 is related to vitamin D levels, which sustains the production of the antimicrobial peptide cathelicidin and subsequently leads to killing of intracellular tubercle bacilli [74]. In accordance, genes associated with the vitamin D receptor pathway are upregulated in wild type zebrafish larvae while they are downregulated in *tlr2* mutant after *M. marinum* infection [36]. This suggests that the higher susceptibility of the

tlr2 mutant to *M. marinum* and *M. avium* infection may be caused by impaired antimicrobial capacity of macrophages. Our observations of higher intracellular *M. avium* burdens in the *tlr2* mutants also supports this suggestion. The absence of differences in the intracellular bacterial burden found in *tlr2* mutant zebrafish after infection with *M. marinum* may have been caused by quicker death of infected macrophages in *M. marinum*-infected larvae. This hypothesis needs to be further validated.

Different mechanisms of *tlr2*-mediated defense against different mycobacterial species are apparently manifested in different effects on leukocyte behavior. In this study, we found that both macrophages and neutrophils moved faster in *tlr2* wild type larvae than in *tlr2* mutants after Mma20 infection, while *tlr2* deficiency did not affect neutrophil migration in MAC 101 infection. The meandering index of *tlr2* mutant macrophages was lower than the *tlr2* wild type macrophages in MAC 101 infection (Fig. 8). This altered leukocyte behavior suggests that chemokine expression profiles may be different in *tlr2* mutant zebrafish after infection by mycobacterial species. We previously reported that the expression levels of *cxcl11aa* and *cxcll11ac* after Mm infection was higher in 4 dpi *tlr2*$^{+/-}$ compared to 4 dpi *tlr2*$^{-/-}$ mutant zebrafish larvae [36]. Here we show that the chemokine gene expression profiles are different between the larvae infected with Mma20 and MAC 101 at the late infection stage in this study (Fig. 4). In future research we would like to investigate whether these differences in expression profiles can also be observed in the initial infection stage.

Materials and Methods

Zebrafish husbandry

The husbandry of adult zebrafish lines and all zebrafish experiments described in this study was in accordance with guidelines from the local animal welfare committee (DEC) of the university (License number: protocol 14,198), in compliance with the international guidelines specified by the EU Animal Protection Directive 2010/63/EU, and was conducted according to standard protocols (www.zfin.org). There was no adult zebrafish sacrificed in this study. All experiments were done with zebrafish larvae developed within 5 days post fertilization (dpf), therefore prior to the free-feeding stage and did not fall under animal experimentation law according to the EU Animal Protection Directive 2010/63/EU. Zebrafish eggs and larvae were cultured and grown at 28.5◦C in egg water (60 g/ml Instant Ocean sea salts). Zebrafish larvae were anesthetized

with egg water containing 0.02% buffered 3-aminobenzoic acid ethyl ester (Tricaine, Sigma-Aldrich, Netherlands) for bacterial infection and imaging experiments.

The ABTL wild type zebrafish strain, *tlr2*^{sa19423} mutant (ENU-mutagenized) and its wild type siblings or the following transgenic lines: *Tg (Mpeg1:EGFP)*^{gl22}, *tlr2*$^{+/+}$ *Tg (mpeg1:mCherry-F);TgBAC (mpx: EGFP)* and *tlr2*$^{-/-}$ *Tg (mpeg1:mCherry-F);TgBAC (mpx: EGFP)* were used for this study [29, 36].

Bacterial strain culture

The *Mycobacterium marinum* m20 (Mma20), the *Mycobacterium avium Chester* (also called MAC 101, ATCC® 700898™), Mma20 expressing mCherry fluorescent protein [23], MAC 101 containing the Wasabi expression vector pSMT3 (Addgene, plasmid 26589), and MAC 101 expressing DsRed through pND239 plasmid [75] were used in this study to induce infection in zebrafish embryos. The Mma20 and MAC 101 without any fluorescent protein were grown at 28.5◦C in Middlebrook 7H9 broth with acid-albumin-dextrose-catalase (ADC) enrichment or Middlebrook 7H10 agar with 10% oleic acid-albumin-dextrose-catalase (OADC) enrichment. The Mma20 mCherry, MAC 101 Wasabi and MAC 101 DsRed were grown in the same medium or plates with hygromycin 50 µg/mL.

Alexa Fluor dye staining of mycobacteria

To visualize the interaction between the mycobacteria and leukocytes, the succinimidyl esters (NHS ester) of Alexa Fluor 647 (Invitrogen, A20006) was applied to stain the mycobacteria. The dye was dissolved in high-quality, anhydrous dimethylsulfoxide (DMSO) at a final concentration of 5 mg/mL for preparing the reactive dye solution. For this method, Mma20 and MAC101 were cultured in 7H9 broth based on the description above and were harvest in their logarithmic phase. The mycobacterial strains were re-suspended in 250 µL 0.1 M sodium bicarbonate buffer ($NaHCO_3$, pH 8.3) and then slowly added 10 µL of the reactive dye solution. The mixture was incubated at room temperature for 20 min. Subsequently, the stained mycobacteria were washed twice by sterile PBS. The Alexa Fluor strained Mma20 and MAC101 were used for the cell tracking and the cell recruitment assay.

Microinjection

Liquid cultures of Mma20 and MAC 101 were harvested and prepared for the microinjection, according to procedures described before in [76]. In short, mycobacterial strains were grown to

the logarithmic phase and harvested by centrifugation and washing three times in sterile PBS. Subsequently, bacterial suspensions were re-suspended in sterile PBS with 2% polyvinylpyrrolidone (PVP40) with the desired concentration by measuring the OD600. An OD600 of 1 corresponds to approximately 10^8 MAC 101, which is the same as Mma20 (data are not shown). Embryos were systemically infected with ~150 CFU mCherry-labeled Mma20 or Wasabi-labeled ~4500 CFU MAC 101 through blood island infection at 28 hpf by using the method described in [76]. For quantification of the bacterial burden, we analyzed the correlation between MAC 101 CFU and average fluorescent signal (Fig. S5). To observe macrophage and neutrophil migration behavior upon mycobacterial infection, zebrafish tailfin infection model was applied [37, 41]. Zebrafish larvae were locally infected in the tail fin at 3 dpf with ~50 CFU Mma20 or MAC 101 as previously described [37, 41].

Imaging and quantification of bacterial burden

Mycobacterial infected ABTL, *tlr2*$^{+/+}$, and *tlr2*$^{-/-}$ zebrafish larvae were imaged at 1 dpi and 4 dpi for the quantification of the bacterial burden changes by using a Leica M205FA fluorescence stereomicroscope, equipped with a Leica DFC 345FX camera. All experiments were performed three times independently and in the same microscope setting. The integrated intensity of bacterial loads was quantified by using Quantifish software (https://github.com/DavidStirling/QuantiFish) [77].

Confocal microscopy imaging

Confocal microscopy imaging was applied for the observation of the granuloma-like cluster and the investigation of the leukocyte migration behavior upon two mycobacterial infections. Observed larvae for each condition were embedded in 1% low melting point agarose (Sigma Aldrich) with 0.02% tricaine and imaged under a Leica TCS SP8 confocal microscope (Leica Microsystems). 4 dpi blood island infected larvae or 3 dpi tail fin infected larvae were imaged with a 20× objective (N.A. 0.75) or a 40× objective (N.A. oil immersion, N.A. 1.3) to observe the phenotype of the granuloma-like clusters upon two different mycobacterial infections. In order to investigate the leukocyte migration behavior upon two mycobacterial infections, living imaging was performed on 1 hpi tail fin infected larvae with a 1 min time interval for 2 h imaging using a 20× objective (N.A. 0.75). Acquisition settings for the living imaging were kept the same across the groups.

RNA isolation, deep sequencing and data analysis

To compare the difference of the larvae infected with *M. marinum* Mma20 infection or *M. avium* MAC 101 infection, the RNAseq data of 4 dpi zebrafish larvae infected with ~250 CFU Mma20 was used (GEO database accession for the RNASeq data: GSE76499) [32]. Fifteen 4 dpi ABTL wild type larvae infected with ~4500 CFU MAC 101 (three replicates) were collected for the total RNA isolation. The same amount of ABTL wild type larvae (three replicates) were injected with sterile PBS as a control group. The total RNAs were isolated by using TRIzol Reagent (Life Technologies) to create RNAseq libraries. Moreover, DNase treatment (Thermo Fisher Scientific, EN0525) was applied to eliminate the effect of the DNA from the samples following the manufacturer's instructions. The concentration and quality of RNAs were assessed by NanoDrop 2000 (Thermo Fisher Scientific, the Netherlands).

The deep sequencing was performed in the company GenomeScan (GenomeScan B. V., Plesmanlaan 1d, 2333 BZ, Leiden, Netherlands). The RNAseq libraries were sequenced by applying a NovaSeq 6000 v1.5 device. Image analysis, base calling, and quality check were done by the Illumina data analysis pipeline RTA3.4.4 and Bclfastq v2.20. Subsequently, RNAseq reads were aligned against the zebrafish genome (GRCz11) by using CLC genomic workbench software (QIAGEN, Cat. 832583). The percent of aligned reads mapping is exceeding 90% among all samples in this study.

The Differential Expression in Two Groups tool from the CLC genomic workbench was used to acquire the differential expressed genes (DEGs) between the mycobacterial infection and its control groups. In brief, the tool performs a statistical differential expression test based on a negative binomial Generalized Linear Model (GLM) (See the user manual of the CLC genomic workbench, page 829: https://resources.qiagenbioinformatics.com/manuals/clcgenomicsworkbench/current/User_Manual.pdf) [78]. The output data were used for further analysis. A cut-oof setting of the FDR p-value < 0.05 and |FoldChange| > 2 was used to define significantly regulated DEGs. Pathvisio 3.3.0 (https://pathvisio.github.io/downloads) was applied for the visualization of the significantly regulated genes in the pathways [79].

Cell tracking and its quantification

The 4D files of leukocyte tracking generated from time-lapse acquisitions were processed by using Imaris x64 7.4 (Bitplane) or ImageJ (NIH, Bethesda, ML, USA). An automatic 3D cell

tracking algorithm in Imaris x64 7.4 (Bitplane) was employed to build macrophage or neutrophil trajectories in the living imaging of mycobacterial infected larvae. The data of the number, mean speed, and meandering index of recruited leukocytes in the infected tail fin region were output from the Imaris software. To confirm the results from the Imaris software, another automatic 3D cell tracking plug-in, 3D Track Foci, was applied [43]. The overall mean speed of macrophages or neutrophils was calculated using the 3D Track Foci for each larva.

Statistical analyses

The statistical analysis of Fig. 1, 5, 6, 8, 9, and Fig. S3 was done by using Graphpad Prism software (Version 9.0.0; GraphPad Software, San Diego, CA, USA). All experiment data in this study are shown as mean ± SD. D' Agostino-Pearson omnibus normality test was performed to determine the normal (Guassian) distribution of the data and unpaired two-tailed t-tests were applied. A parametric test was carried out when the data meets the normal distribution, otherwise the Mann-Whitney test which is a nonparametric test was used. Significance was established at $P < 0.05$ and the other significance levels are indicated as * $P < 0.05$; ** $P < 0.01$; *** $P < 0.001$; **** $P < 0.0001$.

Acknowledgments

This work was supported by a grant from the Innovative Medicines Initiative 2 Joint Undertaking (IMI2 JU) under the RespiriNTM project (Grant No. 853932). We would like to thank our colleagues from Leiden University: Mariëlle C. Haks and Gül Kilinç for supplying us with the pSTM3 Wasabi plasmid, Gerda E.M. Lamers for assistance with confocal laser scanning imaging and Joost J. Willemse for providing microscopic analysis programs. We thank all members of the fish facility team for fish caretaking.

References

1. Hoefsloot W, van Ingen J, Andrejak C, Angeby K, Bauriaud R, Bemer P, et al. The geographic diversity of nontuberculous mycobacteria isolated from pulmonary samples: an NTM-NET collaborative study. Eur Respir J. 2013;42(6):1604-13. Epub 2013/04/20. doi: 10.1183/09031936.00149212. PubMed PMID: 23598956.

2. Nishiuchi Y, Iwamoto T, Maruyama F. Infection Sources of a Common Non-tuberculous Mycobacterial Pathogen, Mycobacterium avium Complex. Front Med (Lausanne). 2017;4:27. Epub 2017/03/23. doi: 10.3389/fmed.2017.00027. PubMed PMID: 28326308; PubMed Central PMCID: PMCPMC5339636.

3. Tortoli E. Microbiological features and clinical relevance of new species of the genus Mycobacterium. Clin Microbiol Rev. 2014;27(4):727-52. Epub 2014/10/04. doi: 10.1128/CMR.00035-14. PubMed PMID: 25278573; PubMed Central PMCID: PMCPMC4187642.

4. Saxena S, Spaink HP, Forn-Cuni G. Drug Resistance in Nontuberculous Mycobacteria: Mechanisms and Models. Biology (Basel). 2021;10(2). Epub 2021/02/13. doi: 10.3390/biology10020096. PubMed PMID: 33573039; PubMed Central PMCID: PMCPMC7911849.

5. Kilinc G, Saris A, Ottenhoff THM, Haks MC. Host-directed therapy to combat mycobacterial infections. Immunol Rev. 2021. Epub 2021/02/11. doi: 10.1111/imr.12951. PubMed PMID: 33565103.

6. Strong EJ, Lee S. Targeting Autophagy as a Strategy for Developing New Vaccines and Host-Directed Therapeutics Against Mycobacteria. Front Microbiol. 2020;11:614313. Epub 2021/02/02. doi: 10.3389/fmicb.2020.614313. PubMed PMID: 33519771; PubMed Central PMCID: PMCPMC7840607.

7. Tomioka H, Sano C, Tatano Y. Host-Directed Therapeutics against Mycobacterial Infections. Curr Pharm Des. 2017;23(18):2644-56. Epub 2016/12/03. doi: 10.2174/1381612822666161202121550. PubMed PMID: 27908271.

8. Inderlied CB, Kemper CA, Bermudez LE. The Mycobacterium avium complex. Clin Microbiol Rev. 1993;6(3):266-310. Epub 1993/07/01. doi: 10.1128/cmr.6.3.266. PubMed PMID: 8358707; PubMed Central PMCID: PMCPMC358286.

9. Griffith DE, Aksamit T, Brown-Elliott BA, Catanzaro A, Daley C, Gordin F, et al. An official ATS/IDSA statement: diagnosis, treatment, and prevention of nontuberculous mycobacterial diseases. Am J Respir Crit Care Med. 2007;175(4):367-416. Epub 2007/02/06. doi: 10.1164/rccm.200604-571ST. PubMed PMID: 17277290.

10. Lam PK, Griffith DE, Aksamit TR, Ruoss SJ, Garay SM, Daley CL, et al. Factors related to response to intermittent treatment of Mycobacterium avium complex lung disease. Am J Respir Crit Care Med. 2006;173(11):1283-9. Epub 2006/03/04. doi: 10.1164/rccm.200509-1531OC. PubMed PMID: 16514112.

11. Park SW, Song JW, Shim TS, Park MS, Lee HL, Uh ST, et al. Mycobacterial pulmonary infections in patients with idiopathic pulmonary fibrosis. J Korean Med Sci. 2012;27(8):896-900. Epub 2012/08/10. doi: 10.3346/jkms.2012.27.8.896. PubMed PMID: 22876056; PubMed Central PMCID: PMCPMC3410237.

12. Verma D, Chan ED, Ordway DJ. The double-edged sword of Tregs in M tuberculosis, M avium, and M absessus infection. Immunol Rev. 2021. Epub 2021/03/14. doi: 10.1111/imr.12959. PubMed PMID: 33713043.

13. Bohlson SS, Strasser JA, Bower JJ, Schorey JS. Role of complement in Mycobacterium avium pathogenesis: in vivo and in vitro analyses of the host response to infection in the absence of complement component C3. Infect Immun. 2001;69(12):7729-35. Epub 2001/11/14. doi: 10.1128/IAI.69.12.7729-7735.2001. PubMed PMID: 11705954; PubMed Central PMCID: PMCPMC98868.

14. Irani VR, Maslow JN. Induction of murine macrophage TNF-alpha synthesis by Mycobacterium avium is modulated through complement-dependent interaction via complement receptors 3 and 4 in relation to M. avium glycopeptidolipid. FEMS Microbiol Lett. 2005;246(2):221-8. Epub 2005/05/19. doi: 10.1016/j.femsle.2005.04.008. PubMed PMID: 15899409.

15. Shin MK, Shin SJ. Genetic Involvement of Mycobacterium avium Complex in the Regulation and Manipulation of Innate Immune Functions of Host Cells. Int J Mol Sci. 2021;22(6). Epub 2021/04/04. doi: 10.3390/ijms22063011. PubMed PMID: 33809463; PubMed Central PMCID: PMCPMC8000623.

16. Shin JI, Shin SJ, Shin MK. Differential Genotyping of Mycobacterium avium Complex and Its Implications in Clinical and Environmental Epidemiology. Microorganisms. 2020;8(1). Epub 2020/01/16. doi: 10.3390/microorganisms8010098. PubMed PMID: 31936743; PubMed Central PMCID: PMCPMC7022546.

17. Andrejak C, Almeida DV, Tyagi S, Converse PJ, Ammerman NC, Grosset JH. Characterization of mouse models of Mycobacterium avium complex infection and evaluation of drug combinations. Antimicrob Agents Chemother. 2015;59(4):2129-35. Epub 2015/01/28. doi: 10.1128/AAC.04841-14. PubMed PMID: 25624335; PubMed Central PMCID: PMCPMC4356827.

18. Gangadharam PR, Perumal VK, Farhi DC, LaBrecque J. The beige mouse model for Mycobacterium avium complex (MAC) disease: optimal conditions for the host and parasite. Tubercle. 1989;70(4):257-71. Epub 1989/12/01. doi: 10.1016/0041-3879(89)90020-2. PubMed PMID: 2626803.

19. Torraca V, Masud S, Spaink HP, Meijer AH. Macrophage-pathogen interactions in infectious diseases: new therapeutic insights from the zebrafish host model. Dis Model Mech. 2014;7(7):785-97. Epub 2014/06/29. doi: 10.1242/dmm.015594. PubMed PMID: 24973749; PubMed Central PMCID: PMCPMC4073269.

20. Tobin DM, May RC, Wheeler RT. Zebrafish: a see-through host and a fluorescent toolbox to probe host-pathogen interaction. PLoS Pathog. 2012;8(1):e1002349. Epub 2012/01/14. doi: 10.1371/journal.ppat.1002349. PubMed PMID: 22241986; PubMed Central PMCID: PMCPMC3252360.

21. Meijer AH, Spaink HP. Host-pathogen interactions made transparent with the zebrafish model. Curr Drug Targets. 2011;12(7):1000-17. Epub 2011/03/04. doi: 10.2174/138945011795677809. PubMed PMID: 21366518; PubMed Central PMCID: PMCPMC3319919.

22. Meijer AH. Protection and pathology in TB: learning from the zebrafish model. Semin Immunopathol. 2016;38(2):261-73. Epub 2015/09/02. doi: 10.1007/s00281-015-0522-4. PubMed PMID: 26324465; PubMed Central PMCID: PMCPMC4779130.

23. van der Sar AM, Spaink HP, Zakrzewska A, Bitter W, Meijer AH. Specificity of the zebrafish host transcriptome response to acute and chronic mycobacterial infection and the role of innate and adaptive immune components. Mol Immunol. 2009;46(11-12):2317-32. Epub 2009/05/05. doi: 10.1016/j.molimm.2009.03.024. PubMed PMID: 19409617.

24. Hato T, Dagher PC. How the Innate Immune System Senses Trouble and Causes Trouble. Clin J Am Soc Nephrol. 2015;10(8):1459-69. Epub 2014/11/22. doi: 10.2215/CJN.04680514. PubMed PMID: 25414319; PubMed Central PMCID: PMCPMC4527020.

25. Oliveira-Nascimento L, Massari P, Wetzler LM. The Role of TLR2 in Infection and Immunity. Front Immunol. 2012;3:79. Epub 2012/05/09. doi: 10.3389/fimmu.2012.00079. PubMed PMID: 22566960; PubMed Central PMCID: PMCPMC3342043.

26. Mukherjee S, Karmakar S, Babu SP. TLR2 and TLR4 mediated host immune responses in major infectious diseases: a review. Braz J Infect Dis. 2016;20(2):193-204. Epub 2016/01/19. doi: 10.1016/j.bjid.2015.10.011. PubMed PMID: 26775799.

27. Uematsu S, Akira S. Toll-Like receptors (TLRs) and their ligands. Handb Exp Pharmacol. 2008;(183):1-20. Epub 2007/12/12. doi: 10.1007/978-3-540-72167-3_1. PubMed PMID: 18071652.

28. Tjarnlund A, Guirado E, Julian E, Cardona PJ, Fernandez C. Determinant role for Toll-like receptor signalling in acute mycobacterial infection in the respiratory tract. Microbes Infect. 2006;8(7):1790-800. Epub 2006/07/04. doi: 10.1016/j.micinf.2006.02.017. PubMed PMID: 16815067.

29. Hu W, van Steijn L, Li C, Verbeek FJ, Cao L, Merks RMH, et al. A Novel Function of TLR2 and MyD88 in the Regulation of Leukocyte Cell Migration Behavior During Wounding in Zebrafish Larvae. Front Cell Dev Biol. 2021;9:624571. Epub 2021/03/05. doi: 10.3389/fcell.2021.624571. PubMed PMID: 33659250; PubMed Central PMCID: PMCPMC7917198.

30. Simpson ME, Petri WA, Jr. TLR2 as a Therapeutic Target in Bacterial Infection. Trends Mol Med. 2020;26(8):715-7. Epub 2020/06/22. doi: 10.1016/j.molmed.2020.05.006. PubMed PMID: 32563557; PubMed Central PMCID: PMCPMC7845793.

31. Davis JM, Clay H, Lewis JL, Ghori N, Herbomel P, Ramakrishnan L. Real-time visualization of mycobacterium-macrophage interactions leading to initiation of granuloma formation in zebrafish embryos. Immunity. 2002;17(6):693-702. Epub 2002/12/14. doi: 10.1016/s1074-7613(02)00475-2. PubMed PMID: 12479816.

32. Benard EL, Rougeot J, Racz PI, Spaink HP, Meijer AH. Transcriptomic Approaches in the Zebrafish Model for Tuberculosis-Insights Into Host- and Pathogen-specific Determinants of the Innate Immune Response. Adv Genet. 2016;95:217-51. Epub 2016/08/10. doi: 10.1016/bs.adgen.2016.04.004. PubMed PMID: 27503359.

33. Ryffel B, Jacobs M, Parida S, Botha T, Togbe D, Quesniaux V. Toll-like receptors and control of mycobacterial infection in mice. Novartis Found Symp. 2006;279:127-39; discussion 39-41, 216-9. Epub 2007/02/07. PubMed PMID: 17278391.

34. Heldwein KA, Fenton MJ. The role of Toll-like receptors in immunity against mycobacterial infection. Microbes Infect. 2002;4(9):937-44. Epub 2002/07/11. doi: 10.1016/s1286-4579(02)01611-8. PubMed PMID: 12106786.

35. Vu A, Calzadilla A, Gidfar S, Calderon-Candelario R, Mirsaeidi M. Toll-like receptors in mycobacterial infection. Eur J Pharmacol. 2017;808:1-7. Epub 2016/10/30. doi: 10.1016/j.ejphar.2016.10.018. PubMed PMID: 27756604.

36. Hu W, Yang S, Shimada Y, Munch M, Marin-Juez R, Meijer AH, et al. Infection and RNA-seq analysis of a zebrafish tlr2 mutant shows a broad function of this toll-like receptor in transcriptional and metabolic control and defense to Mycobacterium marinum infection. BMC Genomics. 2019;20(1):878. Epub 2019/11/22. doi: 10.1186/s12864-019-6265-1. PubMed PMID: 31747871; PubMed Central PMCID: PMCPMC6869251.

37. Hosseini R, Lamers GE, Soltani HM, Meijer AH, Spaink HP, Schaaf MJ. Efferocytosis and extrusion of leukocytes determine the progression of early mycobacterial pathogenesis. J Cell Sci. 2016;129(18):3385-95. Epub 2016/07/30. doi: 10.1242/jcs.135194. PubMed PMID: 27469488.

38. Clay H, Davis JM, Beery D, Huttenlocher A, Lyons SE, Ramakrishnan L. Dichotomous role of the macrophage in early Mycobacterium marinum infection of the zebrafish. Cell Host Microbe. 2007;2(1):29-39. Epub 2007/11/17. doi: 10.1016/j.chom.2007.06.004. PubMed PMID: 18005715; PubMed Central PMCID: PMCPMC3115716.

39. Yang CT, Cambier CJ, Davis JM, Hall CJ, Crosier PS, Ramakrishnan L. Neutrophils exert protection in the early tuberculous granuloma by oxidative killing of mycobacteria phagocytosed from infected macrophages. Cell Host Microbe. 2012;12(3):301-12. Epub 2012/09/18. doi: 10.1016/j.chom.2012.07.009. PubMed PMID: 22980327; PubMed Central PMCID: PMCPMC3638950.

40. Bernut A, Nguyen-Chi M, Halloum I, Herrmann JL, Lutfalla G, Kremer L. Mycobacterium abscessus-Induced Granuloma Formation Is Strictly Dependent on TNF Signaling and Neutrophil Trafficking. PLoS

Pathog. 2016;12(11):e1005986. Epub 2016/11/03. doi: 10.1371/journal.ppat.1005986. PubMed PMID: 27806130; PubMed Central PMCID: PMCPMC5091842.

41. Hosseini R, Lamers GE, Hodzic Z, Meijer AH, Schaaf MJ, Spaink HP. Correlative light and electron microscopy imaging of autophagy in a zebrafish infection model. Autophagy. 2014;10(10):1844-57. Epub 2014/08/16. doi: 10.4161/auto.29992. PubMed PMID: 25126731; PubMed Central PMCID: PMCPMC4198367.

42. Kimmel CB, Ballard WW, Kimmel SR, Ullmann B, Schilling TF. Stages of embryonic development of the zebrafish. Dev Dyn. 1995;203(3):253-310. Epub 1995/07/01. doi: 10.1002/aja.1002030302. PubMed PMID: 8589427.

43. Celler K, van Wezel GP, Willemse J. Single particle tracking of dynamically localizing TatA complexes in Streptomyces coelicolor. Biochem Biophys Res Commun. 2013;438(1):38-42. Epub 2013/07/23. doi: 10.1016/j.bbrc.2013.07.016. PubMed PMID: 23867823.

44. Prevots DR, Marras TK. Epidemiology of human pulmonary infection with nontuberculous mycobacteria: a review. Clin Chest Med. 2015;36(1):13-34. Epub 2015/02/14. doi: 10.1016/j.ccm.2014.10.002. PubMed PMID: 25676516; PubMed Central PMCID: PMCPMC4332564.

45. Nasiri MJ, Calcagno T, Hosseini SS, Hematian A, Nojookambari NY, Karimi-Yazdi M, et al. Role of Clofazimine in Treatment of Mycobacterium avium Complex. Front Med (Lausanne). 2021;8:638306. Epub 2021/05/11. doi: 10.3389/fmed.2021.638306. PubMed PMID: 33968952; PubMed Central PMCID: PMCPMC8099105.

46. Prevots DR, Shaw PA, Strickland D, Jackson LA, Raebel MA, Blosky MA, et al. Nontuberculous mycobacterial lung disease prevalence at four integrated health care delivery systems. Am J Respir Crit Care Med. 2010;182(7):970-6. Epub 2010/06/12. doi: 10.1164/rccm.201002-0310OC. PubMed PMID: 20538958; PubMed Central PMCID: PMCPMC2970866.

47. Tonjum T, Welty DB, Jantzen E, Small PL. Differentiation of Mycobacterium ulcerans, M. marinum, and M. haemophilum: mapping of their relationships to M. tuberculosis by fatty acid profile analysis, DNA-DNA hybridization, and 16S rRNA gene sequence analysis. J Clin Microbiol. 1998;36(4):918-25. Epub 1998/05/23. doi: 10.1128/JCM.36.4.918-925.1998. PubMed PMID: 9542909; PubMed Central PMCID: PMCPMC104661.

48. Weiss G, Schaible UE. Macrophage defense mechanisms against intracellular bacteria. Immunol Rev. 2015;264(1):182-203. Epub 2015/02/24. doi: 10.1111/imr.12266. PubMed PMID: 25703560; PubMed Central PMCID: PMCPMC4368383.

49. Pagan AJ, Yang CT, Cameron J, Swaim LE, Ellett F, Lieschke GJ, et al. Myeloid Growth Factors Promote Resistance to Mycobacterial Infection by Curtailing Granuloma Necrosis through Macrophage Replenishment. Cell Host Microbe. 2015;18(1):15-26. Epub 2015/07/15. doi: 10.1016/j.chom.2015.06.008. PubMed PMID: 26159717; PubMed Central PMCID: PMCPMC4509513.

50. Tobin DM, Vary JC, Jr., Ray JP, Walsh GS, Dunstan SJ, Bang ND, et al. The lta4h locus modulates susceptibility to mycobacterial infection in zebrafish and humans. Cell. 2010;140(5):717-30. Epub 2010/03/10. doi: 10.1016/j.cell.2010.02.013. PubMed PMID: 20211140; PubMed Central PMCID: PMCPMC2907082.

51. Grosset J. Mycobacterium tuberculosis in the extracellular compartment: an underestimated adversary. Antimicrob Agents Chemother. 2003;47(3):833-6. Epub 2003/02/27. doi: 10.1128/AAC.47.3.833-836.2003. PubMed PMID: 12604509; PubMed Central PMCID: PMCPMC149338.

52. Bernut A, Herrmann JL, Kissa K, Dubremetz JF, Gaillard JL, Lutfalla G, et al. Mycobacterium abscessus cording prevents phagocytosis and promotes abscess formation. Proc Natl Acad Sci U S A. 2014;111(10):E943-52. Epub 2014/02/26. doi: 10.1073/pnas.1321390111. PubMed PMID: 24567393; PubMed Central PMCID: PMCPMC3956181.

53. Johansen MD, Kremer L. CFTR Depletion Confers Hypersusceptibility to Mycobacterium fortuitum in a Zebrafish Model. Front Cell Infect Microbiol. 2020;10:357. Epub 2020/08/28. doi: 10.3389/fcimb.2020.00357. PubMed PMID: 32850470; PubMed Central PMCID: PMCPMC7396536.

54. Olson G, McNulty MC, Mullane K, Beavis KG, Tesic V. Cording in Disseminated Mycobacterium chelonae Infection in an Immunocompromised Patient. Lab Med. 2021;52(3):e50-e2. Epub 2020/09/22. doi: 10.1093/labmed/lmaa082. PubMed PMID: 32954440.

55. Hybiske K, Stephens RS. Exit strategies of intracellular pathogens. Nat Rev Microbiol. 2008;6(2):99-110. Epub 2008/01/17. doi: 10.1038/nrmicro1821. PubMed PMID: 18197167.

56. Awuh JA, Flo TH. Molecular basis of mycobacterial survival in macrophages. Cell Mol Life Sci. 2017;74(9):1625-48. Epub 2016/11/21. doi: 10.1007/s00018-016-2422-8. PubMed PMID: 27866220.

57. Ufimtseva E. Mycobacterium-Host Cell Relationships in Granulomatous Lesions in a Mouse Model of Latent Tuberculous Infection. Biomed Res Int. 2015;2015:948131. Epub 2015/06/13. doi: 10.1155/2015/948131. PubMed PMID: 26064970; PubMed Central PMCID: PMCPMC4433666.

58. Cowley S. The biology of HIV infection. Lepr Rev. 2001;72(2):212-20. Epub 2001/08/10. doi: 10.5935/0305-7518.20010028. PubMed PMID: 11495453.

59. Katkoori VR, Basson MD, Bond VC, Manne U, Bumpers HL. Nef-M1, a peptide antagonist of CXCR4, inhibits tumor angiogenesis and epithelialtomesenchymal transition in colon and breast cancers. Oncotarget. 2015;6(29):27763-77. Epub 2015/09/01. doi: 10.18632/oncotarget.4615. PubMed PMID: 26318034; PubMed Central PMCID: PMCPMC4695024.

60. Torraca V, Tulotta C, Snaar-Jagalska BE, Meijer AH. The chemokine receptor CXCR4 promotes granuloma formation by sustaining a mycobacteria-induced angiogenesis programme. Sci Rep. 2017;7:45061. Epub 2017/03/24. doi: 10.1038/srep45061. PubMed PMID: 28332618; PubMed Central PMCID: PMCPMC5362882.

61. Doncker AV, Balabanian K, Bellanne-Chantelot C, de Guibert S, Revest M, Bachelerie F, et al. Two cases of disseminated Mycobacterium avium infection associated with a new immunodeficiency syndrome related to CXCR4 dysfunctions. Clin Microbiol Infect. 2011;17(2):135-9. Epub 2010/02/13. doi: 10.1111/j.1469-0691.2010.03187.x. PubMed PMID: 20148920.

62. Link DC. Neutrophil homeostasis: a new role for stromal cell-derived factor-1. Immunol Res. 2005;32(1-3):169-78. Epub 2005/08/18. doi: 10.1385/IR:32:1-3:169. PubMed PMID: 16106067.

63. Torraca V, Cui C, Boland R, Bebelman JP, van der Sar AM, Smit MJ, et al. The CXCR3-CXCL11 signaling axis mediates macrophage recruitment and dissemination of mycobacterial infection. Dis Model Mech. 2015;8(3):253-69. Epub 2015/01/13. doi: 10.1242/dmm.017756. PubMed PMID: 25573892; PubMed Central PMCID: PMCPMC4348563.

64. Roecklein JA, Swartz RP, Yeager H, Jr. Nonopsonic uptake of Mycobacterium avium complex by human monocytes and alveolar macrophages. J Lab Clin Med. 1992;119(6):772-81. Epub 1992/06/11. PubMed PMID: 1593222.

65. Schorey JS, Carroll MC, Brown EJ. A macrophage invasion mechanism of pathogenic mycobacteria. Science. 1997;277(5329):1091-3. Epub 1997/08/22. doi: 10.1126/science.277.5329.1091. PubMed PMID: 9262476.

66. Mold C. Role of complement in host defense against bacterial infection. Microbes Infect. 1999;1(8):633-8. Epub 1999/12/28. doi: 10.1016/s1286-4579(99)80063-x. PubMed PMID: 10611740.

67. Reiling N, Holscher C, Fehrenbach A, Kroger S, Kirschning CJ, Goyert S, et al. Cutting edge: Toll-like receptor (TLR)2- and TLR4-mediated pathogen recognition in resistance to airborne infection with Mycobacterium tuberculosis. J Immunol. 2002;169(7):3480-4. Epub 2002/09/24. doi: 10.4049/jimmunol.169.7.3480. PubMed PMID: 12244136.

68. Drennan MB, Nicolle D, Quesniaux VJ, Jacobs M, Allie N, Mpagi J, et al. Toll-like receptor 2-deficient mice succumb to Mycobacterium tuberculosis infection. Am J Pathol. 2004;164(1):49-57. Epub 2003/12/26. doi: 10.1016/S0002-9440(10)63095-7. PubMed PMID: 14695318; PubMed Central PMCID: PMCPMC1602241.

69. Feng CG, Scanga CA, Collazo-Custodio CM, Cheever AW, Hieny S, Caspar P, et al. Mice lacking myeloid differentiation factor 88 display profound defects in host resistance and immune responses to Mycobacterium avium infection not exhibited by Toll-like receptor 2 (TLR2)- and TLR4-deficient animals. J Immunol. 2003;171(9):4758-64. Epub 2003/10/22. doi: 10.4049/jimmunol.171.9.4758. PubMed PMID: 14568952.

70. Sweet L, Schorey JS. Glycopeptidolipids from Mycobacterium avium promote macrophage activation in a TLR2- and MyD88-dependent manner. J Leukoc Biol. 2006;80(2):415-23. Epub 2006/06/09. doi: 10.1189/jlb.1205702. PubMed PMID: 16760377.

71. Marinho FA, de Paula RR, Mendes AC, de Almeida LA, Gomes MT, Carvalho NB, et al. Toll-like receptor 6 senses Mycobacterium avium and is required for efficient control of mycobacterial infection. Eur J Immunol. 2013;43(9):2373-85. Epub 2013/05/30. doi: 10.1002/eji.201243208. PubMed PMID: 23716075.

72. Carvalho NB, Oliveira FS, Duraes FV, de Almeida LA, Florido M, Prata LO, et al. Toll-like receptor 9 is required for full host resistance to Mycobacterium avium infection but plays no role in induction of Th1 responses. Infect Immun. 2011;79(4):1638-46. Epub 2011/02/09. doi: 10.1128/IAI.01030-10. PubMed PMID: 21300776; PubMed Central PMCID: PMCPMC3067546.

73. Thoma-Uszynski S, Stenger S, Takeuchi O, Ochoa MT, Engele M, Sieling PA, et al. Induction of direct antimicrobial activity through mammalian toll-like receptors. Science. 2001;291(5508):1544-7. Epub 2001/02/27. doi: 10.1126/science.291.5508.1544. PubMed PMID: 11222859.

74. Liu PT, Stenger S, Li H, Wenzel L, Tan BH, Krutzik SR, et al. Toll-like receptor triggering of a vitamin D-mediated human antimicrobial response. Science. 2006;311(5768):1770-3. Epub 2006/02/25. doi: 10.1126/science.1123933. PubMed PMID: 16497887.

75. Manina G, Dhar N, McKinney JD. Stress and host immunity amplify Mycobacterium tuberculosis phenotypic heterogeneity and induce nongrowing metabolically active forms. Cell Host Microbe. 2015;17(1):32-46. Epub 2014/12/30. doi: 10.1016/j.chom.2014.11.016. PubMed PMID: 25543231.

76. Benard EL, van der Sar AM, Ellett F, Lieschke GJ, Spaink HP, Meijer AH. Infection of zebrafish embryos with intracellular bacterial pathogens. J Vis Exp. 2012;(61). Epub 2012/03/29. doi: 10.3791/3781. PubMed PMID: 22453760; PubMed Central PMCID: PMCPMC3415172.

77. Stirling DR, Suleyman O, Gil E, Elks PM, Torraca V, Noursadeghi M, et al. Analysis tools to quantify dissemination of pathology in zebrafish larvae. Sci Rep. 2020;10(1):3149. Epub 2020/02/23. doi: 10.1038/s41598-020-59932-1. PubMed PMID: 32081863; PubMed Central PMCID: PMCPMC7035342.

78. McCarthy DJ, Chen Y, Smyth GK. Differential expression analysis of multifactor RNA-Seq experiments with respect to biological variation. Nucleic Acids Res. 2012;40(10):4288-97. Epub 2012/01/31. doi: 10.1093/nar/gks042. PubMed PMID: 22287627; PubMed Central PMCID: PMCPMC3378882.

79. Kutmon M, van Iersel MP, Bohler A, Kelder T, Nunes N, Pico AR, et al. PathVisio 3: an extendable pathway analysis toolbox. PLoS Comput Biol. 2015;11(2):e1004085. Epub 2015/02/24. doi: 10.1371/journal.pcbi.1004085. PubMed PMID: 25706687; PubMed Central PMCID: PMCPMC4338111.

Supplementary materials

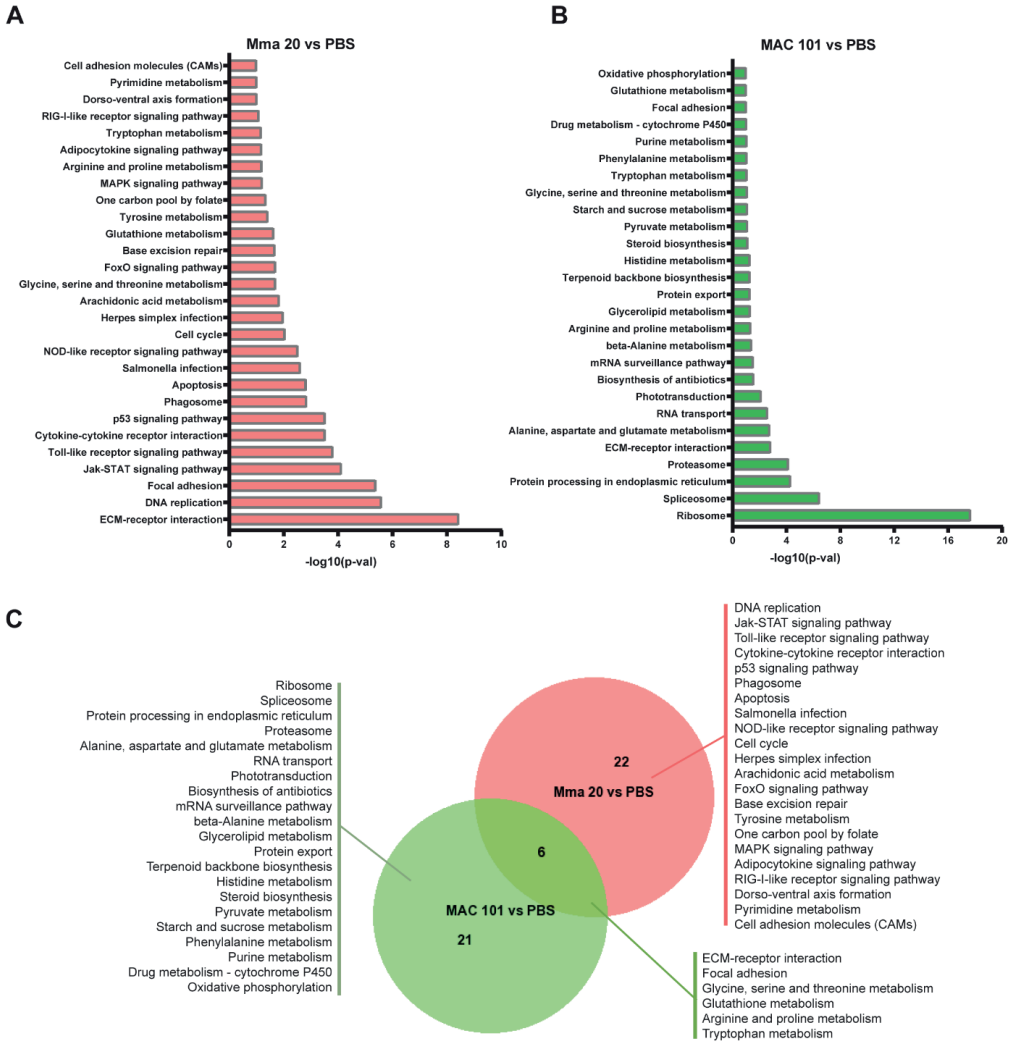

Supplementary figure 1 Significantly enriched KEGG pathways based on DAVID functional analysis. (A) Significantly enriched pathways in zebrafish embryos upon Mma 20 infection. (B) Significantly enriched pathways in zebrafish embryos upon MAC 101 infection. (C) Venn diagram of the enriched KEGG pathways in zebrafish embryos infected with Mma 20 and MAC 101. The comparison was performed on Mma 20 *vs* PBS and MAC 101 *vs* PBS.

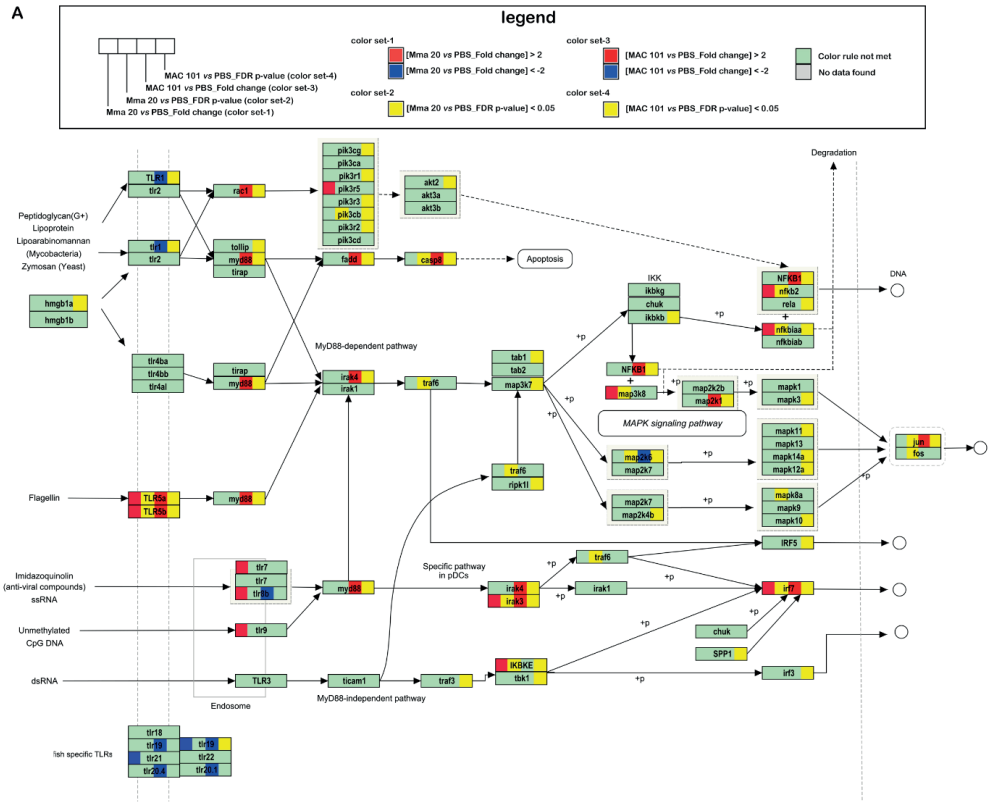

Supplementary figure 2 Toll-like receptor signaling pathway upon *M. marinum* Mma20 or *M. avium* MAC 101 infection. The pathway was adapted from the Wiki pathway. In the visualization, the gene expression in the comparison of Mma20 infection *vs* PBS and MAC 101 infection *vs* PBS are depicted by color (red, upregulated; blue, downregulated; yellow, FDR *p*-value < 0.05).

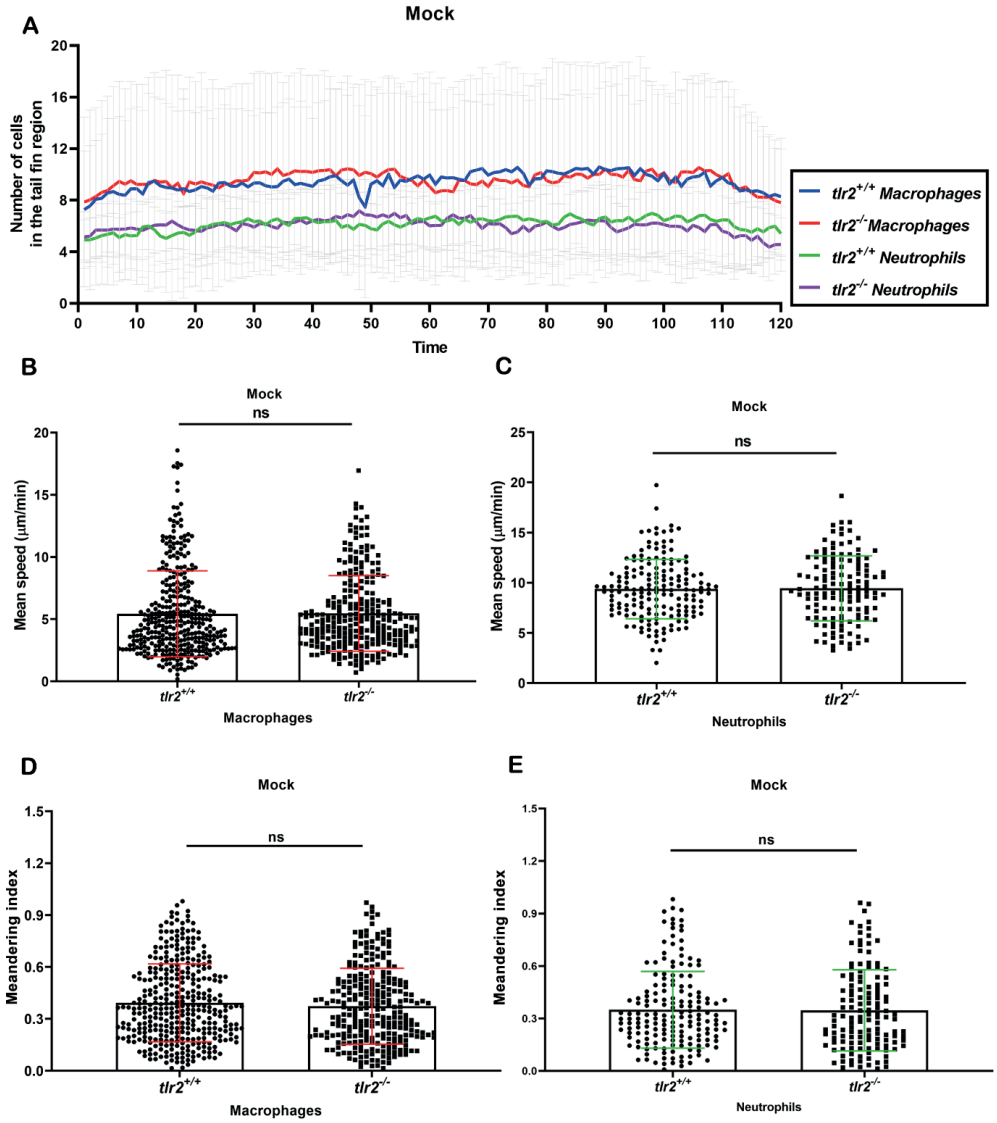

Supplementary figure 3 Quantification of leukocytes behavior in *tlr2* mutant and sibling control larvae after mock injection in tail fin. (A) The number of recruited leukocytes to the tail fin region upon mock infection. (B) The mean speed of tracked macrophages in PBS injected tail fin region. (C) The mean speed of tracked neutrophils in PBS injected tail fin region (D) The meandering index of tracked macrophages in PBS injected tail fin region. (E) The meandering index of tracked neutrophils in PBS injected tail fin region. Data (mean ± SD) were combined from three independent experiments with 5 or 6 fish in $tlr2^{+/+}$ or $tlr2^{-/-}$ group. An unpaired, two-tailed t-test was used to assess significance. ns, non-significant; *, $P < 0.05$, ****, $P < 0.0001$. Scale bar: 100 μm; Sample size (n): 347, 273; 170, 134 (B, D, and C, E).

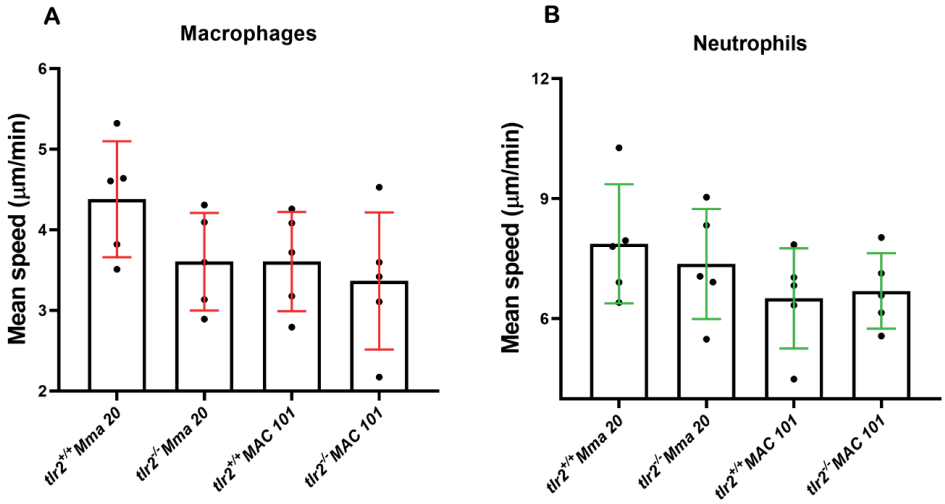

Supplementary figure 4 Quantification of leukocytes overall means speed in *tlr2* mutant and sibling control larvae after *M. marinum* Mma20 or *M. avium* MAC 101 injection in the tail fin. The quantification of the leukocytes overall mean speed was performed by Track Foci plugin. (A) Overall mean speed of macrophages in *tlr2*$^{+/+}$ and *tlr2*$^{-/-}$ zebrafish larvae after Mma 20 or MAC 101 infection. (B) Overall mean speed of neutrophils in *tlr2*$^{+/+}$ and *tlr2*$^{-/-}$ zebrafish larvae after Mma 20 or MAC 101 infection. Each point represents the mean speed of all specific cells from an individual zebrafish.

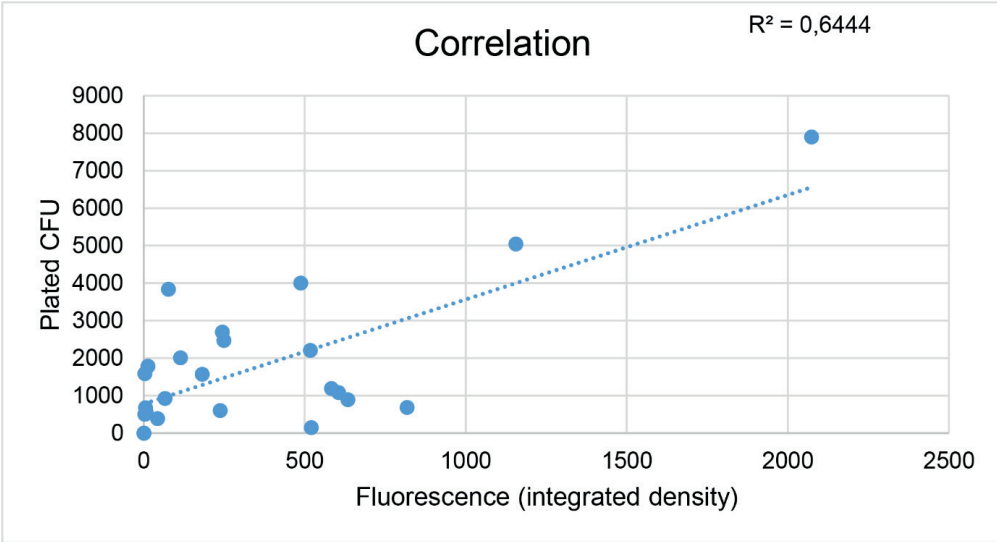

Supplementary figure 5 The correlation between MAC 101 CFU and average fluorescence signal.

Chapter 5

General summary and discussion

1. Zebrafish as a model to study infectious and inflammatory diseases

The activation of the innate immune system depends on the recognition of pathogen-associated molecular patterns (PAMPs) by pattern recognition receptors (PRRs) from the invading pathogens. PRRs are also involved in recognition of damage-associated molecular patterns (DAMPs) from damaged tissues during infection [1, 2]. The Toll-like receptors (TLRs) family is one of the most important member of the PRRs families. The discovery of TLRs as gatekeepers to activate innate immunity was awarded by the 2011 Noble Prize in Physiology or Medicine [3]. It triggered an explosion of research into the functions of TLRs in modulating a broad spectrum of physiological and pathological processes [4, 5]. TLR2 is conserved in most vertebrates and plays an important role in modulating infectious, and inflammatory diseases by recognizing a large number of PAMPs and DAMPs (**Chapter 1**). The broad function of TLR2 makes it a promising therapeutic target (**Chapter 1**). However, the function of TLR2 is still controversial in some studies and its role in several diseases is still inconclusive [6]. Therefore, it is vital to further study how TLR2 signaling functions in the host innate immune responses.

For this purpose, we utilized the zebrafish model to study the function of Tlr2 in inflammation and infection in this thesis. Zebrafish larvae already have a functional innate immune system within 5 days post fertilization at which time the adaptive immune system is not functional yet [7, 8]. This makes zebrafish an excellent model to study the vertebrate innate immunity in the absence of adaptive immunity. Moreover, the zebrafish model is becoming more and more popular in research because of the ease of genetic manipulation, omics studies of large groups of larvae, and live imaging. The last ten years, considerable progress has been made in studying infectious and inflammatory diseases by using the zebrafish model. Van der Vaart et al. found that zebrafish embryos deficient in Myeloid differentiation factor 88 (Myd88), which is a crucial adaptor by all TLRs except for TLR3, are more susceptible to bacterial pathogen infection [9]. This finding is similar to the conclusions derived of studies of MYD88 deficient mutants in human *in vitro* cell cultures and mouse in *vivo* models [9]. In addition, Hosseini et al. reported the function of Myd88 in limiting mycobacterial growth in a tail fin infection zebrafish model [10]. Furthermore, Yang et al. demonstrated that the function of Tlr2 signaling is similar in zebrafish embryos and in mammalian cells. In both systems TLR2 regulates the expression of a similar set of immune genes after the systemic stimulation by the synthetic model lipopeptide ligand Pam3CSK4 [11]. These studies paved the way to further investigate the function of Tlr2 in the zebrafish model. **In Chapter 2**, we studied the function of tlr2 in

defense against *Mycobacterium marinum* infection in zebrafish by measuring infection phenotypes and corresponding transcriptome responses. **In Chapter 3**, we investigated how Tlr2 and Myd88 regulate leukocytes migration behavior in the absence of infection, but with tissue damage, by using a zebrafish tail wounding model. **In Chapter 4**, we studied the function of tlr2 during the infection with *Mycobacterium avium* by comparing it with *M. marinum* infection with special attention to the responsive cell migration behavior.

2. Tlr2 plays a role in defense against mycobacterial infection in zebrafish larvae

In several studies it has been reported that TLR2 polymorphisms increases susceptibility to mycobacterial infection in the human population, although there is a small number of studies that found no effect of TLR2 polymorphisms (**Chapter 1**) [12, 13]. In addition, there is still controversy about the role of TLR2 in host defense against *Mycobacterium tuberculosis* in several rodent studies (**Chapter 1**) [14-16]. **In chapter 2**, we, therefore, generated a *tlr2* zebrafish mutant to study Tlr2 function in innate immune defense during mycobacterial infection. To characterize the effect of *tlr2* mutation, we first compared the transcriptome of homozygous mutant larvae with that of heterozygote larvae in the absence of infection. We found differences in the gene expression profiles of $tlr2^{-/-}$ zebrafish larvae and its control siblings, such as differently expressed genes involved in glycolysis (Chapter 2, Figure 2 and S3). This result is consistent with a previous study in the human *in vitro* and mice *in vivo* models which showed that TLR2 plays a key role to switch the host cellular metabolism toward aerobic glycolysis after *M. tuberculosis* infection [17]. In accordance, a previous study in our lab using zebrafish also suggested that MyD88 plays a role in metabolism [18]. In addition, this study showed that Tlr2 and its adaptor MyD88 are crucial for the response of the host to the microbiome [18]. This indicates that the different gene expression profiles we found in the *tlr2* mutant are caused by a dysfunctional response to the microbiome.

To study the role of Tlr2 in defense against *M. marinum* infection in zebrafish, we injected these bacteria in *tlr2* loss-of-function mutants and their homo- and heterozygote siblings. We found that the bacterial burden was significantly higher in *tlr2* mutants and was accompanied with a higher extracellular bacterial burden and less granulomas than in $tlr2^{+/-}$ and wild-type larvae at 4 dpi (Chapter 2, Figure 3 and 4). This result is consistent with previous studies in mice that show a function of Tlr2 in zebrafish host defense [15, 16, 19]. In addition, our transcriptome analysis showed that the number of up-regulated and down-regulated genes in response to

infection was greatly diminished in infected *tlr2* mutant zebrafish compared to their heterozygotes sibling controls (Chapter 2, Figure 5-7). Moreover, we found many signaling pathways that have been demonstrated to be linked to tuberculous in humans are differentially regulated in *tlr2* mutant zebrafish larvae. For example, we found that the Tlr8 signaling pathway was strongly affected, which indicates that Tlr2 signaling is connected to the function of Tlr8 (Chapter 2, Figure S10). In addition, the vitamin D receptor pathway genes were down-regulated in *tlr2* mutant zebrafish. It has been demonstrated that vitamin D plays an important role to control tuberculosis infection [20]. Therefore, the hyper-susceptibility of *tlr2* mutants to *M. marinum* infection could be caused by aberrant vitamin D signaling. Chemokines constitute the other gene category which was affected by the *tlr2* mutation during *M. marinum* infection. In previous work, Torraca et al, demonstrated that the Cxcr3-Cxcl11 axis was involved in macrophage recruitment after *M. marinum* infection in zebrafish larvae [21]. In agreement, we found that the expression levels of *cxcl11aa* and *cxcl11ac* were significantly lower in the *tlr2* mutant after infection (Chapter 2, Figure 5). This result shows a clear connection between Tlr2 function and macrophage chemotaxis.

3. New insights of Tlr2 functions in regulating leukocyte migration from live imaging

Considering the large number of chemokines that are controlled by Tlr2 (Chapter 2), we hypothesized that Tlr2 is a key factor in the control of chemokine expression in order to regulate cell recruitment in innate immunity. To test this hypothesis, **in Chapter 3**, we first investigated the function of Tlr2 and Myd88 in modulating leukocytes migration behavior in the absence of mycobacterial infection. For this, we utilized a zebrafish tail wounding model which is widely used for anti-inflammatory drugs screening [22, 23]. We found that the number of recruited neutrophils and macrophages was decreased in *tlr2*$^{-/-}$ and *myd88*$^{-/-}$ groups compared to their wild type sibling controls (Chapter 3, Figure 2 and 3). Subsequently, live cell imaging of the tail-wound area in zebrafish was performed in *tlr2* and *myd88* mutants and their corresponding wild type siblings. Leukocyte migration in the *tlr2* and *myd88* mutants upon wounding was analyzed using quantitative analyses of cell migration tracks (Chapter 3, Figure 4 and Table 1). Our results demonstrate that the *tlr2* and the *myd88* mutations affect the migration of neutrophils that are distantly located of a wound by negatively affecting their directional persistence, but not their migration speed (Chapter 3, Figure 5 and 6). Not only the directional persistence of macrophages that are distantly located from a wound was significantly decreased

in the *tlr2* and the *myd88* mutants, but also their migration speed (Chapter 3, Figure 7 and 8). This study shows for the first time that TLR signaling is directly involved in controlling behavior of cell migration of neutrophils and macrophages during wounding, stimulating further studies also in other model systems.

It has been shown previously in mice infection models that TLR signaling is involved in controlling infiltration of neutrophils and macrophages into injured tissues [24, 25]. Moreover, Tlr2 has been demonstrated to regulate the expression of cytokines and chemokines after the recognition of its ligands in both zebrafish and mice models (Chapter 2) [24]. Therefore, the aberrant leukocyte migration behavior, which was observed in *tlr2* and *myd88* mutant zebrafish could be caused by the insufficient level of basal transcripts for chemokines. For the tail wounding, it also could be that DAMPs released by dead cells around the wound do not lead to the secretion of chemokines in the absence of TLR2 signaling. For example, high-mobility group box 1 protein (HMGB1) is a widely studied endogenous danger signal that induces inflammatory response through its direct interaction with DAMPs recognized by TLR2 [26, 27]. Besides, reactive oxygen species (ROS) have been reported to be involved in leukocyte recruitment upon wounding in zebrafish larvae [28, 29]. And it has been demonstrated that the secretion of ROS is mediated by TLRs after tissue injury [30]. Thus, it is interesting to further study whether the generation of ROS may be altered in *tlr2* and *myd88* mutant zebrafish larvae.

4. Differences between TB and NTM infectious learned from zebrafish studies

Nontuberculous mycobacteria (NTM) diseases are defined as diseases caused by mycobacterial pathogens other than *M. tuberculosis* and *Mycobacterium leprae* [31]. Besides TB, NTM infectious diseases have recently attracted wide attention because its prevalence is increasing sharply since 2000 [32]. Although there are existing treatments for NTM infectious diseases, the treatment regimens are long and there is a high frequency of multi-drug resistant cases [33]. Thus, it is urgent to discover novel prevention and therapeutic strategies for patients infected with NTM. **In Chapter 4**, we used zebrafish larvae to establish a *M. avium* infectious model and then characterized *M. avium* infection in larvae by comparing it to *M. marinum* infection, a popular model of tuberculosis infection. It has been reported that innate immune defense against NTM infection is mainly mediated by the TLR signaling pathway [34-36]. Therefore, we first compared the transcriptome profiles of the host responses to infection specifically in relation to TLR signaling. Subsequently, we investigated the function of toll-like receptor

signaling after *M. marinum* and *M. avium* infection to compare the function of Tlr2 in infection with these two different bacteria.

We found *M. marinum* infection is more virulent than *M. avium* infection in zebrafish larvae (Chapter 4, Figure 1). Moreover, we found that *M. avium* is persisting in the macrophages with less extracellular cording compared to *M. marinum* (Chapter 4, Figure 2). *In vivo*, extracellular cording is a morphology of mycobacteria accompanied by necrotic macrophages and extracellularly replicating bacteria which prevent phagocytosis because of the size of the clusters [37, 38]. Bacterial cording is a pathogenic feature associated with hyper-virulence in *M. tuberculosis*, *M. marinum*, *M. abscessus*, *M. fortuitum*, and *M. chelonae* [37, 39-42]. Thus, the observation that *M. marinum* infected larvae show more extracellular cords may be a feature of the higher lethality and bacterial growth resulting from *M. marinum* infection. To obtain explanations for the lower virulence of the *M.avium* infection, and obtain genetic markers for further studies we performed RNAseq deep sequencing to study the whole transcriptome profile in the *M. avium* infection model comparing it to that of *M. marinum* infection model at a systemic level.

We found that *M. avium* has a distinct transcriptome response compared to *M. marinum*, especially regarding to the regulation of the following gene categories: autophagy regulators, matrix remodeling, and cytokines and chemokines (Chapter 4 Figure 3 and 4). In the category of cytokines, chemokines and their receptors, more genes were downregulated specifically in the *M. avium* infection group, such as *il1rga*, *ccr9b*, *cxcr4b*, *ccr6b*, *cxcl11.7*, *ccl36.1*, *cxcl12.b* and *ccl33.3* (Chapter 4, Figure 4). To be noted, the Cxcr4b/Cxcl12 signaling, which is related to HIV pathogenesis, tumor-sustained angiogenesis and mycobacteria-induced angiogenesis, was downregulated in the *M. avium* infection group [43-45]. Furthermore, it has been demonstrated that CXCR4/CXCL12 signaling sustains leukocytes trafficking to inflammatory sites as well as CXCL11 signaling, which mediates the recruitment of macrophages upon mycobacterial infection [46, 47]. Therefore, we hypothesize that the macrophage and neutrophil migration behaviors can be different in zebrafish larvae after infection with different NTM species.

It has been demonstrated that leukocyte migration is important for bacterial clearance, containment, dissemination, and granuloma formation at the early mycobacterial infectious stages [48-51]. In previous chapters, we demonstrated that Tlr2 plays an important role tin defense against *M. marinum* infection (Chapter 2). Furthermore, we found that Tlr2 is involved

in regulating macrophage and neutrophil behavior after tail wounding (Chapter 3). Thus, Tlr2 could also participate in the regulation of migratory behavior of macrophages and neutrophils to the sites of mycobacterial infection. To assess the role of Tlr2 in the regulation of the migration of macrophages and neutrophils, we applied a tail fin infection model **in Chapter 4**, which was described before [48, 52]. *M. marinum* strain Mma20 or *M. avium* strain MAC 101 were injected into 3 days post fertilization (dpf) *tlr2*$^{+/+}$ *Tg (mpeg1:mCherry-F);TgBAC (mpx: EGFP)* and *tlr2*$^{-/-}$ *Tg (mpeg1:mCherry-F);TgBAC (mpx: EGFP)* larvae (Chapter 4, Figure 7). We conclude that macrophages play an important role in the response to both mycobacterial infections because more recruited macrophages were observed in the infected area (Chapter 4, Figure 8). The migration speed of macrophages is faster towards Mma20 infection sites (Chapter 4, Figure 8). We found that neutrophils moved faster in *tlr2* wild type larvae than in *tlr2* mutants after Mma20 injection, while *tlr2* deficiency did not affect neutrophil migration after MAC101 injection (Chapter 4, Figure 8). This altered leukocyte behavior suggests that chemokine expression profiles may be different in *tlr2* mutant zebrafish after infection by mycobacterial species.

5. Perspectives for future studies

5.1 The investigation of host and mycobacteria interactions by using zebrafish larvae

In Chapter 4, we first developed a *M. avium* infection model in zebrafish which makes it possible to directly observe the host and *M. avium* interactions *in vivo*. Through this model, we observed different phenotypes of granuloma-like clusters in zebrafish larvae after infecting with different mycobacteria (Chapter 4, Figure 2). Furthermore, the transcriptome analysis showed that the expression of the genes belonging to the category of autophagy regulator genes was significantly affected in *M. avium*-infected zebrafish larvae (Chapter 4, Figure 4). Therefore, it is interesting to compare the autophagy response and ultrastructure of granulomas resulting from infection by different species of mycobacterial clusters. For this purpose, in the near future we will apply transmission electron microscopy (TEM) and 3D block-face scanning electron microscopy (block-face SEM).

In addition, in Chapter 4, we found that Tlr2 is involved in the regulation of the migration of macrophages and neutrophils in response to infection. Interestingly, the results of cell tracking suggest that *tlr2* regulates the macrophages and neutrophils in different ways after infection by different mycobacterial species. To obtain explanations for further studies of the effect of the

tlr2 mutation on mycobacterial infection, in the future, we will investigate whether differences in expression profiles of chemokines can be observed in the early infection stage. We would also like to study whether the changes of leukocyte migration behavior in *Tlr2* mutants are due to alterations of signals from the infection site or whether they are caused cell autonomous defects in migratory abilities of the myeloid cells in the *tlr2* mutant. Thus, we will apply cell transplantation techniques to investigate the non-intrinsic and intrinsic functions of myeloid cells in the *tlr2* mutant after wounding and mycobacterial infection.

5.2 Automated processing of zebrafish live imaging and mathematic modeling

In Chapter 3 and Chapter 4, we performed a large number of cell tracking experiments to quantify cell migration behaviors. Cell migration is an important physiological parameter for many pathological processes, including inflammatory responses [23], immune defense [48], and metastasis of malignant tumor cells [53]. Single-cell tracking using confocal real-time imaging is one of the most popular methods to analyze cell migration [54]. With the development of confocal laser scanning microscopy, it is easier to acquire massive live imaging data. However, there are many bioinformatic steps needed to be done following the acquisition of imaging. These involve the processing of large data sets, segmenting cell migration trajectories, visualization and quantification of the trajectories, and importantly, interpretation of the biological significance from the large data sets. Currently, manual data analysis is still required to assist automated data analysis. Furthermore, the availability of user friendly software programs still lags behind the requirements of researchers in the field.

Some recent reviews have summarized in detail the available commercial and free software or plug-ins for live imaging processing in cell migration studies [54, 55]. The TrackMate plug-in for ImageJ software (NIH, Bethesda, MD, USA), Volocity (Improvision; PerkinElmer Life and Analytical Sciences), and IMARIS (Bitplane) are widely used in zebrafish studies. However, still quite a large number of researchers choose manually tracking methods for zebrafish *in vivo* cell tracking, like ManualTrack plug-in, or MTrackJ plug-in for ImageJ software. This is because most of the software was designed for tracking movement of big particles or *in vitro* cell migration. However, the shape of cells *in vivo* is irregular, which makes the segmentation of the trajectories difficult and frequently results in over-segmentation [56]. Failure to segment the trajectories of cells correctly is the main reason for tracking errors. Examples of errors are that that, the trajectory output from the software is not from the same cell or that the tracked trajectory is broken in several parts. Moreover, the movement of cells *in vivo* is more

complicated than *in vitro*, especially during dynamic immune responses. Modelling of cell migration *in vivo* is not simply based on Brownian motion or Autoregressive motion, but needs to assume a combination of multiple complex motions. Single tracking algorithms in some commercial software programs results in tracking errors, which makes the quantification of trajectory unreliable. Therefore, it is necessary to establish new algorithm models based on *in vivo* movements of cells in a specific situation. In Chapter 3, we investigated the cell migration behavior regulated by Toll-like receptor signaling in tail-wounded zebrafish larvae through a manual tracking method. These manual tracking data provide a solid ground, which paves the way to develop improved cell tracking plug-ins for *in vivo* cell tracking studies in zebrafish larvae. Consequently, we plan to develop further optimized automatic tracking methods based on the large data sets in Chapter 3.

To study the mechanistic basis of the differences in cell migratory behaviors, mathematical models can provide new insights. Chemokine and ROS gradients can be modeled by partial differential equations (PDEs). These can be incorporated into cell chemotaxis models, such as random walk models, phase field models, or the Cellular Potts model, with varying degrees of cell resolution, to study leukocyte migration. Such models could provide quantitative insights into how chemokines and ROS gradients affect the migration behavior of the leukocytes, and how the cells change these gradients by binding or secretion of chemokines or by absorption and metabolizing ROS [57] which is known to affect the robustness of chemotaxis [58]. Using Bayesian inference on tracking data, one can infer a number of chemotaxis parameters, such as the flow rate, diffusion coefficient and production time of the chemoattractant [59].

6. Conclusion

A broad understanding of the innate immune system is important for host-targeted approaches for the treatment of diseases. In this thesis, we demonstrated that Tlr2 plays a crucial role in the host innate immune system. **In Chapter 2**, we show the roles of Tlr2 signaling in host defense against infection at the transcriptome level and cellular level by studying *M. marinum* infection in a tlr2 mutant. Moreover, the *tlr2*$^{-/-}$ mutant zebrafish strain described in Chapter 2 proved highly useful for the study of innate immune mechanisms underlying mycobacterial infection. **In Chapter 3,** we found that *tlr2* and *myd88* are involved in responses to tail wounding by regulating the behavior and speed of leukocyte migration *in vivo*. The large data sets acquired from Chapter 3 will be further used for developing new cell tracking algorithms and

mathematical modeling. **In Chapter 4**, we characterized a new *M. avium* infection model in zebrafish that can be further used to study the interaction between the host and NTM bacteria.

References

1. Gong T, Liu L, Jiang W, Zhou R. DAMP-sensing receptors in sterile inflammation and inflammatory diseases. Nat Rev Immunol. 2020;20(2):95-112. Epub 2019/09/29. doi: 10.1038/s41577-019-0215-7. PubMed PMID: 31558839.
2. Akira S, Uematsu S, Takeuchi O. Pathogen recognition and innate immunity. Cell. 2006;124(4):783-801. Epub 2006/02/25. doi: 10.1016/j.cell.2006.02.015. PubMed PMID: 16497588.
3. Volchenkov R, Sprater F, Vogelsang P, Appel S. The 2011 Nobel Prize in physiology or medicine. Scand J Immunol. 2012;75(1):1-4. Epub 2011/11/08. doi: 10.1111/j.1365-3083.2011.02663.x. PubMed PMID: 22053831.
4. Kawai T, Akira S. Toll-like receptors and their crosstalk with other innate receptors in infection and immunity. Immunity. 2011;34(5):637-50. Epub 2011/05/28. doi: 10.1016/j.immuni.2011.05.006. PubMed PMID: 21616434.
5. Fitzgerald KA, Kagan JC. Toll-like Receptors and the Control of Immunity. Cell. 2020;180(6):1044-66. Epub 2020/03/14. doi: 10.1016/j.cell.2020.02.041. PubMed PMID: 32164908.
6. Simpson ME, Petri WA, Jr. TLR2 as a Therapeutic Target in Bacterial Infection. Trends Mol Med. 2020;26(8):715-7. Epub 2020/06/22. doi: 10.1016/j.molmed.2020.05.006. PubMed PMID: 32563557; PubMed Central PMCID: PMCPMC7845793.
7. van der Vaart M, Spaink HP, Meijer AH. Pathogen recognition and activation of the innate immune response in zebrafish. Adv Hematol. 2012;2012:159807. Epub 2012/07/20. doi: 10.1155/2012/159807. PubMed PMID: 22811714; PubMed Central PMCID: PMCPMC3395205.
8. Meijer AH, Spaink HP. Host-pathogen interactions made transparent with the zebrafish model. Curr Drug Targets. 2011;12(7):1000-17. Epub 2011/03/04. doi: 10.2174/138945011795677809. PubMed PMID: 21366518; PubMed Central PMCID: PMCPMC3319919.
9. van der Vaart M, van Soest JJ, Spaink HP, Meijer AH. Functional analysis of a zebrafish myd88 mutant identifies key transcriptional components of the innate immune system. Dis Model Mech. 2013;6(3):841-54. Epub 2013/03/09. doi: 10.1242/dmm.010843. PubMed PMID: 23471913; PubMed Central PMCID: PMCPMC3634667.
10. Hosseini R, Lamers GEM, Bos E, Hogendoorn PCW, Koster AJ, Meijer AH, et al. The adapter protein Myd88 plays an important role in limiting mycobacterial growth in a zebrafish model for tuberculosis. Virchows Arch. 2021;479(2):265-75. Epub 2021/02/10. doi: 10.1007/s00428-021-03043-3. PubMed PMID: 33559740.
11. Yang S, Marin-Juez R, Meijer AH, Spaink HP. Common and specific downstream signaling targets controlled by Tlr2 and Tlr5 innate immune signaling in zebrafish. BMC Genomics. 2015;16:547. Epub 2015/07/26. doi: 10.1186/s12864-015-1740-9. PubMed PMID: 26208853; PubMed Central PMCID: PMCPMC4514945.

12. Texereau J, Chiche JD, Taylor W, Choukroun G, Comba B, Mira JP. The importance of Toll-like receptor 2 polymorphisms in severe infections. Clin Infect Dis. 2005;41 Suppl 7:S408-15. Epub 2005/10/21. doi: 10.1086/431990. PubMed PMID: 16237639.

13. Jafari M, Nasiri MR, Sanaei R, Anoosheh S, Farnia P, Sepanjnia A, et al. The NRAMP1, VDR, TNF-alpha, ICAM1, TLR2 and TLR4 gene polymorphisms in Iranian patients with pulmonary tuberculosis: A case-control study. Infect Genet Evol. 2016;39:92-8. Epub 2016/01/18. doi: 10.1016/j.meegid.2016.01.013. PubMed PMID: 26774366.

14. Tjarnlund A, Guirado E, Julian E, Cardona PJ, Fernandez C. Determinant role for Toll-like receptor signalling in acute mycobacterial infection in the respiratory tract. Microbes Infect. 2006;8(7):1790-800. Epub 2006/07/04. doi: 10.1016/j.micinf.2006.02.017. PubMed PMID: 16815067.

15. Drennan MB, Nicolle D, Quesniaux VJ, Jacobs M, Allie N, Mpagi J, et al. Toll-like receptor 2-deficient mice succumb to Mycobacterium tuberculosis infection. Am J Pathol. 2004;164(1):49-57. Epub 2003/12/26. doi: 10.1016/S0002-9440(10)63095-7. PubMed PMID: 14695318; PubMed Central PMCID: PMCPMC1602241.

16. McBride A, Konowich J, Salgame P. Host defense and recruitment of Foxp3(+) T regulatory cells to the lungs in chronic Mycobacterium tuberculosis infection requires toll-like receptor 2. PLoS Pathog. 2013;9(6):e1003397. Epub 2013/06/21. doi: 10.1371/journal.ppat.1003397. PubMed PMID: 23785280; PubMed Central PMCID: PMCPMC3681744.

17. Lachmandas E, Beigier-Bompadre M, Cheng SC, Kumar V, van Laarhoven A, Wang X, et al. Rewiring cellular metabolism via the AKT/mTOR pathway contributes to host defence against Mycobacterium tuberculosis in human and murine cells. Eur J Immunol. 2016;46(11):2574-86. Epub 2016/11/05. doi: 10.1002/eji.201546259. PubMed PMID: 27624090; PubMed Central PMCID: PMCPMC5129526.

18. Koch BEV, Yang SX, Lamers G, Stougaard J, Spaink HP. Intestinal microbiome adjusts the innate immune setpoint during colonization through negative regulation of MyD88 (vol 9, 4099, 2018). Nat Commun. 2019;10. doi: ARTN 526

10.1038/s41467-019-08456-y. PubMed PMID: WOS:000456829800002.

19. Konowich J, Gopalakrishnan A, Dietzold J, Verma S, Bhatt K, Rafi W, et al. Divergent Functions of TLR2 on Hematopoietic and Nonhematopoietic Cells during Chronic Mycobacterium tuberculosis Infection. J Immunol. 2017;198(2):741-8. Epub 2016/12/07. doi: 10.4049/jimmunol.1601651. PubMed PMID: 27920273; PubMed Central PMCID: PMCPMC5224966.

20. Liu PT, Krutzik SR, Modlin RL. Therapeutic implications of the TLR and VDR partnership. Trends Mol Med. 2007;13(3):117-24. Epub 2007/02/06. doi: 10.1016/j.molmed.2007.01.006. PubMed PMID: 17276732.

21. Rougeot J, Torraca V, Zakrzewska A, Kanwal Z, Jansen HJ, Sommer F, et al. RNAseq Profiling of Leukocyte Populations in Zebrafish Larvae Reveals a cxcl11 Chemokine Gene as a Marker of Macrophage Polarization During Mycobacterial Infection (vol 10, 832, 2019). Front Immunol. 2019;10. doi: ARTN 2720

10.3389/fimmu.2019.02720. PubMed PMID: WOS:000503244800001.

22. Renshaw SA, Loynes CA, Trushell DM, Elworthy S, Ingham PW, Whyte MK. A transgenic zebrafish model of neutrophilic inflammation. Blood. 2006;108(13):3976-8. Epub 2006/08/24. doi: 10.1182/blood-2006-05-024075. PubMed PMID: 16926288.

23. Xie Y, Meijer AH, Schaaf MJM. Modeling Inflammation in Zebrafish for the Development of Anti-inflammatory Drugs. Front Cell Dev Biol. 2020;8:620984. Epub 2021/02/02. doi: 10.3389/fcell.2020.620984. PubMed PMID: 33520995; PubMed Central PMCID: PMCPMC7843790.

24. Moles A, Murphy L, Wilson CL, Chakraborty JB, Fox C, Park EJ, et al. A TLR2/S100A9/CXCL-2 signaling network is necessary for neutrophil recruitment in acute and chronic liver injury in the mouse. J Hepatol. 2014;60(4):782-91. doi: 10.1016/j.jhep.2013.12.005. PubMed PMID: WOS:000333106600015.

25. Xu YF, Zhou Y, Lin HY, Hu HY, Wang YX, Xu G. Toll-like receptor 2 in promoting angiogenesis after acute ischemic injury. Int J Mol Med. 2013;31(3):555-60. doi: 10.3892/ijmm.2013.1240. PubMed PMID: WOS:000314905500008.

26. Soehnlein O, Lindbom L. Phagocyte partnership during the onset and resolution of inflammation. Nat Rev Immunol. 2010;10(6):427-39. Epub 2010/05/26. doi: 10.1038/nri2779. PubMed PMID: 20498669.

27. Bianchi ME. HMGB1 loves company. J Leukoc Biol. 2009;86(3):573-6. Epub 2009/05/06. doi: 10.1189/jlb.1008585. PubMed PMID: 19414536.

28. Niethammer P, Grabher C, Look AT, Mitchison TJ. A tissue-scale gradient of hydrogen peroxide mediates rapid wound detection in zebrafish. Nature. 2009;459(7249):996-9. Epub 2009/06/06. doi: 10.1038/nature08119. PubMed PMID: 19494811; PubMed Central PMCID: PMCPMC2803098.

29. Katikaneni A, Jelcic M, Gerlach GF, Ma Y, Overholtzer M, Niethammer P. Lipid peroxidation regulates long-range wound detection through 5-lipoxygenase in zebrafish. Nat Cell Biol. 2020;22(9):1049-55. Epub 2020/09/02. doi: 10.1038/s41556-020-0564-2. PubMed PMID: 32868902; PubMed Central PMCID: PMCPMC7898270.

30. Mittal M, Siddiqui MR, Tran K, Reddy SP, Malik AB. Reactive oxygen species in inflammation and tissue injury. Antioxid Redox Signal. 2014;20(7):1126-67. Epub 2013/09/03. doi: 10.1089/ars.2012.5149. PubMed PMID: 23991888; PubMed Central PMCID: PMCPMC3929010.

31. Hoefsloot W, van Ingen J, Andrejak C, Angeby K, Bauriaud R, Bemer P, et al. The geographic diversity of nontuberculous mycobacteria isolated from pulmonary samples: an NTM-NET collaborative study. Eur Respir J. 2013;42(6):1604-13. Epub 2013/04/20. doi: 10.1183/09031936.00149212. PubMed PMID: 23598956.

32. Prevots DR, Marras TK. Epidemiology of human pulmonary infection with nontuberculous mycobacteria: a review. Clin Chest Med. 2015;36(1):13-34. Epub 2015/02/14. doi: 10.1016/j.ccm.2014.10.002. PubMed PMID: 25676516; PubMed Central PMCID: PMCPMC4332564.

33. Saxena S, Spaink HP, Forn-Cuni G. Drug Resistance in Nontuberculous Mycobacteria: Mechanisms and Models. Biology (Basel). 2021;10(2). Epub 2021/02/13. doi: 10.3390/biology10020096. PubMed PMID: 33573039; PubMed Central PMCID: PMCPMC7911849.

34. Ryffel B, Jacobs M, Parida S, Botha T, Togbe D, Quesniaux V. Toll-like receptors and control of mycobacterial infection in mice. Novartis Found Symp. 2006;279:127-39; discussion 39-41, 216-9. Epub 2007/02/07. PubMed PMID: 17278391.

35. Heldwein KA, Fenton MJ. The role of Toll-like receptors in immunity against mycobacterial infection. Microbes Infect. 2002;4(9):937-44. Epub 2002/07/11. doi: 10.1016/s1286-4579(02)01611-8. PubMed PMID: 12106786.

36. Vu A, Calzadilla A, Gidfar S, Calderon-Candelario R, Mirsaeidi M. Toll-like receptors in mycobacterial infection. Eur J Pharmacol. 2017;808:1-7. Epub 2016/10/30. doi: 10.1016/j.ejphar.2016.10.018. PubMed PMID: 27756604.

37. Pagan AJ, Yang CT, Cameron J, Swaim LE, Ellett F, Lieschke GJ, et al. Myeloid Growth Factors Promote Resistance to Mycobacterial Infection by Curtailing Granuloma Necrosis through Macrophage Replenishment. Cell Host Microbe. 2015;18(1):15-26. Epub 2015/07/15. doi: 10.1016/j.chom.2015.06.008. PubMed PMID: 26159717; PubMed Central PMCID: PMCPMC4509513.

38. Tobin DM, Vary JC, Jr., Ray JP, Walsh GS, Dunstan SJ, Bang ND, et al. The lta4h locus modulates susceptibility to mycobacterial infection in zebrafish and humans. Cell. 2010;140(5):717-30. Epub 2010/03/10. doi: 10.1016/j.cell.2010.02.013. PubMed PMID: 20211140; PubMed Central PMCID: PMCPMC2907082.

39. Grosset J. Mycobacterium tuberculosis in the extracellular compartment: an underestimated adversary. Antimicrob Agents Chemother. 2003;47(3):833-6. Epub 2003/02/27. doi: 10.1128/AAC.47.3.833-836.2003. PubMed PMID: 12604509; PubMed Central PMCID: PMCPMC149338.

40. Bernut A, Herrmann JL, Kissa K, Dubremetz JF, Gaillard JL, Lutfalla G, et al. Mycobacterium abscessus cording prevents phagocytosis and promotes abscess formation. Proc Natl Acad Sci U S A. 2014;111(10):E943-52. Epub 2014/02/26. doi: 10.1073/pnas.1321390111. PubMed PMID: 24567393; PubMed Central PMCID: PMCPMC3956181.

41. Johansen MD, Kremer L. CFTR Depletion Confers Hypersusceptibility to Mycobacterium fortuitum in a Zebrafish Model. Front Cell Infect Microbiol. 2020;10:357. Epub 2020/08/28. doi: 10.3389/fcimb.2020.00357. PubMed PMID: 32850470; PubMed Central PMCID: PMCPMC7396536.

42. Olson G, McNulty MC, Mullane K, Beavis KG, Tesic V. Cording in Disseminated Mycobacterium chelonae Infection in an Immunocompromised Patient. Lab Med. 2021;52(3):e50-e2. Epub 2020/09/22. doi: 10.1093/labmed/lmaa082. PubMed PMID: 32954440.

43. Cowley S. The biology of HIV infection. Lepr Rev. 2001;72(2):212-20. Epub 2001/08/10. doi: 10.5935/0305-7518.20010028. PubMed PMID: 11495453.

44. Katkoori VR, Basson MD, Bond VC, Manne U, Bumpers HL. Nef-M1, a peptide antagonist of CXCR4, inhibits tumor angiogenesis and epithelialtomesenchymal transition in colon and breast cancers. Oncotarget. 2015;6(29):27763-77. Epub 2015/09/01. doi: 10.18632/oncotarget.4615. PubMed PMID: 26318034; PubMed Central PMCID: PMCPMC4695024.

45. Torraca V, Tulotta C, Snaar-Jagalska BE, Meijer AH. The chemokine receptor CXCR4 promotes granuloma formation by sustaining a mycobacteria-induced angiogenesis programme. Sci Rep. 2017;7:45061. Epub 2017/03/24. doi: 10.1038/srep45061. PubMed PMID: 28332618; PubMed Central PMCID: PMCPMC5362882.

46. Link DC. Neutrophil homeostasis: a new role for stromal cell-derived factor-1. Immunol Res. 2005;32(1-3):169-78. Epub 2005/08/18. doi: 10.1385/IR:32:1-3:169. PubMed PMID: 16106067.

47. Torraca V, Cui C, Boland R, Bebelman JP, van der Sar AM, Smit MJ, et al. The CXCR3-CXCL11 signaling axis mediates macrophage recruitment and dissemination of mycobacterial infection. Dis Model Mech. 2015;8(3):253-69. Epub 2015/01/13. doi: 10.1242/dmm.017756. PubMed PMID: 25573892; PubMed Central PMCID: PMCPMC4348563.

48. Hosseini R, Lamers GE, Soltani HM, Meijer AH, Spaink HP, Schaaf MJ. Efferocytosis and extrusion of leukocytes determine the progression of early mycobacterial pathogenesis. J Cell Sci. 2016;129(18):3385-95. Epub 2016/07/30. doi: 10.1242/jcs.135194. PubMed PMID: 27469488.

49. Clay H, Davis JM, Beery D, Huttenlocher A, Lyons SE, Ramakrishnan L. Dichotomous role of the macrophage in early Mycobacterium marinum infection of the zebrafish. Cell Host Microbe. 2007;2(1):29-39. Epub 2007/11/17. doi: 10.1016/j.chom.2007.06.004. PubMed PMID: 18005715; PubMed Central PMCID: PMCPMC3115716.

50. Yang CT, Cambier CJ, Davis JM, Hall CJ, Crosier PS, Ramakrishnan L. Neutrophils exert protection in the early tuberculous granuloma by oxidative killing of mycobacteria phagocytosed from infected macrophages. Cell Host Microbe. 2012;12(3):301-12. Epub 2012/09/18. doi: 10.1016/j.chom.2012.07.009. PubMed PMID: 22980327; PubMed Central PMCID: PMCPMC3638950.

51. Bernut A, Nguyen-Chi M, Halloum I, Herrmann JL, Lutfalla G, Kremer L. Mycobacterium abscessus-Induced Granuloma Formation Is Strictly Dependent on TNF Signaling and Neutrophil Trafficking. PLoS Pathog. 2016;12(11):e1005986. Epub 2016/11/03. doi: 10.1371/journal.ppat.1005986. PubMed PMID: 27806130; PubMed Central PMCID: PMCPMC5091842.

52. Hosseini R, Lamers GE, Hodzic Z, Meijer AH, Schaaf MJ, Spaink HP. Correlative light and electron microscopy imaging of autophagy in a zebrafish infection model. Autophagy. 2014;10(10):1844-57. Epub 2014/08/16. doi: 10.4161/auto.29992. PubMed PMID: 25126731; PubMed Central PMCID: PMCPMC4198367.

53. Paul CD, Bishop K, Devine A, Paine EL, Staunton JR, Thomas SM, et al. Tissue Architectural Cues Drive Organ Targeting of Tumor Cells in Zebrafish. Cell Syst. 2019;9(2):187-206 e16. Epub 2019/08/26. doi: 10.1016/j.cels.2019.07.005. PubMed PMID: 31445892; PubMed Central PMCID: PMCPMC8276582.

54. Meijering E, Dzyubachyk O, Smal I. Methods for cell and particle tracking. Methods Enzymol. 2012;504:183-200. Epub 2012/01/24. doi: 10.1016/B978-0-12-391857-4.00009-4. PubMed PMID: 22264535.

55. Masuzzo P, Van Troys M, Ampe C, Martens L. Taking Aim at Moving Targets in Computational Cell Migration. Trends Cell Biol. 2016;26(2):88-110. Epub 2015/10/21. doi: 10.1016/j.tcb.2015.09.003. PubMed PMID: 26481052.

56. Grau V, Mewes AU, Alcaniz M, Kikinis R, Warfield SK. Improved watershed transform for medical image segmentation using prior information. IEEE Trans Med Imaging. 2004;23(4):447-58. Epub 2004/04/16. doi: 10.1109/TMI.2004.824224. PubMed PMID: 15084070.

57. Dona E, Barry JD, Valentin G, Quirin C, Khmelinskii A, Kunze A, et al. Directional tissue migration through a self-generated chemokine gradient. Nature. 2013;503(7475):285-+. doi: 10.1038/nature12635. PubMed PMID: WOS:000326894200056.

58. Tweedy L, Knecht DA, Mackay GM, Insall RH. Self-Generated Chemoattractant Gradients: Attractant Depletion Extends the Range and Robustness of Chemotaxis. PLoS Biol. 2016;14(3):e1002404. Epub 2016/03/18. doi: 10.1371/journal.pbio.1002404. PubMed PMID: 26981861; PubMed Central PMCID: PMCPMC4794234.

59. Manolopoulou I, Matheu MP, Cahalan MD, West M, Kepler TB. Bayesian Spatio-Dynamic Modeling in Cell Motility Studies: Learning Nonlinear Taxic Fields Guiding the Immune Response. J Am Stat Assoc. 2012;107(499):855-65. doi: 10.1080/01621459.2012.655995. PubMed PMID: WOS:000309793400001.

Samenvatting

1. Zebravis als model om infectie- en ontstekingsziekten te bestuderen

De activering van het aangeboren immuunsysteem hangt af van de herkenning van pathogeen-geassocieerde moleculaire patronen (PAMP's) van de binnendringende pathogenen door patroonherkenningsreceptoren (PRR's). PRR's zijn tevens betrokken bij de herkenning van schade-geassocieerde moleculaire patronen (DAMP's) van beschadigde weefsels bij infectie. De familie van Toll-like receptoren (TLR's) is een van de belangrijkste leden binnen de PRR-families. De ontdekking van TLR's als poortwachters om de aangeboren immuniteit te activeren heeft in 2011 de Nobelprijs voor Fysiologie of Geneeskunde toegekend gekregen. Dit heeft een explosie aan onderzoek naar de functies van TLR's bij het moduleren van een breed spectrum van fysiologische en pathologische processen veroorzaakt. TLR2 is geconserveerd binnen de meeste gewervelde dieren en speelt een belangrijke rol bij het moduleren van infectie- en ontstekingsziekten doordat het een groot aantal PAMP's en DAMP's herkent (Hoofdstuk 1). De brede functie van TLR2 maakt het een veelbelovend therapeutisch doelwit (Hoofdstuk 1). De functie van TLR2 is echter nog steeds controversieel in sommige studies en de rol ervan bij verschillende ziekten is nog steeds onduidelijk. Het is daarom van vitaal belang om verder te onderzoeken hoe TLR2-signalering functioneert in de aangeboren immuunrespons van de gastheer.

Met dit doel hebben we in dit proefschrift gebruik gemaakt van het zebravismodel om de functie van Tlr2 bij ontsteking en infectie te bestuderen. Zebravislarven hebben al binnen 5 dagen na de bevruchting een functioneel aangeboren immuunsysteem, terwijl op dat moment het adaptieve immuunsysteem nog niet functioneel is. Dit maakt de zebravis een uitstekend model om de aangeboren immuniteit van gewervelde dieren te bestuderen in de afwezigheid van adaptieve immuniteit. Bovendien wordt het zebravismodel alsmaar populairder in studies vanwege het gemak van genetische manipulatie, omics-studies van grote groepen larven en live-imaging. De afgelopen tien jaar is er met behulp van het zebravismodel aanzienlijke vooruitgang geboekt bij het bestuderen van infectie- en ontstekingsziekten . Van der Vaart *et al.* ontdekten dat zebravis embryo's met een tekort aan myeloïde differentiatiefactor 88 (Myd88), een cruciale adapter voor alle TLR's behalve TLR3, vatbaarder zijn voor bacteriële infectie met pathogenen. Deze bevinding is vergelijkbaar met de conclusies uit studies van MYD88-deficiënte mutanten in menselijke celculturen *in vitro* en *in vivo*-muismodellen. Daarnaast

rapporteerden Hosseini *et al.* dat Myd88 betrokken is bij het beperken van mycobacteriële groei in een zebravismodel met staartvininfectie. Yang *et al.* toonden aan dat de functie van Tlr2-signalering vergelijkbaar is tussen zebravis embryo's en zoogdiercellen. In beide systemen reguleert TLR2 de expressie van een vergelijkbare set immuun genen na de systemische stimulatie door het synthetische lipopeptide-ligand Pam3CSK4. Deze studies hebben de weg vrijgemaakt om de functie van Tlr2 in het zebravismodel verder te onderzoeken. In Hoofdstuk 2 hebben we de functie van *tlr2* in de afweer van zebravissen tegen *Mycobacterium marinum*-infectie bestudeerd door de fenotypes bij infectie en de corresponderende transcriptoom veranderingen te meten. In Hoofdstuk 3 hebben we onderzocht hoe Tlr2 en Myd88 het migratiegedrag van leukocyten reguleren in afwezigheid van een infectie, maar met weefselbeschadiging, door gebruik te maken van een zebravisstaartwondmodel. In Hoofdstuk 4 hebben we de functie van tlr2 bij infectie met *Mycobacterium avium* bestudeerd door het te vergelijken met *M. marinum* infectie, met speciale aandacht voor het responsieve celmigratie gedrag.

2. Tlr2 speelt een rol bij de afweer tegen mycobacteriële infectie bij zebravislarven

In verschillende studies is gemeld dat TLR2-polymorfismen de gevoeligheid voor mycobacteriële infectie in de menselijke populatie verhogen, al is er een klein aantal studies die geen effect van TLR2-polymorfismen hebben gevonden (Hoofdstuk 1). Daarnaast is er nog steeds controverse over de rol van TLR2 in de afweer van de gastheer tegen *Mycobacterium tuberculosis* in verschillende knaagdierstudies (Hoofdstuk 1). In hoofdstuk 2 hebben we daarom een *tlr2* zebravismutant gecreëerd om de functie van Tlr2 in de aangeboren immuunafweer tijdens mycobacteriële infectie te bestuderen. Om het effect van *tlr2*-mutatie te karakteriseren, vergeleken we eerst het transcriptoom van homozygoot mutante larven met dat van heterozygote larven zonder infectie. We vonden verschillen in de genexpressieprofielen van *tlr2*$^{-/-}$ zebravislarven en controle –larven van dezelfde ouders, zoals verschillend tot expressie gebrachte genen die betrokken zijn bij glycolyse (Hoofdstuk 2, Figuur 2 en S3). Dit resultaat komt overeen met een eerdere studie in het menselijke in vitro model en *in vivo* muismodel die aantoonden dat TLR2 een sleutelrol speelt bij het omschakelen van het cellulaire metabolisme van de gastheer naar aerobe glycolyse na *M. tuberculosis*-infectie. Een eerdere zebravisstudie in ons laboratorium suggereerde hiermee in overeenstemming dat ook MyD88 een rol speelt in het metabolisme. Bovendien toonde deze studie aan dat Tlr2 en zijn adapter MyD88 cruciaal zijn voor de reactie van de gastheer op het microbioom. Dit geeft aan dat de

verschillende genexpressieprofielen die we in de tlr2-mutant vonden, worden veroorzaakt door een disfunctionele reactie op het microbioom.

Om de rol van Tlr2 in de afweer tegen *M. marinum*-infectie bij zebravissen te bestuderen, injecteerden we deze bacteriën in mutanten zonder functioneel *tlr2* en homo- en heterozygote blarven van dezelfde ouders. We ontdekten dat de bacteriële belasting significant hoger was in *tlr2*-mutanten en vergezeld ging met een hogere extracellulaire bacteriële belasting en minder granulomen dan in *tlr2*$^{+/-}$ en wildtype larven op 4 dpi (Hoofdstuk 2, Figuur 3 en 4). Dit resultaat is vergelijkbaar met eerdere studies bij muizen die een functie van Tlr2 in de verdediging van de zebravisgastheer laten zien. Bovendien toonde onze transcriptoom analyse aan dat het aantal opwaartse en neerwaartse gereguleerde genen als reactie op infectie sterk verminderd was in geïnfecteerde *tlr2* mutante zebravissen in vergelijking met de heterozygote controlevissen van dezelfde ouders (Hoofdstuk 2, Figuur 5-7). Bovendien vonden we dat veel signaalroutes waarvan is aangetoond dat ze verband houden met tuberculose bij mensen, differentieel worden gereguleerd in *tlr2*-mutante zebravislarven. We ontdekten bijvoorbeeld dat de Tlr8-signaleringsroute sterk werd beïnvloed, wat aangeeft dat Tlr2-signalering verband houdt met de functie van Tlr8 (hoofdstuk 2, figuur S10). Bovendien werden de genen van de vitamine D-receptorroute neerwaarts gereguleerd in *tlr2*-mutante zebravissen. Het is aangetoond dat vitamine D een belangrijke rol speelt bij de bestrijding van tuberculose-infectie. Daarom kan de hypergevoeligheid van *tlr2*-mutanten voor *M. marinum*-infectie worden veroorzaakt door afwijkende vitamine D-signalering. Chemokines vormen de andere gencategorie die werd beïnvloed door de *tlr2*-mutatie bij *M. marinum*-infectie. In eerder werk toonden Torraca *et al*. aan dat de Cxcr3-Cxcl11-as betrokken was bij de rekrutering van macrofagen na infectie met *M. marinum* in zebravislarven [21]. In overeenstemming hiermee vonden we dat de expressieniveaus van *cxcl11aa* en *cxcl11ac* significant lager waren in de *tlr2*-mutant na infectie (Hoofdstuk 2, Figuur 5). Dit resultaat toont een duidelijk verband tussen de Tlr2-functie en chemotaxis van macrofagen.

3. Nieuwe inzichten in Tlr2-functies bij het reguleren van leukocytmigratie door live-imaging

Gezien het grote aantal chemokinen dat aangestuurd wordt door Tlr2 (Hoofdstuk 2), veronderstelden we dat Tlr2 een sleutelfactor is in de controle van chemokine-expressie om celrekrutering in aangeboren immuniteit te reguleren. Om deze hypothese te testen, hebben we in Hoofdstuk 3 eerst de rol van Tlr2 en Myd88 onderzocht bij het moduleren van het

migratiegedrag van leukocyten in afwezigheid van mycobacteriële infectie. Hiervoor gebruikten we een zebravisstaartverwondingsmodel dat veel wordt gebruikt voor het screenen van ontstekingsremmende geneesmiddelen. We ontdekten dat het aantal gerekruteerde neutrofielen en macrofagen afnam in *tlr2*$^{-/-}$ en *myd88*$^{-/-}$ groepen in vergelijking met de wildtype individuen van dezelfde ouders (Hoofdstuk 3, Figuur 2 en 3). Vervolgens werd live-cel-imaging van het staartwondgebied in zebravissen uitgevoerd in *tlr2*- en *myd88*-mutanten en de overeenkomstige wildtype vissen van dezelfde ouders. Leukocytmigratie in de *tlr2* en *myd88* mutanten na verwonding werd geanalyseerd met behulp van kwantitatieve analyses van celmigratie sporen (Hoofdstuk 3, Figuur 4 en Tabel 1). Onze resultaten laten zien dat de *tlr2* en de *myd88* mutaties de migratie van neutrofielen die zich ver van een wond bevinden beïnvloeden door hun directionele persistentie negatief te beïnvloeden, maar niet hun migratiesnelheid (Hoofdstuk 3, Figuur 5 en 6). Van macrofagen ver van de wond was niet alleen de directionele persistentie was significant verminderd in de *tlr2* en de *myd88* mutanten, maar ook hun migratiesnelheid (Hoofdstuk 3, Figuur 7 en 8). Deze studie toont voor het eerst aan dat TLR-signalering direct betrokken is bij het sturen van het celmigratie gedrag van neutrofielen en macrofagen tbij verwonding, Dit stimuleert verdere studies stimuleert, waaronder ook in andere modelsystemen.

Eerder is in infectiemodellen van muizen aangetoond dat TLR-signalering betrokken is bij het aansturen van infiltratie van neutrofielen en macrofagen in beschadigde weefsels. Bovendien is aangetoond dat Tlr2 de expressie van cytokinen en chemokinen reguleert na de herkenning van zijn liganden in zowel zebravis- als muizenmodellen (Hoofdstuk 2). Daarom kan het afwijkende migratiegedrag van leukocyten, dat werd waargenomen in *tlr2* en *myd88* mutante zebravissen, worden veroorzaakt door het onvoldoende niveau van basale transcripten voor chemokinen. Voor de staartverwonding kan het ook zijn dat DAMP's die worden afgegeven door dode cellen rond de wond niet leiden tot de afscheiding van chemokinen in afwezigheid van TLR2-signalering. High-mobility group box 1-eiwit (HMGB1) is bijvoorbeeld een veel bestudeerd endogeen gevaarsignaal dat een ontstekingsreactie induceert door zijn directe interactie met DAMP's die worden herkend door TLR2. Bovendien is beschreven dat reactieve zuurstofsoorten (ROS) betrokken zijn bij de rekrutering van leukocyten na verwonding in zebravislarven. Tevens is aangetoond dat de secretie van ROS wordt gemedieerd door TLR's na weefselbeschadiging. Het is dus interessant om verder te onderzoeken of ROS-productie in reactie op verwonding is veranderd in zebravislarven met mutaties in de *tlr2* en *myd88* genen.

4. Verschillen tussen tbc en NTM-infecties geleerd uit zebravisstudies

Niet-tuberculeuze mycobacteriën (NTM) infectieziekten worden gedefinieerd als ziekten veroorzaakt door andere mycobacteriële pathogenen dan *M. tuberculosis* en *Mycobacterium leprae*. Naast TBC hebben NTM-infectieziekten de laatste tijd veel aandacht gekregen omdat de prevalentie ervan sinds 2000 sterk is toegenomen. Hoewel er behandelingen zijn voor NTM-infectieziekten, is de behandelingsduur lang en komen multiresistente gevallen frequent voor. Het is dus dringend nodig om nieuwe preventie- en therapeutische strategieën te ontdekken voor patiënten besmet met NTM. In Hoofdstuk 4 hebben we zebravislarven gebruikt om een infectiemodel van *M. avium* te ontwikkelenen vervolgens *M. avium*-infectie in larven gekarakteriseerd door het te vergelijken met *M. marinum*-infectie, een populair model van tuberculose-infectie. Eerder is gemeld dat de aangeboren afweer tegen NTM-infectie voornamelijk gemedieerd wordt door de TLR-signaleringsroute. Daarom hebben we eerst de transcriptoom profielen van de gastheer in reactie op infectie vergeleken, specifiek met betrekking tot TLR-signalering. Vervolgens hebben we de functie van toll-like receptorsignalering na infectie met *M. marinum* en *M. avium* onderzocht om de functie van Tlr2 bij infectie met deze twee verschillende bacteriën te vergelijken.

We vonden dat *M. marinum* infectie virulenter is dan *M. avium* infectie in zebravislarven (Hoofdstuk 4, Figuur 1). Bovendien vonden we dat *M. avium* stand houdt in de macrofagen met minder extracellulaire koorden vergeleken met *M. marinum* (Hoofdstuk 4, Figuur 2). Extracellulaire koordvorming is een *in vivo* morfologie van mycobacteriën vergezeld van necrotische macrofagen en extracellulair replicerende bacteriën die fagocytose voorkomen vanwege de grootte van de clusters. Bacteriële koordvorming is een pathogeen kenmerk dat geassocieerd is met hypervirulentie bij *M. tuberculosis*, *M. marinum*, *M. abscessus*, *M. fortuitum* en *M. chelonae*. De observatie dat met *M. marinum* geïnfecteerde larven meer extracellulaire koorden vertonen, kan dus een kenmerk zijn van de hogere letaliteit en bacteriegroei als gevolg van *M. marinum*-infectie. Om de lagere virulentie van de *M. avium*-infectie te verklaren en om genetische markers te verkrijgen voor verdere studies, voerden we RNAseq-deep sequencing uit om het hele transcriptoom profiel in het *M. avium*-infectiemodel te bestuderen en het op een systemisch niveau te vergelijken met dat van het *M. marinum*-infectiemodel .

We vonden dat *M. avium* een duidelijke transcriptoom respons heeft in vergelijking met *M. marinum*, vooral met betrekking tot de regulatie van de volgende gencategorieën:

autofagieregulatoren, matrixremodellering en cytokinen en chemokinen (Hoofdstuk 4, Figuur 3 en 4). In de categorie van cytokinen, chemokinen en hun receptoren werden meer genen gedownreguleerd specifiek in de *M. avium*-infectiegroep, zoals *il1rga*, *ccr9b*, *cxcr4b*, *ccr6b*, *cxcl11.7*, *ccl36.1*, *cxcl12.b* en *ccl33.3* (Hoofdstuk 4, Figuur 4). Opgemerkt moet worden dat de *Cxcr4b / Cxcl12*-signalering, die gerelateerd is aan HIV-pathogenese, tumor-geïnduceerde angiogenese en door mycobacteriën geïnduceerde angiogenese, werd gedownreguleerd in de *M. avium*-infectiegroep. Verder is aangetoond dat CXCR4/CXCL12-signalering de leukocytentransport naar ontstekingsplaatsen ondersteunt, evenals CXCL11-signalering, die de rekrutering van macrofagen bij mycobacteriële infectie bemiddelt. Daarom veronderstellen we dat het migratiegedrag van macrofagen en neutrofielen anders kan zijn in zebravislarven na infectie met verschillende NTM-soorten.

Er is aangetoond dat leukocytmigratie belangrijk is voor het opruimen van bacteriën, het inperken alsook verspreiden van bacteriën, en het vormen van granulomen in de vroege mycobacteriële infectieuze stadia. In voorgaande hoofdstukken hebben we aangetoond dat Tlr2 een belangrijke rol speelt in de afweer tegen *M. marinum* infectie (Hoofdstuk 2). Verder vonden we dat Tlr2 betrokken is bij het reguleren van het gedrag van macrofagen en neutrofielen na beschadiging van de staart (Hoofdstuk 3). Tlr2 zou dus ook kunnen deelnemen aan de regulatie van het migratiegedrag van macrofagen en neutrofielen naar de plekvan mycobacteriële infectie. Om de rol van Tlr2 in de regulatie van de migratie van macrofagen en neutrofielen te beoordelen, hebben we een staartvininfectiemodel toegepast in Hoofdstuk 4, dat eerder is beschreven. Hierbij werden bacteriën van ofwel de *M. marinum*-stam Mma20 ofwel de *M. avium*-stam MAC 101 geïnjecteerd 3 dagen na de bevruchting (dpf) in larven met *tlr2*$^{+/+}$ *Tg (mpeg1:mCherry-F); TgBAC (mpx: EGFP)* en *tlr2*$^{-/-}$ *Tg (mpeg1:mCherry -F);TgBAC (mpx: EGFP)* genotype (Hoofdstuk 4, Figuur 7). We concluderen dat macrofagen een belangrijke rol spelen in de respons op beide mycobacteriële infecties omdat er meer gerekruteerde macrofagen werden waargenomen in het geïnfecteerde gebied (Hoofdstuk 4, Figuur 8). De migratiesnelheid van macrofagen is hoger naar Mma20-infectieplaatsen (Hoofdstuk 4, Figuur 8). We vonden dat neutrofielen sneller bewogen in *tlr2* wildtype larven dan in *tlr2* mutanten na Mma20 injectie, terwijl *tlr2* deficiëntie geen invloed had op de migratie van neutrofielen na MAC101 injectie (Hoofdstuk 4, Figuur 8). Dit veranderde leukocytengedrag suggereert dat chemokine-expressieprofielen anders kunnen zijn in *tlr2*-mutante zebravissen na infectie door mycobacteriële soorten.

5. Perspectieven voor toekomstige studies

5.1 Het onderzoek naar interacties tussen gastheer en mycobacteriën met behulp van zebravislarven

In Hoofdstuk 4 hebben we eerst een *M. avium* infectiemodel ontwikkeld in zebravissen dat het mogelijk maakt om de gastheer en *M. avium* interacties *in vivo* direct te observeren. Met dit model hebben we verschillende fenotypes van granuloma-achtige clusters waargenomen in zebravislarven geïnfecteerd met verschillende mycobacteriën (Hoofdstuk 4, Figuur 2). Verder toonde de transcriptoom analyse aan dat de expressie van de genen die behoren tot de categorie van autofagieregulator genen significant werd beïnvloed in met *M. avium* geïnfecteerde zebravislarven (Hoofdstuk 4, Figuur 4). Daarom is het interessant om de autofagie respons en ultrastructuur van granulomen als gevolg van infectie door verschillende soorten mycobacteriële clusters te vergelijken. Voor dit doel zullen we in de nabije toekomst transmissie-elektronenmicroscopie (TEM) en 3D block-face scanning elektronenmicroscopie toepassen (blok-face SEM).

Daarnaast vonden we in Hoofdstuk 4 dat Tlr2 betrokken is bij de regulatie van de migratie van macrofagen en neutrofielen als reactie op infectie. Interessant is dat de resultaten van celtracking suggereren dat *tlr2* de macrofagen en neutrofielen op verschillende manieren reguleert na infectie door verschillende mycobacteriële soorten. Om verklaringen te verkrijgen voor verdere studies van het effect van de *tlr2*-mutatie op mycobacteriële infectie, zullen we in de toekomst onderzoeken of verschillen in expressieprofielen van chemokinen kunnen worden waargenomen in het vroege infectiestadium. We zouden ook willen onderzoeken of de veranderingen in het migratiegedrag van leukocyten in Tlr2-mutanten te wijten zijn aan veranderingen in signalen afkomstig van de infectieplaats of dat ze worden veroorzaakt door celautonome defecten in het migrerend vermogen van de myeloïde cellen in de *tlr2*-mutant. We zullen daarom celtransplantatie technieken toepassen om de niet-intrinsieke en intrinsieke functies van myeloïde cellen in de tlr2-mutant na verwonding en mycobacteriële infectie te onderzoeken.

5.2 Geautomatiseerde verwerking van live-beeldvorming van zebravissen en wiskundige modellering

In Hoofdstuk 3 en Hoofdstuk 4 hebben we een groot aantal celtracking experimenten uitgevoerd om celmigratie gedrag te kwantificeren. Celmigratie is een belangrijke fysiologische parameter

voor veel pathologische processen, waaronder ontstekingsreacties, immuunafweer en metastase van kwaadaardige tumorcellen. Tracking van individuele cellen met behulp van confocale real time beeldvorming is een van de meest populaire methoden om celmigratie te analyseren. Met de ontwikkeling van confocale laser scanning microscopie is het gemakkelijker om enorme hoeveelheden live beeldgegevens te verkrijgen. Er zijn echter veel bioinformatische stappen vereist die moeten worden uitgevoerd na de verwerving van beeldvorming. Deze omvatten de verwerking van grote datasets, het segmenteren van celmigratie trajecten, visualisatie en kwantificatie van de trajecten, en belangrijker nog, de interpretatie van de biologische betekenis van de grote datasets. Momenteel is handmatige gegevensanalyse nog steeds vereist om geautomatiseerde gegevensanalyse te ondersteunen. Bovendien blijft de beschikbaarheid van gebruiksvriendelijke softwareprogramma's nog steeds achter bij de eisen van onderzoekers in het laboratorium.

Sommige recente beoordelingen hebben de beschikbare commerciële en gratis software of plug-ins voor live-beeldverwerking in celmigratie studies in detail samengevat. De TrackMate-plug-in voor ImageJ-software (NIH, Bethesda, MD, VS), Volocity (Improvision; PerkinElmer Life and Analytical Sciences) en IMARIS (Bitplane) worden veel gebruikt in zebravisstudies. Toch kiezen nog steeds een vrij groot aantal onderzoekers voor handmatige trackingmethoden voor in vivo celtracking van de zebravis, zoals de ManualTrack-plug-in of de MTrackJ-plug-in voor ImageJ-software. Dit komt omdat de meeste software is ontworpen voor het volgen van beweging van grote deeltjes of in vitro celmigratie. De vorm van cellen in vivo is echter onregelmatig, wat de segmentatie van de trajecten bemoeilijkt en vaak resulteert in over segmentatie. Het niet correct segmenteren van de trajecten van cellen is de belangrijkste reden voor fouten in de tracking. Voorbeelden van fouten zijn dat de trajectuitvoer van de software niet van een en dezelfde cel afkomstig is of dat het gevolgde traject in verschillende delen is onderbroken. Bovendien is de beweging van cellen in vivo ingewikkelder dan in vitro, vooral tijdens dynamische immuun responsen. Modellering van celmigratie in vivo is niet alleen gebaseerd op Brownse beweging of autoregressieve beweging, maar moet een combinatie van meerdere complexe bewegingen aannemen. Enkele trackingalgoritmen in sommige commerciële softwareprogramma's resulteren in trackingfouten, wat de kwantificatie van het traject onbetrouwbaar maakt. Daarom is het noodzakelijk om nieuwe algoritmemodellen vast te stellen op basis van in vivo bewegingen van cellen in een specifieke situatie. In Hoofdstuk 3 onderzochten we het celmigratie gedrag dat wordt gereguleerd door Toll-like receptorsignalering in staartver wonde zebravislarven door middel van een handmatige

trackingmethode. Deze handmatige trackinggegevens bieden een solide basis, die de weg vrijmaakt om betere cel tracking-plug-ins te ontwikkelen voor in vivo cel trackingstudies bij zebravislarven. Daarom zijn we van plan om verder geoptimaliseerde automatische trackingmethoden te ontwikkelen op basis van de grote datasets in hoofdstuk 3.

Om de mechanistische basis van de verschillen in cel migratiegedrag te bestuderen, kunnen wiskundige modellen nieuwe inzichten verschaffen. Partiële differentiaalvergelijkingen (PDE's) kunnen chemokine- en ROS-gradiënten modelleren. Deze kunnen worden opgenomen in cel chemotaxis-modellen, zoals random walk-modellen, faseveldmodellen of het Cellular Potts-model, met verschillende gradaties van cel resolutie, om leukocytmigratie te bestuderen. Dergelijke modellen kunnen kwantitatieve inzichten verschaffen in hoe chemokinen en ROS-gradiënten het migratiegedrag van de leukocyten beïnvloeden, en hoe de cellen deze gradiënten veranderen door chemokines te binden of uit te scheiden of door ROS te absorberen en te metaboliseren waarvan bekend is dat het de robuustheid van chemotaxis beïnvloed. Met behulp van Bayesiaanse inferentie op trackinggegevens kan men een aantal chemotaxisparameters afleiden, zoals de stroomsnelheid, diffusiecoëfficiënt en productietijd van de chemoattractant.

6. Conclusie

Een breed begrip van het aangeboren immuunsysteem is belangrijk voor gastheergerichte benaderingen voor de behandeling van ziekten. In dit proefschrift hebben we aangetoond dat Tlr2 een cruciale rol speelt in het aangeboren immuunsysteem van de gastheer. In Hoofdstuk 2 laten we de rol van Tlr2-signalering in de afweer van de gastheer tegen infectie op transcriptoom niveau en cellulair niveau zien door *M. marinum*-infectie in een *tlr2*-mutant te bestuderen. Bovendien bleek de *tlr2*$^{-/-}$ mutante zebravisstam beschreven in Hoofdstuk 2 zeer nuttig te zijn voor de studie van aangeboren immuun mechanismen die ten grondslag liggen aan mycobacteriële infectie. In Hoofdstuk 3 hebben we gevonden dat *tlr2* en *myd88* betrokken zijn bij reacties op staartverwonding door het gedrag en de snelheid van leukocytmigratie *in vivo* te reguleren. De grote datasets verkregen uit hoofdstuk 3 zullen verder worden gebruikt voor het ontwikkelen van nieuwe cel tracking algoritmen en wiskundige modellering. In Hoofdstuk 4 hebben we een nieuw *M. avium* infectiemodel in de zebravis gekarakteriseerd dat verder kan worden gebruikt om de interactie tussen de gastheer en NTM-bacteriën te bestuderen.

List of abbreviations

AB/TL: AB/Tupfel long fin

CFU : colony-forming units

CLSM: confocal laser scanning microscopy

DEGs: differential expressed genes

Dpf: days post fertilization

Dpi: days post injection

EGPF: enhanced Green fluorescent protein

FDR: false discovery rate

FACS: Fluorescence-activated cell sorting

GSEA: Gene-Set Enrichment Analysis

HDT: host-directed therapies

Hpf: hours post fertilization

Hpi: hours post injection

Hpw: hours post wounding

Mpeg1: macrophage expressed gene 1

Mpx: Myeloperoxidase

Mm: *Mycobacterium marinum*

Mtb: *Mycobacterium tuberculosis*

MAC: *Mycobacterium avium complex*

NMD: non-sense mediated mRNA decay

NTM: nontuberculous mycobacteria

qPCR: quantitative polymerase chain reaction

RNAseq: Deep sequencing of cDNA derived from polyA RNA

SNEA: Sub-Network Enrichment Analysis

TB: tuberculosis

Tg: transgenic

Curriculum vitae

Wanbin Hu was born on May 8th, 1991 in Luoyang, Henan, China. After graduating from Luoyang No. 3 High School in 2010, she started a Bachelor's program in Biotechnology at the Faculty of Life Science at Henan Normal University, Xinxiang, China. In 2014, she obtained her BSc degree.

In 2014, she started to pursue a Master's degree at Dalian Ocean University, Dalian, China. In her first year of graduate school, she was hired as an assistant graduate counselor. In 2016, she was awarded the "Third Prize of Excellent Paper" in the 2016 Dalian China-Japan-Korea Graduate Student Academic Forum. In the same year, she was awarded the "National Scholarship for Postgraduates". She was awarded twice the "Three Merits Student award", and awarded twice the "First Class Academic Scholarship" of Dalian Ocean University during her master's education. As a graduate student, her study mainly focused on the impact of environmental stress on morphology and physiology in marine life. In 2017, she was awarded "Outstanding Graduates in Dalian" and "Outstanding Graduate of Dalian Ocean University" certificates based on her master thesis "Transcriptome study on the response of sea urchin larvae to seawater acidification".

After completion of her MSc degree in 2017, she was awarded a scholarship from the China Scholarship Council (CSC) to carry out a PhD research project at the Institute of Biology of Leiden University under the supervision of Prof. Herman P. Spaink and Prof. Fons J. Verbeek. In this thesis, she investigated the function of toll-like receptor 2 in the innate immune system by using the zebrafish infectious model and zebrafish inflammatory model. The results of the research were published in BMC Genomics, British Journal of Pharmacology, and Frontiers in Cell and Developmental Biology. Currently, she is working as a postdoc at the Institute of Biology Leiden on non-tuberculous mycobacterial infections funded by the Innovative Medicines Initiative (IMI) of the European Union.

Publication list

1. **Hu W**, van Steijn L, Li C, Verbeek FJ, Cao L, Merks RM, Spaink HP. A novel function of TLR2 and MyD88 in the regulation of leukocyte cell migration behavior during wounding in zebrafish larvae. Frontiers in cell and developmental biology. 2021;9.
2. Van Wijk RC, **Hu W**, Dijkema SM, van den Berg DJ, Liu J, Bahi R, Verbeek FJ, Simonsson US, Spaink HP, Van der Graaf PH, Krekels EH. Anti-tuberculosis effect of isoniazid scales accurately from zebrafish to humans. British journal of pharmacology. 2020 Dec;177(24):5518-33.
3. **Hu W**, Yang S, Shimada Y, Münch M, Marín-Juez R, Meijer AH, Spaink HP. Infection and RNA-seq analysis of a zebrafish *tlr2* mutant shows a broad function of this toll-like receptor in transcriptional and metabolic control and defense to *Mycobacterium marinum* infection. BMC genomics. 2019 Dec;20(1):1-8.